ALLIGATOR RIVERS ANALOGUE PROJECT

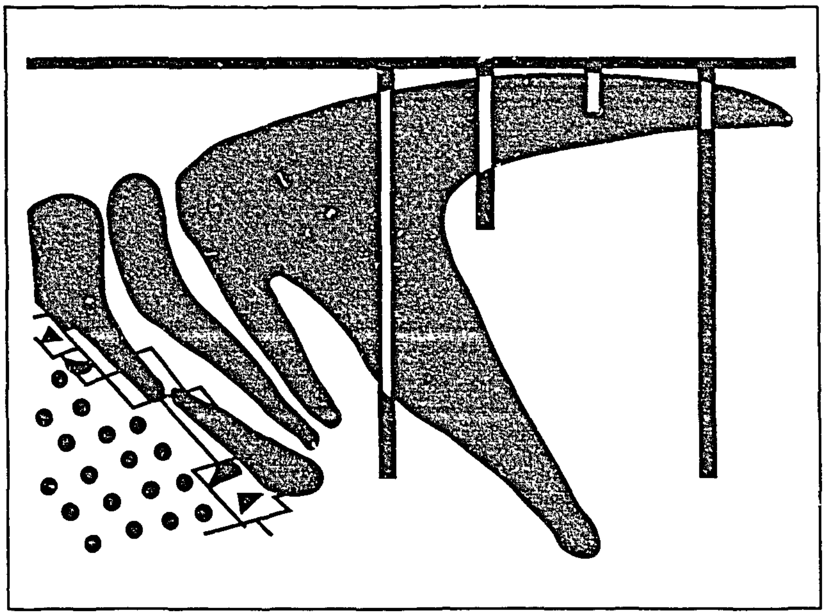

ISBN 0-642-59934-3

DOE/HMIP/RR/92/078

SKI TR 92:20-8

FINAL REPORT
VOLUME 8

CHEMISTRY AND MINERALOGY OF ROCKS AND SOILS

1992

AN OECD/NEA INTERNATIONAL PROJECT MANAGED BY:
AUSTRALIAN NUCLEAR SCIENCE AND TECHNOLOGY ORGANISATION

ALLIGATOR RIVERS ANALOGUE PROJECT

FINAL REPORT

VOLUME 8

CHEMISTRY AND MINERALOGY

OF ROCKS AND SOIL

R. Edis[1]

L. Cao[2], J. Cashion[3], D. Klessa[4], A.J. Koppi[4], T. Murakami[5], T. Nightingale[1], T. Payne[1], A. Snelling[6] and N. Yanase[5]

[1]Australian Nuclear Science and Technology Organisation
Private Mail Bag 1, Menai, NSW, 2234, Australia

[2]University of Sydney, Department of Geology and Geophysics
Sydney, NSW 2006, Australia

[3]Monash University, Department of Physics
Clayton, Vic. 3168, Australia

[4]University of Sydney, Department of Soil Science
Sydney, NSW 2006, Australia

[5]Japan Atomic Energy Research Institute
Tokai Research Establishment, Tokai-Mura, Naka-Gun, Ibaraki-Ken, Japan

[6]Consultant Geologist
PO Box 302, Sunnybank, Qld 4109, Australia

PREFACE

The Koongarra uranium ore deposit is located in the Alligator Rivers Region of the Northern Territory of Australia. Many of the processes that have controlled the development of this natural system are relevant to the performance assessment of radioactive waste repositories. An Agreement was reached in 1987 by a number of agencies concerned with radioactive waste disposal, to set up the International Alligator Rivers Analogue Project (ARAP) to study relevant aspects of the hydrological and geochemical evolution of the site. The Project ran for five years.

The work was undertaken by ARAP through an Agreement sponsored by the OECD Nuclear Energy Agency (NEA). The Agreement was signed by the following organisations: the Australian Nuclear Science and Technology Organisation (ANSTO); the Japan Atomic Energy Research Institute (JAERI); the Power Reactor and Nuclear Fuel Development Corporation of Japan (PNC); the Swedish Nuclear Power Inspectorate (SKI); the UK Department of the Environment (UKDoE); and the US Nuclear Regulatory Commission (USNRC). ANSTO was the managing participant.

This report is one of a series of 16 describing the work of the Project; these are listed below:

No.	Title	Lead Author(s)
1	Summary of Findings	P Duerden, D A Lever, D A Sverjensky and L R Townley
2	Geologic Setting	A A Snelling
3	Geomorphology and Paleoclimatic History	K-H Wyrwoll
4	Geophysics, Petrophysics and Structure	D W Emerson
5	Hydrogeological Field Studies	S N Davis
6	Hydrogeological Modelling	L R Townley
7	Groundwater Chemistry	T E Payne
8	Chemistry and Mineralogy of Rocks and Soils	R Edis
9	Weathering and its Effects on Uranium Redistribution	T Murakami
10	Geochemical Data Bases	D G Bennett and D Read
11	Geochemical Modelling of Secondary Uranium Ore Formation	D A Sverjensky
12	Geochemical Modelling of Present-day Groundwaters	D A Sverjensky
13	Uranium Sorption	T D Waite
14	Radionuclide Transport	C Golian and D A Lever
15	Geochemistry of ^{239}Pu, ^{129}I, ^{99}Tc and ^{36}Cl	J T Fabryka-Martin
16	Scenarios	K Skagius and S Wingefors

CONTENTS

ABBREVIATIONS

AES	Atomic Emission Spectrometry
ARAP	Alligator Rivers Analogue Project
ANSTO	Australian Nuclear Science and Technology Organisation
CDB	Citrate Dithionite Bicarbonate
CSIRO	Commonwealth Scientific Research Organisation
CV	Coefficient of Variation
DNAA	Delayed Neutron Activation Analysis
EDS	X-Ray Energy Dispersive Spectroscopy
EMA	Electron Microprobe Analysis
HREE	Heavy Rare Earth Element
ICP-MS	Inductively Coupled Plasma Mass Spectrometry
INAA	Instrumental Neutron Activation Analysis
JAERI	Japan Atomic Energy Research Institute
MDL	Minimum Detection Limits
PIGME	Proton Induced Gamma-ray Emission
PIXE	Proton Induced X-ray Emission
PAAS	Post Archaean Australian Shales
REE	Rare Earth Element
SEM	Scanning Electron Microscope
TAO	Tamms Acid Oxalate
TEM	Transmission Electron Microscopy
WDS	Wavelength Dispersive Spectrometry
XRD	X-ray Diffraction
XRF	X-ray Fluorescence

EXECUTIVE SUMMARY

The chemistry and mineralogy of rock and soil at Koongarra have been investigated with the aim of gaining understanding about the migration of radionuclides. Of central interest was the mobility and retardation of uranium over long timescales. In addition, data was collected to provide a geochemical framework of the Koongarra system. This was necessary for the application, testing and development of transport and geochemical models, and to allow a realistic evaluation of the transferability of the results.

Data were collected to clarify the extent and direction of the redistribution of uranium from the primary ore body. Leaching and deposition of uranium are strongly linked to weathering processes. Uranium concentrations in the weathered and transition zones are high compared to the unweathered parent material for at least 300 m from the source. The apparent direction of the plume is mainly due south to south-south west, and corresponds well with many hydrochemical and geophysical parameters. The most important zones of enrichment appear to be near the base of weathering, and in the very shallow zone. The shallow component appears to be more widespread than the deeper component, but accounts for only a small proportion of the mobilised uranium.

The main mineral constituents of the host schists are quartz, chlorite and muscovite. Small amounts of graphite, sulfides, garnets, feldspars and remnant biotite also occur, particularly outside of the primary ore zone. The forms and abundances of the mineral constituents greatly affect weathering processes, final products, groundwater chemistry and radionuclide-mineral interactions. The abundances of major rock constituents vary spatially over the site, however, zones of generally similar mineralogy can be delineated. Within the primary ore zone, the nature of the chlorite is mainly magnesium-rich. Outside of this inner halo of hydrothermal alteration, iron-rich chlorite tends to dominate. In the weathered zone above the primary ore body, kaolinite is the only significant clay mineral. Near the base of weathering, there is a thin layer of vermiculite. Down-gradient, where the degree of hydrothermal alteration of the rock is less, smectite also becomes a significant component of the weathered zone.

Goethite, hematite and ferrihydrite are the major iron oxides present at Koongarra. They occur as fissure and remnant schistosity coatings, dispersed clay coatings, and nodules. The different forms of iron oxide probably play different roles in the capture and storage of otherwise mobile species. The amount of iron oxides is very variable, with occasional bands of bleached clay juxtaposed with iron rich bands. The greatest heterogeneity in the distribution of iron appears to be with the crystalline phases. The concentration of ferrihydrite, estimated by chemical extraction, was between 7 and 29 mg/g, making up an average of 10% of the total iron. Lithiophorite is the only manganese mineral identified in the weathered zone, and mainly occurs coating fissures and remnant schistosity. Coatings of iron and manganese oxy-hydroxides on pore and fissure surfaces are well placed for contact with migrating species.

Areas of depletion and enrichment of elements of interest were determined. The concentration and distribution of elements potentially significant to radionuclide migration were determined. Associations between various elements, and between elements and minerals were examined. In the unweathered rock, uranium appears to be associated with a few trace elements, but not with any major rock forming elements. There has been very little penetration of uranium into the quartz chlorite matrix from fissures; an apparent diffusivity of 10^{-24} m^2s^{-1} was estimated.

In the secondary ore body (weathered), uranium is correlated with phosphorus, and the uranyl phosphate mineral saleeite has been detected, particularly near the base of weathering. The concentration of phosphorus within the secondary ore body is not significantly greater than elsewhere. This suggests that the formation of uranyl phosphates is not due to a phosphate concentration anomaly. The main source of phosphorus at Koongarra is fluorapatite, however, a non-apatite phase of phosphorus is also present within the inner halo of alteration. Further down-gradient, uranium is correlated with iron and iron oxide associated elements.

The area of primary mineralisation is characterised by marked relative enrichment of heavy rare earth elements, compared to the regional host rock. This may reflect conditions during ore genesis. The heavy rare earth elements are the most accessible to the groundwater, and may therefore be preferentially transported. Cerium appears to be preferentially taken up into inaccessible phases, compared to other rare earth elements, probably into oxides of iron and manganese. The association of uranium with mineral phases was studied using various microscopic and chemical techniques. In the weathered zone, uranium was found to be associated with secondary oxides of iron and manganese. Phase selective extraction schemes showed that the uranium in the weathered zone is mainly accessible to the groundwater (adsorbed or associated with amorphous phases, 10-73%), or entrapped within crystalline iron oxides (<27-82%). The relationship with iron oxy-hydroxide appears to be of a diffuse nature, indicative of sorption as the initial mechanism for association. However within manganese phases, uranium is almost exclusively associated with "hot spots" containing a cerium oxide phase. This cerium phase occurs as small globules, approximately 2 μm in diameter, and is probably a mixed oxide of cerium and uranium. The mechanism for the cerium-uranium association is not clear, but probably involves a redox interaction between manganese and cerium. Anomalously high concentrations of cerium were not found in the bulk Koongarra rock.

Uranium series disequilibria has been extensively examined, particularly in the weathered zone of Koongarra. The isotopes of central interest were ^{238}U, ^{234}U, ^{230}Th and ^{226}Ra. In the unweathered zone, the ore material and the host rock were at approximate secular equilibrium, except for a small apparent depletion of ^{226}Ra. In the weathered rock, above the primary mineralised zone, high $^{230}Th/^{234}U$ activity ratios indicate strong recent leaching of uranium. In these leached areas, the $^{234}U/^{238}U$ activity ratios are high; above unity in the bulk rock and near unity in the accessible phases (extractable with Tamms acid oxalate (TAO)). This indicates a net preferential leaching of ^{238}U relative to ^{234}U. The most intensely leached samples came from near the surface, near the up-flow boundary of the primary ore.

The most intense recent accumulation of uranium appears to have occurred near the base of weathering, about 0-50 m from the down-flow boundary of primary ore. This highlights the importance of the early stages of weathering to the migration and retardation of uranium. Samples having low $^{230}Th/^{234}U$ activity ratios, indicating deposition of uranium, also contained low $^{234}U/^{238}U$ activity ratios. Beyond about 50 m down-gradient, both activity ratios tend to increase with distance. At distances greater than about 100 m from the primary ore, deposition of uranium seems to have occurred particularly SSW of the deposit, and is most pronounced near the surface.

Sequential extraction data showed that the highest $^{234}U/^{238}U$ activity ratios were from resistant phases with low uranium contents, such as quartz and muscovite. The amount of excess ^{234}U appeared to be related to the amount of uranium present in the crystalline iron oxide phases, and iron oxides were frequently observed coating minerals. The high activity ratios in the resistant phases suggest that α-recoil emplacement of ^{234}Th is a significant process occurring at Koongarra. Other mechanisms may also be operating to reduce the mobility of ^{234}U.

The following scenario for the development of disequilibria between ^{234}U and ^{238}U is proposed. The onset of weathering causes the rapid dissolution of the primary uranium minerals, resulting in the congruent liberation of ^{238}U and ^{234}U. This is followed by preferential entrapment of ^{234}U through processes such as α-recoil emplacement, which results in an apparent preferential leaching of ^{238}U. This leads to high $^{234}U/^{238}U$ activity ratios in leached samples and low ratios in depositional samples down-gradient. Beyond about 50 m down-gradient, uranium mobilised from the primary ore makes a smaller contribution to the total accessible uranium. It is likely that relatively stable minerals that contain uranium, such as zircon and monazite, would preferentially leach ^{234}U relative to ^{238}U due to the physical location of the uranium, resulting in higher $^{234}U/^{238}U$ activity ratios of the accessible and groundwater uranium. It is suggested that where the uranium content in accessible phases is high, the accessible (or solution) $^{234}U/^{238}U$ activity ratio will generally tend to decrease with time or distance due to preferential retardation of ^{234}U.

Estimates of the partitioning of ^{238}U and ^{230}Th between groundwaters and solid phases were made using several approaches. The uranium isotope ratio in the TAO-extractable fractions were generally similar to those in the groundwater, suggesting that TAO-extraction removes material accessible to exchange with the groundwater. Using the TAO-extractable uranium, partition coefficients of 0.5-1 $\times 10^3$ mL/g were calculated. Bulk rock data gave partition coefficients of 1-45 $\times 10^3$ mL/g. Near the base of weathering, the $^{234}U/^{238}U$ activity ratio in the groundwater tended to increase with increasing bulk rock partition coefficient.

In summary, considerable information has been gathered on the migration of uranium at Koongarra. Widely applicable data has been collected on; the importance of early stages of weathering in radionuclide mobility; the behaviour of uranium in weathered environments; the development of isotopic disequilibria under weathering conditions; the behaviour of rare earth elements; and the associations of uranium with mineral phases.

ACKNOWLEDGMENTS

We gratefully acknowledge the financial support of the organisations which sponsored the Alligator Rivers Analogue Project (ARAP).

We are grateful to the many individuals and organisations who were involved in the ARAP, in particular Peter Duerden for management of the ARAP; Robin Lowerson for administrative assistance and; David Garton for technical assistance. Further assistance was provided by; David Cohen, Terry Wall and other staff of the Applied Physics Program at Ansto; John Fardy, Steven Short, Henri Wong and other staff of the Environmental Science Program at Ansto; Chris Matulis, Les Dale and other staff of the CSIRO at Lucas Heights; Hiroshi Isobe, Toshi Ohnuki and other staff of JAERI at Tokai; Gordon Thorogood, Cliff Ball and other staff of the Advanced Materials Program at Ansto; staff of the Electron Microscope Unit and Soil Science Department of the University of Sydney, particularly David Cockayne and Chris Conoley; Dimitri Sverjensky and Ali Komninou of Johns Hopkins University; Bob Treloar and other staff of the Northern Territory Department of Mines and Energy and; staff of the Office of the Supervising Scientist at Jabiru.

The work described in this volume greatly benefited from lengthy discussions and dispatches with the other workers participating in the ARAP. Access to the site, rock and soil samples, and unpublished data and information was kindly provided by Denison Australia, particularly through Grant Watt.

1 INTRODUCTION

This volume contains a description of the distribution of minerals and elements at Koongarra, including the distribution of radionuclides. The Koongarra orebody is situated 225 km east of Darwin in the Northern Territory of Australia. The zone of primary uranium mineralisation has been intersected by weathering conditions, and this has resulted in the formation of a secondary ore zone and dispersion fan in the weathered zone. A detailed description of the location and the geology of the site is given in Volume 2 of this Series.

The uranium distribution over the site was investigated to determine the extent and direction of uranium migration from the primary uranium mineralisation. The depth patterns of uranium concentration were also investigated to elucidate depths of uranium mobility/retardation.

The distribution of elements, rock and minerals, and how they may affect uranium mobility, or indicate interactions between uranium and solid phases, were considered. Multi-elemental analyses were carried out on many samples to provide basic concentration data about various geochemically significant elements, and to elucidate how the elements interact with one another, the solid substrate and the groundwater. This included the analysis of bulk rock samples, visually distinct subsamples, different particle sizes and chemically defined phases. Similarly, mineralogical data supplied information on the substrate reacting with the groundwater.

Extensive studies were undertaken to elucidate the form of uranium in the weathered zone. These involved optical and electron microscopy studies and auto-radiography. Similarly, uranium-mineral and uranium-fracture associations were examined.

Spatial trends of uranium series disequilibria in bulk rock, secondary uranium minerals and different chemically defined phases were obtained. These give information about uranium deposition and leaching, the evolution of the dispersion fan, the roles and relative importance of different mineralogical phases and processes involved in the retardation of radionuclides.

1.1 Uranium-Mineral Associations in the Alligator Rivers Region

Sorption is likely to be the major process in the retardation of uranium under the groundwater conditions that currently apply at Koongarra, and this is the likely case for most radionuclides and other contaminants. Other processes that are sometimes important include coprecipitation and biological uptake (Levinson et al., 1982). The most important mineral phases involved in these retardation processes are the secondary minerals produced as a result of weathering. Secondary minerals, particularly the metal oxides, usually have a much higher sorption capacity than the primary rock forming minerals, such as chlorite. For some elements, such as cesium, weathering products such as illite, vermiculite and smectites, are stronger binders than metal oxides (Ticknor et al., 1989). Secondary minerals tend to have high surface areas, and occur in locations such as lining cracks and fissures which are in close contact with moving groundwater. Secondary minerals of particular relevance to

Koongarra include vermiculite, iron oxides, manganese dioxide, anatase and rutile, and possibly smectite.

Iron oxides

In soil and weathered environments, most uranium is generally associated with iron oxides, due to the high sorption capacity of these minerals for uranium (Gueniot et al., 1982). The strong association of uranium, and other trace elements with secondary iron minerals has been described by many authors (McKenzie, 1975; Zielinski et al., 1986b). Koons et al. (1980) showed that uranium and thorium were often associated with iron oxides at very early stages of weathering of diabasic and granitic rock.

Lowson et al. (1986) measured U/Fe ratios in natural crystalline iron oxides from the nearby Ranger uranium deposits of up to 0.3%, however this may not all have been present as lattice substitution. Fission and α-track autoradiography of weathered samples from Ranger showed that the uranium was concentrated with the iron minerals, particularly in nodules (Gray, 1986). It has been suggested that uranium may be taken up, to a small degree, as a crystal substitute in lepidocrocite (Gueniot et al., 1982), but the evidence for this is not conclusive. Gerth (1987) was unable to incorporate a measurable amount of uranium or thorium into synthetic goethite crystal lattices.

Elemental correlations from bulk weathered Koongarra and Ranger samples indicated that Mn, P, Th, and uranium were significantly positively correlated to iron (Gray, 1986). Phosphorus is an element of particular importance to uranium geochemistry, and it has been shown to be predominantly adsorbed onto iron oxides in weathered systems (Hsu, 1965; Pea and Torrent, 1984). It appears that goethite is a stronger sorbing phase for phosphate than hematite (Colombo et al., 1991).

Manganese oxides

Manganese oxides have been reported to be very tenacious binders of many elements, including uranium (Means et al., 1978). Zielinski et al. (1986b) found that MnO_2 was a stronger binder of uranium than iron oxides in tuff. Radium is also well taken up by manganese oxides, and it has been suggested that this is partially via coprecipitation (Levinson et al., 1982).

Anatase, brookite and rutile

Precipitated hydrous oxides of titanium have been shown to adsorb significant quantities of uranium during the early stages of weathering (Ruzicka and Littlejohn, 1982; Speer et al., 1981). Yamashita et al. (1980) reported the importance of titanium(IV) oxides in scavenging uranium from seawater. Hydrous titanium oxides have been shown to readily adsorb uranyl species from groundwater-like solutions, especially above pH 4.5 (Maya, 1982; Venkataramani and Gupta, 1991).

1.2 Uranium-Element Associations in the Alligator Rivers Region

Correlation coefficients between elements for sites in the Alligator Rivers region have been reported by Ferguson and Winer (1980); Gray (1986), and Nash and Frishman (1983). These studies have mainly concentrated on unweathered rock, although Gray included some weathered zone samples.

Ferguson and Winer (1980) presented statistical analyses of various rock units in the Pine Creek geosyncline, including the Cahill formation and the Kombolgie formation. They also included a site study of the Jabiluka ore deposits. On the regional scale they found that for 143 samples of unweathered rock from the Cahill formation, uranium was correlated with Li, Sc, V, Co, Cu, As, Y, Nb, Mo, W, Pb, and -Rb ($P < 0.05$; "-" denotes an inverse correlation). Gray (1986) produced element-element correlation coefficients for 11 unweathered samples from the Cahill formation, and found that uranium correlated to Ni, As and Pb ($P < 0.05$).

Site studies of rock from the Cahill formation gave similar relationships of elements with uranium as for the regional scale. Nash and Frishman (1983) presented data on samples from the Ranger mine area. For rock containing >250 μg/g uranium, they found uranium correlated to 25 elements, including Li, F, Ti, V, Co, Ni, Pb, Th, -Si and -K. They found that Li, Mg, Sc, V, Cr, Fe, Ni, Y, Sn, Eu, Yb and Pb were significantly enriched, while Na, K, Ca, Mn, Sr, Cs, Ba and Ce were significantly depleted in ore samples from the Ranger uranium deposit. The enrichment values of magnesium and iron reflect the presence of chlorite, which is the host rock for uranium mineralisation in the region.

In the studies by Ferguson and Winer (1980), Nash and Frishman (1983) and Gray (1986), elements that were found to significantly correlate with uranium in rock from the Cahill formation, either locally or regionally, were Li, Be, F, Na, Sc, Ti, V, Co, Ni, Cu, As, Sr, Y, Nb, Mo, W, Pb, Th, -Si, -K and -Rb. An interesting aspect of these results is that uranium did not correlate to any major rock constituent, such as magnesium. In this report some elemental relationships will be discussed with regard to mineralogical implications.

The distribution of rare earth elements (REEs) in the Cahill formation, including some uranium ore bodies, has been studied by McLennan and Taylor (1979, 1980). The Cahill formation generally has a REE signature similar to Post Archaean Australian Shales (PAAS) (Taylor and McLennan, 1985). However, uranium mineralisation zones and particularly uranium-rich material such as uraninite, were associated with a large enrichment of the heavy rare earth elements (HREEs, Eu-Yb), relative to PAAS. The PAAS corrected maxima of rock containing mineralised uranium was at about Tb-Dy (McLennan and Taylor, 1979, 1980).

1.3 Evolution of Uranium Series Disequilibria in Natural Systems

A brief review of the development of uranium series disequilibria, particularly in respect to disequilibrium between ^{234}U and ^{238}U is presented here, with the discussion being mainly constrained to systems other than Koongarra. A detailed report on the

ARAP findings at Koongarra is presented in Section 6 for rock samples and Volume 7 of this series for the groundwater investigations.

Disequilibria in weathered rock

Several authors have used uranium series disequilibrium to study the geochemical behaviour of uranium and thorium in the weathering environment (for a review see Rosholt, 1982) Rosholt (1961a, b) studied the accumulation of uranium in sandstone deposits. It was argued that the extreme tendency of both protactinium and thorium to hydrolyse, and their resulting immobility in the geochemical environment, enabled the radiogenic daughters ^{231}Pa and ^{230}Th to be used as markers for recent uranium migration. The assumption was made that these nuclides remained at their point of generation from ^{235}U and ^{234}U respectively.

Rosholt et al. (1963, 1964) studied the isotopic fractionation of uranium in weathered granite and sandstone using mass spectrometry. Uranium-234 was observed to be preferentially leached from some samples, most of which were correspondingly enriched in ^{230}Th. The presence of excess ^{234}U in other samples, together with less than equilibrium amounts of ^{230}Th was taken to indicate a relatively recent accumulation of uranium.

A more detailed study of uranium isotopic composition was reported by Rosholt et al. (1966), on the basis of the relative amounts of uranium and thorium isotopes in a soil profile. Generally they found large excesses of ^{230}Th over ^{234}U in B and C horizons ($^{230}Th/^{234}U$ activity ratios up to 1.7), which were accompanied by low $^{234}U/^{238}U$ activity ratios. They attributed this to preferential leaching of uranium over thorium and of ^{234}U over ^{238}U. In the A horizon the reverse situation generally applied, with lower $^{230}Th/^{234}U$ activity ratios and higher $^{234}U/^{238}U$ activity ratios prevailing.

Hansen (1970) studied a number of soil profiles including one from a warm, dry climate in which the organic content was found to be very low, and as a result thorium mobility was also very low. In this environment uranium was leached far more rapidly than thorium and the degree of loss of uranium could be calculated from the excess of ^{230}Th. In this respect the environment of the Koongarra uranium deposit can be regarded as being similar since the local climate is hot with seasonal rainfall, and the soil organic content is generally low.

Osmond and Cowart (1982) pointed out that ^{234}U deficiencies are commonly observed in granites that have no outward appearance of weathering. The slight penetration of meteoric waters carrying both O_2 and CO_2 was sufficient to cause oxidation and subsequent complexation of uranium. Uranium-234 was normally leached preferentially and, with its 244 ky half-life, the long term effects of even slight weathering could be sustained in the form of measurable $^{234}U/^{238}U$ disequilibria. Guthrie (1991) studied granitic rock, and generally found $^{234}U/^{238}U$ activity ratios of unity, except where intense alteration had occurred and a depletion of ^{234}U was observed. Latham and Schwarcz (1987) studied the relative mobility of uranium, thorium, and radium isotopes in weathered granite and found that radium was the most rapidly mobilised. Samples from which uranium was leached gave $^{234}U/^{238}U$

activity ratios below unity, and most of the uranium in the samples was found associated with zircon and sphene.

A study by Zielinski et al. (1980) of disequilibria in glassy and zeolitised tuff provided a good example of selective ^{234}U removal from a solid. The greatest ^{234}U depletion was found in zeolitised samples and this was attributed to the higher surface area of zeolite. In one sample the $^{234}U/^{238}U$ and $^{230}Th/^{234}U$ activity ratios were 0.51 and 0.97 respectively, indicating that a high degree of selective removal of ^{234}U had not greatly affected the $^{230}Th/^{234}U$ activity ratio. A similar study of zeolitised tuff by Rosholt (1980) revealed $^{234}U/^{238}U$ and $^{230}Th/^{234}U$ activity ratios both in excess of unity. In comparing these two studies, Szabo and Rosholt (1982) suggested that the elevated activity ratios found by Rosholt (1980) were the effects of daughter "emplacement", occurring in the earlier stages of alteration. In the later stages of alteration, the daughter "displacement" mechanisms demonstrated by Zielinski et al. (1980), were thought to predominate. Ghaleb et al. (1990) found that leaching of uranium from lacustrine carbonate occurred without uranium isotope fractionation, due to rapid dissolution of the principal uranium bearing phase.

The assumption of thorium and protactinium immobility is a very important one and has been used in numerous studies of the geochemical migration of uranium. Cases of thorium being mobilised have been comparatively rare, and usually involve organic ligands (Chopin, 1988), acidic conditions (Langmuir and Herman, 1980) and high carbonate conditions (Dervin and Faucherre, 1973). At Koongarra, thorium levels in the groundwater were very low, and sensitive to filtration (see Volume 7 of this series). This, along with near neutral pH and low dissolved organic carbon, suggests that thorium solubility at Koongarra is minimal.

Studies of rock/aquifer systems

Osmond and Cowart (1976) published an extensive review of the literature on $^{234}U/^{238}U$ fractionation in groundwater and rock. They stressed the generally higher mobility of ^{234}U over ^{238}U in groundwater systems, and attributed this to selective leaching of ^{234}U from solids and direct recoil of ^{234}Th into the water from solids (possible mechanisms are discussed below in this Section). A range of possible applications of uranium isotopic variation in hydrology were discussed, including an assessment of the degree of mixing of regional aquifers, dating of groundwater systems and uranium exploration.

In systems leaching uranium from within mineral grains, the degree of disequilibria between ^{234}U and ^{238}U in groundwater should reflect the flow rate (Laul and Smith, 1988), with faster flowing systems having greater excess ^{234}U than slow systems. Near unity $^{234}U/^{238}U$ activity ratios may indicate possible nearby uranium deposits (Osmond and Cowart, 1976; Asikainen, 1981). Toulhoat and Beaucaire (1991) studied groundwater from three uraninite deposits, and found that increasing $^{234}U/^{238}U$ activity ratio was correlated with decreasing Eh, decreasing uranium concentration, and the ratio of uranium concentration in the rock to the uranium concentration in solution. In general, oxidised waters encountering uranium accumulations, showed high uranium concentrations and low $^{234}U/^{238}U$ activity ratios. They also found lower

$^{234}U/^{238}U$ activity ratios in zones of massive mineralisation at the Cigar Lake uranium deposit than in dispersed ore. Andrews and Kay (1983) suggested that the evolution of $^{234}U/^{238}U$ disequilibria is dependant upon the uranium content of the rock relative to the solution, and to the degree of contact between solid surfaces and the solution.

One of the more extreme examples of a very recent accumulation of uranium was reported by Zielinski et al. (1986a). Ore-grade concentrations of uranium found in organic-rich sediments had $^{234}U/^{238}U$ activity ratios between 1.30 and 1.38 while the $^{230}Th/^{234}U$ activity ratios were between 0.008 and 0.11. The very low $^{230}Th/^{234}U$ activity ratios indicated that the deposit was only a few thousand years old, placing its origin in the late quaternary period.

Longworth et al. (1989) reported uranium series disequilibria at a natural analogue site at Broubster, UK. At this site uranium from a vein of mineralisation in limestone was advected to a peat bog. Over 90% of the uranium in this bog was associated with organic phases. Samples from above the uranium source yielded $^{234}U/^{238}U$ and $^{230}Th/^{234}U$ activity ratios greater than unity, while down-gradient, in peat samples, these ratios were both below unity. This suggests preferential mobility of ^{238}U from the uranium source limestone. At another analogue study site at Needles Eye, Scotland, Scott et al. (1991) found $^{234}U/^{238}U$ activity ratios in groundwater, down-gradient from pitchblende veins, to be below unity. The source pitchblende was in secular equilibrium with respect to ^{238}U, ^{234}U, and ^{230}Th.

Disequilibria in unweathered rock

Fractionation between ^{238}U, ^{234}U and ^{230}Th is generally less common in unweathered rock than in weathered rock, owing to the lower degree of groundwater penetration and the lower solubility of uranium in the reduced (tetravalent) state. Since this topic is of only limited relevance to the present study it will not be examined in detail here. An extensive study of uranium and thorium isotopic composition of 84 unweathered rock samples was reported by Rosholt (1983). In the majority of samples, $^{234}U/^{238}U$ and $^{230}Th/^{234}U$ activity ratios were within 5% of unity although there were some notable exceptions. Schwarcz et al. (1982) reviewed the possible mechanisms that can give rise to various patterns of disequilibria in unweathered rock. Recent volcanic rock studied by Gill and Williams (1990), contained $^{234}U/^{238}U$ activity ratios of unity, reflecting isotopic equilibrium in magma.

Mechanisms of $^{234}U/^{238}U$ fractionation

Although $^{230}Th/^{234}U$ disequilibria may be attributed in part to chemical differences between uranium and thorium, this is not the case for fractionation between ^{234}U and ^{238}U. Most authors dismiss the possibility that chemical fractionation between ^{238}U and the short-lived intermediates ^{234}Pa and ^{234}Th could play a significant role, particularly in the case of preferential daughter mobility. However, the case of decreased daughter mobility has not been extensively discussed. Three mechanisms for the development of high $^{234}U/^{238}U$ activity ratios have been extensively reviewed and are described here.

Direct alpha-recoil transfer of ^{234}Th across phase boundaries

The law of conservation of momentum implies that an alpha decay will impart significant momentum to the newly formed nucleus, causing it to recoil for distances of up to 60 nm in solids. This is sufficient for the nucleus to cross a phase boundary, be it from a solid to a liquid or vice versa. Kigoshi (1971) immersed fine grains of uraniferous zircon in dilute nitric acid solutions and found that there was a time-dependent increase in the level of ^{234}Th in the aqueous phase. This increase could be directly related to the half-life of ^{234}Th and resulted in the ^{234}Th activity in the solution being approximately an order of magnitude higher than that of longer-lived radionuclides such as ^{234}U, ^{230}Th and ^{238}U. This result was attributed to direct alpha-recoil of ^{234}Th from the solid into the water. The enrichment of ^{234}U in many natural aquifers was attributed to this mechanism. Kigoshi went on to suggest that water permeating the interstitial regions of minerals would become enriched in ^{234}Th. Several authors, including Sakanoue and Komura (1971) Rosholt (1983), and Szabo (1982), have also proposed that alpha recoil at the solid-liquid interface can result in the nucleus being implanted further into the solid.

Hashimoto et al. (1981) measured the ^{234}Th recoil range in amorphous UO_2 and U_3O_8 to be 13.2 and 16.9 $\mu g/cm^2$ respectively, corresponding to distances of 12 and 20 nm respectively. Hashimoto et al. (1985) also reported theoretical calculations of the recoil distances of several natural alpha decays in a range of common minerals, giving recoil ranges for ^{234}Th of 15-38 nm. Rossler (1983) claimed that the recoil distance of 20 nm was small compared to the most abundant grain sizes and that consequently the direct recoil mechanism could not be an important source of $^{234}U/^{238}U$ disequilibrium in solids.

Increased susceptibility to leaching caused by alpha decay

Whether or not the decay-induced recoil causes the nucleus to cross a phase boundary, the decay will inevitably result in severe dislocation of the nucleus, leaving it in a damaged site within the mineral. This can render the nucleus more susceptible to leaching. Kigoshi (1971), in an extension of the experiment on direct alpha recoil injection into water, suggested that where an alpha decay had left a recoil track near the surface, a preferential path of ^{234}U diffusion into the water would be provided. The presence of alpha-recoil tracks has been shown to increase the rate of weathering of many minerals, including sphene (Gleadow and Lowring, 1974) and allanite, apatite, monazite and xenotime (Petit et al., 1985a).

Eyal and Kaufman (1982) and Eyal (1982) demonstrated the preferential loss of radiogenic uranium and thorium isotopes from monazite. This was attributed to alpha recoil damage, and was postulated to be a potential release mechanism for alpha-emitting nuclides in buried nuclear waste. Eyal and Fleischer (1985a, 1985b) suggested that the loss of crystallinity caused by alpha decay (metamictisation) progressively diminished due to self-annealing of minerals.

Petit et al. (1985b) argued that alpha-recoil related models for disequilibria between ^{238}U and ^{234}U require improbably low mineral dissolution rates. They suggested that a more probable mechanism of fractionation involved a change in the oxidation state between ^{234}U and ^{238}U. Similarly, alpha track annealing rates appear to be high, which would further decrease the effect of alpha recoil on the incongruent dissolution of uranium bearing minerals.

Oxidation of ^{234}U from the +4 to the +6 state

It has been proposed that preferential dissolution could occur as a result of the ^{234}U being formed in the more soluble hexavalent state by decay of tetravalent ^{238}U. This could occur either as a result of the decay process itself (which involves an alpha and two beta decays) or by the relocation of ^{234}U in a more oxidising environment. Cherdyntsev (1968) favoured the latter mechanism, while Rosholt et al. (1963, 1964) favoured a mechanism of electron stripping caused by alpha decay in combination with recoil damage.

Preferential retardation of daughter nuclides

Disequilibria in secondary uranium accumulations have almost always been interpreted purely in terms of ^{234}U being the more mobile isotope. This implied that any accumulation in which the $^{234}U/^{238}U$ activity ratios exceeded unity was anomalous and could only be explained in terms of a multi-stage migration of uranium. Several authors have reported such occurrences with varying explanations, including Chalov (1959), Lively et al. (1979), Carl and Meyer (1984), Carl (1985), Sakanoue and Komura (1971), Rosholt (1980, 1983), Longworth et al. (1989), Scott et al. (1991) and many case studies of the Alligator Rivers Region (see below). Here, it will be argued that such a situation can often be explained in terms of preferential leaching of ^{238}U over ^{234}U.

Sequential extraction studies of weathered material, from the vicinity of ore bodies in the Alligator Rivers Region, show trends of increasing concentration of daughter nuclides (relative to parents) in phases of increasing inaccessibility (Airey et al., 1983; 1985; Shirvington, 1980a; 1980b; 1983; Lowson et al., 1986, 1992; Gray, 1986; and Short, 1988). This trend was observed down the chain to ^{226}Ra. While most of the uranium occurred in amorphous (adsorbed or in amorphous materials) and crystalline iron oxides, the strongest relative enrichment of daughter nuclides occurred in resistate minerals (such as clays, quartz and accessory minerals). Proposed mechanisms for daughter enrichment include direct recoil emplacement (Airey et al., 1983; Lowson et al., 1986; Short, 1988), preferential entrapment of thorium (eg ^{234}Th) (Gray, 1986), and inclusion into clay crystal lattices following recoil emplacement (Shirvington, 1983).

Short (1988) argued that since resistant minerals dominated the rock volume, the probability of recoil emplacement was high and could account for the observed disequilibria. Airey et al. (1985) presented results of a series of experiments whereby ^{226}Ra and ^{228}Th were added to suspensions of illite, montmorillonite, and kaolinite. After ingrowth of ^{224}Ra to secular equilibrium with ^{228}Th, the aqueous and solid phase extractions were analysed for ^{224}Ra and ^{226}Ra. The ratio of $^{224}Ra/^{226}Ra$ was depleted in the solution, and increased with increasingly aggressive leaching of the solid phase. This was interpreted as evidence of direct recoil emplacement, with the ^{224}Ra, the product of α-decay of ^{228}Th, being emplaced into inaccessible phases.

The probability of recoil emplacement, and therefore preferential entrapment of daughter nuclides, may be increased under a number of circumstances. These include a high accessible surface area of the solid and high surface affinity of the parent radionuclide (minimising the distance the recoiling nucleus needs to travel for emplacement), and unsaturated conditions (minimising the chances of the recoiling nucleus being stopped by water). One of the aims of the current program was to consider mechanisms for the development of uranium series disequilibrium.

1.4 Uranium Series Disequilibria in the Alligator Rivers Region

Several studies of uranium series disequilibria have been undertaken in the Alligator Rivers region, particularly in the vicinity of uranium deposits, to study the movement of radioactive elements. These include studies at Austatom, Nabarlek, Jabiluka, Ranger and Koongarra. Discussion of uranium series disequilibria in rocks from Koongarra is presented in Section 6.

Austatom

The Austatom prospect consists of a secondary uranium mineralisation in fully weathered schist of the Cahill Formation, unconformably overlain by Kombolgie sandstone, and underlain by dolerite. There is limited surface expression of the deposit, which runs to a depth of about 70 m.

Shirvington (1980a,b) found slight depletion of ^{234}U (activity ratio 0.95) in weathered rock containing 730 μg/g uranium. Leaching the sample with 1.6 M HNO_3 yielded $^{234}U/^{238}U$ activity ratios between 0.69-0.42. Shirvington also found that extractants which formed strong complexes with uranium, such as dilute HCl and K_2CO_3, gave higher $^{234}U/^{238}U$ activity ratios than the dilute HNO_3 extracts. This indicates preferential leaching of ^{238}U relative to ^{234}U. Since the less accessible ^{234}U was in a different chemical environment, a chemical fractionation process was suggested, probably in conjunction with a physical mechanism such as α-recoil. Shirvington (1983) later suggested that retardation of ^{234}U relative to ^{238}U only occurred in the presence of smectite and/or illite, and not in the presence of kaolinite only. From this it was suggested that isomorphous substitution into clay crystal lattices was responsible for the different leachabilities of ^{234}U, possibly following α-recoil emplacement of the ^{234}Th nuclide.

Nabarlek

The Nabarlek orebody was located within intensely deformed quartz-chlorite, quartz-mica and chlorite mica schist, in the absence of graphitic or dolomitic units. The uranium mineralisation consisted of pitchblende, with a halo of secondary minerals (Anthony, 1975; Hegge et al., 1980). The top of the orebody had been exposed to weathering, and some leaching of the ore near the surface had apparently taken place.

Shirvington (1980 a,b) studied $^{234}U/^{238}U$ disequilibria in weathered rock from Nabarlek, both in whole rock and in dilute HNO_3 extracts. Above the orebody, and near the surface just down-gradient of the source, bulk $^{234}U/^{238}U$ activity ratios were greater than unity (1.02-1.14). With distance from the source the $^{234}U/^{238}U$ activity ratio decreased, and outside the ore zone also decreased with depth in the weathered zone (minimum value measured 0.95). The 1.6M HNO_3 extracts gave $^{234}U/^{238}U$ activity ratios slightly less than unity (0.88-0.95), which were constant with depth in the dispersion fan.

Airey et al. (1983) measured $^{234}U/^{238}U$, $^{230}Th/^{234}U$ and $^{226}Ra/^{230}Th$ in 32 bulk weathered rock samples. Generally the $^{234}U/^{238}U$ activity ratios were near unity, ranging from 0.80 to 1.15. Samples with $^{234}U/^{238}U$ activity ratios greater than unity were generally from leached zones, such as the near surface. Depositional sites generally had $^{234}U/^{238}U$ activity ratios less than 1. Leaching zones were generally characterised by $^{230}Th/^{234}U$ activity ratios greater than 1 (0.94-2.85) and deposition zones by values less than 1 (0.51 to 1.01). Most leaching zone samples were from within 1 m of the ground surface. Values for $^{226}Ra/^{230}Th$ were very variable, between 0.86 and 1.85, with highest values coming from the shallow leaching zone samples.

Gray (1986) examined disequilibria in samples from within 2 m of the surface in different chemically and magnetically defined phases. High gradient magnetic separation was used to separate iron-rich phases such as iron oxides, from iron poor phases such as clays and quartz. The $^{234}U/^{238}U$ activity ratio in "accessible" phases (defined by extraction with Tamm's acid oxalate reagent (TAO)) were similar in magnetic and non-magnetic phases, and were generally less than unity. Values for the $^{230}Th/^{234}U$ activity ratios in TAO extracts were lower in the magnetically enriched fractions (0.2-1.07) than the non-magnetic fractions (0.76-2.3). This suggests release of uranium, but not of ^{230}Th, from inaccessible sites of the crystalline iron oxides. The $^{234}U/^{238}U$ and $^{230}Th/^{234}U$ activity ratios in citrate dithionite extracts (estimating crystalline iron oxides) were higher than the corresponding TAO extract. Gray postulated that uranium, and particularly thorium, were incorporated into crystalline iron oxides either as occlusions or as lattice substitutes, and this was a partial explanation for disequilibrium, at least between ^{234}U and ^{230}Th.

Groundwaters from the vicinity of the Nabarlek deposit gave $^{234}U/^{238}U$ activity ratios of between 0.76-1.1, with trends of increasing values with decreasing uranium concentration. This further illustrates preferential leaching of ^{238}U from the deposit (Airey et al. 1983, 1985).

Jabiluka

The Jabiluka No. 1 ore deposit is situated in the Cahill Formation, coinciding with an erosional window from which the unconformably overlying Kombolgie sandstone has been removed. The host rock is mainly chlorite and/or graphite schists (Hegge et al., 1980). No surface expression of the deposit has been observed, but weathering to a depth of about 15 m (Airey et al., 1985) has probably intersected the top of the mineralised zone. Mineralisation principally consists of pitchblende, with minor coffinite and brannerite (Hegge et al., 1980). The Jabiluka No. 2 ore deposit, about 300 m from No. 1, is overlain by 20-220 m of sandstone. This has prevented oxidation and weathering of the host schist. Airey et al. (1982) reported bulk rock activity ratios for weathered material from Jabiluka No. 1 of 0.92-1.10 for $^{234}U/^{238}U$ and 0.45-1.72 for $^{230}Th/^{234}U$. The low $^{234}U/^{238}U$ activity ratios were from samples which also gave low $^{230}Th/^{234}U$ activity ratios, suggesting that recently deposited uranium was enriched in ^{238}U.

Unweathered rock from Jabiluka No. 1 (Airey et al., 1982) and Jabiluka No. 2 (Airey et al., 1983; Nightingale, 1988a) gave $^{234}U/^{238}U$ activity ratios of approximately unity, and $^{230}Th/^{234}U$ activity ratios often significantly less than unity (0.68-0.99). This suggests that the processes leading to a preferential leaching of ^{238}U do not occur under unweathered conditions. Groundwaters from Jabiluka No. 2 gave $^{234}U/^{238}U$ activity ratios of 1.17-3.67 which further illustrates a lack of preferential ^{238}U mobility under unweathered conditions.

Nightingale (1988a) examined the variation of activity ratios with distance from the surface of a fracture in unweathered rock. The fracture surface was coated with uranium rich material, probably calcite, containing 7600 μg/g uranium. The $^{234}U/^{238}U$ activity ratio fell sharply from a value of just above unity at the fracture surface, to a minimum of 0.63 about 1 cm into the rock. The ratio then rose to 1.05 about 3 mm further into the rock. Leaching with a mild extractant (1M sodium acetate, pH 5) gave solutions further enriched in ^{234}U. This suggests that ^{234}U is more leachable than ^{238}U, and this is reflected in the groundwater ratios for unweathered rock. The $^{230}Th/^{234}U$ activity ratio was close to unity through the core sample. At the fracture surface, the $^{226}Ra/^{230}Th$ activity ratio was less than unity, but quickly increased with distance to about 6.5 about 0.5 cm into the rock. This suggests that radium is more mobile in the unweathered environment than uranium, and that some ^{226}Ra generated and mobilised within the fracture material had become incorporated in the rock.

Ranger

The two main orebodies at Ranger, No. 1 and No. 3, are separated by about 1500 m of barren rock. Both have been the subject of uranium series disequilibrium studies. The uranium mineralisation at the No. 1 orebody extends to the surface with the top 15-35 m being in the oxidised weathered zone. The primary mineralisation is pitchblende, with minor quantities of brannerite. In the weathered zone, uranium is found as saleeite, sklodowskite, gummite and metatorbernite (Eupene et al., 1975). The No. 3 orebody is similar to No. 1, but with lower concentrations of uranium.

Airey et al. (1983), Lowson et al. (1986) and Short (1988) reported results for bulk and sequential chemical extraction analyses for a series of weathered samples from a drill hole near the No. 1 orebody. Airey et al. (1983), reported bulk disequilibrium results, and found $^{234}U/^{238}U$ activity ratios between 0.68 and 0.99, with the lowest value from near the base of weathering (21 m). $^{230}Th/^{234}U$ activity ratios were generally above unity, except for one sample containing approximately 10 times more uranium than other samples (378 μg/g at 13 m), which gave a value of 0.90. Accessible phases (estimated by TAO extraction) gave values of $^{234}U/^{238}U$ generally below unity, which were similar to those for nearby groundwater (Airey et al., 1982). The lowest $^{234}U/^{238}U$ activity ratios were from samples with the lowest $^{230}Th/^{234}U$ activity ratios. This suggests that recently accumulated uranium contained an excess of ^{238}U.

Airey et al. (1983), Lowson et al. (1986) and Short (1988) suggested that the net transfer of ^{234}U, ^{230}Th and ^{226}Ra to resistate phases against the concentration gradient required a physical driving force such as α-recoil.

Weathered zone samples (to a depth of 11 m) from Ranger orebody No. 3 were studied by Lowson et al. (1992), using selective chemical extractants. Almost all the uranium was present in TAO-extractable and crystalline iron phases. They found that $^{234}U/^{238}U$ activity ratios in TAO-extractable and crystalline iron phases were constant with depth. The data showed an excess of ^{238}U (relative to ^{234}U) in TAO-extractable (accessible) phases in the secondary ore zone, near unity values of $^{239}U/^{238}U$ in crystalline iron phases, and an excess of ^{234}U in resistate phases. The $^{230}Th/^{234}U$ in activity ratios in TAO extracts were generally less than unity, while $^{230}Th/^{234}U$ in crystalline iron oxide phases and resistates were generally above unity. These results again suggest a preferential mobility of ^{238}U compared to ^{234}U, with a daughter enrichment in less accessible phases, such as crystalline iron oxides.

Summary

At all the uranium deposits studied in the Alligator Rivers region, where uranium has been mobilised due to the intersection of weathering with mineralisation, there appears to be a preferential leaching of ^{238}U. Fixation of uranium and daughter nuclides appears to occur in amorphous sites (including sorption sites) and in crystalline iron oxides. Additionally, preferential daughter enrichment in less accessible phases, such as crystalline iron oxides, has been detected.

In unweathered sites, including samples showing recent deposition of uranium ($^{230}Th/^{234}U$ activity ratios <1), no evidence was found for preferential mobility of ^{238}U. This suggests that weathered zone processes are central to the development of this type of disequilibrium, and that a chemical mechanism is at least a component to the preferential mobility of ^{238}U.

2 SAMPLING AND ANALYTICAL TECHNIQUES

Rock and soil samples from Koongarra were collected and analysed to provide information on - the extent of the migration of uranium from the primary orebody; the environments in which the most intense leaching and deposition occur; the relationships between uranium, other elements and minerals present; the forms in which uranium occurs in association with the solid phase; and the nature of the rocks and soils present. The geological setting is described in Volume 2 of this series.

Sampling procedures are discussed in the relevant sections, and a brief description of all the samples analysed during the ARAP is given in Appendix 1. A listing of analyses conducted on each sample and the uranium content where available is also included. The methods used for different analyses are discussed individually, and where appropriate further information is given in the appendices. Figure 2.1 shows in plan view the location of sites from which samples were collected, and Figures 2.2 and 2.4 show cross-sectional views through the orebody.

Three types of holes were drilled to collect samples, inclined diamond drill holes (DDH-series), vertical holes (PH-, C-, M- and W-series), and shallow auger holes (including AD-series). DDH-series holes were drilled at an angle (45°-50° from horizontal, declining toward NW) to facilitate core recovery and intersect strata. DDH-series, PH-series, and some auger holes were drilled prior to the ARAP.

2.1 Uranium Assays

A large number of uranium assays were carried out by Noranda Australia on material from many of the core, bore and auger holes drilled before the commencement of the ARAP (1987) (see also Volume 2 of this series). During the ARAP, a selection of samples from previously collected core and pulp, and material from new sites drilled in 1988 and auger holes drilled in 1991 were also assayed. Sample assays are available from all the holes shown in Figure 2.1; Appendix 1 includes descriptions of samples assayed during the ARAP.

The samples analysed by Noranda Australia were prepared by splitting core and analysing approximately 1.5 m of core or equivalent pulp material. Samples were generally taken for the length of the profile from which material was recoverable. For the auger holes, sampled either by Noranda Australia or the ARAP, subsamples of pulp material were taken about every 30-60 cm. For core and pulp samples from sites drilled in 1988 (W-, M-, and C-series) representative subsamples of about 20 cm of core/pulp were taken every metre. About 50 g of sample was crushed in a tungsten carbide rotary mill, to pass through a 100 BS mesh sieve, then dried at 110°C overnight. All uranium assays were by delayed neutron activation analysis (DNAA) at Ansto, using the reactor MOATA. Contours of uranium concentration were developed using the Surfer contouring package.

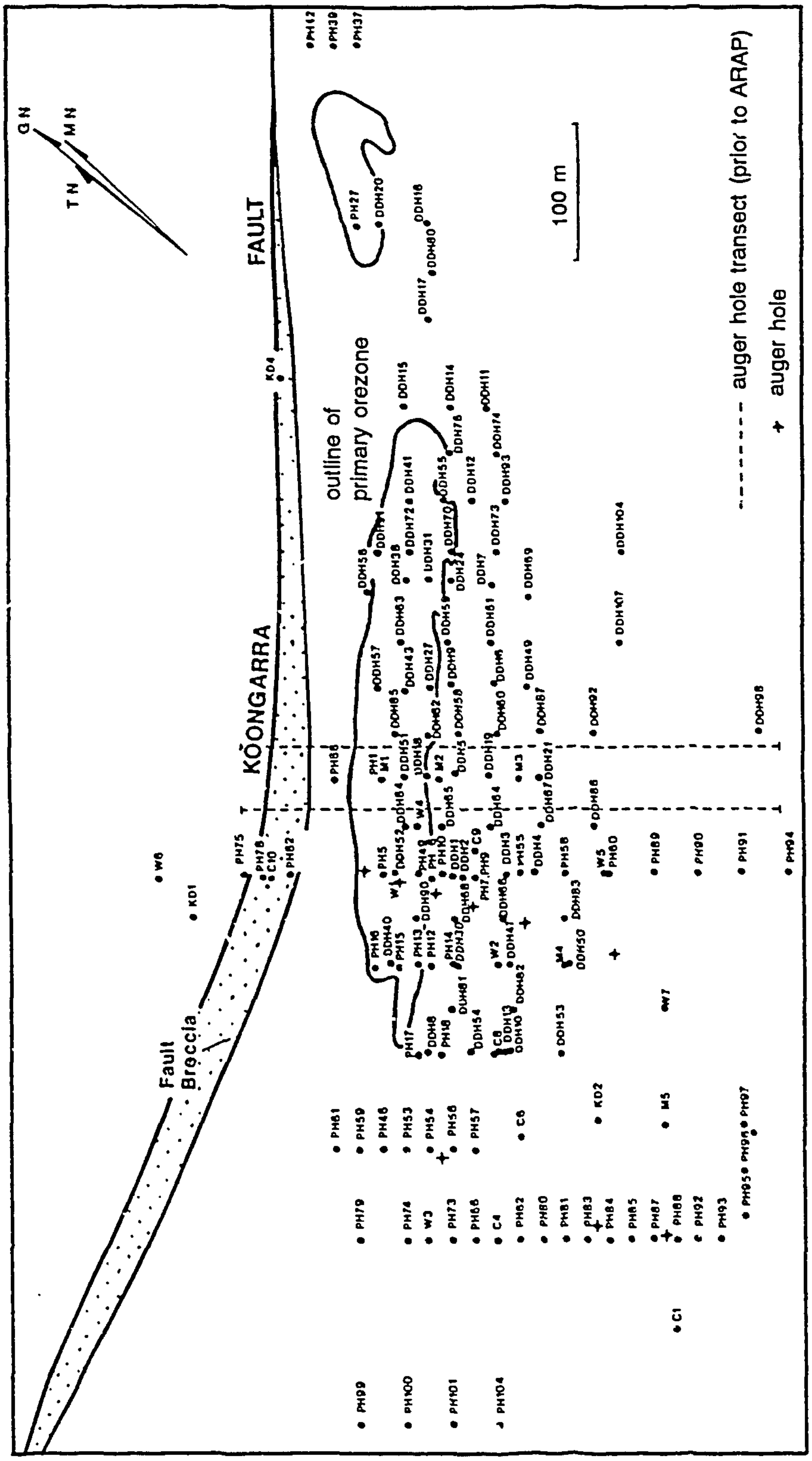

FIGURE 2.1 Location of holes from which samples were collected (plan view)

2.2 Elemental Analyses

Prior to the ARAP, multi-elemental analyses had been reported for many samples by Ferguson and Winer (1980) and Tucker (1975) (see also Volume 2 of this series). The results for samples analysed prior to the ARAP are presented in Appendix 4.3. The samples analysed were mainly unweathered rock.

Elemental concentrations in a selection of samples from the ARAP 1988 drilling were determined using proton induced X-ray and γ-ray emission spectroscopy (PIXE-PIGME), X-ray fluorescence (XRF), and instrumental neutron activation analysis (INAA). Depths of sampling from sites W1, W2, W3, W4, W5, W7, C1, C4, C6, C7, C8 and M4 were chosen to represent shallow (~5 m), mid-weathered (~13 m) and transition (~23 m) zones, and in the case of the C- and M-series profiles, the unweathered (39 m) zone. Elemental concentrations in chemically defined phases were also determined using inductively coupled plasma-mass spectrometry (ICP-MS) and atomic emission spectrometry (AES), in conjunction with the uranium series disequilibria measurements.

A more intensive sampling and analysis program was undertaken for sites M1, M2 and M3. The majority of samples were whole rock, with some subsampling of visibly different zones and of different particle sizes. These sites were chosen to represent three different zones of the site: The leached primary zone (M1); the secondary ore zone (M2) and; a zone of dispersed uranium (M3). Samples from these three sites were also analysed using thin section, mineralogical and radiochemical techniques. Figure 2.2 shows in cross-section the sampling positions in M1, M2 and M3.

2.2.1 PIXE-PIGME

The concentration of many elements in bulk rock were determined using PIXE-PIGME by the Accelerator Applications Group at ANSTO. The samples were crushed to <100 BS mesh size, mixed with graphite spiked with 0.5% ruthenium and pressed into 13 mm diameter pellets. The pellets, together with four reference standards chosen to have similar compositions and stopping powers, were bombarded with 2.6 MeV protons from a 3 MV Van de Graaff accelerator using a target current of ~150 nA, a 3 mm diameter beam spot size and an accumulated charge of 90 μC.

PIGME provided data on the elements Li, F, Na, Mg and Al. PIXE provided information on Si, S, Cl, K, Ca, Ti, V, Cr, Mn, Fe, Co, Ni, Cu, Zn, Ga, As, Se, Br, Rb, Sr, Y, Zr, Nb, Mo, Ba, Pb, Th and U.

Elements from Si upwards were measured using a Si(Li) X-ray detector fitted with a standard pinhole filter consisting of 2 mm thick perspex with a 3.8% hole and a layer of 50 μm Mylar. This tailors the spectrum so that there is a balance between the light elements which are prolific sources of X-rays and the heavy elements which are present in trace amounts. The lighter elements Li, F, Na, Mg and Al were measured simultaneously using a separate Ge(Li) γ-ray detector.

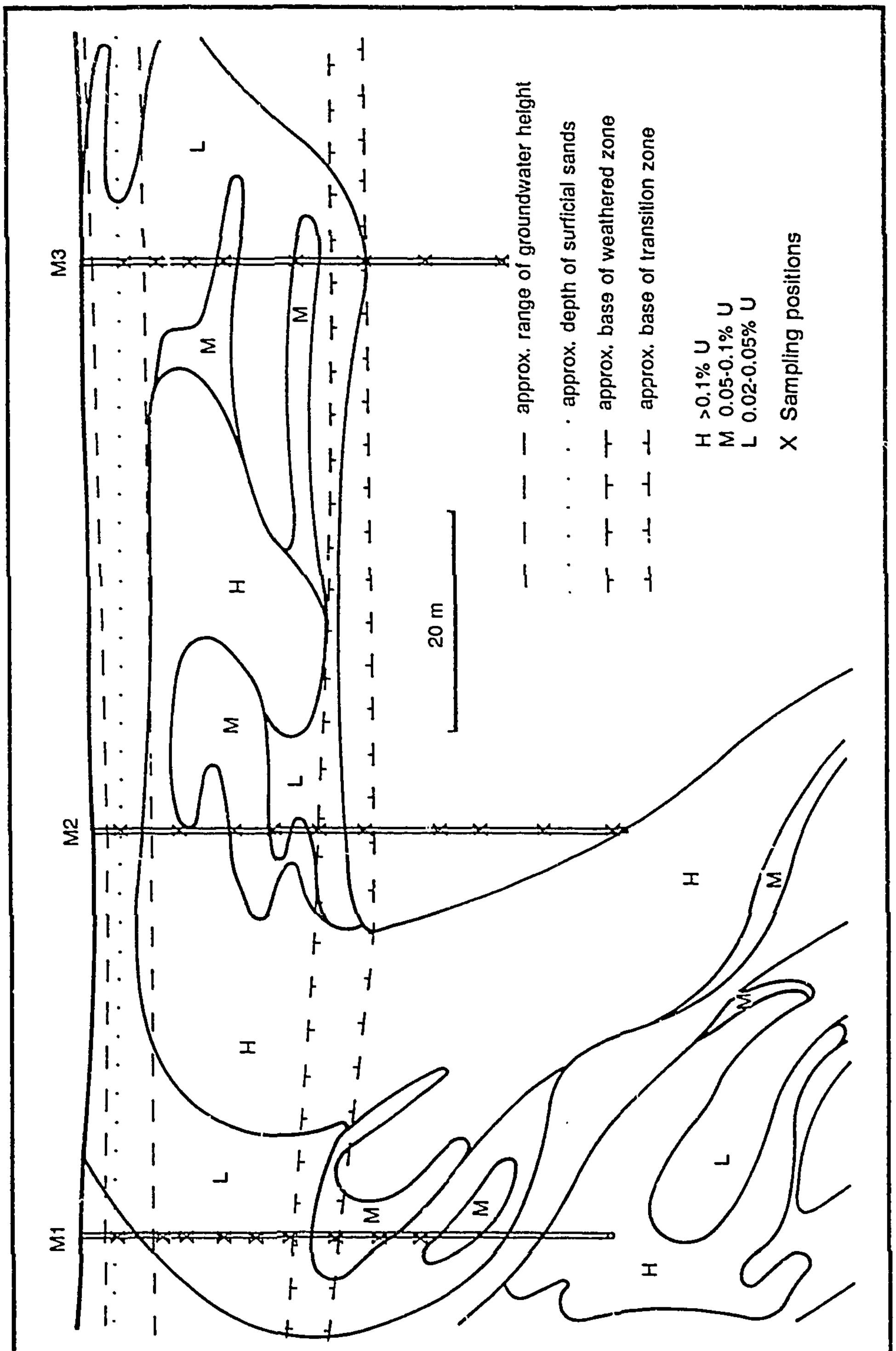

FIGURE 2.2 Section through the orebody showing the locations of samples collected and from holes M1, M2 and M3.

Analysis was carried out using the PIXAN program to determine elemental peak areas. As these samples are mainly soil and rock, an iterative X-ray yield calculation was used to estimate the composition of major elements (assumed present in oxide form) and hence the matrix corrections necessary to estimate concentrations. An initial average matrix concentration of 12% Fe_2O_3, 62% SiO_2, 18% Al_2O_3, 3% K_2O, 2% MgO, 2% TiO_2 and 1% CaO was assumed for all samples. The concentrations obtained for this average matrix were then fine-tuned by iterating for each sample until the matrix concentrations fed into the program became the same as those produced by the program.

Table 2.1 lists the Minimum Detection Limits (MDL) in μg/g for 90 μC runs, and represent a conservative estimate of the detection limit in these types of samples.

Uranium values were obtained by three techniques; PIXE, DNAA and INAA. Figure 2.3 shows a comparison of uranium concentration determined by the three methods.

TABLE 2.1

ELEMENTS AND MINIMUM DETECTION LIMITS (MDL) IN PIXE-PIGME ANALYSIS

Element	MDL (μg/g)	Element	MDL (μg/g)	Element	MDL (μg/g)
PIXE		Co	20	Nb	14
Si	1650	Ni	19	Mo	18
S	200	Cu	4	Pb	22
Cl	100	Zn	3.5	Th	40
K	50	Ga	3.5	U	30
Ca	45	As	2.6	PIGME	
Ti	27	Br	3.2	F	20
V	30	Rb	13	Li	10
Cr	20	Sr	6.5	Na	50
Mn	20	Y	5	Mg	4000
Fe	15	Zr	5.5	Al	4000

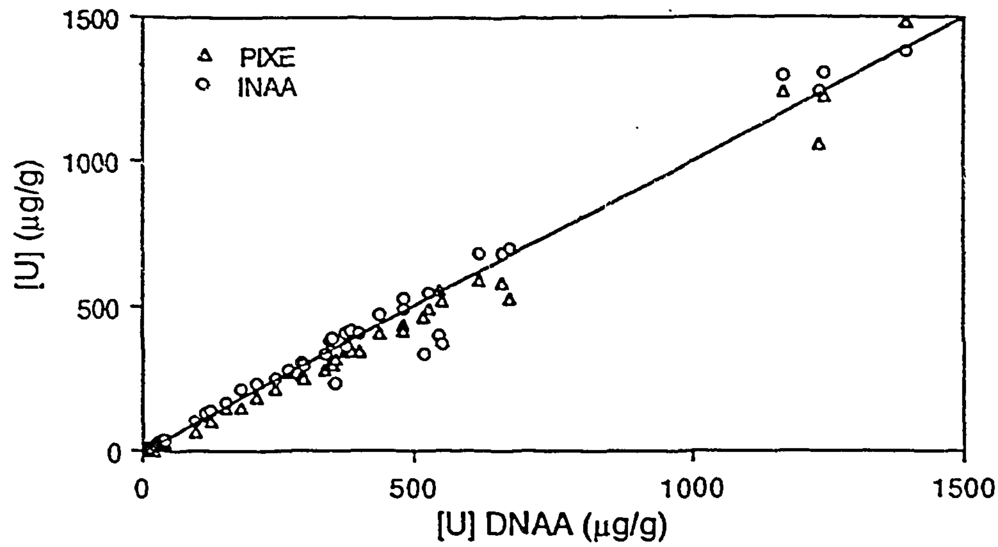

FIGURE 2.3 Uranium concentrations in samples from holes M1, M2 and M3, determined by PIXE, DNAA and INAA

2.2.2 X-ray fluorescence (XRF)

Phosphorus was determined by XRF for the sampies that were analysed using PIXE-PIGME, except when the amount of subsample was too small. Samples were analysed using a Philips PW 145010 X-ray spectrometer, using niobium as an internal standard (9:1 sample:Nb). Three standards (SO1, SO4 and SY2, Canadian Centre for Mineral and Energy Technology) were used to construct a calibration curve between 600 and 1900 μg/g phosphorus, and these gave an r^2 value of 0.998 for a linear calibration passing through the origin.

2.2.3 Instrumental neutron activation analysis (INAA)

The M1, M2 and M3 samples analysed by PIXE-PIGME were also analysed by INAA for the concentrations of rare earth elements and uranium. The analysis, which included corrections for interferences by uranium, were carried out by the Industrial Technology Program, Ansto.

2.2.4 ICP-MS and AES

Sequential chemical extraction schemes were used to determine uranium series disequilibria in different chemically defined phases (see Section 2.5). Some of the extracts were also analysed by ICP-MS and AES to determine concentrations of other elements associated with these phases. The analyses were carried out by the CSIRO Environment Protection Research Group, Lucas Heights.

2.3 Bulk Mineralogical Analyses

2.3.1 X-ray diffraction (XRD)

Samples for random powders were taken from core and pulp samples and dried at 50°C. Random powder XRD was also used to examine samples before and after chemical extraction and density separation. Bulk samples were crushed using a tungsten carbide ring grinder. Random powder diffractograms were also collected for sand fractions (20-45 μm) and clay fractions (<2 μm) from samples from sites M1, M2 and M3. Diffractograms from 2° to 75° 2θ were collected using a Philips PW 1050/70 broad focus diffractometer. Copper (Kα) radiation was used, at 55 kV and 40 mA, with apertures: divergent 1.0°, receiving 0.2 mm, and anti-scatter 1.0°. A monochromator was used to remove K(β) lines. The diffractometer was calibrated using tetradecanol reference standard, St. Austel kaolinite, and highly crystalline mica. Some random powders of samples for bulk elemental analyses were analysed using a Siemens Kristalloflex Diffraktometer system, with scatter, sample and second slits of 1°, focus slit of 0.05° and crystal slit of 0.6°. Cobalt (Kα) radiation was used with 55 kV and 40 mA. Proportions of minerals present were estimated from XRD peak heights and elemental analysis.

The method for treatments of oriented clay films, and interpretation of patterns followed the procedures given in Brindley and Brown (1980). A Philips PW 1050/70 diffractometer was used, with Cu(Kα) radiation. Treatments used included magnesium saturation, potassium saturation, glyceration, and heating to 300 and 550°C.

2.3.2 Mössbauer spectroscopy

A sample used for sorption experiments (W2 14 m, see Volume 13 of this series) was subsampled according to iron oxide banding. It was noticed that the sample was generally red, but bands of clayey material, up to 1 cm thick, ran throughout the core. These bands were white and grey to black, and were flanked by yellow to orange material, up to 1 cm thick, followed by red material which made up the bulk of the sample. The subsamples were analysed using Mössbauer spectroscopy at the Physics Department, Monash University. Procedural details are given in Appendix 2.

2.4 Microscopy

2.4.1 Thin section preparation

Thin sections were prepared of samples from profiles M1, M2, M3, DDH92 and DDH119. The samples were vacuum impregnated with a polyester resin, diluted with acetone, following the procedure of FitzPatrick (1984). The resin polymerisation was triggered by gamma irradiation (about 7.5 kGy) in a gamma irradiation pond at ANSTO, Lucas Heights; thin sections, of size 26 mm × 46 mm × 25 μm and 100 mm × 65 mm × 25 μm, were prepared, using aluminium oxide powders and wet and dry papers of grades 360-1200 for grinding, and tin oxide powder for polishing. Samples were fixed to glass slides using Araldite or Loctite UV cure resin. Thin sections were examined with plane and cross polarised transmitted light, and reflected light. See Figure 2.2 for the location of samples from the M-series profiles. To avoid heavy metal contamination, no catalyst was added.

2.4.2 Scanning electron microscopy (SEM)

Thin section samples were cleaned by ultrasonification with freon for about 10 minutes. They were then mounted onto aluminium stubs and coated with about 300 nm of evaporated carbon. A Philips 505 scanning electron microscope was used in conjunction with an EDAX PV9900 EDS system. The SEM was operated at an accelerating voltage of 20 keV, and a spot size of 20 or 50 nm. Secondary electron images and single element maps were collected. EDS spectra of spot analyses were collected over 100 seconds.

2.4.3 Electron microprobe

Thin section samples were examined using an ETEC Siemens Autoprobe electron microprobe. Wavelength dispersive spectrometry (WDS) was used for quantitative analysis of selected elements, while EDS was used for full spectral checks. Spot analyses were done on areas and features of interest, including fracture filling chlorites, matrix chlorites, fissure coatings, uranium minerals and areas of high α-activity. Analyses were corrected for matrix effects (atomic number, absorption and fluorescence) using a standard routine. The spatial associations of elements was determined from X-ray maps.

The probe was operated at 14.2 keV with a spot size of 50 nm, and was calibrated for Na, Mg, Al, Si, P, S, K, Ca, Ti, Mn, Fe, Ce, Pb and U. Qualitative EDS was used to ensure all elements detectable were analysed. Line scans for uranium and iron were made across fractures and uranium minerals and backscattered electron images were collected from analysed areas.

2.4.4 Transmission electron microscopy (TEM)

Manganese-rich areas were hand picked from the M2 10 m sample. The subsamples were ground and examined by electron diffraction and EDS, using a Philips EM430 300 kV TEM, with an EDAX X-ray detector and TN 5500 MCA. TEM was also used to compare samples before and after phase selective chemical extraction.

2.4.5 Alpha-track autoradiography

α-Track autoradiographs were prepared for all the thin section samples. CR39 and Tastrak plastic film was used as the solid state nuclear track detectors. The film was placed flat against the cleaned polished surface of a thin section, and left in contact for exposure times of 2 to 672 hours. After exposure, the film was etched in 6.25M NaOH for 6 hours at 75°C, as described by Ellis and Wall (1982). For analysis, the etched film was placed over the thin section and the α-tracks were aligned with features of similar shape. The autoradiograph and thin section were examined simultaneously with a petrological or mineralogical microscope.

Changes in α-track density were studied with distance from fissures and veins. A graticule with a 10×10 grid was placed in the microscope eye piece; each grid square at $40\times$ magnification was 25×25 μm, and at $10\times$ magnification, 100×100 μm. One row of squares was placed next to and parallel to a feature and the number of tracks in each grid square was recorded. Usually about ten grids were analysed along each feature.

2.5 Uranium Series Disequilibria

Disequilibria between uranium series isotopes was determined in whole rock samples, in chemically defined phases of weathered rock, and in individual crystals of secondary uranium minerals. Chemical extractants were used to investigate the degree of disequilibria in mineral phases with different accessibility of contained uranium to groundwater. Figure 2.4 shows in cross section the holes and positions from which some of the samples were analysed (see Figure 2.1 for position of holes in plan view), and the sample descriptions are included in Appendix 1. Twenty-five five stage sequential extractions, 93 two stage extractions, 17 secondary uranium mineral (saleeite) analyses and 102 bulk rock analyses, were conducted on 125 samples from 32 sites (drill holes).

2.5.1 Sequential extraction schemes

The use of selective chemical extractions in geochemistry and soil science is reviewed in Appendix 3. The aim of such schemes is to utilise a series of reagents, in order of increasing aggressiveness, to dissolve particular phase types in order of decreasing accessibility to water. Here a brief description of the scheme used in this study is given.

Selection of extraction reagents

Five chemical reagents were selected to dissolve particular phases of interest in weathered rock from Koongarra. These reagents were chosen on the basis of the minerals present in the rock, and the geochemical significance of phases with respect to the mobility of uranium. The uranium concentrations and the major minerals in the rock samples studied by a five stage extraction procedure, are given in Table 2.2.

Quartz, mica, zeolite, clay minerals (smectite, vermiculite and kaolinite), iron minerals (hematite and goethite), titanium minerals (anatase and rutile) and uranium minerals (pitchblende and sklodowskite) are the major mineral components of these samples. Uranium minerals, such as saleeite, autunite and torbernite, and iron minerals, such as pyrite, limonite and chalcopyrite, are common at Koongarra. Consequently an extraction procedure was selected for adsorbed species, amorphous iron phases, crystalline iron phases, clays and remaining resistant phases such as quartz. The effects of these extractions on the mineral components of the rock were checked using XRD, TEM, and chemical analyses of the extracts.

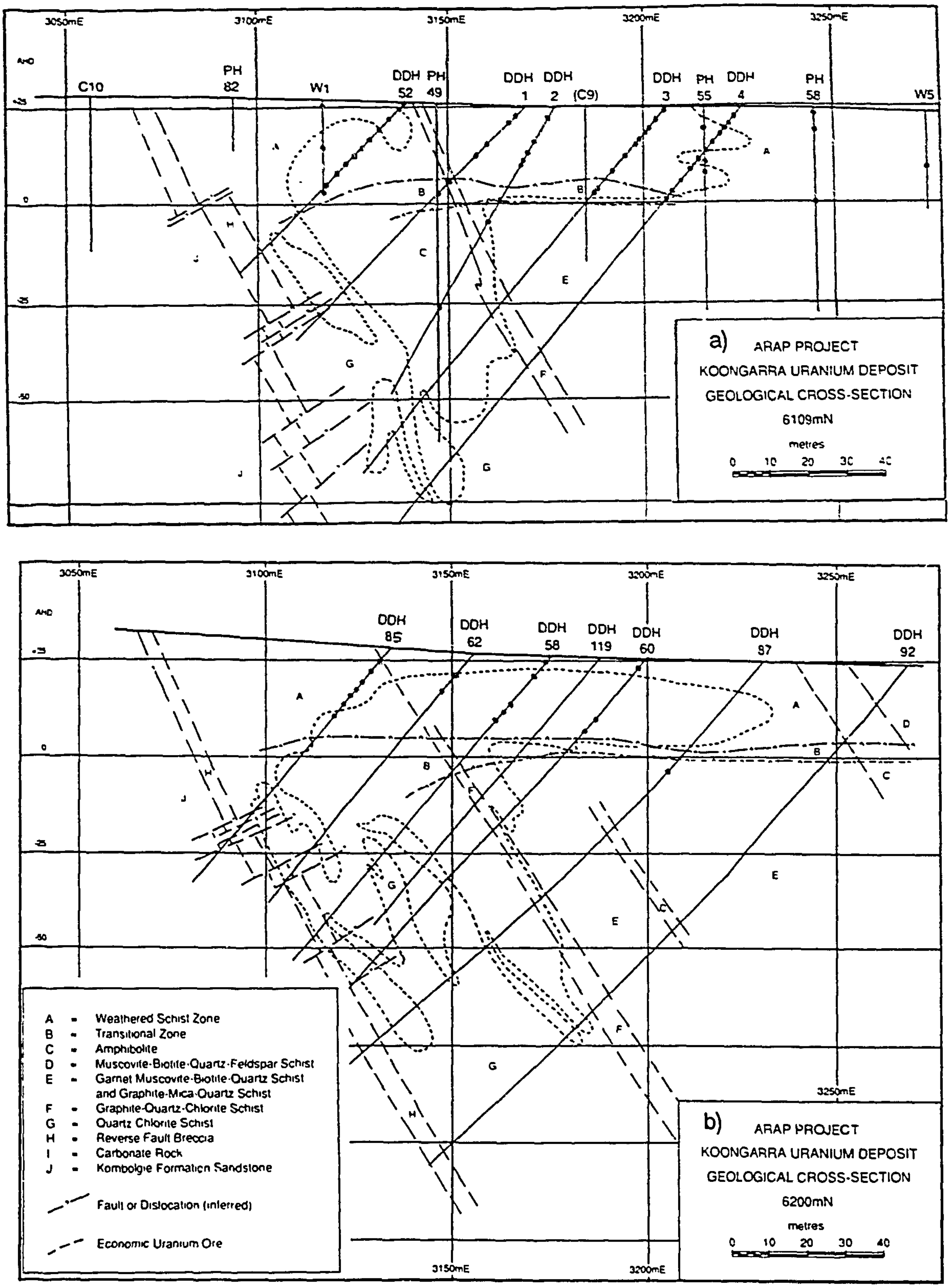

FIGURE 2.4 Location of the sampling sites for uranium series studies from two transects. a) transect DDH52-PH94 and b) transect DDH85-DDH87

TABLE 2.2

URANIUM CONCENTRATION AND MAJOR MINERALS IN SAMPLES STUDIED BY FIVE STAGE SEQUENTIAL EXTRACTION

Drill hole	Depth (m)	[U] (μg/g)	Major minerals
DDH1	4.7	2271	hematite, goethite, kaolinite and quartz
DDH1	19.4-20.5	82300	sklodowskite, chlorite, kaolinite, vermiculite, mica, zeolite and quartz
DDH2	33.0-34.3	82500	pitchblende, kaolinite, smectite, vermiculite, mica, zeolite and quartz
DDH3	10.5-11.7	769	goethite, kaolinite, vermiculite and quartz
DDH3	16.3-17.5	965	goethite, vermiculite, mica and quartz
DDH4	14-15.2	536	goethite, kaolinite, vermiculite, anatase and quartz
DDH54	13.5-15	963	goethite, kaolinite, vermiculite and quartz
PH55	18.3-19.8	316	goethite, kaolinite, vermiculite and quartz
PH56	13.5-15	323	goethite, chlorite, vermiculite, mica and quartz
DDH58	9.12	1700	goethite, kaolinite, mica and quartz
DDH58	18.2	4620	kaolinite, mica, zeolite and quartz
DDH58	21.2	1090	chlorite, mica, zeolite and quartz
DDH58	24.3	726	chlorite, mica, zeolite and quartz
DDH87	24.3	61.4	chlorite, zeolite, rutile and quartz
DDH85	6.07	44.6	vermiculite, chlorite, mica and quartz
DDH85	9.12	377	goethite, hematite, kaolinite and quartz
DDH85	15.2	186	goethite, vermiculite, kaolinite, mica and quartz
DDH85	21.2	443	hematite, vermiculite, kaolinite, mica and quartz
DDH62	9.12	605	hematite, kaolinite, mica and quartz
DDH62	15.2	5907	hematite, kaolinite, mica and quartz

Table 2.3 gives the different target phases and procedure for each extraction.

TABLE 2.3

SUMMARY OF SEQUENTIAL EXTRACTION PROCEDURE

Reagent	Minerals dissolved	Extraction conditions
1) Morgan's solution 1M NaOAc adjusted to pH 5.0 with HOAc	Carbonate minerals, adsorbed trace elements	40 mL/g sample, shaken for 4 hours
2) Tamm's acid oxalate (TAO) 10.9 g/L Oxalic acid + 16.1 g/L Ammonium oxalate pH 3.0	Adsorbed trace elements, amorphous minerals of Fe, Al and Si (eg. ferrihydrite), secondary uranium minerals	40 mL/g sample, shaken in the dark for 4 hours
3) Citrate dithionite bicarbonate (CDB) 0.3M Tri-sodium citrate 0.2M Sodium hydrogen carbonate 1 g/g sample Sodium dithionite, pH 8.5	Crystalline iron oxides, hydroxides and oxy-hydroxides	60 mL/g sample, stirred for 30 min. at 85 °C, filtered and repeated
4) 6M HCl	Clay minerals (vermiculite, smectite, kaolinite), uranium oxides	Stirred for 2 hours at 85 °C
5) Digestion (and fusion)	Remaining resistant minerals (quartz, muscovite)	$HF/HClO_4$ digestion, sodium carbonate/borax fusion

Sequential extraction procedure

Approximately 50 g of rock was crushed in a tungsten carbide ring mill, with about 1 g of crushed rock being sequentially treated with the extraction solutions. At the end of each extraction step, the suspended material and the solution were separated by centrifugation followed by filtration through 0.45 μm filters. The residue was washed with 10 mL of the extractant solution and filtered, then washed with 10 mL of distilled water and filtered, combining the filtrates. The combined residue was dried in a desiccator to constant mass and weighed. Some of the residues were then examined by XRD analysis to determine the constituent residual minerals, and the effect of the extraction. The residues were then treated with the next extraction solution. Details of the target phases and the steps in the five stage extraction procedure are given below. A discussion of the phases removed from the samples by the procedure is included in Section 6.2.

Fraction 1. Adsorbed species and carbonate minerals.

The sample was shaken with 40 mL of Morgan's solution (1M sodium acetate, adjusted to pH 5.0 with acetic acid, Morgan (1935))

Fraction 2. Amorphous phases of iron (including ferrihydrite), aluminium and silicon, and secondary uranium minerals

The residue of Fraction 1 was shaken with 40 mL of Tamm's acid oxalate (TAO; 10.9 g/L oxalic acid + 16.1 g/L ammonium oxalate, buffering at pH 3.0, in the dark at ambient temperature for 4 hours (Tamm 1922, 1934, modified by McKeague and Day, 1966). The TAO-extractable fraction is approximately that fraction which is amorphous, and accessible to interaction with the groundwater.

Fraction 3. Crystalline iron oxides

The residue from Fraction 2 was stirred with 40 mL CDB solution (1 g sodium dithionite and 60 mL of 0.3 M trisodium citrate + 0.2 M sodium hydrogen carbonate) at 85 °C for 30 minutes, and repeated once (Coffin, 1961). The first and second extracts were combined, and refluxed with aqua-regia until the solution became transparent. This was required to avoid precipitation of sulfides.

Fraction 4. Clay and some refractory minerals

The residue from stage 3 was stirred with 60 mL of 6 M HCl at 85°C for 2 hours. This stage was aimed at dissolving clay minerals and contained species.

Fraction 5. All remaining resistant minerals

The residue from stage 4 was heated to dryness with 5 mL perchloric acid and 25 mL hydrofluoric acid in a platinum crucible. The sample was fused with sodium carbonate (1 g/g sample) and sodium tetraborate (2 g/g sample). The residue was then dissolved in 6 M HCl.

The uranium, thorium and sometimes radium in the extraction solutions were then purified using the anion exchange method for chemical separation. Lead-210 was analysed using gamma spectrometry.

A number of samples were analysed using only a two stage extraction scheme, which included a TAO extraction followed by total dissolution of the residue. The TAO extraction procedure was used to estimate of amounts of radionuclides accessible to, and potentially in equilibrium with the groundwater. Multi-phase extraction results were also converted to two phase extraction data by combining Morgans and TAO extractions for TAO-extractable (accessible), and CDB, HCl and fusion fractions for residual (inaccessible).

2.5.2 Whole rock and single crystal digestions

The analysis of uranium minerals was conducted after total dissolution by hydrofluoric and perchloric acids. Saleeite crystals from DDH52, DDH84, DDH65 and DDH64 were analysed. For bulk rock samples where greater than about 0.1 g was required, a carbonate/borax fusion was included after the acid digestion.

Saleeite crystals from DDH65 27 m and DDH84 22 m were sequentially leached in 0.1M, 1M and 6M HCl to dissolve the crystals from the outside to the centre. The samples used appeared to be single crystals. The crystals were placed on 0.45 µm membrane filters set in filtration units; and immersed in HCl for the required period (1 to 30 minutes). The solution was then removed and the crystal washed with distilled water. The procedure was repeated until the crystal was fully dissolved.

2.5.3 Alpha spectrometry

The majority of the analyses of ^{238}U, ^{235}U, ^{234}U, ^{232}Th, ^{230}Th, ^{235}U and ^{226}Ra were by alpha spectrometry. After the sample was extracted or dissolved, the resulting solution was converted to a 6-9 M solution of HCl. Most of the samples were prepared using the anion exchange method. Yield tracers were added prior to chemical separation steps; ^{236}U or ^{232}U were used for uranium determinations, ^{229}Th for thorium and ^{133}Ba for radium.

a) Solvent extraction method

A method slightly modified from that of Sill (1977) was used. The flow scheme of this chemical separation procedure is shown in Figure 2.5. Thorium was co-precipitated from the HCl solution with barium sulfate. The uranium and thorium were purified using solvent extraction with the amine solution Aliquat-336. The uranium and thorium were back extracted from the organic phase, dissolved in an electrolyte solution and electroplated onto a stainless steel planchette. The activities of each radionuclide were measured by alpha spectrometry, using a silicon surface barrier detector, installed in an Ortec 676A Alpha-King spectrometer, with a Canberra 85 multi-channel analyser (MCA) for data processing.

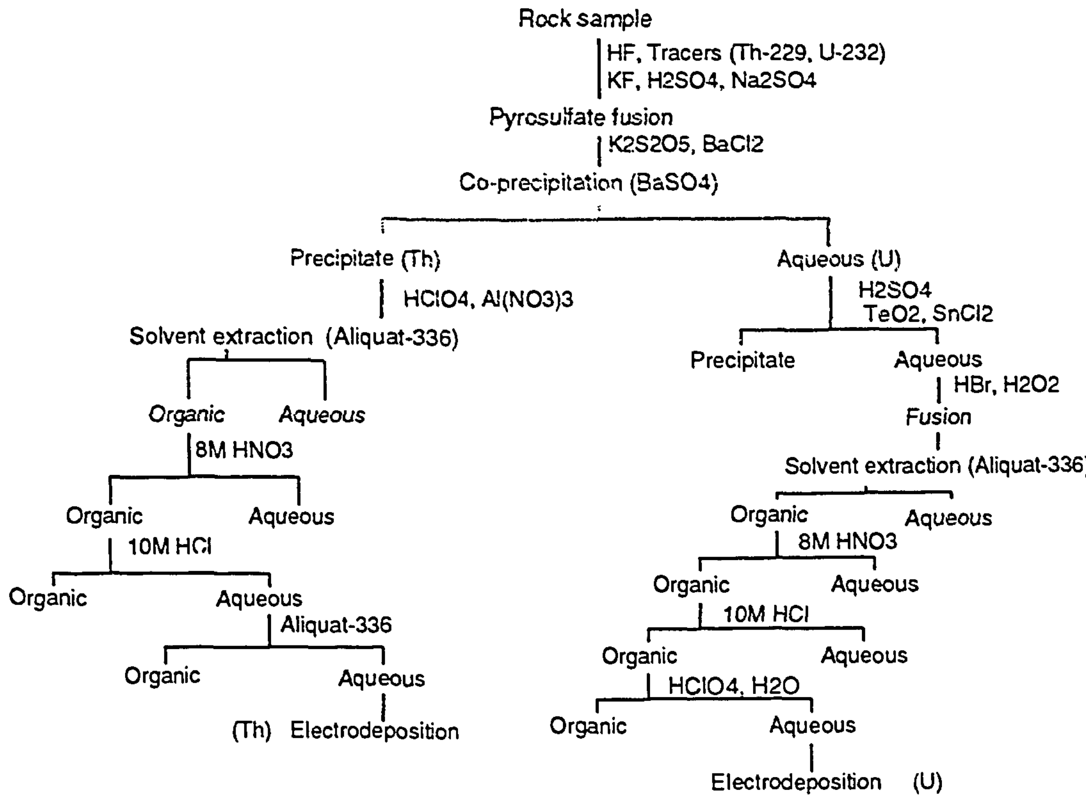

FIGURE 2.5 Flow scheme of chemical separation for uranium and thorium using a solvent extraction method.

b) Anion exchange method

A chemical separation method modified from Airey et al. (1982) was used with the flow scheme shown in Figure 2.6. Uranium isotopes and iron were separated from a 6M HCl solution using a chloride-form anion exchange resin (AG1X8). Iron and uranium were separated using solvent extraction. Thorium isotopes were separated from a 8M HNO_3 solution using nitrate-form resin. Electrodeposition and counting was as described above, with additional Ortec 576 and Canberra Quad spectrometers, and data processing using Canberra MCAs and MCA emulation software (Maestro II). The analysis of ^{226}Ra by alpha spectrometry involved co-precipitation of radium (and ^{133}Ba) with barium sulfate. The activity of ^{226}Ra was determined by alpha spectrometry, and the yield tracer ^{133}Ba was determined by gamma spectrometry.

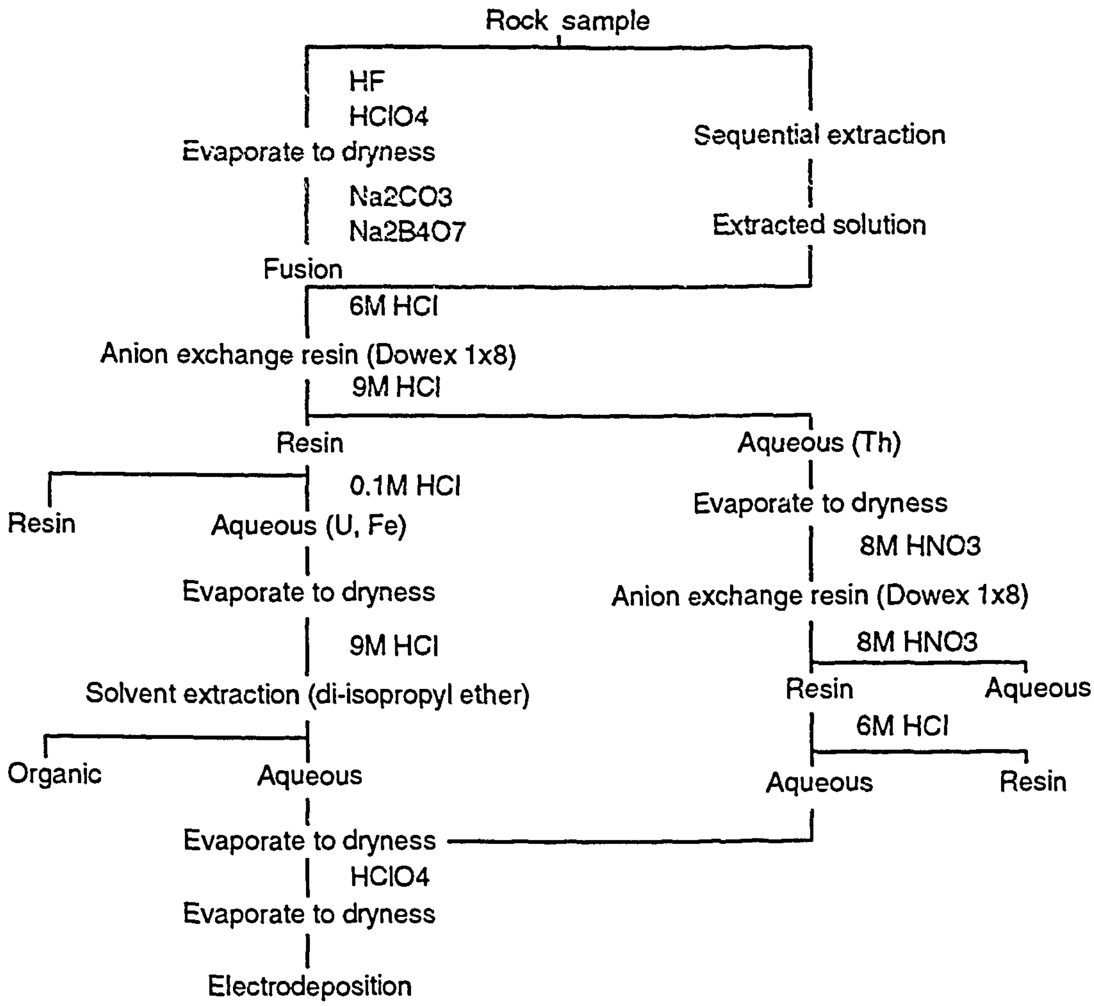

FIGURE 2.6 Flow scheme of chemical separation for uranium and thorium using an anion exchange procedure.

2.5.4 Gamma spectrometry

Ortec planar type and LO-AX germanium detectors were used for low energy gamma-ray determination in 2 and 10 gram samples respectively. The peaks used for the concentration determination were ^{231}Pa (27.5 keV), ^{210}Pb (46.5 keV), ^{234}Th (for ^{238}U) (63.0 keV), ^{230}Th (67.7 keV), ^{235}U (163.3 keV), ^{214}Bi (for ^{226}Ra) (609 keV), ^{228}Ac (for ^{228}Ra) (338 keV) and ^{40}K (1462 keV). Figure 2.7 shows an example of the gamma-ray spectrum for the sample from DDH62 15.2 m.

Samples from PH73 13.5-15 and 18.0-19.5 m were sieved to obtain five fractions: <105, 105-250, 250-500, 500-1000 and 1000-2000 μm. Each fraction was separately analysed by gamma spectrometry.

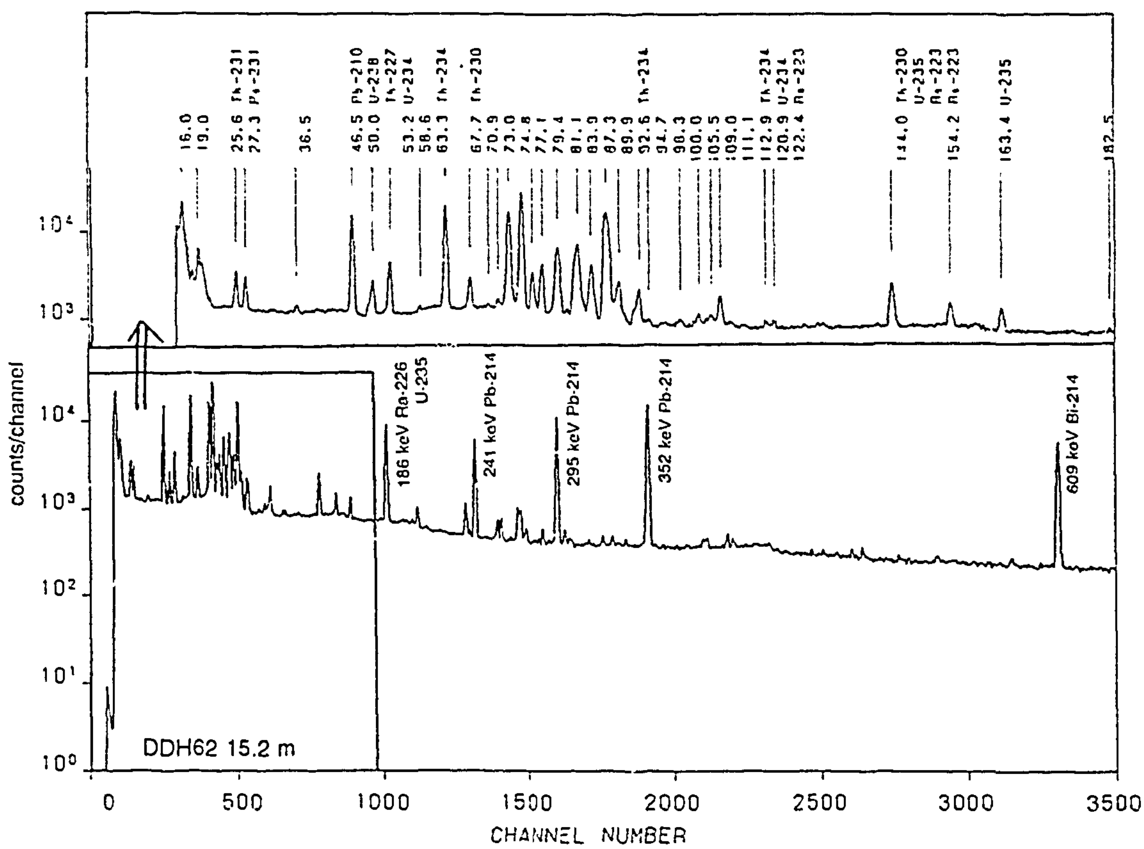

FIGURE 2.7 Typical gamma-ray spectrum showing peak identification

3 BULK MINERALOGY AT KOONGARRA

The nature and distribution of the host rock minerals at Koongarra have been discussed by Ewers and Ferguson (1980); Foy and Pedersen (1975); Pedersen (1978); Snelling (1980a, 1980b) and Tucker (1975), all of whom concentrated principally on the unweathered schist, and by Gray (1986), who included some discussion of the weathered zone components. Mineral studies are also presented in Volumes 2 and 9 of this series.

3.1 Unweathered Rock Components

The unweathered rock in the vicinity of the deposit can be divided into five major rock series;

1 The low uranium Kombolgie Formation sandstone and conglomerate;

2 The quartz chlorite schist, with siliceous bands and containing the ore, extending about 50 m from the sandstone;

3 A graphitic quartz chlorite hanging wall unit, approximately 5 m thick containing pyritic and graphitic chlorite quartz breccia, which defines the south-east boundary of the primary ore;

4 Quartz muscovite chlorite schist, with garnetiferous, pyritic, and graphitic sections, and possibly some amphibolite. This extends for about 100 m from the graphitic hanging wall unit;

5 Quartz muscovite, biotite and feldspar schists, with occasional amphibolite.

These rock units are also discussed in Volume 2 of this series, where the relative abundance of minerals in the three main series schists are tabulated. A distinctive primary hydrothermal alteration halo has been observed around the mineralisation at Koongarra, and an inner and an outer halo have been identified. The inner alteration halo contains the primary uranium mineralisation, and extends up to 50 m from the ore. Further details about the hydrothermal alteration are given in Volume 2 of this series.

Quartz occurs as the principal mineral of the sandstone, as a general schist component, as veins through the schist, as the principle component of the surficial sands, and as a gravel component throughout soil profiles.

Chlorite is the only major rock forming mineral, apart from quartz, common to all the Alligator Rivers region uranium deposits (Ewers and Ferguson, 1980). It occurs throughout the unweathered rock at Koongarra as replacement of biotite and as cementing and fracture filling material. Pervasive chloritisation occurred to about 130 m from the Koongarra reverse fault (Snelling, 1989), with the most intense chloritisation occurring in the primary mineralised zone. With increasing alteration, chlorite was found replacing biotite, garnet, hornblende, feldspars, and even muscovite (Snelling 1980a).

Many studies have been made on the composition of chlorites at Koongarra, mainly utilising microprobe analysis of individual grains (see Volume 2 of this series); Ewers and Ferguson, 1980; Gray, 1986; Edis, 1991; (Volume 9 of this series). These studies showed that two main types of chlorite make up the schist, fine grained magnesium-rich chlorite (groundmass chlorite) containing little iron, and a coarser grained chlorite containing much more iron. In Volume 9 the two types of chlorite have been characterised for drill holes DDH3 and DDH4. The average cell formulae for the two types are:-

iron-rich: $(Mg_{2.24}Fe_{2.61}Al_{1.14})(Si_{2.89}Al_{1.11})O_{10}(OH)_8$

magnesium-rich: $(Mg_{3.40}Fe_{1.12}Al_{1.28})(Si_{3.00}Al_{1.00})O_{10}(OH)_8$

The iron-rich chlorite grains were tens to hundreds of microns wide, while the magnesium-rich chlorites were less than 10 μm. The atom ratio of magnesium to iron in the two forms can be used as a guide to their relative proportion in bulk samples. In the iron-rich form, the average atom ratio Mg/Fe is 0.86, and for the magnesium-rich form it is 3.04.

The atom ratio of Mg/Fe has been determined from the bulk elemental analysis of many samples in which chlorite was a principle component (data from Appendix 4). Corrections were made for pyrite in the samples (it was assumed that all sulfur in the samples was present as pyrite (FeS_2)), and the potassium analysis was noted for consideration of a major iron contribution by biotite. It was then assumed that all remaining iron and magnesium was present as chlorite; where there was evidence that other minerals may be making a significant contribution to the iron or magnesium content of the rock, the analyses were not used.

From this analysis, it appears that north of the graphitic hanging wall unit, in or near the primary ore zone and within the inner halo of alteration, magnesium rich chlorite is dominant. However, south of the graphitic hanging wall unit, down-gradient of the primary ore zone, the more iron-rich form is dominant.

Generally, fracture/breccia filling chlorite is magnesium- and aluminium-rich, similar to the groundmass chlorite. Ewers and Ferguson (1980) observed that the Fe^{2+}/Fe^{3+} ratio of chlorite appears to decrease with increasing uranium content of the rock, and that chlorite from Koongarra tends to be more iron-rich than that from other deposits. The most iron-rich chlorites at Koongarra were adjacent to pyrite grains, and the most magnesium rich were adjacent to uraninite (Snelling, 1980a). The types of chlorite present have been described in terms of Hey (1954) taxonomy as from iron-rich ripidolite to pycnochlorite (Snelling, 1980a), and from chlinochlore (IIb) (Gray, 1986) to penninite (Snelling, 1980a). Differences in type and structure of chlorite may reflect conditions during ore genesis, or the degree of hydrothermal alteration; and may give rise to a range of weathering products with differing potential for interaction with uranium.

Muscovite is present (in varying amounts) throughout the unweathered and weathered schist units at Koongarra, but is especially abundant SE of the graphitic hanging wall unit. The form of the muscovite is likely to be 2M1 (Gray, 1986). Fine white mica (sericite) is also present and may occur as an alteration product of K-feldspars (Ewers and Ferguson, 1980).

Small amounts of biotite remain unchloritised, particularly outside of the quartz chlorite schist, SE of the graphitic hanging wall unit. Some stacking disorders in chlorite observed in some chlorite grains probably result from incomplete chloritisation of the biotite; remnants of which persist as stacking faults (Murakami and Isobe, 1990). Foy and Pedersen (1975) reported the presence of feldspar in several drill cores, particularly south of the graphitic hanging wall unit, and noted the presence of partially to completely chloritised hornblende. Garnet was observed to be either completely chloritised or surrounded by an outer layer of chlorite (Snelling, 1980a), and also occurred SE of the graphitic hanging wall.

Dolomite is intersected S and NE of the mineralised zone in unweathered rock (see Volume 4 of this series). Some of the siliceous units nearer to the ore body may represent silicified carbonates (Ewers and Ferguson, 1980).

Graphite is not confined to any one of the mine series schist units, but is by far most abundant in the graphitic quartz chlorite schist hanging wall unit. The graphite forms thin films along the foliation and shear planes, often accompanied by pyrite, chalcopyrite and galena. The graphite persists into the weathered zone without the sulfides, and from the results of stable isotope studies it was postulated that the graphite is of a biogenic origin (Donelly and Ferguson, 1980).

Intense and pervasive hematitic alteration is frequently present in the ore zone schist near the Koongarra reverse fault, often resulting in colouration of the whole rock. Hematite also occurs as a result of weathering, and often occurs where secondary uranium minerals were formed from in situ alteration of uraninite.

Apatite was found in the unweathered quartz chlorite schist, in quantities of up to 2% of the rock (Pedersen, 1978) and is the only phosphate mineral identified in the unweathered rock. Phosphorus was correlated with calcium in unweathered samples, further illustrating the occurrence of phosphorus as apatite. However, there was insufficient calcium to account for all the phosphorus as apatite in some samples from within the inner halo of alteration (see Section 4.1, phosphorus). Apatite is possibly present as inclusions in chlorite and pyrite grains, and is the likely source of phosphorus for the formation of uranyl phosphate minerals and complexes. Analyses of apatite grains are given in Table 3.1; the major form of apatite is likely to be fluorapatite. An as yet unidentified phase containing phosphorus, aluminium, and rare earth elements has been found from within the primary ore zone (A. Komninou, Pers. Comm., 1992). This phase may be related to florencite.

TABLE 3.1

ANALYSIS OF APATITES FROM WITHIN THE INNER ALTERATION HALO
(analyst: A. Komninou)

	Apatite 1		Apatite 2		Apatite 3	
	Weight %	Atoms per 12 oxygens	Weight %	Atoms per 12 oxygens	Weight %	Atoms per 12 oxygens
SiO_2	0.77	0.064	0.37	0.031	0.02	0.002
Al_2O_3	0.99	0.097	0.15	0.015	0.07	0.007
FeO	0.12	0.008	0.21	0.015	0.08	0.006
MnO	0.15	0.011	0.25	0.018	0.05	0.004
MgO	0.06	0.007	0.05	0.006	0.02	0.002
CaO	53.78	4.800	53.66	4.804	56.20	5.014
K_2O	0.04	0.004	0.01	0.001	0.00	0.000
SO_4	0.01	0.002	0.01	0.002	0.00	0.000
P_2O_5	41.93	2.957	42.79	3.027	42.34	2.985
F	2.81	0.740	3.24	0.856	2.47	0.650
Cl	0.00	0.000	0.02	0.003	0.01	0.001
Total	100.66		100.76		101.25	
O=F,Cl	1.18		1.37		1.04	
Total	99.48		99.39		100.21	
F/(F+OH)		0.740		0.858		0.650

Apatite grain 1: DDH4 44.5 m, in groundmass chlorite (30 μm diameter)
Apatite grain 2: DDH4 44.5 m, inside a quartz grain (30 μm diameter)
Apatite grain 3: DDH4 32 7 m, from a quartz vein (300 μm diameter)

The distribution of apatite and phosphorus throughout the schist units suggests that it is of primary metamorphic origin. However, the presence of apatite occluded in pyrite grains suggests a superimposed hydrothermal generation of apatite, which, although not significantly increasing the amount of phosphorus present, may affect the distribution of uranyl phosphates.

Traces of magnetite were found in the quartz chlorite schist (Snelling, 1980a). Sulfides were found in trace amounts in most unweathered rock units of the site, but are particularly abundant in and near the graphitic hanging wall unit (Snelling, 1980a). Sulfides detected included pyrite (FeS_2), chalcopyrite [$(CuFe)S_2$] and, near the primary ore zone, galena (PbS). Sulfides were probably important in the regulation of redox conditions of the system, and possibly led to the development of a redox barrier for uranium when in high concentrations.

3.2 Weathered Zone Components

Weathering of the schist appears to have occurred to a depth of approximately 25-30 m over the site. Near the reverse fault the weathered zone extends down to about 50 m. This greater depth of weathering near the fault may be a result of interactions with oxidising groundwater crossing the fault from the sandstone, or may be related to the oxidation of graphite causing more intense weathering conditions in this area.

Vermiculite, probably the major initial weathering product of chlorite, occurs at the base of weathering in the transition zone, in a band up to 5 m thick, grading from unweathered chlorite to fully kaolinised vermiculite at approximately 25-30 m depth (see Volume 9 of this series).

Kaolinite is the dominant clay mineral in the weathered zone, resulting from the weathering of vermiculite, residual biotite, garnet, feldspar, smectite (Gray, 1986; see also Volume 9 of this series), and possibly directly from the weathering of chlorite (Volume 12). Above the primary ore zone it was the only secondary clay mineral detected.

Smectite was identified in various amounts throughout the weathered zone, and may have been formed from the weathering of vermiculite (Murakami et al., 1990), or directly from the weathering of chlorite (Gray, 1986). Montmorillonite and biedellite were identified by Gray (1986). Very little smectite has been found above the primary mineralised zone, and the amount appears to increase with distance down-gradient. Smectite appears to most abundant above the feldspathic schists, which begin near the tip of the dispersion fan. The smectite abundance appears to be reflected by the concentrations of magnesium in the weathered zone (see Section 4).

Muscovite appears to be very resistant to weathering, and in some samples, particularly SE of the graphitic hanging wall unit, dominates the weathered zone mineralogy. Thin section analysis of muscovite grains suggest it weathers almost directly to kaolinite, probably with an illite intermediate. Illite occurs in varying amounts throughout the weathered zone, probably formed from the degradation of muscovite and sericite.

Iron oxides (including oxy-hydroxides) are very important mineral phases in the weathered and weathering environment. At Koongarra they occur coating clays, fissures and remnant schistosity planes, and form nodules, ferruginous gravel and ferricrete. The different forms of iron oxide probably play different roles in the capture and storage of radionuclides. The formation and properties of iron oxides have been extensively reviewed (for example, Schwertmann and Taylor, 1989).

Iron oxides at Koongarra appear to influence the distribution of uranium, phosphorus, vanadium, arsenic, manganese, nickel, copper and zinc. The distribution of iron oxides is very heterogenous, with many weathered samples showing strong zonation, going from bleached and gleyed heavy clay, containing about 2% iron, to red micaceous material with up to 20% iron oxide, over a few centimetres.

The three main iron oxides identified in the weathered zone at Koongarra are hematite, goethite, and the "amorphous" iron oxide ferrihydrite. Hematite appears to be most abundant in the weathered primary ore zone, and goethite is the dominant crystalline iron oxide down-gradient. Ferrihydrite was only detected directly in one sample, using Mössbauer spectroscopy, but its presence has been suggested in many samples from extraction with Tamms acid oxalate. Based on these extractions, the amount of ferrihydrite has been estimated to be 7-29 mg/g, with 4-48% of the iron as an amorphous (TAO-extractable) phase. Most of the observed variation of iron content in bulk samples was accounted for by variations in the concentrations of crystalline, inaccessible iron oxides (not TAO-extractable). The concentration range for goethite was estimated to be 2-19%, assuming all the "crystalline" iron was present in this form.

A sample used for sorption experiments (W2 14 m, see Volume 13 of this series) was subsampled for a study of the iron oxides. In general, the sample was a red colour, but throughout the core ran bands of clayey material, up to about 1 cm thick. These bands were white and grey to black, and were much wetter than the bulk of the sample. These gleyed bands were flanked by yellow to orange material, up to 1 cm thick, followed by the red material which made up the bulk of the sample. Each band was sampled for analysis by Mössbauer spectroscopy and PIXE-PIGME (see Appendix 2 for a full description of the Mössbauer analysis).

Table 3.2 summarises the Mössbauer and elemental analysis of the different zones in sample W2 14 m. The variation in the iron content appears to be largely accounted for by variation in the amount of goethite and ferrous iron present. There were similar amounts of ferrihydrite in the three subsamples, 48-70 mg/g. This amount of ferrihydrite is above the range estimated by extraction with TAO, however, this may be expected considering the nature of the material sampled. It is possible that some of the ferrihydrite detected in the samples resulted from post-sampling oxidation of Fe^{2+}.

Both rutile and anatase occur at Koongarra. Rutile occurs as acicular inclusions in chlorite grains at and below the base of weathering. Gray (1986) suggested a greater abundance of anatase than rutile in the weathered zone. Weaver (1976) suggested that titanium precipitates as an "amorphous" hydrous gel which becomes crystalline. While Weaver did not directly observe this "amorphous" gel, Fitzpatrick et al. (1978) found that up to 36% of soil titanium was soluble in TAO extractions, and was probably "amorphous". In the present study of weathered samples from Koongarra, only up to about 5% of total titanium was TAO extractable.

TABLE 3.2

ELEMENTAL AND IRON OXIDE COMPOSITION OF BANDS OF MATERIAL FROM W2 14 m

	Grey	Orange	Red	General
% Fe as Fe^{2+}	27	5	1.4	
% Fe as goethite	>14	69	61	
% Fe as ferrihydrite	59	26	38	
% Fe	6.1	11	15	6.5
% FeO	2.1	0.7	0.3	
% goethite	>1.4	13	15	
% ferrihydrite	6.1	4.8	9.7	
% Al_2O_3	22	17	13	11
% SiO_2	53	47	51	83
% K_2O	0.3	0.8	0.3	2.1
% MgO	3.5	3.0	3.7	2.1
mg/g Ca	2.0	1.1	0.3	0.5
mg/g Ti	2.0	5.1	12.6	2.6
mg/g Mn	0.4	0.2	1.5	1.5
μg/g Pb	141	117	25	53
μg/g U	71	290	297	165

Zircon has been detected in the quartz chlorite schist (Snelling, 1980a) as inclusions in biotite (Ewers and Ferguson, 1980) and possibly chlorite, and has also been detected in trace amounts in the weathered zone. Monazite has been observed in weathered zone samples and may be an important source of rare earth elements. Zeolite traces were detected by XRD in partially weathered and unweathered rock.

Manganese oxide coatings were observed along fissures and remnant schistosity in weathered and partially weathered rock (Noranda, unpublished), and are often associated with iron oxide accumulations. Manganese oxides are most abundant down-gradient of the primary ore zone, with up to 3% MnO_2 in very manganese rich samples (see Section 4). From XRD and bulk elemental analysis, the main form of secondary manganese oxide appears to be lithiophorite [$(Al,Li)MnO_2(OH)_2$], which has been frequently identified in Australian soil, but rarely elsewhere (McKenzie, 1989).

The manganese oxides in soil are often reported to be "amorphous" (Childs, 1975; McKeague et al., 1968; Sidhu et al., 1977). In this study an average of 47.5% of manganese present in the weathered zone at Koongarra was extractable by Tamms acid oxalate reagent, which suggested a large proportion of manganese present as, or associated with, amorphous phases. The position of the manganese phases as fissure coatings suggests a cycling of the manganese involving dissolution by reduction followed by deposition under more oxic conditions. The position of these phases in potential transport pathways places them in an ideal position for contact with migrating species. At Koongarra, manganese oxides seem to play a strong role in determining the distribution of barium, cobalt, lithium, rare earth elements (particularly cerium), and uranium.

Mineral assemblages and particle size distributions in three profiles

The mineral components of three profiles have been studied in detail. The three profiles M1, M2 and M3, represented the zone of leached primary mineralisation, the secondary ore zone, and the zone of dispersed uranium, respectively. Weathered material from each profile was examined by light microscope for modal analysis (45-100 μm fraction) and by XRD (20-45 μm and <2 μm fractions). Bulk samples were also analysed by XRD and PIXE-PIGME.

An optical examination of the 45-100 μm (fine sand) fraction revealed major differences in the mineralogical composition of samples from each site, and this was further modified by depth (see Figure 3.1). Whilst quartz was ubiquitous to all samples, proportions of altered biotite, muscovite and chlorite varied. In M1, chlorite appeared at and below 16 m, and in M2, at 25 m. The muscovite and altered biotite content was greater at M2 than at M1 or M3. At M2, the biotite concentration tended to decrease with depth, whilst at M1 and M3 it was largely restricted to the top 4 metres.

Examination of the very fine sand fraction (20-45 μm) by XRD (see Table 3.3) indicated that chlorite was absent in all sampled depths of M3. Chlorite was present at M1 deeper than 19 m, and deeper than 25 m at M2. No biotite was detected by XRD in any of the samples. Muscovite was found throughout M2, but only in samples from 13 m and 21 m at M1, and 7 m and 13 m at M3. Kaolinite was present in all the 20-45 μm samples examined.

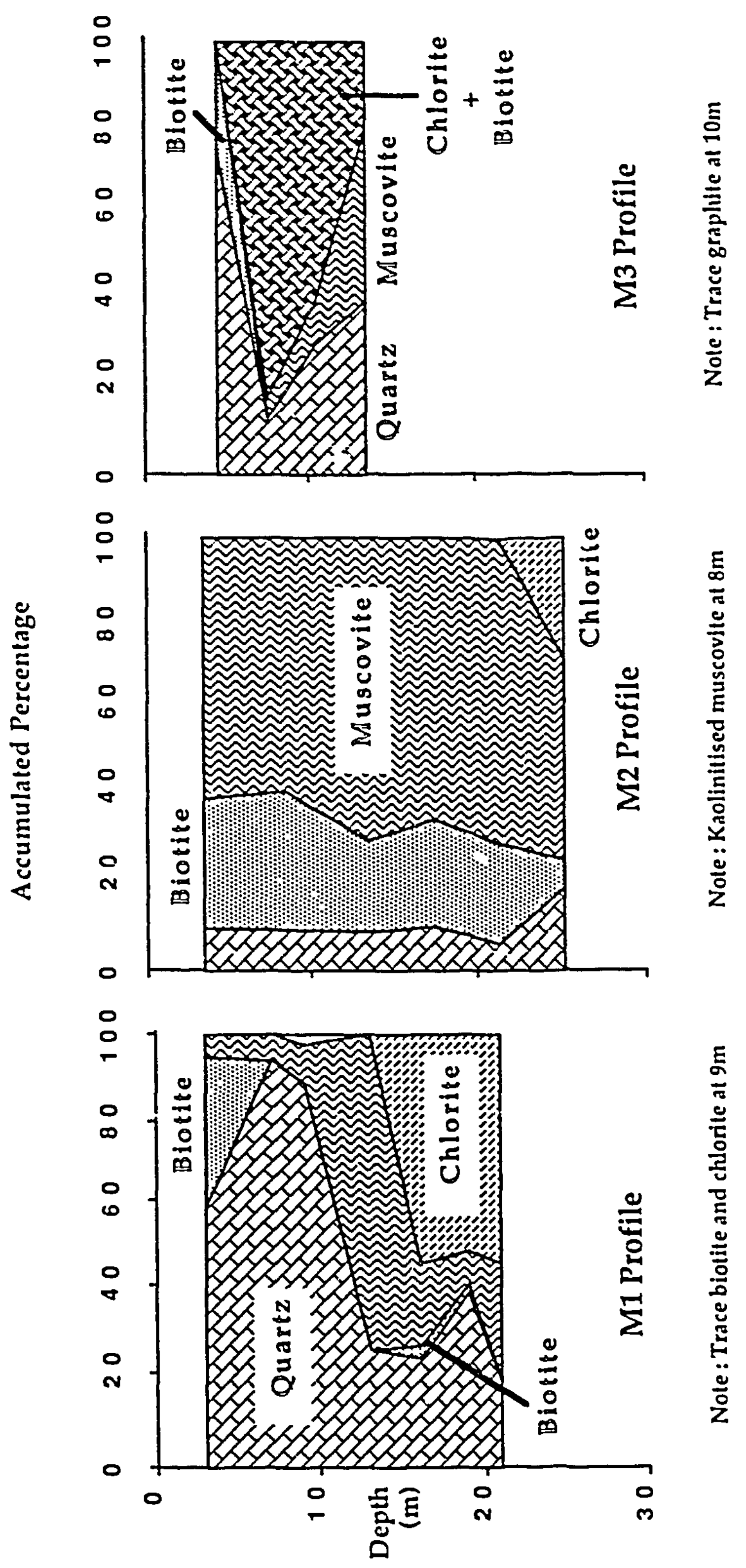

FIGURE 3.1 Estimated proportions (optically by light microscope) of minerals in the 100-45 μm of weathered material in the M1, M2 and M3 profiles

TABLE 3.3

MINERALOGICAL COMPOSITION OF THE 20-45 μm SAND FRACTIONS OF THE M1, M2 AND M3 PROFILES BY XRD

Hole	Depth (m)	Quartz	Muscovite	Chlorite	Kaolinite
M1	3	*			*
	7	*			*
	9	*			*
	13	*	*		*
	16	*			*
	19	*		*	*
	21	*	*	*	*
M2	3	*	*		*
	8	*	*		*
	13	*	*		*
	17	*	*		*
	21	*	*	*	*
	25	*	*		*
M3	4	*			*
	7	*	*		*
	10	*			*
	13	*	*		*

When the clay fraction was investigated by XRD (see Figure 3.2), the dominant minerals found were:

M1: kaolinite, illite, smectite and chlorite
M2: kaolinite, illite, smectite, vermiculite and chlorite
M3: kaolinite, illite, smectite, interstratified chlorite/smectite

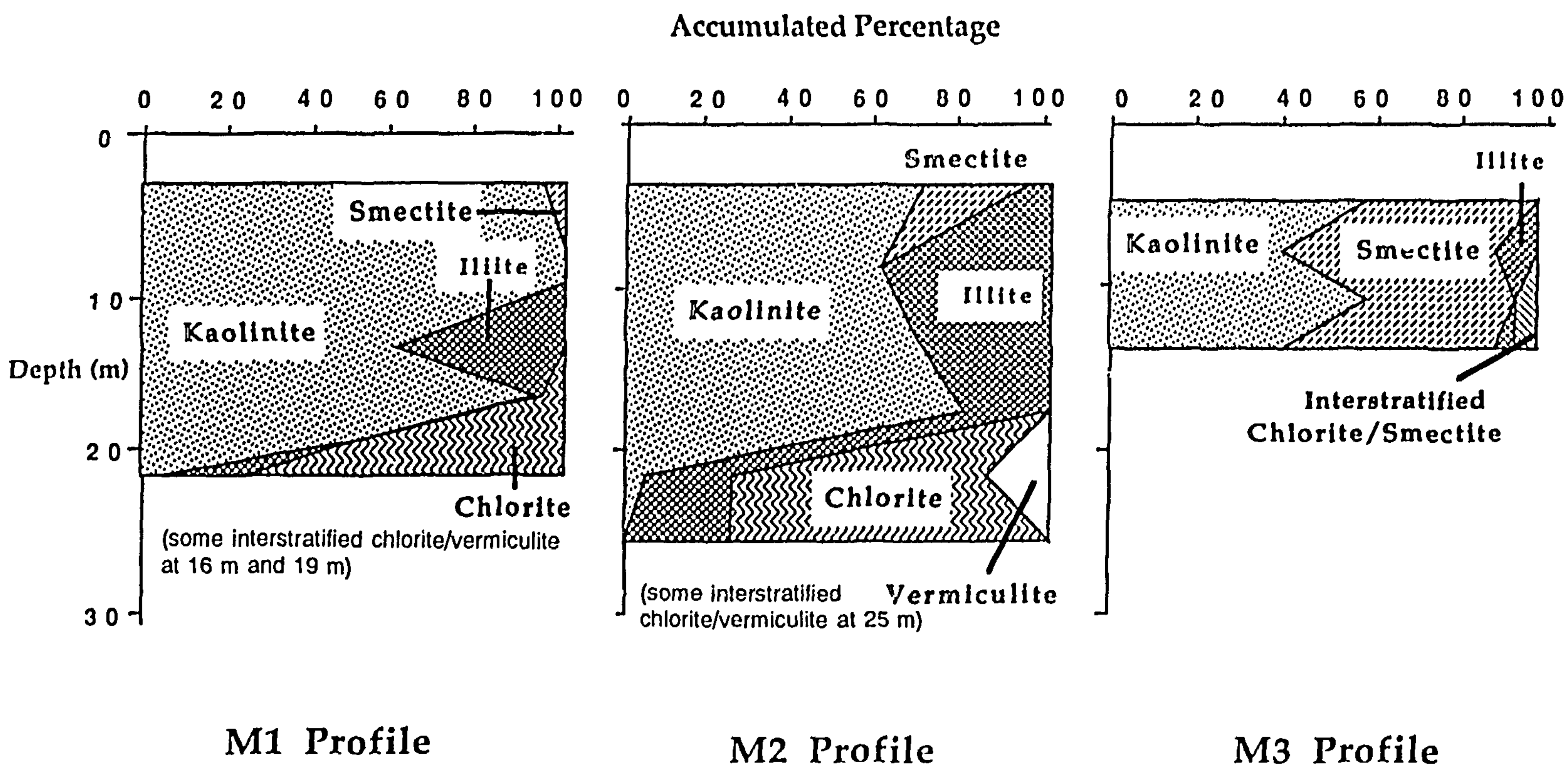

FIGURE 3.2 Estimated proportions (semi-quantitatively by XRD) of minerals in the <2 μm fraction of weathered material in the M1, M2 and M3 profiles

In M3, smectite along with kaolinite dominated the clay fraction. Chlorite in M1 and M2 was mainly restricted to mainly 19 m and below. In M2, vermiculite (15%) was found along with chlorite (60%) and illite (20%) in relatively freshly weathered material (21 m). While illite was present throughout M2, its distribution was limited largely to the 13 m depth in M1. The collective proportion of illite and interstratified chlorite/smectite in M3 was small (<10%) and located only in the 7-13 m depths. Investigation of the smectite found in the surface samples, by XRD, revealed a dioctahedral form of biedellite/montmorrillonite (see Figure 3.3) following identification procedures described in Brindley & Brown (1980).

Tables 3.4, 3.5 and 3.6 give the mineral components for bulk samples down the three profiles, using random powder XRD data and elemental data from PIXE-PIGME (see Section 4). Because of the apparent simplicity of the weathered zone mineral assemblage at M1 and M2, estimates of the relative abundances of kaolinite, mica, quartz and iron oxides were made. For this calculation, all potassium was assumed to be present in mica minerals and mica was assumed to consist of 10% K_2O and 30% Al_2O_3 (Deer et al., 1983). All remaining aluminium was assumed to be in kaolinite, and kaolinite was assumed to consist of 40% Al_2O_3 and 46% SiO_2 (Deer et al., 1983). The remaining SiO_2 was assumed to be quartz.

Particle size characteristics varied between the three profiles and within the profiles (see Figure 3.4). One of the most marked differences between the sites was in the clay (<2 µm) content. Samples from M1 had the greatest clay content, with profiles M2 and M3 having similar clay contents and distribution. Clay content decreased with depth in all profiles. Changes in clay content with depth were smooth in profiles M2 and M3, but in M1 peaks occurred at depths 3 m (34%), 9 m (30%) and 16 m (24%). The clay peaks in M1 were matched by a similar pattern for silt (2-20 µm), and relatively low concentrations of gravel (2-5 mm). When the possible confounding effect of the large variation in gravel content was removed, the same trends in chlorite content remained. Whilst maximum gravel concentrations were found near the surface of M2 and M3, this trend was not observed for profile M1.

Soil and Surficial Deposits

The soil of the Alligator Rivers region has been described by Christian and Stewart (1952); Gray (1986); Stewart (1956); Story et al. (1976); Wells (1979), and White et al. (1982). The soil profiles at Koongarra were generally described as lateritic, with an abundance of ferruginous nodules and possibly ferricrete fragments over most of the site. Much of the land surface is overlayed by surficial sands, apparently remnants of the Kombolgie sandstone, up to 3 m thick (Noranda, unpublished; Snelling, 1984; White et al., 1982). White et al. (1982) presented a soil study of the Koongarra valley region, dividing up the area into six landform categories. The landforms of particular interest to this study occur in undulating upland terrain. These are areas away from the sandstone plateau, scarps and scree slopes, and away from low lying drainage floors. The soil of the upland terrain land forms is of variable depth, from shallow (<60 cm), to deep (>100 cm). The profiles often bottomed out onto massive ferruginous gravel and stone. These lateritic gravels

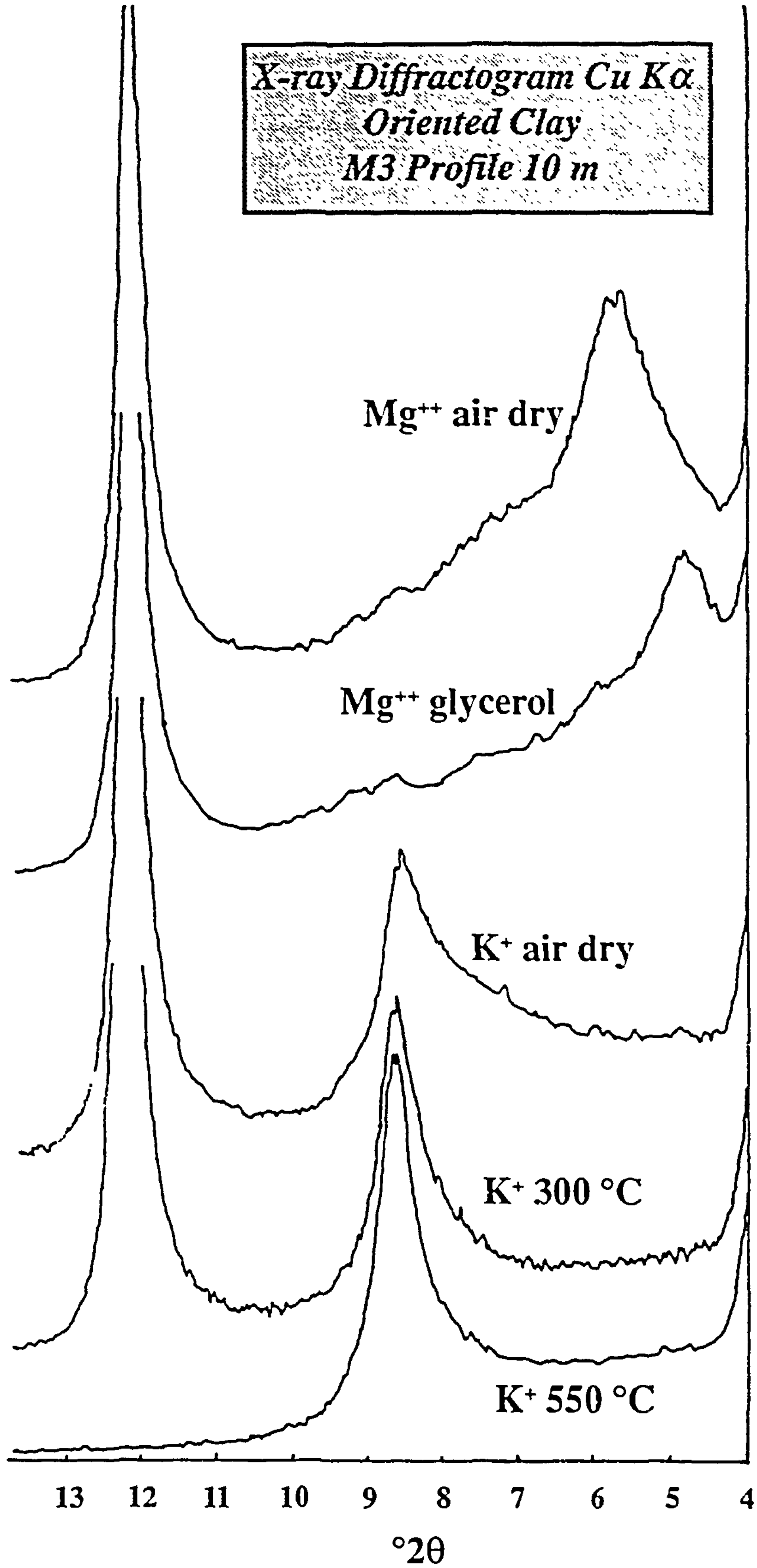

FIGURE 3.3 X-ray diffractogram (CuKα) for an oriented clay (< 2 μm), from M3 10 m

often occurred throughout the profile, and made up to 80% of the surface layer. Generally the soil is gravelly, sandy to loamy, and classified as yellow or red massive earths (White et al., 1982). The surface is usually sandy to gravelly loamy sand, with occasional lateritic outcrops (Snelling, 1984; White et al., 1982). Occasional mottling was observed in some profiles and the soil was often observed to be hydrophobic (White et al., 1982). Short et al (1989) estimated the age of pisolith rinds from Ranger to be about 176 ky old.

TABLE 3.4

MINERAL COMPONENTS OF SAMPLES FROM PROFILE M1

	% Mineral abundances			
Sample	Mica	Kaolinite	Quartz	Fe-oxides
M1 3 m general	<2	46	38	13
M1 3 m red	<1.4	37	52	16
M1 7 m white	<1.6	35	69	1.8
M1 7 m red	<1.2	27	60	14
M1 9 m white	<0.6	42	61	1.2
M1 9 m red	<0.2	28	36	28
M1 13 m white	23	29	45	0.9
M1 13 m brown	26	36	24	16
M1 16 m general	<1.2	49	29	17
M1 16 m orange	<0.6	59	26	17
M1 19 m	~0.5% mica, quartz, trace chlorite and/or vermiculite, kaolinite and Fe oxides			
M1 23 m	~3.5% mica, quartz, chlorite, trace kaolinite, possibly trace vermiculite and Fe oxides			
M1 27 m	~1.5% mica, quartz, chlorite			
M1 31 m	~1.1% mica, quartz, chlorite			
M1 37 m	~6.6% mica, quartz, chlorite			
M1 43 m	~12.1% mica quartz, chlorite			
M1 49 m	~7.2% mica, quartz, chlorite			

TABLE 3.5

MINERAL COMPONENTS OF SAMPLES FROM PROFILE M2

	% Mineral abundances			
Sample	Mica	Kaolinite	Quartz	Fe-oxides
M2 3 m <2 mm	10	33	44	14
M2 3 m >2 mm	4	9	76	11
M2 8 m <2 mm	35	20	30	13
M2 13 m <2 mm	45	16	25	12
M2 13 m 45-100 μm	65	17	10	9
M2 17 m <2 mm	37	17	38	11
M2 17 m >2 mm	6	3	88	3
M2 21 <2 mm	40	20	29	12
M2 25 m <2 mm	23	quartz, chlorite, muscovite, trace interstratified chlorite/vermiculite		
M2 25 m >2 mm	16	quartz, chlorite, trace vermiculite		
M2 32 m	21	quartz, chlorite, muscovite		
M2 36 m	1	quartz, chlorite		
M2 42 m	0.4	quartz, chlorite		
M2 48 m	6.2	quartz, chlorite, possibly talc, pyrite, graphite, uraninite		

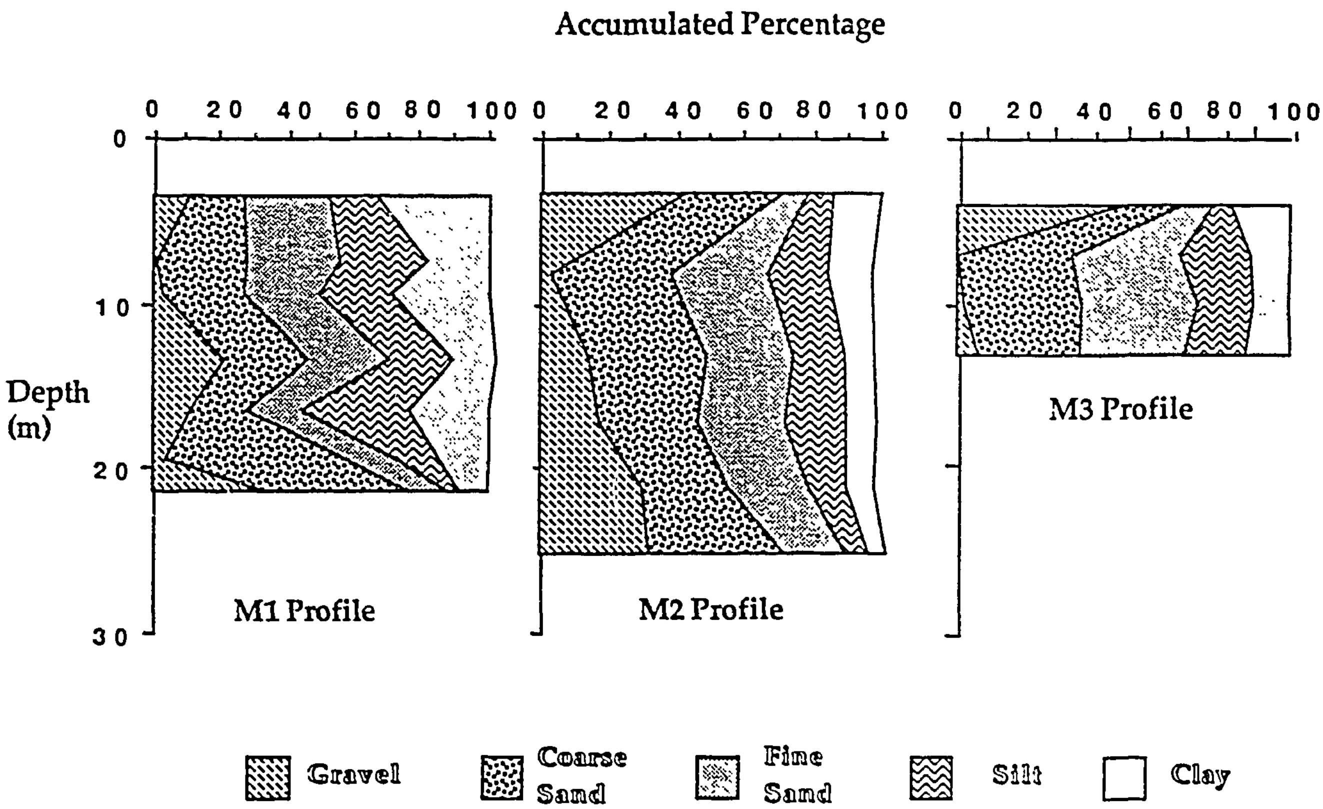

FIGURE 3.4 Particle size analysis of the M1, M2 and M3 profiles

TABLE 3.6

MINERAL COMPONENTS OF SAMPLES FROM PROFILE M3

Sample	Minerals identified
M3 4 m	quartz, kaolinite, Fe oxide, smectite
M3 7 m	kaolinite, quartz, smectite, trace mica
M3 10 m general	quartz, kaolinite, smectite, chlorite/smectite interstatified, lithiophorite, Fe oxides
M3 13 m general	quartz, kaolinite, smectite, mica (~18%), Fe oxides
M3 13 m white	quartz, kaolinite, mica (~17%)
M3 13 m yellow	quartz, kaolinite, trace smectite, mica (~11%), Fe oxide, possibly trace brookite or anatase
M3 13 m black	quartz, kaolinite, lithiophorite, trace smectite, Fe oxides, mica (~8%)
M3 15 m	quartz, kaolinite, chlorite/smectite interstratified
M3 20 m	quartz, chlorite, mica (~5%), possibly some vermiculite
M3 26 m	quartz, chlorite, mica (~6%)
M3 32 m	quartz, chlorite, mica (~12)

ROCK AND SOIL CHEMISTRY

4.1 The Distribution of Elements In Material From Three Profiles

Forty-eight samples from three vertical profiles through different zones of the Koongarra uranium deposit, were analysed by PIXE-PIGME for 30 elements. X-ray fluorescence was used for analysing the phosphorus content, DNAA was used for uranium, which was also included in the PIXE set, and INAA was used for the analysis of rare earth elements and also uranium. The three profiles were:

M1: Primary mineralised zone, uranium leached from the weathered zone.

M2: Secondary mineralised zone.

M3: Adsorbed zone, where uranium was proposed to be adsorbed onto matrix constituents.

For some of the samples, subsamples of visually distinct zones, or different particle size ranges, were analysed separately. The elemental concentration data for each sample/subsample are given in Table 1 of Appendix 4, except for the rare earth data which is given in Table A4.2. Here the data have been arranged to produce concentration profiles for elements present in quantities detectable by the techniques employed, and to determine associations between elements. The distribution of elements between TAO-extractable (estimating accessible) and inaccessible phases are discussed in Section 4.3, and also referred to here.

Elemental Concentration Profiles

Figures 4.1 to 4.25 show the depth profiles of F, Li, Na, Al, Mg, Si, P, S, K, Ca, Ti, V, Cr, Mn, Fe, Ni, Cu, Zn, Ga, As, Rb, Y, Zr, Pb and U, at M1, M2 and M3. Different subsamples for the same depth have been plotted separately, to show the degree of heterogeneity in the samples and the impact of particular kinds of subsampling on element concentrations. Elements analysed, but present at levels below the detection limits, were sulfur at M1; lead at M3, and Se, Br, Sr, Nb, Mo and Th in all drill cores.

Element-Element Correlations

Correlation matrices were calculated for measured elements using the Statview statistical package. Matrices were calculated using the data in two forms including and excluding the SiO_2 component. The transformation for the SiO_2 excluded data was:

$$X/(\%\ \text{total oxides} - \%SiO_2)$$

where X = sample value for an element concentration.

This gave concentration values for the non-SiO_2 fraction. This transformation was considered of interest because SiO_2 tended to dominate the mass of the system while essentially being geochemically inert.

For the calculation of correlation coefficients, only weathered samples were considered, and samples from each profile were treated separately. The null hypothesis tested was that the correlation coefficient between each element was zero. In discussions about associations between elements, more emphasis has been given to the SiO_2 adjusted data. The sample sizes from which correlation coefficients were calculated were smaller than ideal, but it was felt that correlations between elements using data from the same profile, would give better guides to element-element associations than from pooled data from many profiles. Consequently the risk of a dramatic effect from an outlier is high, and this needs to be considered when elucidating associations. Very few unweathered samples were analysed in this study. However, Ferguson and Winer (1980) compiled a large set of analyses of Cahill Formation rocks, which included many samples from the Koongarra deposit. Values for unweathered samples from, or in the vicinity of, the Koongarra No.1 ore body were recompiled into three groups according to uranium contents:

uranium concentration > 500 μg/g

40 μg/g < uranium concentration < 500 μg/g

uranium concentration < 40 μg/g.

Correlation matrices for the three concentration groups were developed using the method described above. The concentrations of elements in individual samples are given in Appendix 4.3. The three uranium concentration groups were chosen to represent highly mineralised, weakly mineralised and intermediately mineralised samples, and samples away from the mineralisation.

Some major elements may be useful as mineralogical indicators, and are therefore useful in discussing associations between minerals and elements. For example, iron in the weathered zone indicates iron oxides (including oxy-hydroxides), whereas silicon is a major constituent of quartz, clays, mica, chlorite and altered chlorite. Aluminium indicates clays, mica or chlorite, potassium indicates mica, and magnesium often indicates chlorite in unweathered samples, and smectite in weathered samples. Depending on the values for potassium and magnesium, aluminium can sometimes be used to more specifically indicate clays, such as kaolinite.

Fluorine

A common occurrence of fluorine in rock and soil, is as a substitute for hydroxyl groups in many minerals, particularly micas, chlorites and phosphates (Kabata-Pendias and Pendias, 1984). The most common fluorine mineral is the fluorine end-member of apatite, fluoroapatite ($Ca_{10}(PO_4)_6F_2$). Fluorine is readily adsorbed by clays, and as a consequence its mobility is usually slight. In Koongarra samples fluorine followed the distribution of potassium. This suggests a predominant association of fluorine with mica. Fluorine occurred in similar concentrations in the three M profiles, and appeared not to be greatly affected by iron oxide zoning. At M2, fluorine appeared to be most concentrated in the 45-100 μm fraction, reflecting a grain size dominated by mica (Figure 4.1).

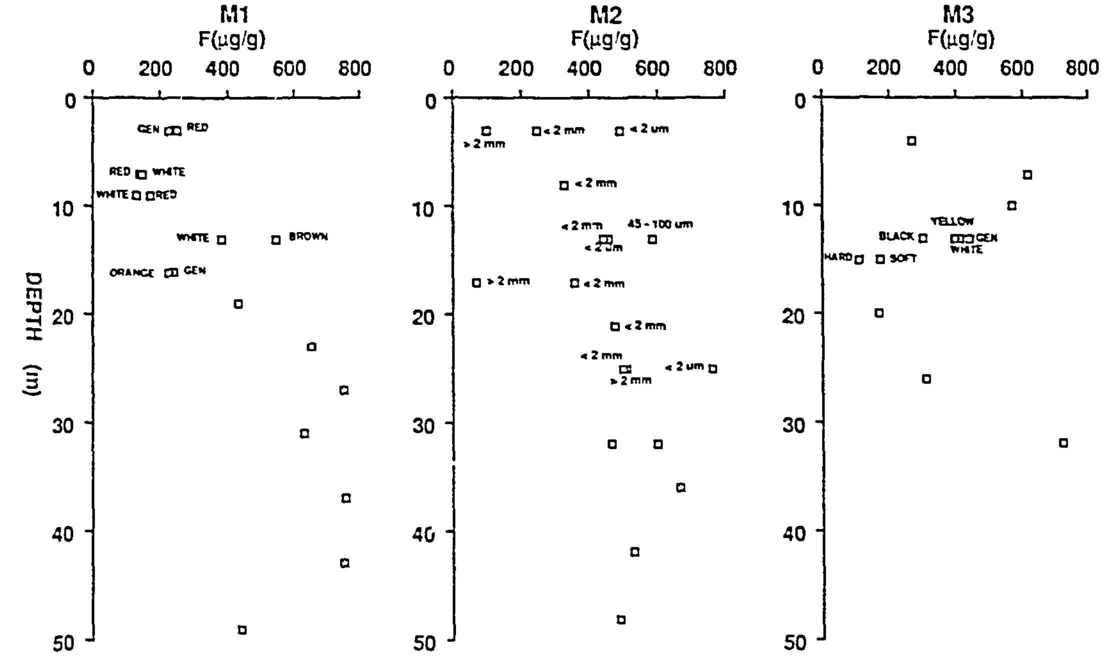

FIGURE 4.1 Fluorine concentration depth profiles from holes M1, M2 and M3 (point labels denote subsamples. Points with no labels, or GEN were general bulk samples)

Lithium

The depth profile for lithium at M1 suggests a leaching of lithium from the weathered zone, while the distribution at M3 suggests an accumulation, especially near fissures where manganese coatings occurred (Figures 4.2 and 4.14). In weathered M1 samples, lithium was correlated with Al, Ti and Zr, suggesting possible associations with clays, TiO_2, and zircon. In the unweathered, high uranium concentration group, lithium correlated with elements that may be expected to occur with resistant minerals like zircon and monazite (Zr, Th, Y, Hf). In the unweathered, low and medium uranium concentration groups, lithium was correlated to chlorite elements like Mg and Fe(II). At M3 there appeared to be an association between lithium and manganese. Lithium was insensitive to iron oxide zoning but was strongly affected by manganese zoning, suggesting scavenging, or coprecipitation, of lithium by manganese. Lithium may be a component of the manganese phase, such as in lithiophorite [$(Al,Li)MnO_2(OH)_2$].

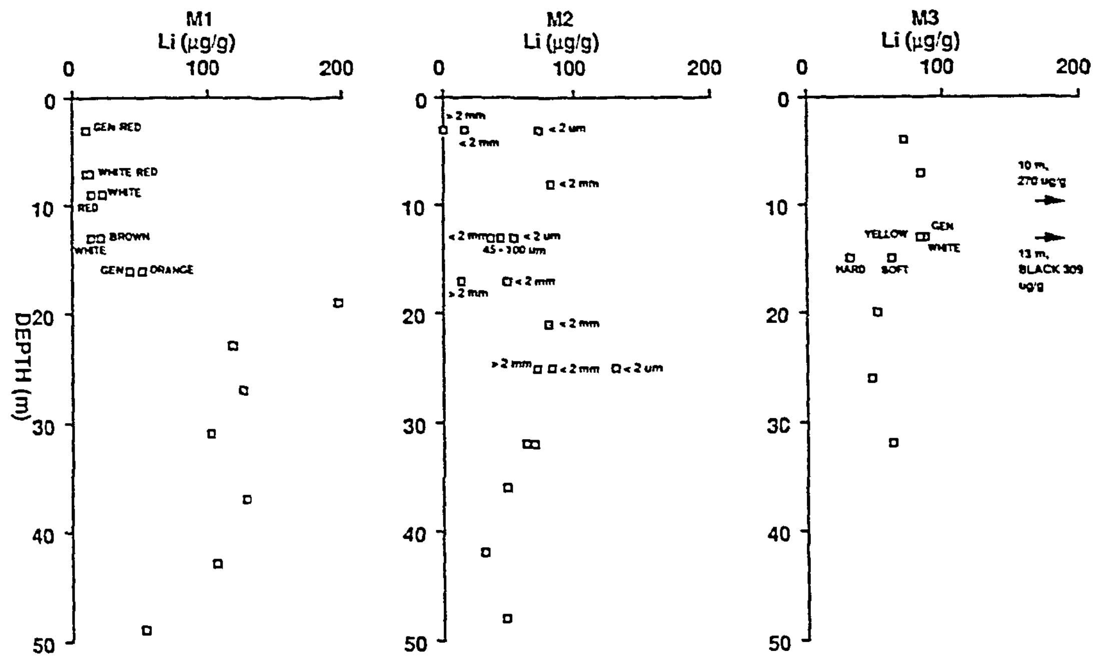

FIGURE 4.2 Lithium concentration depth profiles from holes M1, M2 and M3 (point labels denote subsamples. Points with no labels, or GEN were general bulk samples)

Sodium

In the unweathered low and intermediate uranium concentration groups, and the weathered zone at M1 and M2, sodium tended to correlate with aluminium and potassium, suggesting a relationship with micas (Figure 4.3).

Aluminium

Aluminium was present mainly in clay, mica and chlorite and was used as an indicator of these minerals. Aluminium was used as an indicator specifically for clays, where these were the dominant aluminium-containing phases. In M1 weathered samples, elements which appeared to be associated with aluminium were F, Li, Na, Ca, Ti, Zr and Ga. In M2 weathered samples, only gallium was correlated with aluminium, and in M3 weathered samples F, K and Rb (mica) correlated with aluminium. Gallium has a very similar geochemistry to aluminium (Kabata-Pendias and Pendias, 1984) and would be expected to often follow the same distributions as observed here (Figure 4.4).

The unweathered samples described by Ferguson and Winer (1980) contained very similar amounts of aluminium in the three uranium concentration groups, but had quite different correlating element sets. Elements that correlated with aluminium in two of the groups were Ti, K, F, Sc, Na, Rb, Zr and Be. This suggests a relationship with mica.

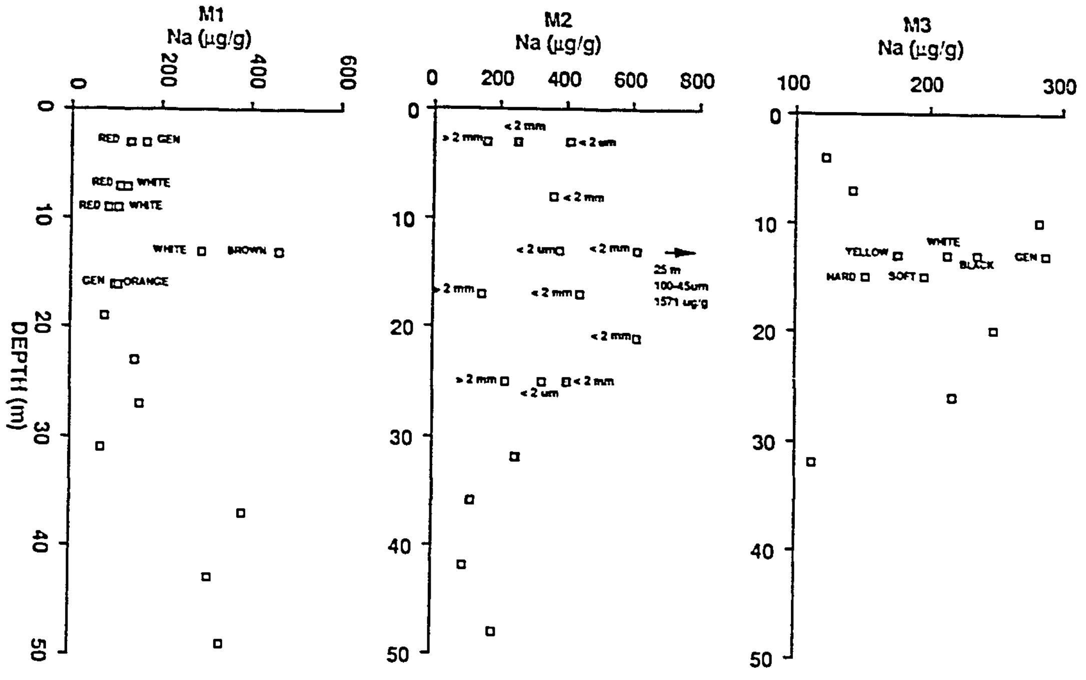

FIGURE 4.3 Sodium concentration depth profiles from holes M1, M2 and M3 (point labels denote subsamples. Points with no labels, or GEN were general bulk samples)

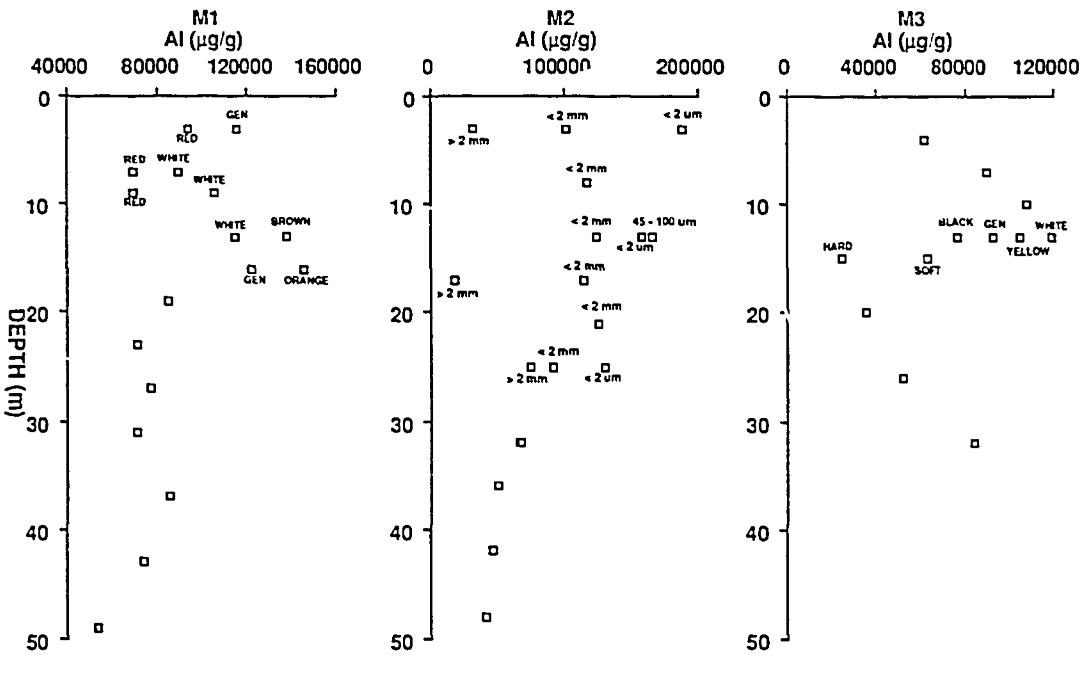

FIGURE 4.4 Aluminium concentration depth profiles from holes M1, M2 and M3 (point labels denote subsamples. Points with no labels, or GEN were general bulk samples)

Magnesium

Magnesium concentrations were very depth dependent as shown in Figure 4.5. Much higher concentrations were present in unweathered than weathered samples, owing to the high mobility of magnesium after the alteration of chlorite and vermiculite, which are the major sources of magnesium. In weathered samples from M1 and M2, there were only a few samples in which magnesium was detectable. In the M3 weathered samples, magnesium correlated with F, K, Rb, Ti and Zr. The association with titanium and zirconium may be through the observed presence of acicular inclusions of rutile and zircon in chlorite grains. There did, however, appear to be a mutual association of these elements with mica. M3 contained larger amounts of potassium than M1 or M2, suggesting a more micaceous material, as was observed visually and by XRD. The higher magnesium concentrations at M3 may reflect a greater abundance of smectite in the weathered zone.

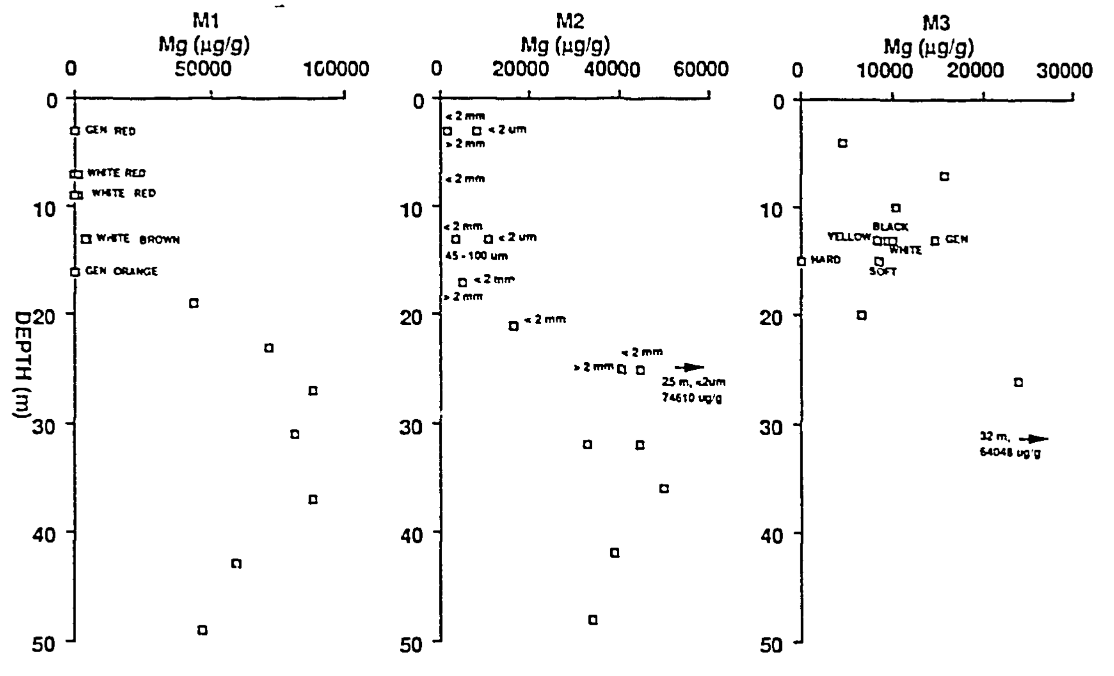

FIGURE 4.5 Magnesium concentration depth profiles from holes M1, M2 and M3 (point labels denote subsamples. Points with no labels, or GEN were general bulk samples)

No differences in the amount of magnesium in mineralised and unmineralised areas were observed for unweathered rock. Although all the Cahill Formation uranium deposits occur in chlorite schist, mineralised zones did not appear to contain more chlorite than unmineralised zones. Magnesium correlated negatively with elements representing quartz and mica (Si, K, Rb), and correlated positively with nickel and Fe(II) in the high and medium uranium concentration groups. The relationship of Fe(II) with magnesium was possibly from high Fe(II) chlorites associated with uranium mineralisations. Nickel may also have been included in the interlayer hydroxide sheet of chlorite (Barnhisel and Bertsch, 1989), but this has not been reported for Alligator Rivers region chlorites.

Silicon

Silicon (Figure 4.6) was present in quartz, but also in the alumino-silicates. Silicon was negatively correlated with many elements, including some alumino-silicate elements.

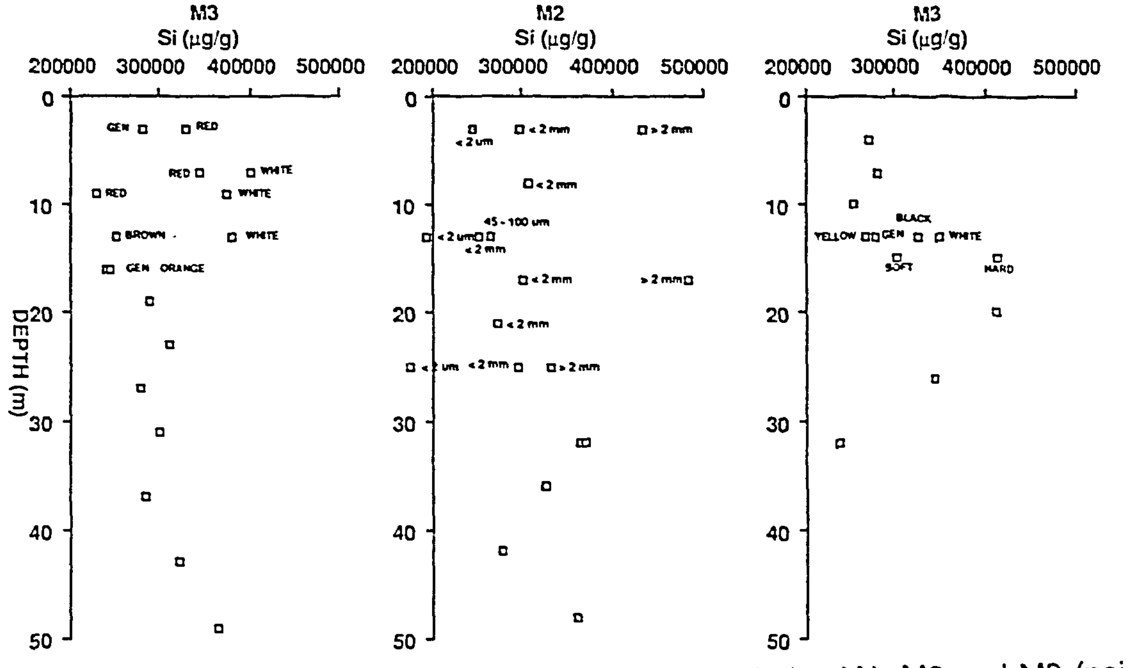

FIGURE 4.6 Silicon concentration depth profiles from holes M1, M2 and M3 (point labels denote subsamples. Points with no labels, or GEN were general bulk samples)

In unweathered samples from the Ferguson and Winer data set (1980), SiO_2 consistently made up about 62% of each sample. No positive correlations between silicon and other elements were observed, and several negative correlations were apparent with major rock forming and trace elements (Fe(II), Mg, Zn, Ti, Al, Li, Sc, Ni, F).

Phosphorus

Phosphorus was present in similar quantities in all the M series profiles (Figure 4.7), although M2 and possibly M3, had higher values in the unweathered rock. At M1, phosphorus appeared to be associated with the iron oxides, and was also correlated with uranium and arsenic. The correlation with uranium at M1 suggests that uranyl phosphates may have been present in this zone.

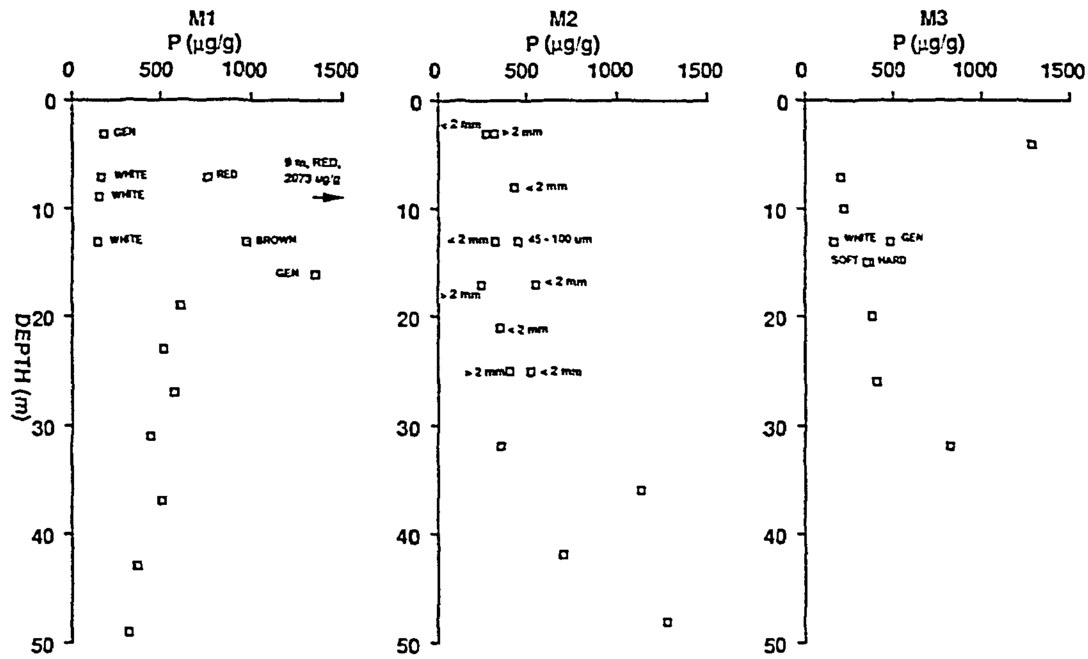

FIGURE 4.7 Phosphorus concentration depth profiles from holes M1, M2 and M3 (point labels denote subsamples. Points with no labels, or GEN were general bulk samples)

Subsampling of iron-rich zones showed that uranium was most concentrated in these areas. Uranyl phosphates may be unevenly distributed throughout the iron oxide containing matrix, and may be more concentrated in the vicinity of fissures and remnant schistosity. At M2, in the weathered zone, phosphorus was also correlated with iron (and hence iron oxides), and with uranium. As the samples came from the zone of uranyl phosphates, much of the uranium is likely to have been in such a form. In weathered M3 samples, phosphorus was correlated with iron and copper, but not with uranium.

Phosphorus was generally associated with iron oxides in the weathered zone and phosphorus was also associated with uranium in zones where uranium mineralisation may have occurred (M1 and M2). In unweathered M-series samples, high phosphorus concentrations were associated with high concentrations of U, Pb, S, Ca, V, Cu, As and Y. All showed higher than usual values in the high grade primary ore zone material at the bottom of M2. Snelling (1980a) observed apatite inclusions in some grains of pyrite, and this was possibly the nature of the relationship between P, Ca and S in the unweathered samples. The high uranium concentration sample from M2 48.5-50 m was from just below the graphite hanging wall unit, and contained high sulfide concentrations.

On the basis of calcium concentrations, it appears that phosphorus was present in forms other than apatite in some unweathered samples from within the inner alteration halo. These samples were from; M1 (27 and 29 m, maximum of 69% and 66% of phosphorus as apatite respectively), DDH49 (83 m), DDH21 (96 and 130 m), DDH5 (48, 79, 84 and 58 m). Phosphorus in unweathered samples from the Ferguson and

Winer set (1980) was very variable in concentration and did not appear to be higher in mineralised zones. Phosphorus correlated to calcium in the high and medium uranium concentration groups, suggesting that apatite was the major phosphorus source, and that other forms of calcium, for example carbonates, were not major contributors to the calcium content. The similar amounts of phosphorus outside of mineralised zones, and the similar amounts in the weathered zone at M1, M2 and M3 suggest that a phosphorus anomaly did not cause the development of the uranyl phosphate zone. Since phosphorus tended to be mobilised only very locally with weathering, a phosphorus anomaly in the weathered zone should have been reflected in the unweathered zone. However, the rock alteration may have changed the mineral form of the phosphate, possibly becoming more available for interaction with uranium.

Sulfur

The distribution of sulfur was very depth dependent, being present in significant quantities only in unweathered samples from M2 and M3 (Figure 4.8). Unweathered samples from M2 contained much more sulfur than samples from M1 or M3. The higher values of sulfur at M2 reflect the proximity of the graphitic hanging wall unit, and the accompanying iron, copper and lead sulfides. At the early stages of weathering, sulfides were probably oxidised to sulfates and leached away.

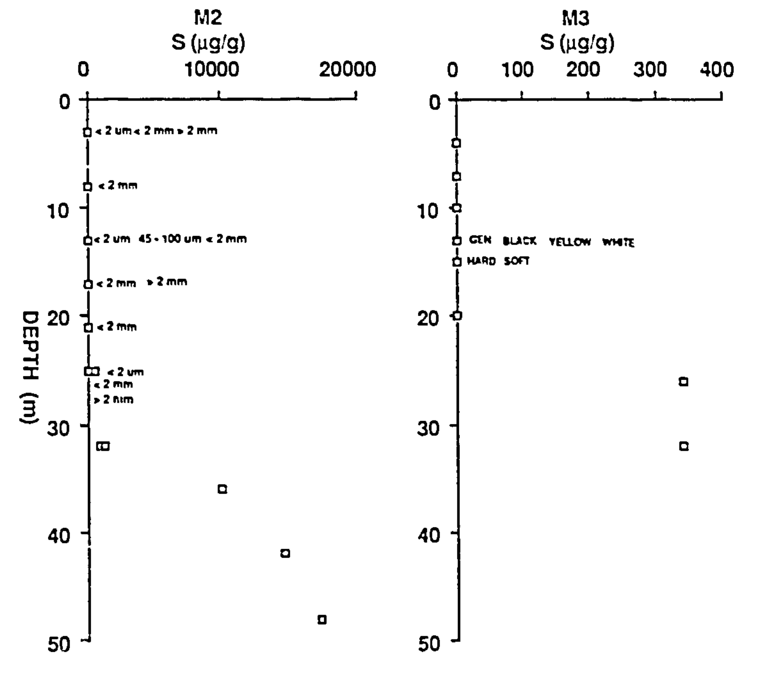

FIGURE 4.8 Sulfur concentration depth profiles from holes M1, M2 and M3 (point labels denote subsamples. Points with no labels, or GEN were general bulk samples)

In unweathered samples analysed by Ferguson and Winer (1980), sulfur was very variable, both in the amount present and correlating elements. Calcium was the only element to correlate with sulfur in two groups. As mentioned earlier, phosphorus correlated to calcium in these samples and a relationship between apatite and sulfides was suggested. In the high uranium concentration group, lead correlated to sulfur, possibly due to the presence of galena. Also, in the high uranium concentration group, sulfur correlated positively with Fe(III) and the light rare earth elements lanthanum and cerium; but was negatively correlated with Zr, Th and Y. The medium uranium concentration range had copper correlated with sulfur, possibly due to the presence of chalcopyrite.

Potassium

In the present study, potassium was used as an indicator of micas. Except for a band of micaceous material at about 13 m, there was less potassium (and mica) in weathered M1 samples compared to M2 and M3, and there was more potassium (and mica) in unweathered M3 samples than those from M1 and M2 (Figure 4.9).

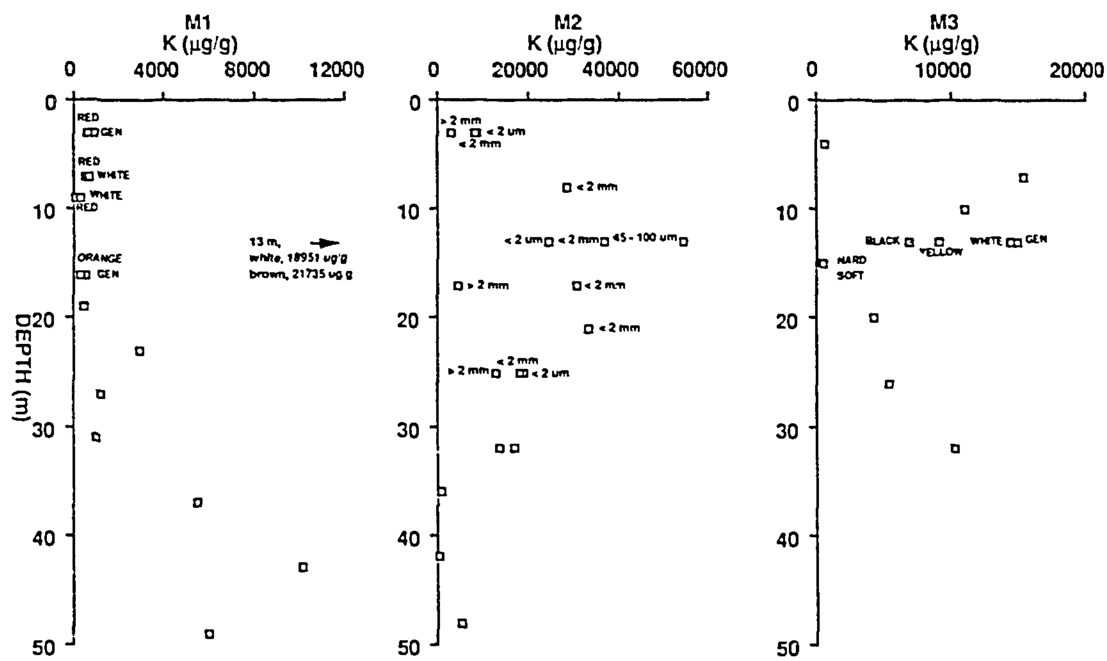

FIGURE 4.9 Potassium concentration depth profiles from holes M1, M2 and M3 (point labels denote subsamples. Points with no labels, or GEN were general bulk samples)

In weathered samples from M1, potassium was correlated with Rb, Y, F, Na and Ca. Rubidium has similar geochemical properties to potassium, and the two are often associated (Kabata-Pendias and Pendias, 1984). Yttrium often reflects rare earth element distributions, particularly light rare earths, which may be related to micas at M1. The main mica types present in the weathered samples are muscovite, and illite. In the unweathered zone, muscovite and sericite were the major micas, with trace biotite. In weathered samples from M2, potassium correlated with rubidium and sodium, and in weathered samples from M3, potassium correlated with Mg, F, Ti, Rb and Zr.

The potassium content in unweathered rocks was very variable, reflecting the uneven distribution of mica in the rocks. The mica content of mineralised samples was not significantly different to that of unmineralised rock.

Calcium

In weathered samples, the relationships with calcium appeared to be different for the three M profiles (Figure 4.10). At M1, calcium appeared to be associated with potassium (micas), while at M2, calcium was only correlated with chromium. At M3, calcium was correlated with iron and with other elements associated with iron oxides (Ga, As, U, Na, Cr, Ni and Zn). Calcium was more concentrated in unweathered samples than weathered samples, especially at M1 and M2. The sources of calcium in unweathered rock probably included apatite and possibly carbonates. In unweathered M1 samples, the Ca/P ratio was close to, or below, that for apatite. However, in samples from M2 and M3, there was an excess of calcium, with as little as 30% of the calcium accounted for apatite. This shows that at M1 there was another source of phosphorus as well as apatite, and that at M2 and M3 there was an additional source of calcium.

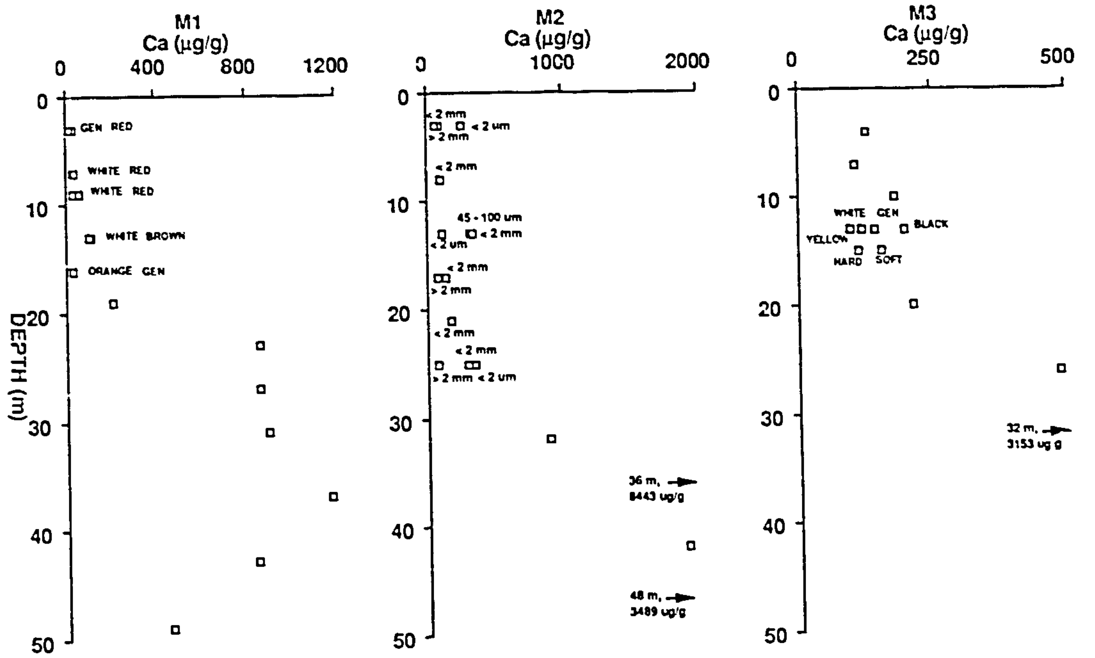

FIGURE 4.10 Calcium concentration depth profiles from holes M1, M2 and M3 (point labels denote subsamples. Points with no labels, or GEN were general bulk samples)

Calcium was present in very variable amounts in unweathered rocks, and was correlated with lead and phosphorus in the high and medium uranium concentration groups. Calcium also correlated with S, V, Fe(II), Nb, Ga, Li and F.

Titanium

In weathered samples, titanium was correlated with zirconium for all profiles.. Zirconium was present in much smaller amounts than titanium and followed the distribution of titanium. Acicular inclusions of rutile, and possibly sphene and zircon, have been observed in chlorite grains from M2 25 m. Rutile and anatase have been observed in the weathered zone at Koongarra, and are likely to be the major source of titanium (Gray, 1986). Titanium is generally assumed to be immobile in weathered systems (Milnes and Fitzpatrick, 1989), which is consistent with the depth profiles at M1 and M2 (Figure 4.11).

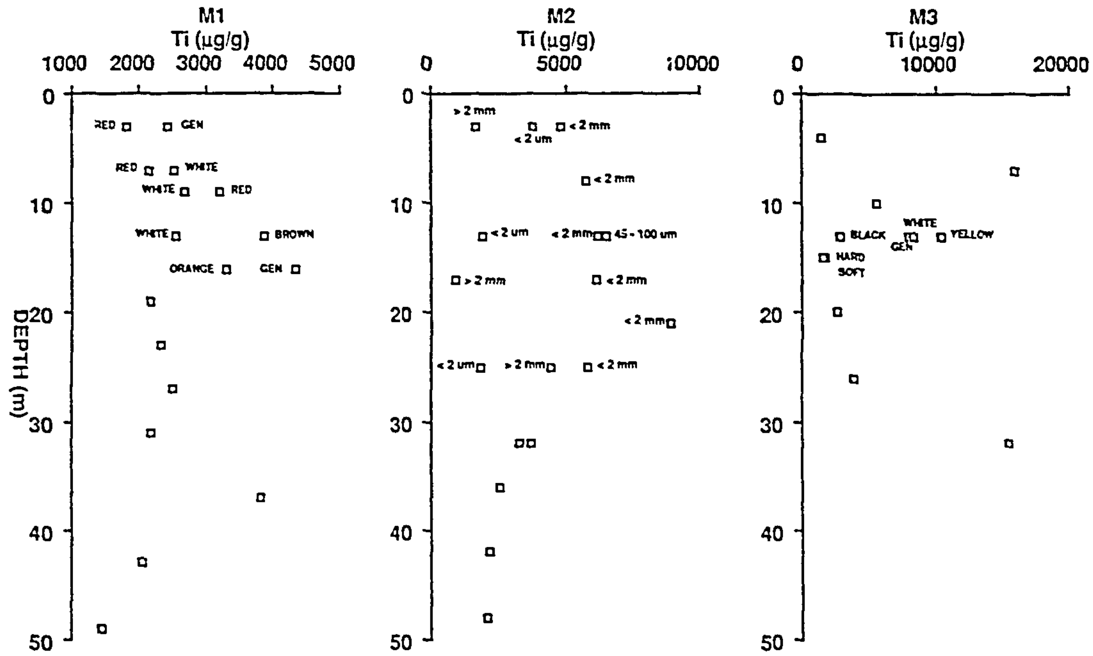

FIGURE 4.11 Titanium concentration depth profiles from holes M1, M2 and M3 (point labels denote subsamples. Points with no labels, or GEN were general bulk samples)

In data for unweathered samples compiled by Ferguson and Winer (1980), titanium was positively correlated to mica related elements (K, Rb, Na, Ba, Zr, Nb, Cs and Sc) in the highest and lowest uranium concentration groups. Biotite in particular may be considered a major initial source of titanium. The correlation of titanium with mica elements may suggest incomplete chloritisation of the biotite.

Vanadium

Vanadium was present in fairly similar and small amounts in the three M profiles (Figure 4.12). Vanadium appeared to be sensitive to iron oxide zoning, being most concentrated in iron-rich areas. At M1 and M2, vanadium was correlated with iron in weathered samples. At M3, vanadium was correlated only with yttrium. Norrish (1975) noted a high degree of association of vanadium with manganese and potassium, but this was not the case here. Norrish also suggested that iron oxides may entrap vanadium, as was observed here. Uranyl vanadate species are more insoluble than phosphates, and a uranyl vanadate of the carnotite-tyuyamunite series has been observed at Koongarra (Tucker, 1975). The amounts of vanadium found, while generally small (<300 µg/g) may influence the mobility of uranium, if present in a suitable form. Between 7 and 38% of the vanadium in weathered samples was "accessible" to the groundwater. Some of the unweathered uranium-rich samples contained much more vanadium than low uranium samples.

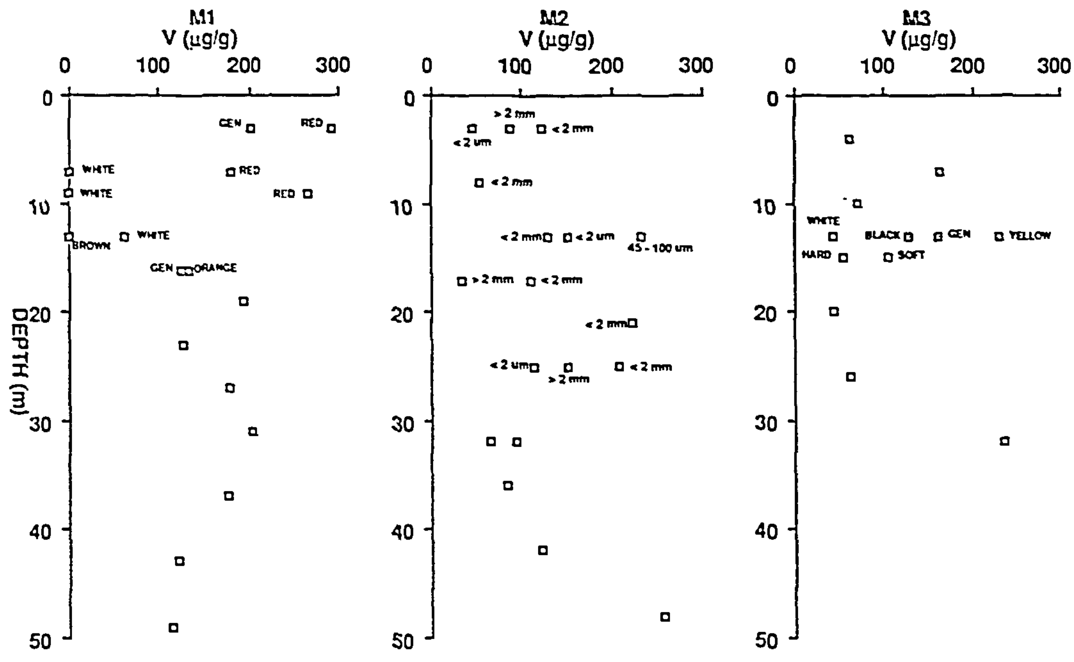

FIGURE 4.12 Vanadium concentration depth profiles from holes M1, M2 and M3 (point labels denote subsamples. Points with no labels, or GEN were general bulk samples)

Chromium

There were no clear trends in the distribution of chromium or in its relationships with other elements (Figure 4.13). Interestingly, chromium appeared to be concentrated in the fractions >2 µm and >2 mm in the M2 profile. Silicon was the only element to have a similar size distribution. In the weathered M3 samples, chromium correlated with uranium, and this may have been because of a relationship with iron oxides.

Manganese

The levels of manganese at M1 were considerably lower than at M2 and M3, especially in the weathered zone (Figure 4.14). At M2, there appeared to be some enrichment, especially in the top 10 m, followed by fairly constant levels with increased depth. M3 samples from 10 m and 13 m contained manganese oxide coatings, leading to the high manganese levels at these depths. These coatings were mainly lithiophorite. Lithium was correlated with manganese in weathered M3 samples. At M2, manganese was correlated with iron and other elements associated with iron oxides. The low values of manganese in weathered compared to unweathered samples at M1, suggest a leaching of manganese from this area with weathering. Furthermore, the low values of manganese in unweathered compared to weathered samples at M3, together with the observation of manganese oxides coating fissures, suggests deposition of manganese in the vicinity of M3 after leaching from an up-gradient position (M1). X-ray diffraction patterns from M1 10 m and 13 m "black", where the most manganese was observed, contained unique peaks which fit closest to lithiophorite as the manganese phase.

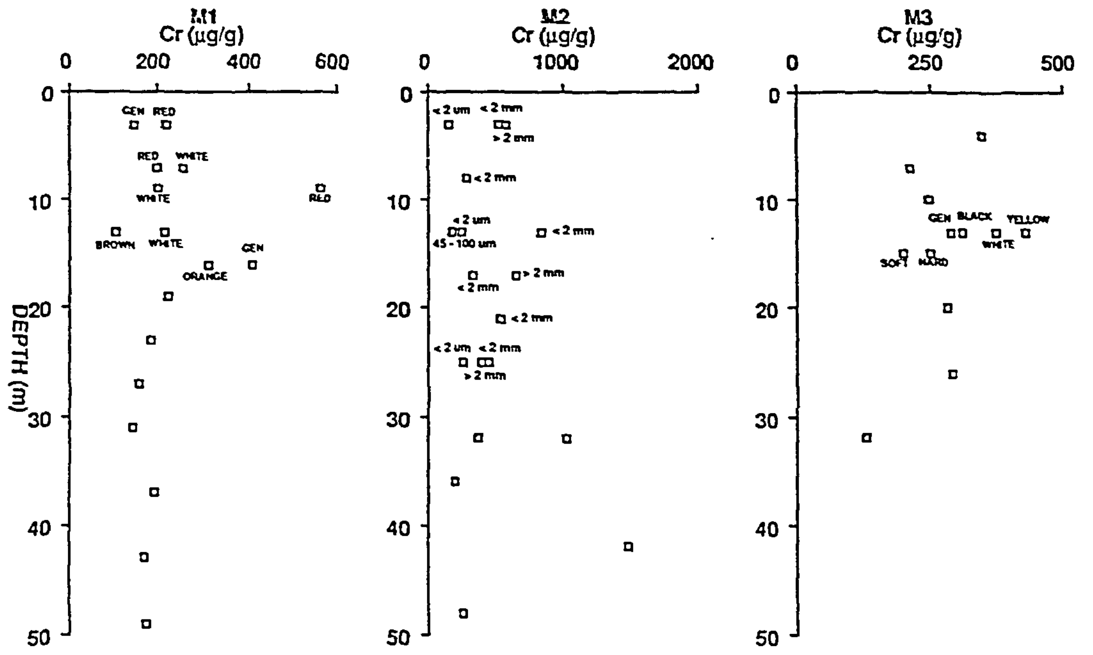

FIGURE 4.13 Chromium concentration depth profiles from holes M1, M2 and M3 (point labels denote subsamples. Points with no labels, or GEN were general bulk samples)

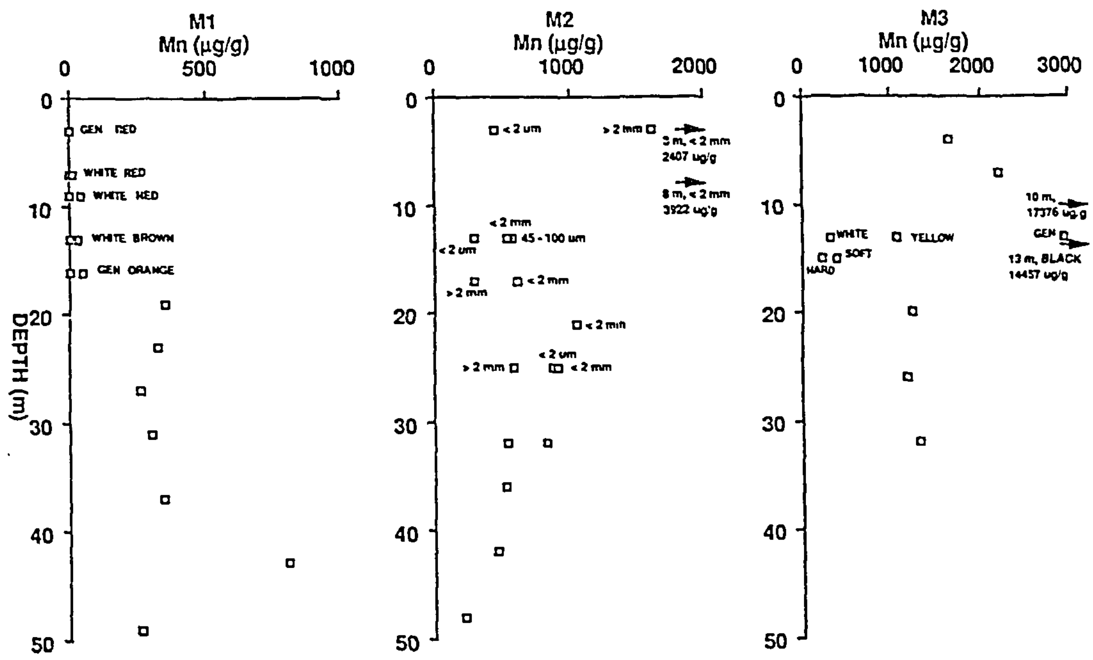

FIGURE 4.14 Manganese concentration depth profiles from holes M1, M2 and M3 (point labels denote subsamples. Points with no labels, or GEN were general bulk samples)

Similar amounts of manganese were present in mineralised and unmineralised unweathered samples. Analysis of manganese nodules in the weathered zone (DDH92 18.0 m) showed that these phases were the only phases that contained detectable quantities of cobalt. Taylor (1968) found that in many soil types, almost all the cobalt was associated with manganese phases. A strong relationship between concentrations of Mn, Ba and Co in phases extractable by Tamms acid oxalate reagent was found in weathered samples from Koongarra (see Section 4.3).

Iron

Iron was used as an indicator for iron oxides in the weathered zone, particularly goethite, hematite and ferrihydrite. The observed concentration of iron oxide was between 1% and 27% Fe_2O_3, with white and red domains being the most iron-depleted and iron-rich zones respectively. In M1 weathered samples, elements that were positively correlated with iron were P, V and As. Other elements that did not correlate significantly, but were much higher in iron-rich than iron-poor zones were Ni, Cu, Zn and U. In M2 weathered samples, the size fraction dependence of iron was variable with depth. At 3 m, iron was most concentrated in the <2 mm fraction, probably due to the formation of small nodules >2 µm. At 13 m and 25 m, iron was most concentrated in the <2 µm fraction, reflecting the fine nature of unaggregated iron oxides (Figure 4.15). Elements that correlated with iron in M2 weathered samples, were P, V and As (as for M1) and Mn, Cu, Y and Zr. In weathered M3 samples, elements that correlated with iron were P, As (as for M1 and M2), Zn, Ca, Ni and U.

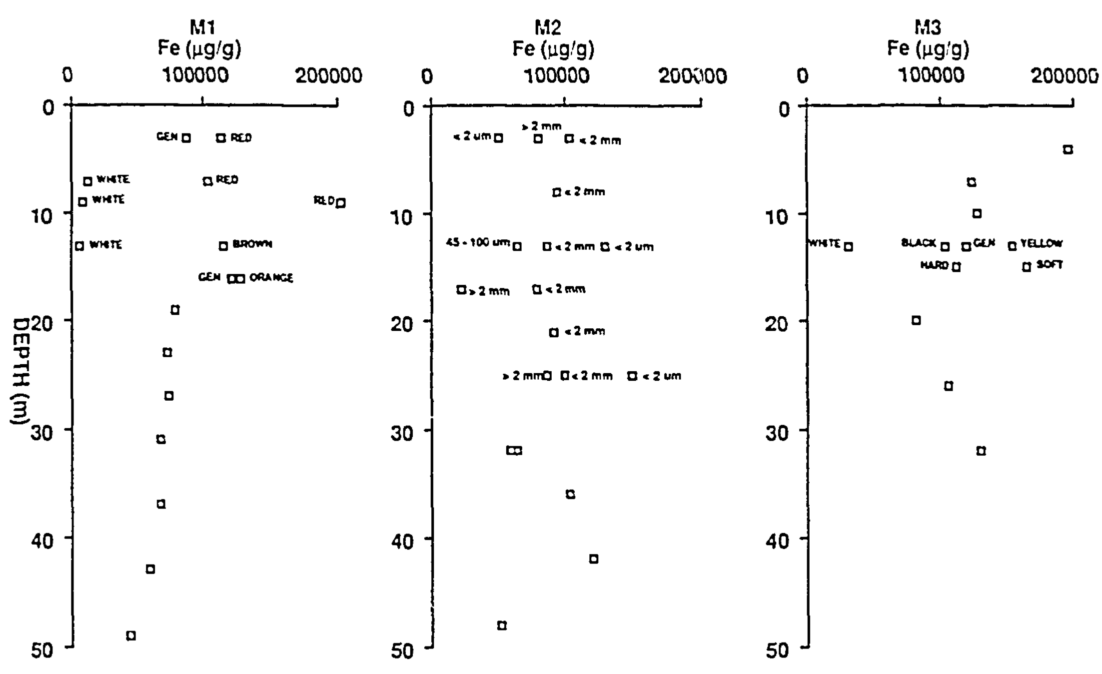

FIGURE 4.15 Iron concentration depth profiles from holes M1, M2 and M3 (point labels denote subsamples. Points with no labels, or GEN were general bulk samples)

From the depth patterns and correlations of elements, it appears that the elements most affected by the distribution of iron oxides were P, As, Mn, V, Ni, Zn, Cu and U. The strengths of these associations varies between profiles and with depth. The distribution of many elements, such as uranium and manganese, may be affected by physical factors, and may be restricted, for example, to the vicinity of fissures (Section 4.5).

In the data compiled by Ferguson and Winer (1980), iron was separated into ferric (Fe_2O_3) and ferrous (FeO) forms. For all uranium concentration groups, the Fe(II):Fe(III) ratios and the amounts of iron present were similar. In the high and medium uranium concentration groups Fe(II) correlated with magnesium, suggesting a high Fe(II) chlorite. Nickel also correlated with Fe(II) in the high uranium concentration group. The correlations with chlorite related elements suggest the presence of high Fe(II) chlorites associated with the uranium mineralisation. Iron(III) did not correlate with uranium or any major rock forming elements. The nature of Fe(III) in unweathered rocks is unclear, but may be due to hematitic alteration of the host rock.

Nickel

Nickel appeared to be associated with iron oxides in weathered samples. At M2 and M3, nickel correlated to uranium . There was more nickel present in unweathered samples from M1 than from M2 or M3 (Figure 4.16). In the unweathered sample data, compiled by Ferguson and Winer (1980), there was little difference in nickel content between mineralised and unmineralised samples, although nickel did correlate with uranium in samples with <40 µg/g uranium. Nickel also correlated with magnesium and Fe(II), which suggests an association with chlorite. Tucker (1975) suggested that elevated nickel concentrations are associated with uranium mineralisation at Koongarra.

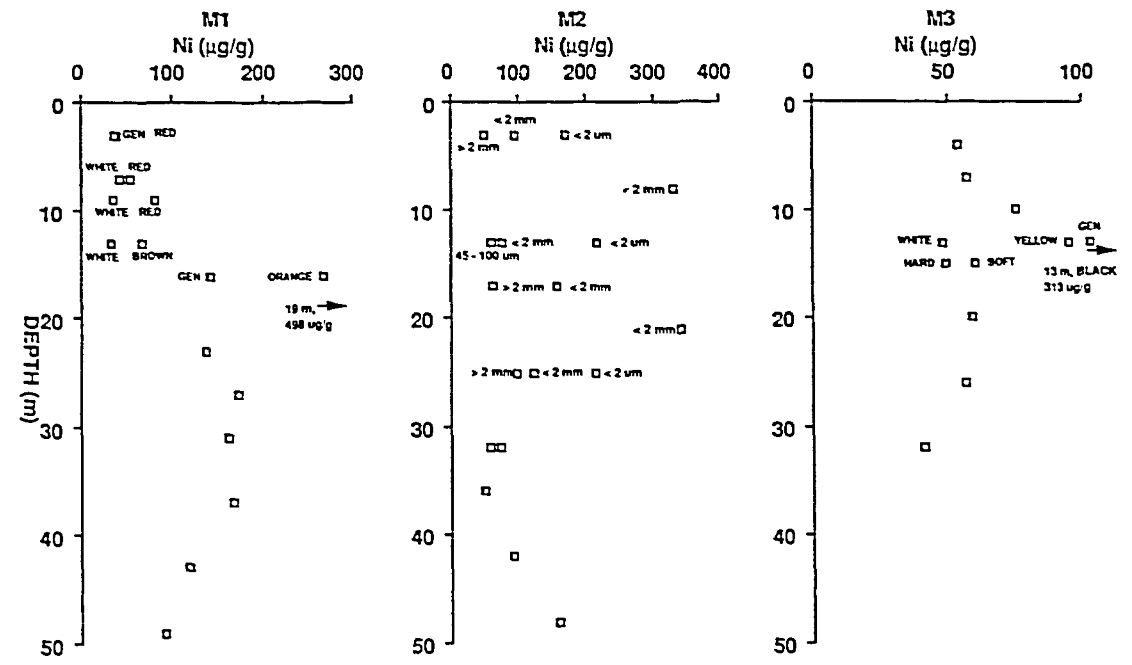

FIGURE 4.16 Nickel concentration depth profiles from holes M1, M2 and M3 (point labels denote subsamples. Points with no labels, or GEN were general bulk samples)

Copper

Copper was generally present in small amounts at M1 compared with M2 and M3, and M2 had far more copper than M3. Copper appeared to be very sensitive to particle size, with the <2 µm fraction being by far the most concentrated (Figure 4.17). Copper was correlated to zinc at M1, iron at M2 and phosphorus at M3. At M1, the copper concentration seemed to be influenced by the distribution of iron oxides. The depth profiles for copper were quite erratic and inconsistent down the three profiles, and did not follow similar trends to any other element. Harter (1979) reported that for subsurface soil horizons adsorption of copper was highly related to vermiculite content. In the present study, copper concentrations appeared to peak near the base of weathering. The three profiles tended to contain more copper in the weathered than the unweathered rock, suggesting a retention of copper through the weathering process.

In unweathered samples, copper correlated to vanadium in the high and medium uranium concentration samples. In the medium uranium concentration group copper correlated to sulfur. This suggests that chalcopyrite is an important copper phase. Chalcopyrite has been detected directly by SEM/EDS and microprobe, particularly in association with graphite and pyrite.

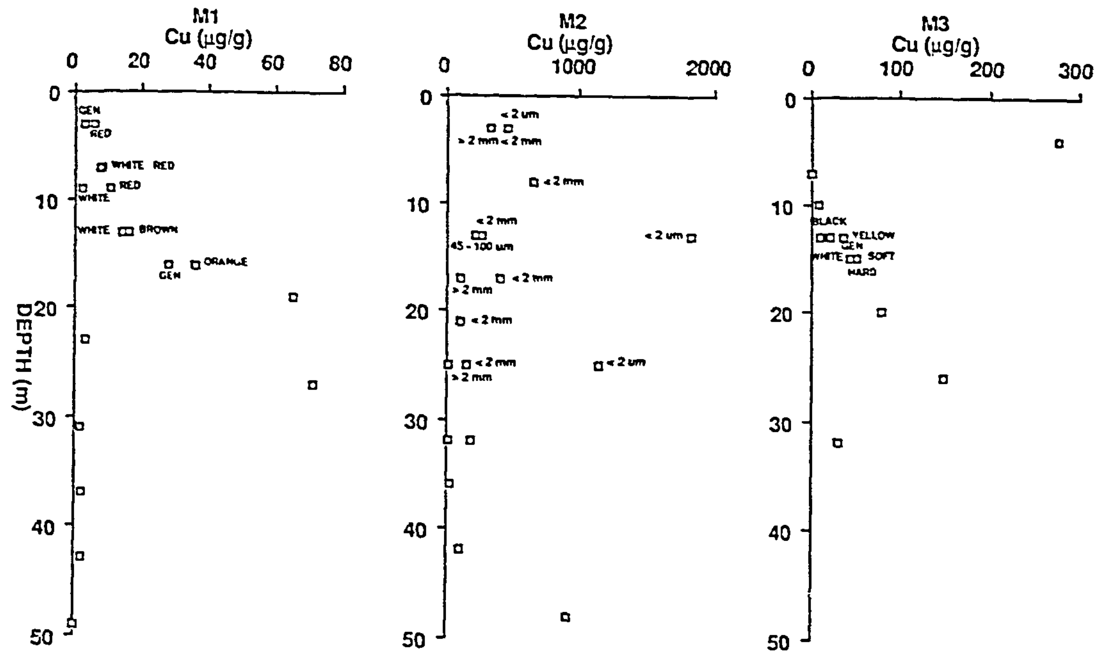

FIGURE 4.17 Copper concentration depth profiles from holes M1, M2 and M3 (point labels denote subsamples. Points with no labels, or GEN were general bulk samples)

Zinc

Zinc occurred in similar concentrations in the three M profiles, and similarly to copper, was very particle size dependent. At M2, zinc was most concentrated in the <2 µm fractions (Figure 4.18). At M1 and M2, the zinc concentrations peaked near the base of weathering. In M1 weathered samples, zinc appeared to correlate with uranium, as well as copper, and at M3, zinc correlated with iron oxides.

Gallium

Generally gallium followed the distribution of aluminium, and was present only in trace amounts (Figure 4.19). During weathering, gallium behaves like aluminium, and is often correlated to clay fractions in soils. Gallium also often shows a correlation with iron and manganese oxides (Kabata-Pendias and Pendias, 1984). In M3 weathered samples, gallium correlated with three elements that correlated with iron oxides (Ca, As, U). In unweathered samples (Ferguson and Winer, 1980), the gallium concentration was similar for the high and medium uranium concentration samples, which contained more gallium than the low uranium concentration samples.

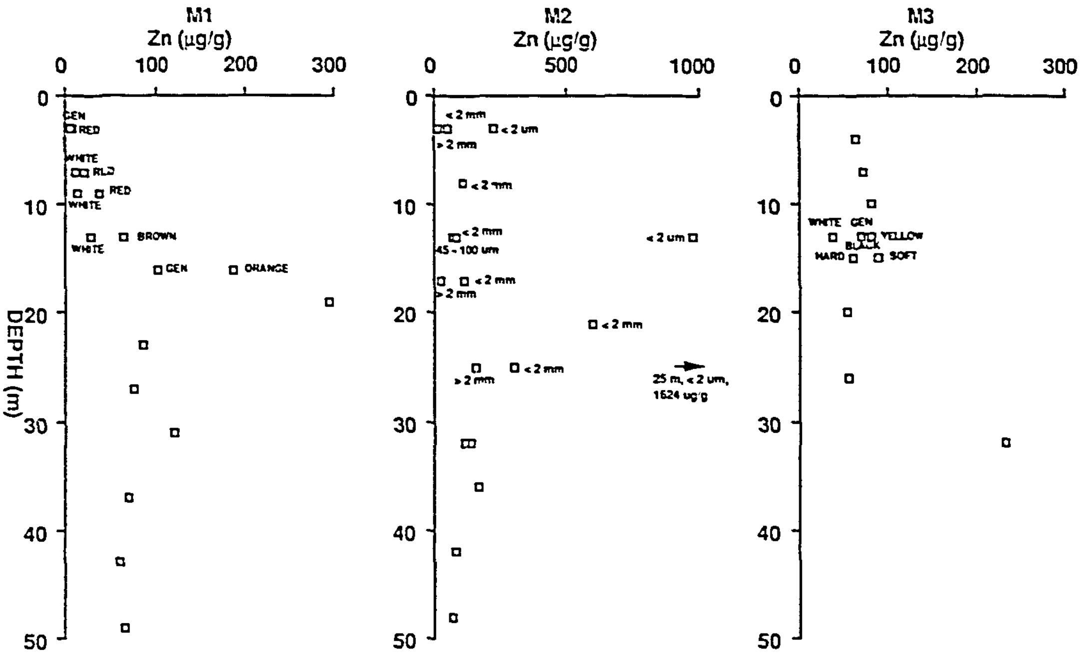

FIGURE 4.18 Zinc concentration depth profiles from holes M1, M2 and M3 (point labels denote subsamples. Points with no labels, or GEN were general bulk samples)

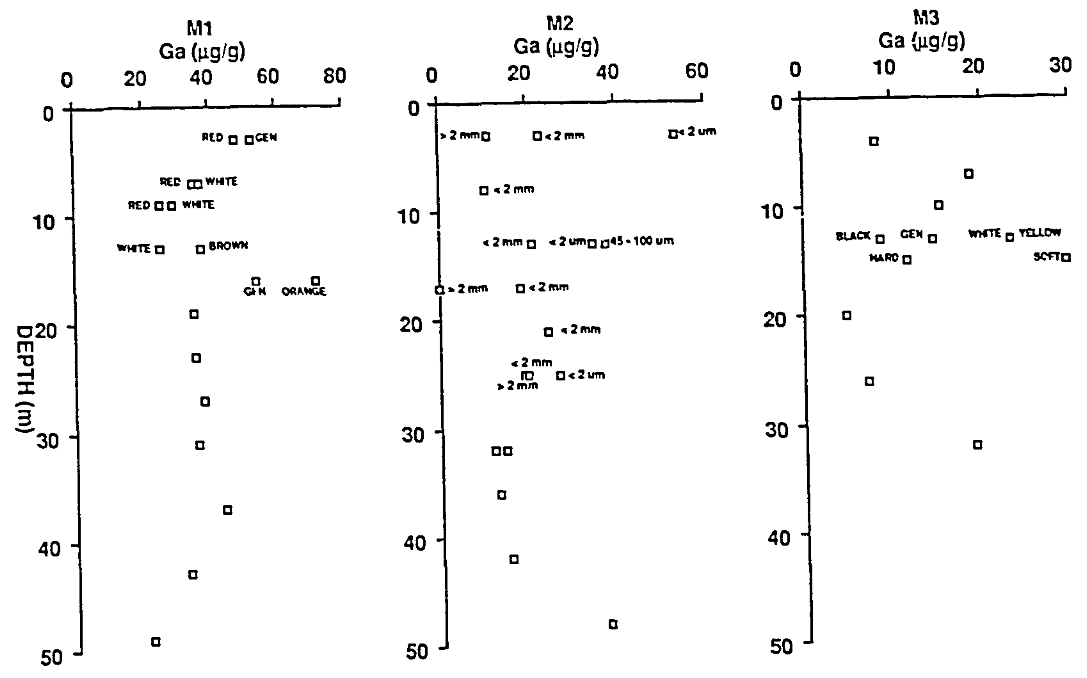

FIGURE 4.19 Gallium concentration depth profiles from holes M1, M2 and M3 (point labels denote subsamples. Points with no labels, or GEN were general bulk samples)

Arsenic

Generally present in trace amounts, arsenic appeared to be greatly affected by the distribution of iron oxides in the weathered zone, correlating with iron in the three profiles. A strong relationship between arsenic and iron oxides has been reported by several authors (eg. Belzille and Tessier, 1990). In the unweathered zone, arsenic was probably present with pyrite, being most concentrated in the high grade primary ore zone at the bottom of M2 (Figure 4.20).

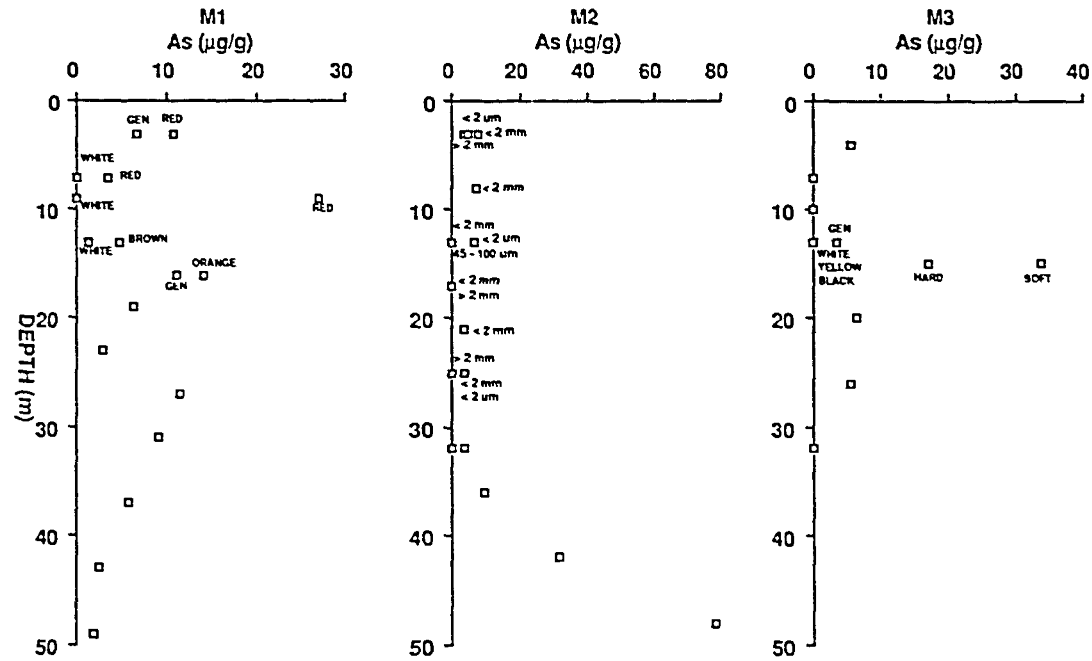

FIGURE 4.20 Arsenic concentration depth profiles from holes M1, M2 and M3 (point labels denote subsamples. Points with no labels, or GEN were general bulk samples)

Rubidium

Rubidium (Figure 4.21) was generally closely associated with potassium owing to similar geochemistry during weathering. Rubidium always correlated to potassium (mica) for the unweathered samples presented by Ferguson and Winer (1980).

Yttrium

Although present in trace amounts, yttrium may indicate the distribution of light rare earth elements. Similar concentrations of yttrium were observed in the three M profiles, with the largest amount being present in the sample from the bottom of M2 (high grade ore) (Figure 4.22). Yttrium was correlated with zirconium at M2 and M3, suggesting that zircon may be a major source of rare earth elements in the weathered zone. At M1, yttrium was correlated with potassium (mica). Yttrium correlated with zirconium in the high uranium concentration range samples and with various rare earth elements (La, Ce, Hf) in unweathered samples.

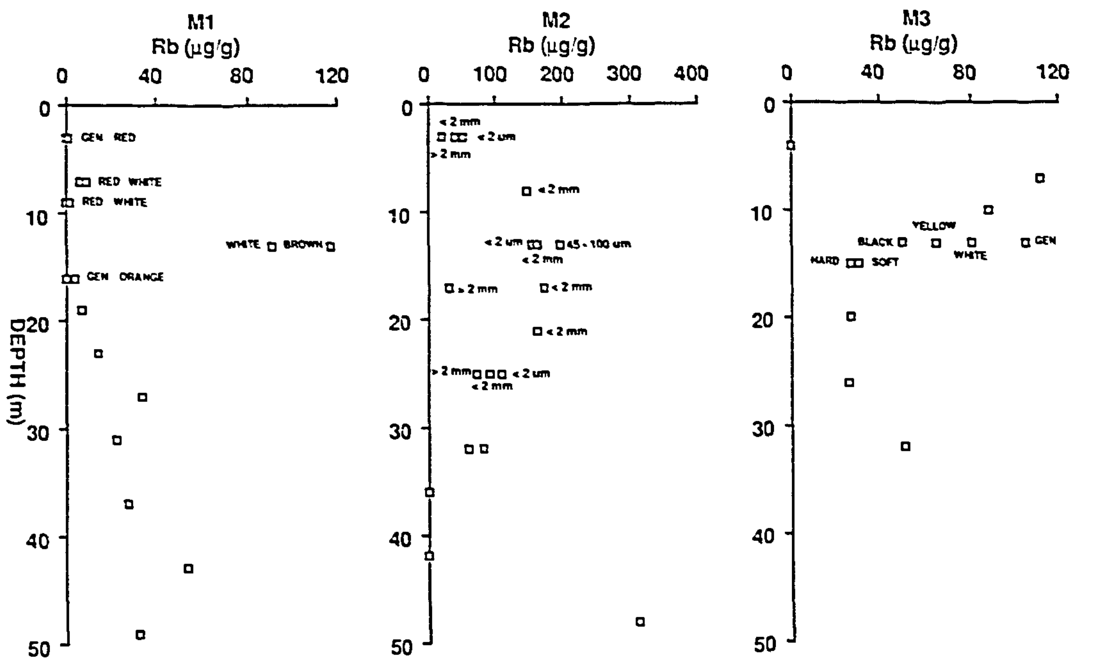

FIGURE 4.21 Rubidium concentration depth profiles from holes M1, M2 and M3 (point labels denote subsamples. Points with no labels, or GEN were general bulk samples)

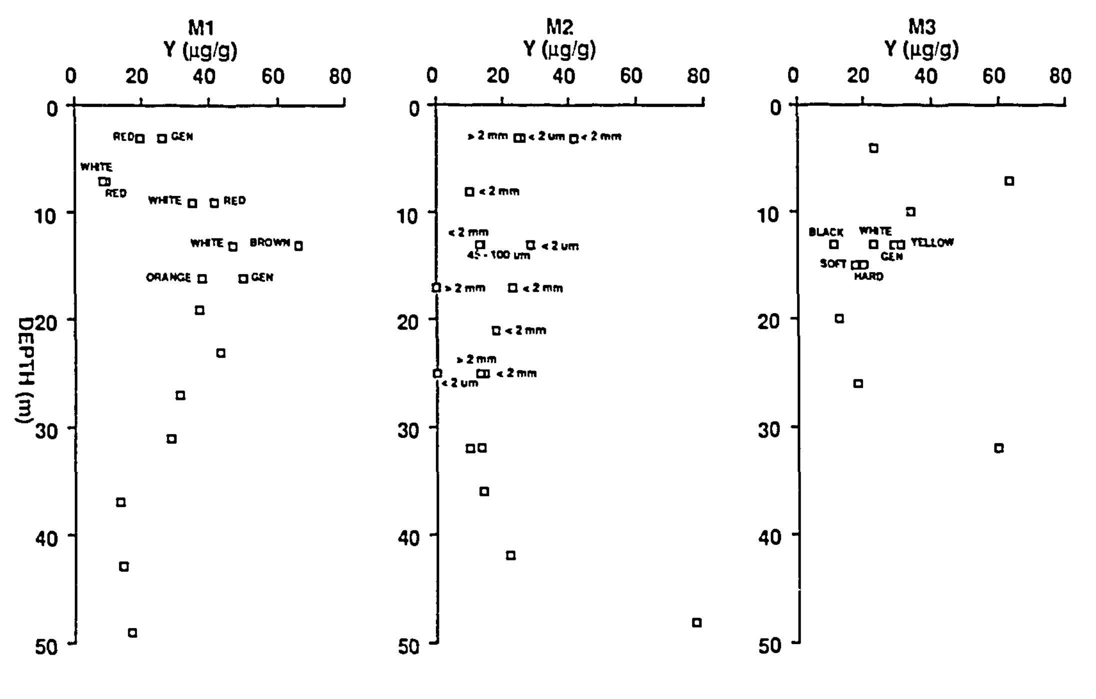

FIGURE 4.22 Yttrium concentration depth profiles from holes M1, M2 and M3 (point labels denote subsamples. Points with no labels, or GEN were general bulk samples)

Zirconium

Zirconium has a similar geochemistry to titanium and correlated with titanium in weathered samples from M1 and M3 and in unweathered, low uranium concentration samples. Zirconium occurs in zircon grains, with some also present in sphene. Zircon may be a major source of ^{232}Th and rare earth elements (see the discussion on yttrium). Zircon grains have been found in the weathered schist at Koongarra. In unweathered samples with high and medium uranium concentration, zirconium correlated with thorium and yttrium.

Zirconium is considered to be an immobile element (Milnes and Fitzpatrick, 1989) that tends to become enriched with weathering and the removal of other constituents. This appeared to be the case at M1 and M2, but the zirconium distribution was erratic at M3, troughing at the base of weathering (Figure 4.23). The weathered zone at Koongarra has a bulk density approximately 20% less than that of the unweathered rock (see Volume 4 of this series). At M1 and M2, the concentration of zirconium in the weathered zone is approximately twice that of the unweathered zone (1.9 and 2.2 times respectively on average). This suggests a loss of about 50% of the rock material by mass due to weathering, corresponding to a reduction in rock volume of about 38%.

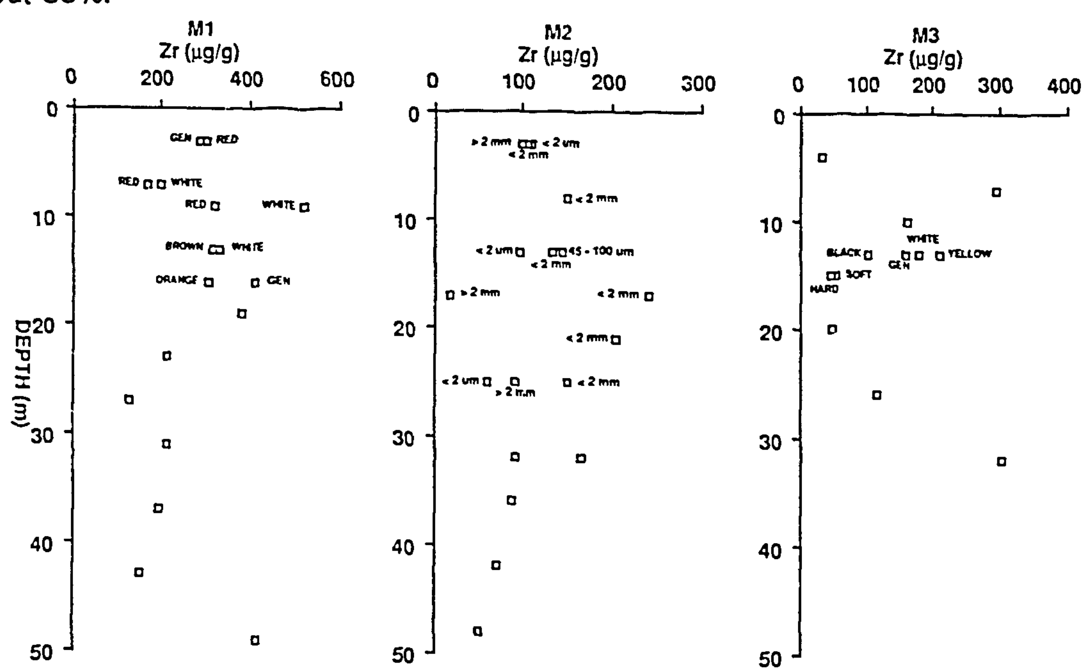

FIGURE 4.23 Zirconium concentration depth profiles from holes M1, M2 and M3 (point labels denote subsamples. Points with no labels, or GEN were general bulk samples)

Lead

Lead concentrations were generally below detection limit in the weathered zone, except at M1, where lead correlated with uranium. At M2 all values of lead in the weathered zone, except at 3 m and 8 m, were below detection limits. Levels of lead were generally higher in the weathered zone of M1 than M2, even though there was much more uranium in the M2 weathered samples. This illustrates the greater mobility of uranium than lead and that uranium was leached from the weathered zone at M1. In the sample from M2 3 m, the levels of lead were higher than the levels of uranium. This suggests that uranium may have been leached from this material; from the size fractionation it would appear that the lead was associated with small iron oxide nodules. The highest value for lead was obtained from the high grade ore zone at the bottom of M2 (Figure 4.24).

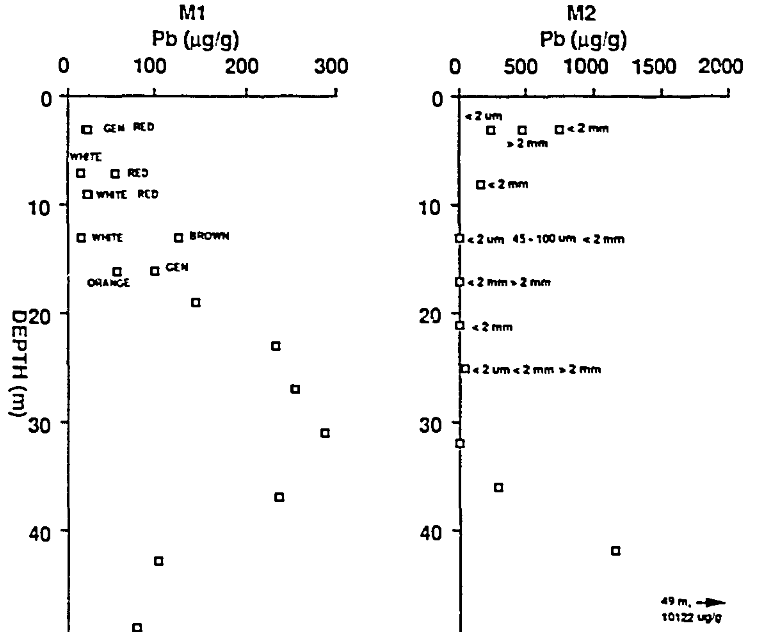

FIGURE 4.24 Lead concentration depth profiles from holes M1 and M2 (point labels denote subsamples. Points with no labels, or GEN were general bulk samples)

Lead was much more concentrated in unweathered mineralised samples than in low or medium uranium concentration samples. Lead correlated with uranium in unweathered samples containing medium uranium concentrations. In the high uranium concentration samples, lead correlated positively with S, Ca and Cu, and negatively correlated with Al, Ti, Na and Th; the correlation with sulfur suggests a relationship with sulfides, such as galena. The much larger amount of lead in mineralised samples, compared to barren rock, suggests a large radiogenic origin of much of the lead. However, some of the samples with <40 µg/g uranium also contained significant amounts of lead, up to 300 µg/g, which suggests an authigenic component of the lead concentration.

Uranium

At M1, the levels of uranium in the weathered zone were depleted compared to the unweathered samples, whereas at M2 and M3, most uranium was in the weathered

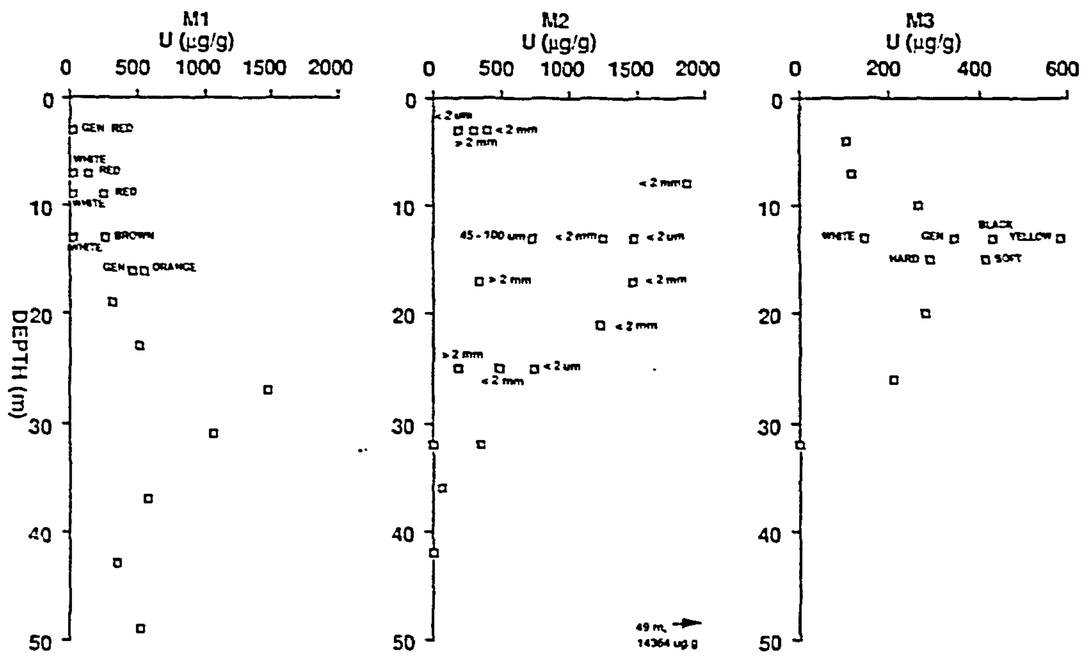

FIGURE 4.25 Uranium concentration depth profiles from holes M1, M2 and M3 (point labels denote subsamples. Points with no labels, or GEN were general bulk samples)

zone (except for the high grade ore sample at the bottom of M2) (Figure 4.25). At M1, uranium correlated with phosphorus, suggesting the possibility of uranyl phosphates, and was sensitive to iron oxide zoning. In weathered M2 samples, the uranium again correlated with phosphorus and followed a similar size fractionation to iron. At M3 weathered samples, uranium was not correlated with phosphorus, but was correlated with iron. Table 4.1 compares the amounts of uranium and phosphorus, and gives the proportion of phosphorus that could be included in uranyl phosphates. It can be seen that in all cases there is ample phosphorus present for all the uranium to be in the form of uranyl phosphates. This suggests that a phosphorus concentration anomaly, superimposing the uranyl phosphate zone, is not required to account for the presence of uranyl phosphate minerals. At M1, uranium was also correlated with lead and zinc, and at M2 also with nickel and rubidium. At M3, uranium was also correlated with other elements correlated with iron (Ca, Ni, Zn and As), as well as with Na, Cr and Ga.

In unweathered M-series samples, uranium appeared to be associated with a block of trace elements; P, S, V, Cu, Ga, Rb, Y, Nb and Pb. These elements may be involved in the uranium mineralisation near the graphitic hanging wall unit. In unweathered samples from the Ferguson and Winer (1980) data set, uranium did not correlate with any major rock-forming element. Nash and Frishman (1983) also found that uranium did not correlate with any major elements at Ranger, and Ferguson and Winer (1980) reported a similar result for Jabiluka.

TABLE 4.1

URANIUM AND PHOSPHORUS CONTENTS OF WEATHERED SAMPLES

Hole/Depth	Subsample	[P] (µg/g)	[U] (µg/g)	U/P (g/g)*
M1 3 m	general	176	28	0.14
M1 7 m	red	761	143	0.24
M1 7 m	white	161	31	0.23
M1 9 m	red	2073	247	0.14
M1 9 m	white	148	31	0.22
M1 13 m	brown	973	265	0.27
M1 13 m	white	137	21	0.21
M1 16 m	general	1350	462	0.38
M1 19 m	general	605	317	0.58
M1 23 m	general	519	512	1.1
M1 27 m	general	575	1481	2.4
M1 31 m	general	438	1061	2.8
M2 3 m	<2 mm	275	401	1.6
M2 3 m	>2 mm	319	296	1.1
M2 8 m	<2 mm	429	1858	4.5
M2 13 m	45-100 µm	446	720	1.6
M2 13 m	<2 mm	322	1246	3.6
M2 17 m	<2 mm	550	1462	2.8
M2 17 m	<2 mm	245	336	1.6
M2 21 m	<2 mm	343	1221	3.6
M2 25 m	<2 mm	522	488	1.0
M2 25 m	>2 mm	406	188	0.52
M3 4 m	general	1285	103	0.10
M3 7 m	general	199	117	0.59
M3 10 m	general	218	262	1.3
M3 13 m	general	481	345	0.79
M3 15 m	hard	363	290	0.95
M3 20 m	general	379	276	0.89

* U/P for saleeite = 7.7 (g/g)

Ferguson and Winer (1980) reported significant correlations between uranium and other elements, over a number of uranium concentration ranges, for the pooled data of Cahill Formation rocks. Elements correlating with uranium in different uranium concentration groups, at the 95% level of confidence were:

uranium concentration > 500 μg/g : As, Nb, La, Ce, Mo, Pb, Sc and Co.

uranium concentration > 40 μg/g : As, Nb, Cu, W, Mo, Pb, Sc and Co.

uranium concentration < 40 μg/g : P.

Some elements (Sc, Co, Cu, P, La and Ce) correlated to uranium in Cahill Formation rocks at the regional scale, but not for unweathered rocks at Koongarra. Lanthanum and cerium (the light rare earth elements) were negatively correlated to uranium at Koongarra. Manganese, Cs, Sn and Ni correlated with uranium at Koongarra, but not at the regional scale; tin and nickel seemed to be uniquely associated with the Koongarra mineralisation (cf Ferguson and Winer (1980) and Nash and Frishman (1983)). At Koongarra, the relationships between uranium and Sn, Y, La and Ce, appeared to be the reverse to that observed regionally and at Jabiluka.

Rare earth elements

The Cahill Formation rocks in the Northern Territory have a pattern of rare earth elements similar to Post-Archaean Australian Sediments (PAAS) (McLennan and Taylor, 1979, 1980). Rare earth element patterns in samples from M1, M2 and M3 were compared to PAAS, by first normalising the concentrations to the samples La value, then normalising the value to the corresponding concentration of the element in PAAS.

Figure 4.26 shows representative plots of La and PAAS corrected rare earth element concentrations. Most samples from M1 showed patterns similar to that shown by M1 31, having much larger amounts of heavy rare earth elements (HREEs) with a maximum at about Dy. The exceptions were subsamples of heavy bleached clay bands, the unusually micaceous sample at 13 m and the surficial sample. These samples had trends similar to PAAS. Both weathered and unweathered schist samples from M1 gave high HREE patterns.

Virtually all samples from M2 showed REE patterns near to PAAS, as for M2 32 m. The exception was at 25 m, where higher relative HREE contents were observed. Samples from M3 also gave similar trends to PAAS (M3 31 m in Figure 4.26). An exception was the high manganese subsample from M3 13 m, which showed an enriched HREE pattern, similar to those observed for samples from M1. The fissure

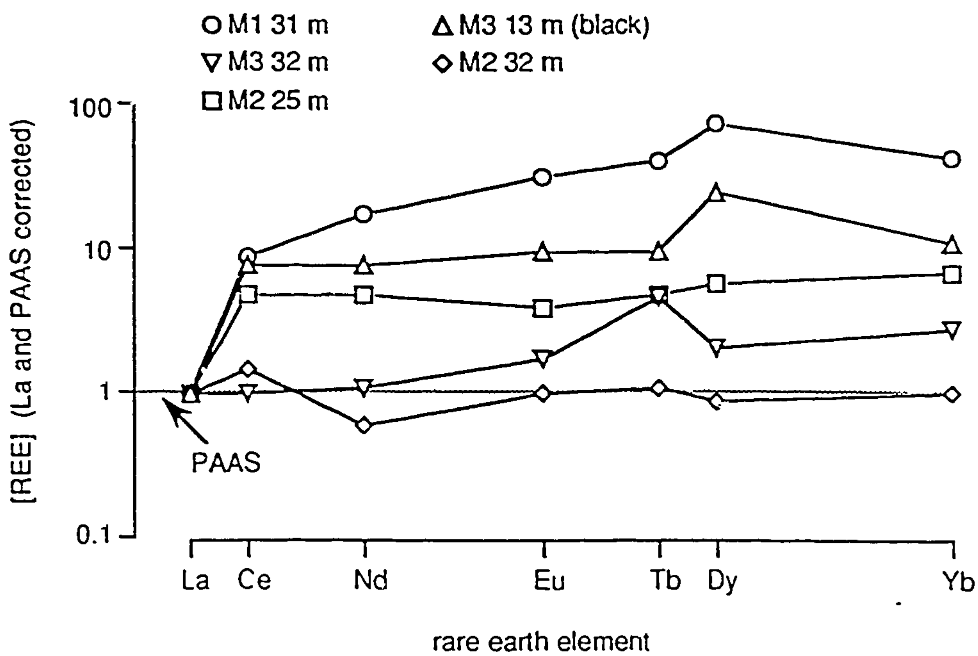

FIGURE 4.26 PAAS and La normalised rare earth element contents of representative samples from M1, M2 and M3

coating material may reflect the pattern of REEs in the groundwater, since it can be regarded as a precipitate, and not the bulk rock.

The patterns of the REEs in samples from M1, suggest that the primary mineralised area is characterised by a negative La anomaly, and is relatively very high in HREEs, with a maxima at about dysprosium. This is similar to published data on high uranium concentration samples from the Cahill Formation (McLennan and Taylor, 1979, 1980). Similar relative REE patterns occurred at the base of weathering at M2 (25 m) and in an M3 sample containing large amounts of manganese coating fissures (13 m black). Trends of REEs similar to the zone of primary mineralisation may suggest contact of the sample by water from that zone.

Bleached heavy clay bands and the surficial sample at M1 showed similar REE patterns to PAAS and samples from non-mineralisation zones at Koongarra. Two possible explanations may be proposed; that these samples never experienced the REE signature of the mineralised zone, either at the time of primary mineralisation or during weathering, or, that the weathering and pedological processes involved in these samples, including redox processes, resulted in the preferential leaching of HREEs. Here we propose that the uranium mineralisation was associated with the deposition of REEs greatly enriched with HREEs, and that this occurred preferentially in chlorite/biotite phases. This would explain near PAAS patterns at M1 13 m. This HREE enriched inprint would be in geochemically different positions to the pre-existing suite in zircon and monazite. Consequently it may be expected that the HREEs may be preferentially leached from the bleached clay zones.

4.2 The Distribution of Elements Over the Site

An elemental analysis of over 110 samples has been carried out, both within the ARAP project, and previously. The samples included material from W-series water sampling points, some samples from south of the deposit, and samples being used in the sorption program. Where available, samples from four depths were selected, representing shallow (near the base of surficial sands), mid-weathered, deep weathered/transition, and unweathered zones. The complete set of data is included in Appendix 4.

There appears to be a general depletion of magnesium from the weathered zone, but with a more intensive removal from W1, W4, C7, and M1 and M2 than from other sites. These holes are located north-west of the graphitic hanging wall unit and within the inner halo of hydrothermal alteration. Magnesium-rich chlorites tend to be dominant within the inner alteration halo, whilst outside of this zone iron-rich forms tend to dominate (Section 3).

Carbonate has been observed in unweathered samples from C1, but C1 samples did not show relatively high magnesium or calcium concentrations. Outside of the inner alteration halo, there is a general excess of calcium relative to phosphorus for apatite to be the dominant calcium containing mineral in the unweathered zone. Calcium levels at all sites were strongly depleted in the weathered zone.

Sulfur has also been lost from the weathered zone, after oxidation of sulfide. However, shallow samples at W3 and W4 contained measurable sulfur, probably as sulfates. In the unweathered zone, sulfide seemed widely distributed south of the graphitic hanging wall unit, except in the vicinity of M4, C6 and C8.

The distribution of potassium, reflecting the concentration of mica (with a mass ratio of about 12:1 for mica:potassium), was very heterogeneous, due to the presence of bands of mica. There did appear to be less potassium in samples from the inner alteration halo (such as M1 and W1), than in those outside that zone.

Manganese appears to be strongly depleted in the near surface except near C8 and M4. Manganese is depleted from the weathered zone at depth from W1 and M1. Slight depletion may have occurred at the other sites except at C1, M4, C7, M2 and M3 which appear to have gained some manganese. Iron also seems to be depleted in the weathered zone around W1 and M1 and possibly W4.

No regions of very high or very low phosphorus were identified, except in association with the unweathered graphitic hanging wall unit (eg M2 49 m), where phosphorus concentrations were high. In unweathered samples, phosphorus tended to correlate with calcium, and calcium tended to correlate with sulfur. This suggests an association between apatite (as the major source of phosphorus) and sulfide zones. Calcium tended to be strongly leached from the weathered zone, but phosphorus was not so sensitive to weathering. Some unweathered samples from within the inner halo of alteration had an excess of phosphorus relative to calcium for it to be present only as apatite.

Titanium, which may reflect biotite or TiO_2 was less concentrated in samples from W1, M1, W4, M2 and W3 than at the other sites. The depth patterns of titanium concentration suggest little leaching with weathering, and at sites C8 and C4 there was a possible enrichment of titanium near the surface. Generally, the samples contained similar amounts of silicon, mainly representing quartz. Surficial samples from W3 and W4 contained more quartz than the other samples, possibly from surficial sand contamination and intense weathering. The distribution of uranium is described in Section 5 of this Volume.

4.3 Elements in Accessible and Inaccessible Phases

Tamm's acid oxalate (TAO) extractions were carried out on several weathered zone samples, as part of the uranium series disequilibria program. Twenty six extracts and residual digests were analysed to estimate the amounts of elements accessible for interaction with the groundwater (TAO-extractable); the results for the ICP-MS and AES analyses are given in Appendix 5. A spectral scan was also used to obtain semi-quantitative values for many more elements, and these results are given in Table 3 of Appendix 5.

The main constituents of the TAO-extractable phases (excluding oxygen), were Fe, Al and Mg, and occasionally manganese and potassium, (concentrations >1 mg/g in the extractable phase). Iron and aluminium correspond to the major expected amorphous phases, such as ferrihydrite, while magnesium is the major exchangeable cation in the system. The concentration of silicon was not determined, owing to acidification of the samples and probable precipitation of silica. If dissolution of clay minerals had occurred during this extraction, it was probably minor considering that the percentage of total aluminium extracted was generally small.

Manganese, Co, Cu, U, P and Pb were the elements that were consistently highly extractable, with averages of >25% extracted; on some occasions >25% of the iron was extractable. These elements are those with distributions expected to be controlled by iron and manganese oxides in the non-mineralised zone. Manganese had the highest average extractability (47.5%), illustrating the dissolution of MnO_2 by TAO (Mendelovici and Sagarzau, 1991). Elements with consistently low percentage extractable (<10%) were Rb, Zr, K, Al, Ti and the light REEs. These elements represent the more stable minerals such as muscovite (Rb, K, Al), clays (Al), zircon (Zr, REEs) and anatase and rutile (Ti). If all the zirconium and titanium is assumed to be present as zircon and TiO_2, respectively, there was an average of about 350 μg/g zircon and about 0.4% TiO_2 in the samples.

The concentrations and extractability of most elements was very variable. This is particularly the case for iron, which has a concentration range in the extractable phases of 1.3-17.5 mg/g and an extractability of 2-60%. Some of the heterogeneity can be accounted for by considering the sample descriptions. If all unweathered and very surficial samples are discounted, the range of iron concentrations in extractable phases becomes 4.6-17.5 mg/g and the extractability 5-48%.

The iron results for samples in the weathered zone are summarised in Table 4.2. The data is separated into two groups according to the total iron content of the samples; Fe <50 mg/g, and Fe >50 mg/g. This also has the effect of grouping mineralogically different samples. The samples with <50 mg/g iron were mainly pale or limonitic and highly micaceous samples from along the DDH52-PH94 transect, away from the ore zone. The range of concentrations of extractable iron for this group was 4.6-14.5 mg/g, with an average of 10 mg/g. The percentage extractable iron for this group was 12-48%, with an average of 30%. The group with total iron content >50 mg/g generally had more colour, contained less mica and were mostly evolved from chloritic schist. For this group the range of extractable iron concentrations was 5.0-17 mg/g, with an average of 10.3 mg/g, and the percentage extractable iron range was 4-17%, with an average of 10.3%. This shows that the two groups had similar amounts of extractable iron, but very different amounts of non-extractable iron oxides. TAO extraction dissolves amorphous material, while the residual contains the crystalline iron oxides.

At most of the sites providing samples with total Fe >50 mg/g, different depths gave similar extractabilities of iron, and to a lesser extent uranium. The $Fe_{amorphous}/Fe_{crystalline}$ ratio for this group ranged from 0.04 to 0.20, with an average of 0.12. The concentration of ferrihydrite in the weathered zone samples, assuming a composition of about $5Fe_2O_3.9H_2O$, would have ranged from about 7 to 29 mg/g, assuming that all iron extracted was from ferrihydrite (see also Section 3.2). If we assume that all the non-extractable iron was present as goethite, then the concentration of goethite would have been about 2 to 20%.

No correlations of element concentrations with iron were observed in the extracts. The analysed samples were selected from a large area of the site, and it was expected that the distribution of iron oxides would be independent of many of the factors governing the distribution of other elements (such as uranium) for example the groundwater flow direction. There was, however, an apparent strong relationship between the concentrations of Mn, Ba and Co in the extracts, with $R^2 = 0.852$ between barium and manganese. Radium values did not correlate with Mn, Ba or Co in the extracts, but this may be due to them having different sources. The geochemical behaviour of Ra is very similar to that of barium, and therefore radium may be expected to be preferentially associated with manganese phases, where present. The pattern of manganese in the weathered zone at Koongarra has been shown to be "washed out" (see Section 4.1) from near the primary zone and deposited in fissures down-flow. No other element-element concentration correlations were found.

TABLE 4.2 IRON CONCENTRATIONS IN "ACCESSIBLE" PHASES

Hole	Depth (m)	[Fe] extracted (mg/g)	% Fe extracted	Total [Fe] (mg/g)	Description
total Fe <50 mg/g					
PH60	6.8	8.2	17	48	W QMS pale
PH60	11.5	9.4	20	47	W QMS pale
PH89	9.8	4.6	12	38	W QMS pale
PH89	16	12	44	27	W LQMS pale
PH90	11.5	13	33	40	W QMS pale
PH90	16	8.0	20	40	W LQMS grey brown
PH91	9.9	9.0	48	19	W QMS pale
PH91	14.4	14	38	38	W QMS pale
PH94	9.9	11	45	29	W LQMS + clay
PH94	14.4	10	24	42	W LQMS
total Fe >50 mg/g					
M2	10	8.2	10	82	W QCS
M2	14	7.9	9	88	W QCS
DDH4	11.1	6.2	5	124	W QCMS clay yellow
DDH4	21.1	17	13	135	W QCMS pale brown
PH55	14	17	15	110	W QCMS + clay
M4	11	5.7	5	114	W QCMS
M4	15	5.0	4	125	W QCMC
M5	11	10	11	91	W QCMS
M5	15	11	11	100	W QCMS
PH93	9.9	12	17	72	W QCMS
PH93	14.4	13	13	100	W QCMS

W = weathered, Q = quartz, M = muscovite, S = schist, L = limonitic, C = chlorite

There were many correlations between the percentage of each element extracted by TAO. Elements with a degree of extractability significantly correlated to the extractability of iron were: V, Ni, Cu, P, Al and Ti. The proportion of uranium extracted by TAO was related to the amount of iron extracted in the group of samples with total Fe <50 mg/g. In the more iron and uranium rich groups, the proportion of uranium extracted appeared to be independent of the proportion of iron dissolved, ie $U_{amorphous}/U_{crystalline}$ was not related to $Fe_{amorphous}/Fe_{crystalline}$. The amount of extractable material appeared, to some extent, to be dependent upon the sampling position. Only small amounts of Al, Mg, Fe and Mn were extracted from samples from DDH52, and the amounts seemed to increase with distance, to a maximum around PH55.

Rare Earth Elements

The concentrations of rare earth elements in TAO-extractable and residual phases are included in Appendix 5. The concentrations were determined by ICP-MS, and are quantitative (standardised) for La, Ce, Nd, and Sm, and semi-quantitative for Eu, Gd, Tb, Dy, Ho, Er, Tm, Yb, and Lu. The errors associated with the semi-quantitative results may be up to 20%. Generally the amounts of lanthanum in the samples were similar to amounts in Post-Archaean Average Australian Sedimentary rocks (PAAS) (McLennan and Taylor, 1979). However there are some striking differences in the relative abundances.

Figure 4.27 shows the average percentage of each REE extracted by TAO. For most samples, only a small proportion of the total REE content was extractable, and the light REEs tended to be less extractable than the heavy REEs. There appears to be an increase in the proportion accessible (TAO-extractable) with increasing atomic number, particularly between cerium and dysprosium.

Samples from M2, PH89, PH93 and one sample from PH94 showed high extractability (>10%) of light REEs and the highest extractability of thorium. This suggests dissolution of accessory thorium- and REE-containing minerals such as monazite. Cerium was the least extractable of the REEs, which suggests that cerium is preferentially included into inaccessible, crystalline phases.

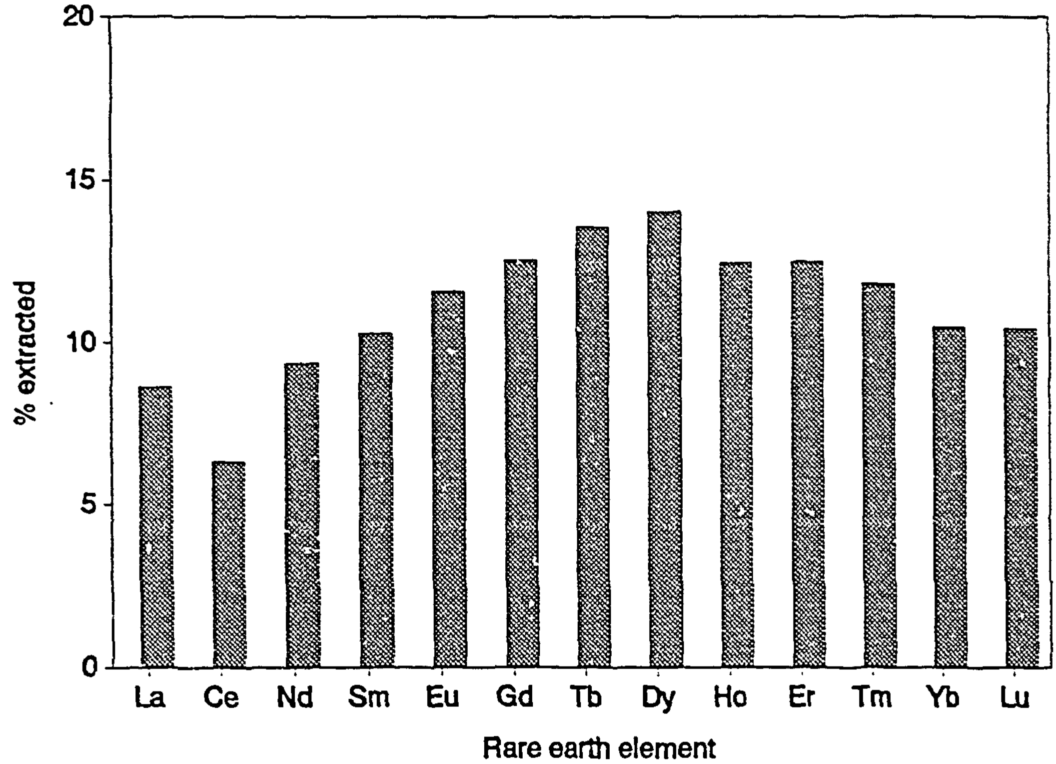

FIGURE 4.27 Average extractability of rare earth elements by TAO (n=22)

The results were normalised to the lanthanum value of the samples, and then to the corresponding values for PAAS (La normalised). The normalised trends of the REEs are shown in Figures 4.28 and 4.29; (a) for TAO and (b) for residual. The trends show that some samples are enriched in the heavy REEs, particularly in the TAO-extractable phases. In accessible phases there was a negative cerium anomaly present in some samples, which was reflected in a positive anomaly in the inaccessible phases (Figure 4.28). This suggests a preferential inclusion of cerium into crystalline, inaccessible phases. The samples that did not show a negative cerium anomaly in the accessible phases (M4, DDH4, PH55 and PH60 in Figure 4.29), were also those most strongly enriched in the heavy REEs. These samples were those nearest to the zones of hydrothermal alteration, except for the M2 samples; site M2 intersects the graphitic hanging wall unit, and this may explain the near PAAS trends.

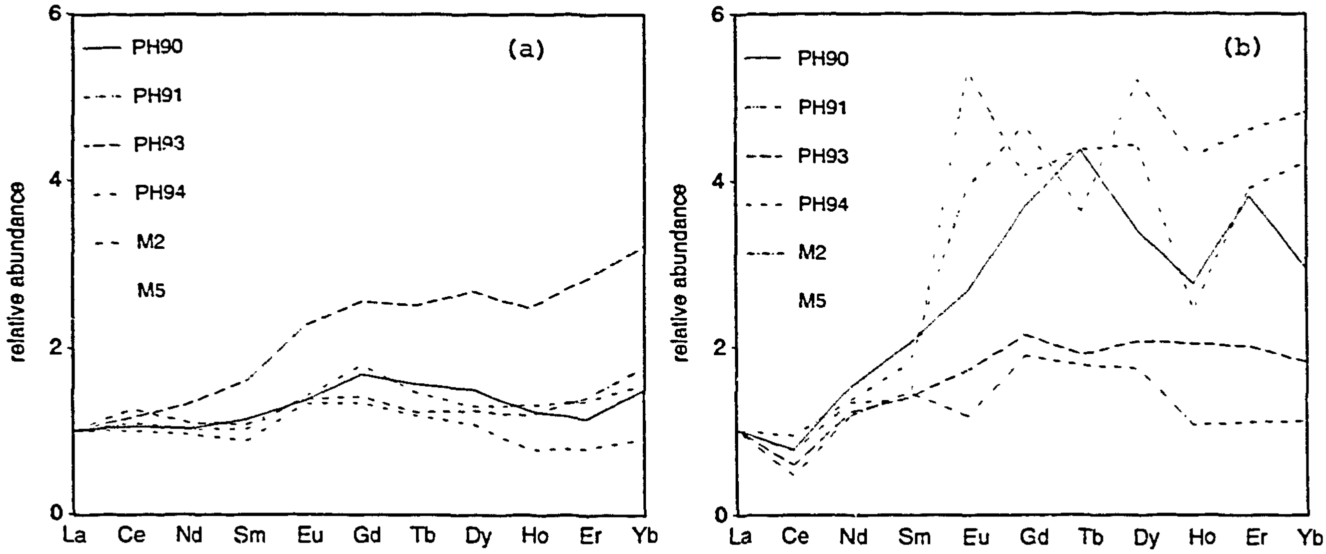

FIGURE 4.28 Rare earth element patterns (normalised to PAAS and La) in a) accessible and, b) inaccessible phases of representative samples

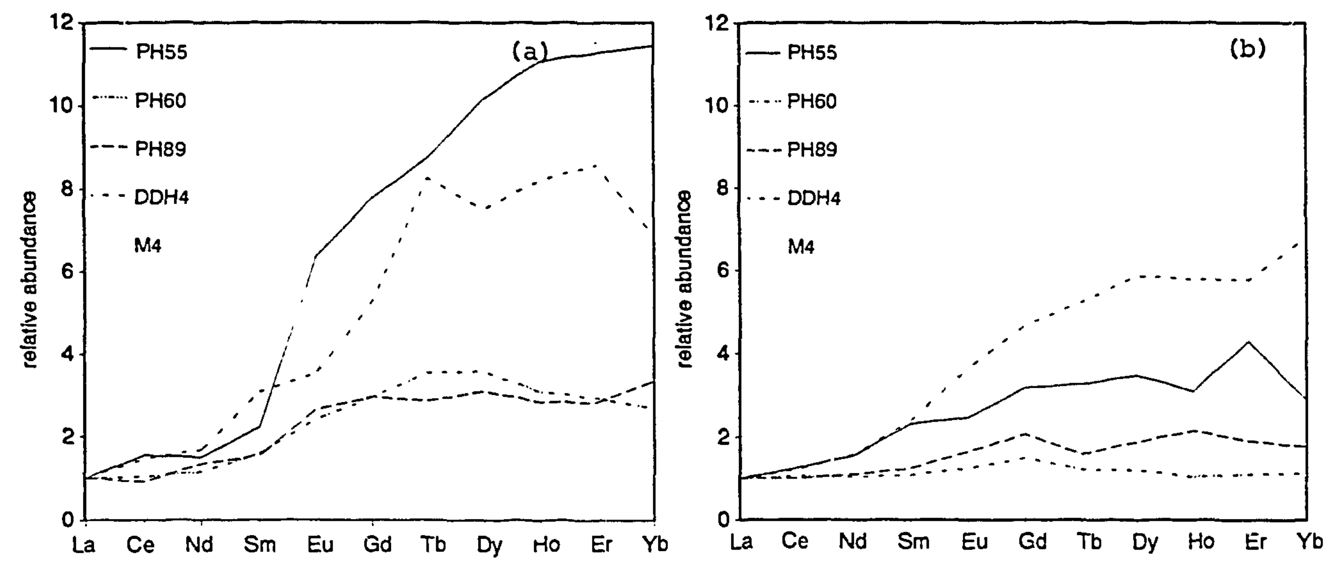

FIGURE 4.29 Rare earth element patterns (normalised to PAAS and La) in a) accessible and b) inaccessible phases of representative samples

4.4 Uranium-mineral Associations

Uranium associations with oxy-hydroxides in weathered rock

Auto-radiographs of thin sections from the weathered zones of drill holes M1, M2, M3 and DDH92 revealed that α-particle emitters were concentrated in iron-rich and manganese-rich areas. Electron microprobe analysis (EMA) and X-ray maps showed that within the iron-rich areas, uranium is associated with iron in a diffuse fashion. Within manganese-rich areas there were smaller areas with high concentrations of uranium in intimate association with cerium. Table 4.3 shows the association of α-activity with different phases in a weathered rock sample from DDH92 (18.4 m). Iron- and manganese-rich features were often present, coating or infilling fissures, and these features contained high amounts of uranium, compared to the bulk rock (see also Volume 9 of this Series).

TABLE 4.3
ASSOCIATION OF α-ACTIVITY WITH DIFFERENT PHASES ON A WEATHERED ROCK THIN SECTION (DDH92, 18.2 m, 672 hr exposure)

	Mineral Phase					
	Quartz	Clay + light Fe-oxide coating	Clay + medium Fe-oxide coating	Clay + heavy Fe-oxide coating	Fe-oxide nodule	Mn-oxide nodule
Track density (α-tracks/mm^2)	0	120	270	385	820	2995
% of total area	39	27	20	11	3	~0.1
% of total α-activity	0	20	34	28	16	~2

Iron-rich zones

The 25 m depth of M2 is at the base of the weathered zone in which alteration of iron-bearing minerals such as biotite and chlorite has led, in part, to the formation of iron oxy-hydroxides. At this depth, high density α-tracks were matched by the presence of optically-identified red-brown areas of iron oxy-hydroxides which may be composed of either hematite, ferrihydrite (or even lepidocrocite) or a mixture of the two, containing a mean uranium concentration of 0.9% (Table 4.4). Opaque yellow zones of iron-rich material at 25 m, probably goethite, gave low background α-emissions. The uranium enrichment is most likely due to sorption on iron oxy-hydroxide surfaces, since the correlation between uranium and iron and other elements, as determined by electron microprobe analysis, is rather poor (Figure 4.30) and points towards a non-stoichiometric uranium-rich phase. However, the possible presence of some secondary micro-crystalline minerals, such as saleeite, more than an order of magnitude smaller than the microprobe scale of analysis (ie less than about 0.3 μm diameter), cannot be discounted.

TABLE 4.4
MEAN ELEMENTAL COMPOSITION (%) OF IRON OXY-HYDROXIDES IN M2
(ELECTRON MICROPROBE)

	17 m depth (n=22)			21 m depth (n=11)			25 m depth (n=25)		
	mean	range	CV (%)	mean	range	CV (%)	mean	range	CV (%)
Al	2.6	0.4-4.7	38	3.7	0.7-6.9	61	3.9	1.1-9.3	56
Si	2.9	1.8-4.4	22	2.8	1.3-4.9	51	3.1	0.5-9.3	70
P	0.3	0.1-0.8	53	0.3	0.1-0.6	58	0.6	0.1-1.6	68
U	2.6	0.6-3.9	26	1.4	0.6-3.0	45	0.9	0.2-1.8	46
Ti	0.2	0.01-1.3	178	0.04	0.00-0.21	129	0.08	0.00-0.24	89
Ce	0.09	0.00-0.32	102	0.09	0.00-0.22	93	0.09	0.00-0.30	84
Mn	0.03	0.00-0.11	91	0.04	0.02-0.07	41	0.05	0.00-0.21	80
Fe	56	44.8-61.3	7	45.4	35.7-56.3	17	43.2	19.4-60.9	24

CV = Coefficient of variation

Examination of high density α-track areas, from the 21 m and 17 m depths of M2, showed that these were derived from an iron-rich mineral phase but, in contrast to the 25 m depth, they were yellow under reflected light, indicative of a goethite dominant phase. Elemental X-ray maps (Figure 4.31) show a clear spatial association of uranium and iron and a weaker association of phosphorus with these elements. In the centre and bottom left of this figure, the occurrence of two bright areas containing U, P and Th indicates the presence of rarely encountered remnant monazite. From numerous microprobe analyses uranium and iron contents were again poorly correlated and the average uranium concentration increased in the order 17 m > 21 m > 25 m.

Correlation matrix

Variable	P	U	Ce	Fe	Mn
P	1.0000	0.4821	0.1264	0.4722	0.2403
U	0.4821	1.0000	-0.0059	0.4111	-0.1675
Ce	0.1264	-0.0059	1.0000	0.1869	-0.0190
Fe	0.4722	0.4111	0.1869	1.0000	-0.1099
Mn	0.2403	-0.1675	-0.0190	-0.1099	1.0000

Scatter plots

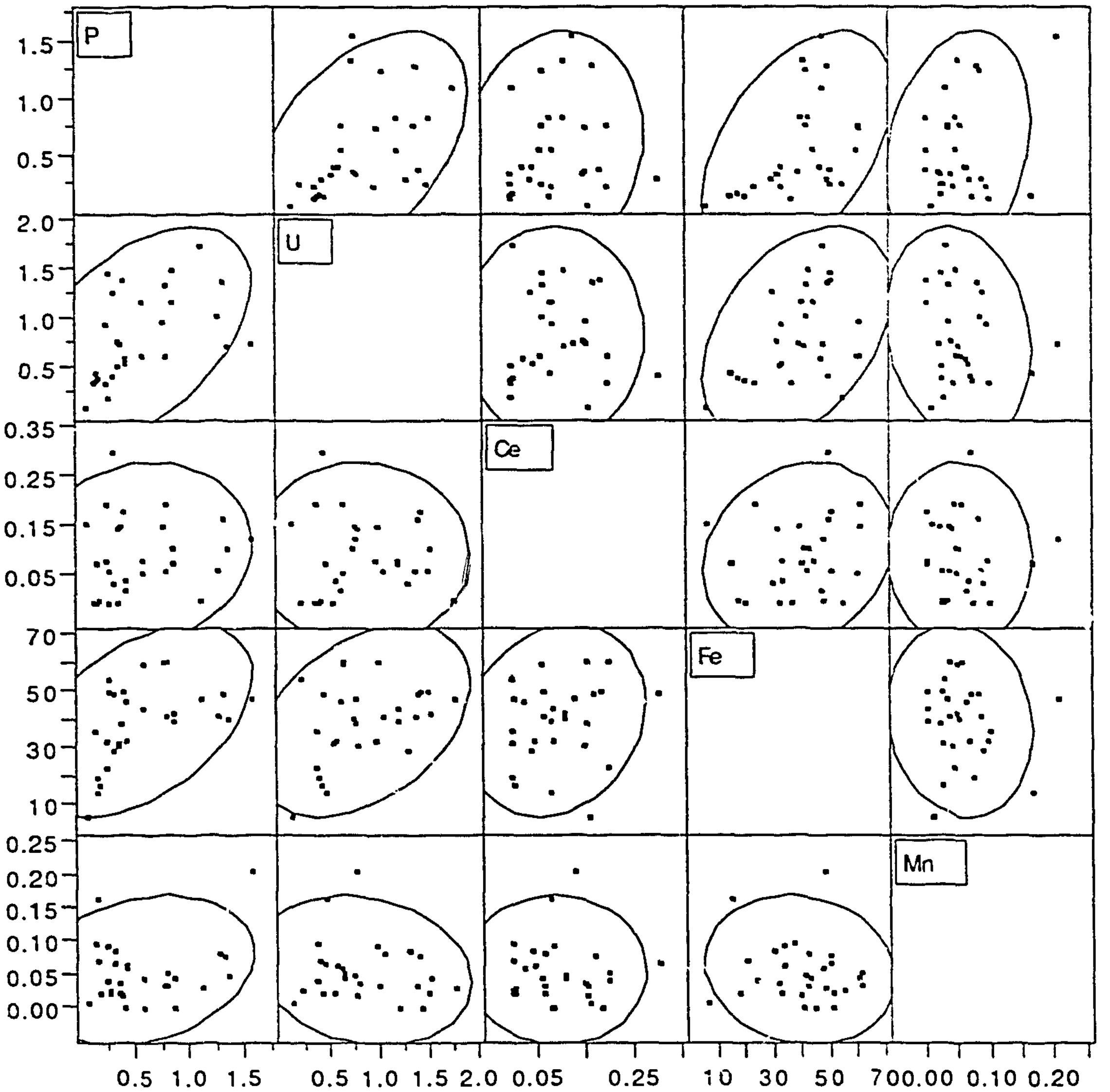

FIGURE 4.30 Correlation matrix and scatter plots of elements (%) in the iron-rich zones at M2 25 m

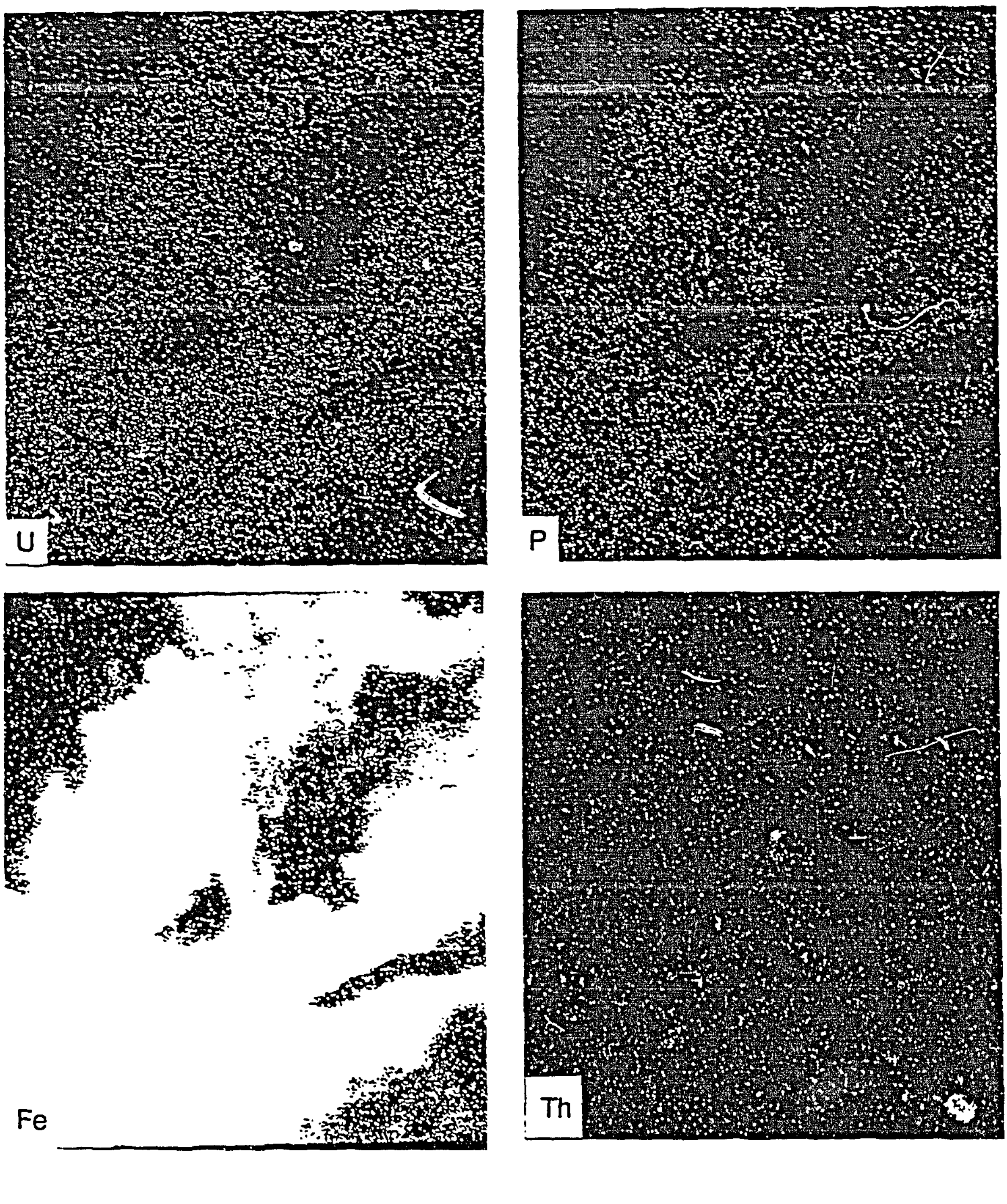

FIGURE 4.31 X-ray maps of U, P, Fe and Th from a goethite-rich area at M2 21 m. The width of the area in each micrograph is 125 μm

When the microprobe data of the iron rich zones from 17 m, 21 m and 25 m depths are combined, iron is positively and significantly ($P < 0.01$) correlated with uranium (Figure 4.32). This may simply reflect a combination of effects arising from ageing, in that young iron oxy-hydroxides such as ferrihydrite will tend to be poorly structured and show low apparent iron contents when analysed. In addition, a shorter contact time with uranium-enriched groundwater compared with aged material means less opportunity for uranium adsorption. Hence the highest total iron and uranium contents will be shown by aged and well-crystalline goethite even though surface reactivity may not be as great as ferrihydrite.

The uranium concentration is relatively low (<4%) and appears to be distributed throughout the secondary iron depositions in a diffuse fashion. This suggests an adsorption process of UO_2^{2+} onto oxy-hydroxide surfaces. This adsorbed uranium would become progressively occluded as further iron is deposited, or as the crystalline structure changes with ageing. Uranium is unlikely to replace iron in the crystal structures of iron-minerals (Gerth, 1987).

Manganese-rich zones

Back-scattered electron images of black, opaque manganese-rich areas from M2 at 8 m were found to be associated with relatively high α-emissions. Uranium was localised within the many small bright areas, but not throughout the manganese area (Figure 4.33). The mean elemental composition of manganese oxy-hydroxides at 8 and 17 m depths is given in Table 4.5. Compared with the iron-rich zones, the average uranium concentration was 4-10 times greater in manganese-rich zones. X-ray maps (Figure 4.34) show that the manganese and uranium are in juxtaposition, and that the uranium is intimately associated with cerium. Microprobe data (Table 4.5) show that uranium concentrations may be as high as 17% and cerium as high as 61% and that these two elements are strongly correlated (Figure 4.35). In these manganese-rich areas of M2, high uranium concentrations were only found together with high cerium concentrations. Where cerium and uranium occur together, iron seems to play no role (Figures 4.34 and 4.35).

Correlation matrix

Variable	P	U	Ce	Fe	Mn
P	1.0000	-0.2320	0.0650	-0.2035	0.3932
U	-0.2320	1.0000	0.0906	0.5925	-0.2120
Ce	0.0650	0.0906	1.0000	0.0593	-0.0535
Fe	-0.2035	0.5925	0.0593	1.0000	-0.1782
Mn	0.3932	-0.2120	-0.0535	-0.1782	1.0000

Scatter plots

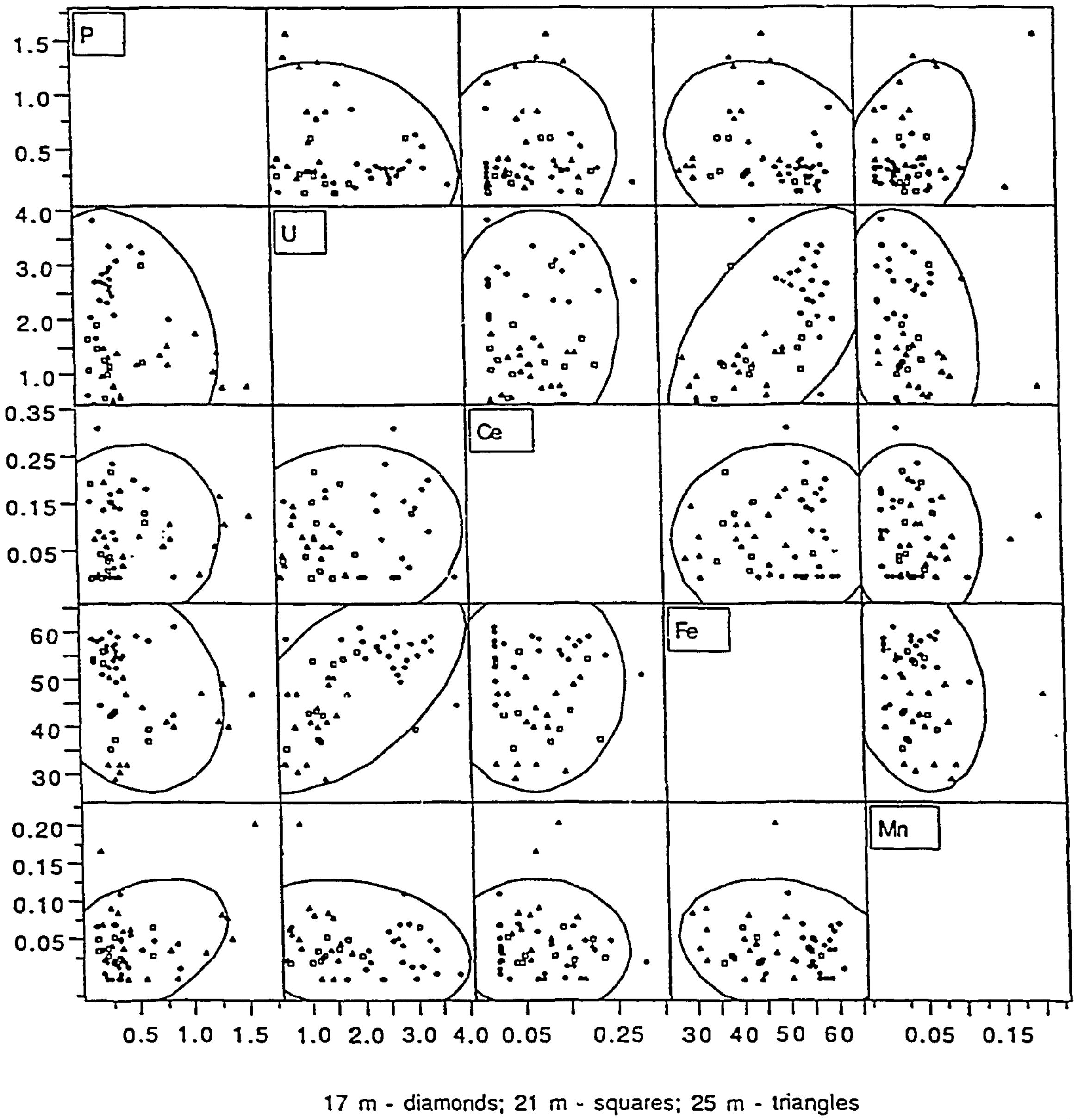

FIGURE 4.32 Correlation matrix and scatter plots of elements (%) in iron-rich zones at M2 17 m, 21 m and 25 m

FIGURE 4.33 Back scattered electron image of a manganese-rich area from M2 8 m. Bright areas contain highest U concentrations (width of micrograph area is 0.5 mm)

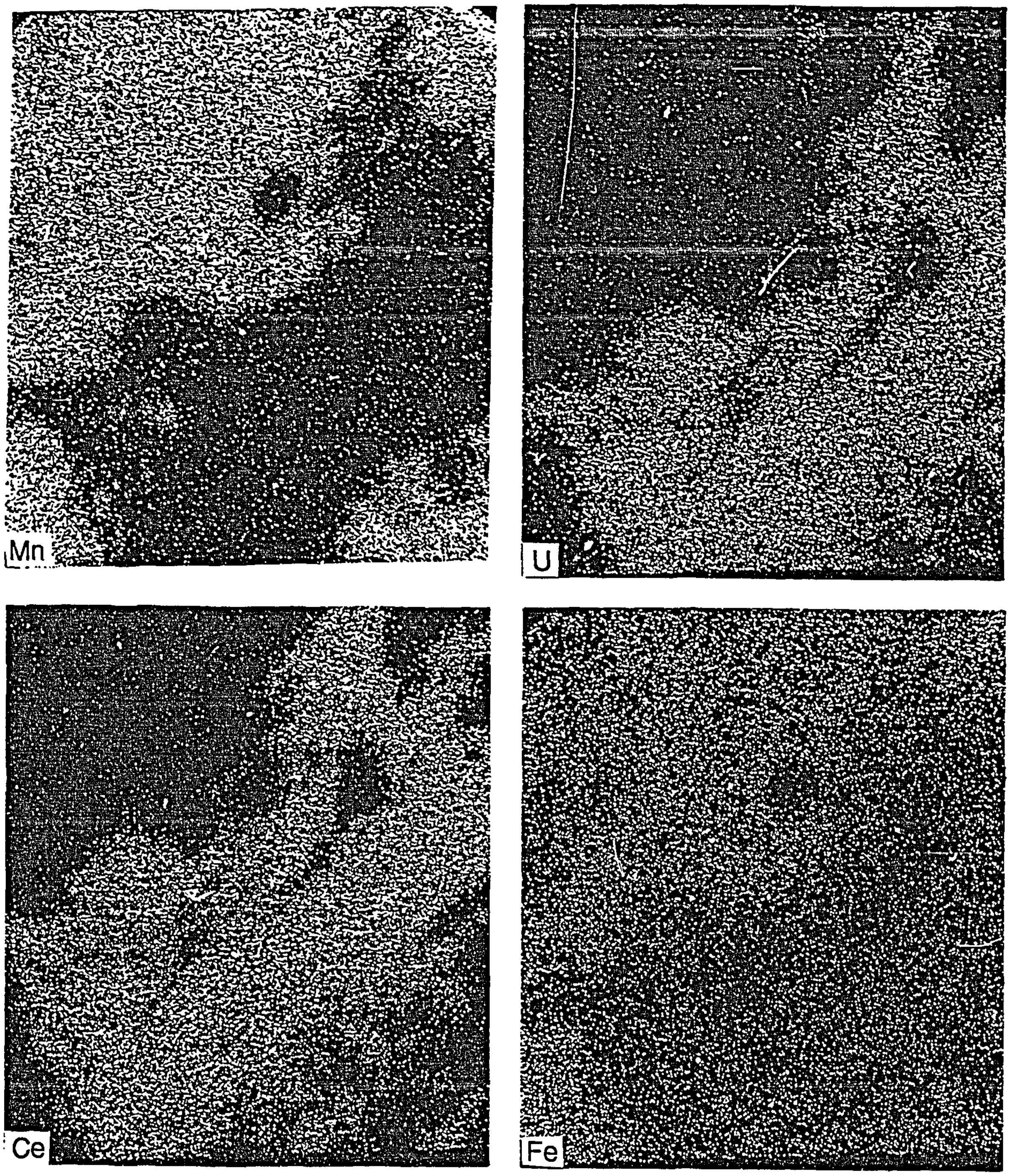

FIGURE 4.34 X-ray maps of Mn, U, Ce and Fe from a manganese-rich area from M2 17 m. (width of micrograph area is 62.5 μm)

Correlation matrix

Variable	P	U	Ce	Fe	Mn
P	1.0000	-0.0983	0.1254	-0.1605	-0.0816
U	-0.0983	1.0000	0.8169	-0.4200	-0.4934
Ce	0.1254	0.8169	1.0000	-0.5305	-0.6513
Fe	-0.1605	-0.4200	-0.5305	1.0000	0.1305
Mn	-0.0816	-0.4934	-0.6513	0.1305	1.0000

Scatter plots

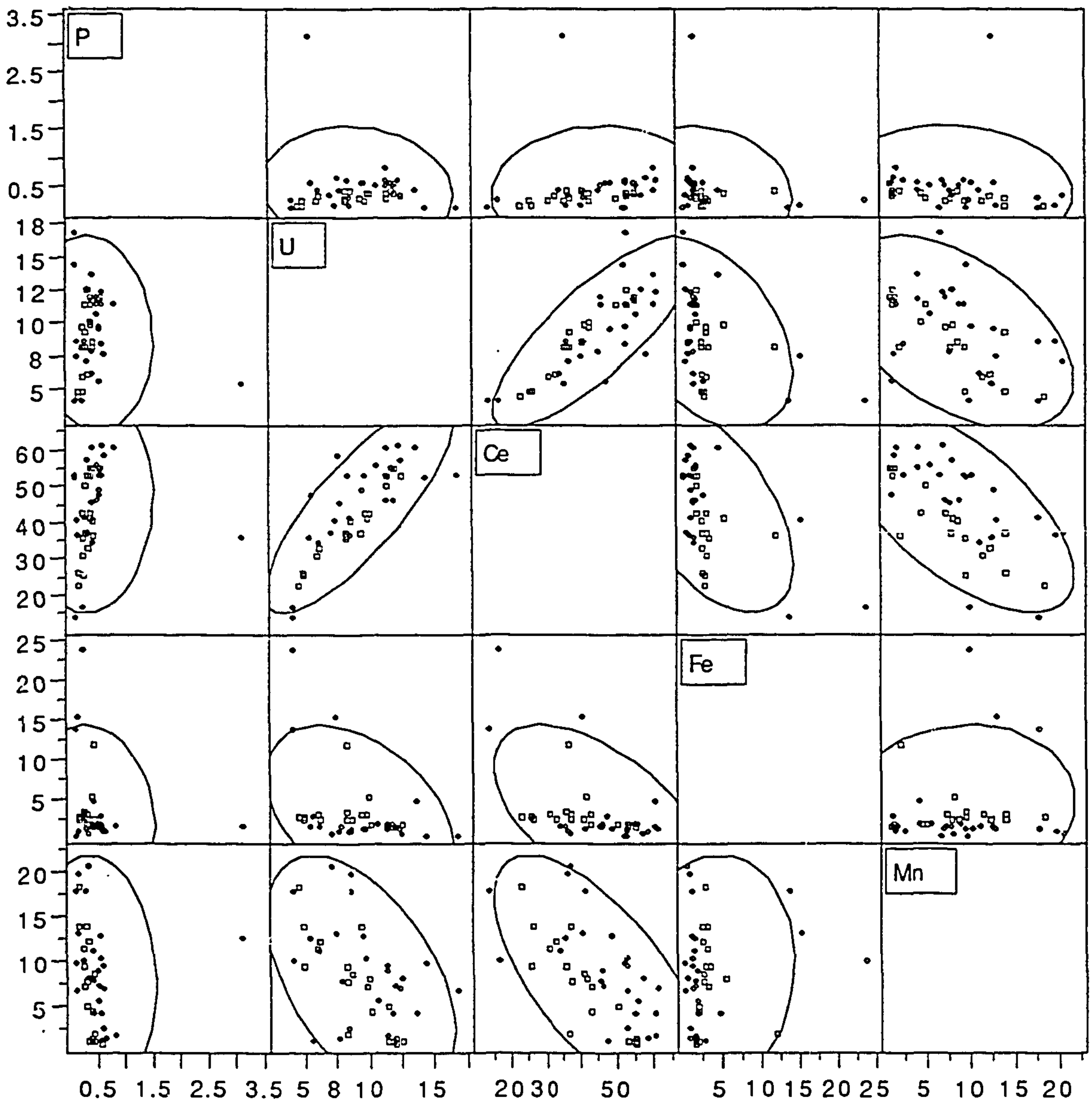

8 m diamonds; 17 m squares

FIGURE 4.35 Correlation matrix and scatter plots of elements (%) in a manganese-rich zone at M2 8 m and 17 m

TABLE 4.5 MEAN ELEMENTAL COMPOSITION (%) OF U-RICH ZONES IN MANGANESE OXY-HYDROXIDES AT M2 (ELECTRON MICROPROBE)

	8 m depth (n=25)			17 m depth (n=11)		
	Mean	Range	CV (%)	Mean	Range	CV (%)
Al	4.7	0.9-9.4	51	5.4	0.7-8.2	41
Si	2.1	0.2-12.2	135	3.2	1.1-5.3	37
P	0.5	0.1-3.1	109	0.3	0.2-0.6	32
U	9.5	4.0-16.8	34	8.9	4.4-12.6	30
Ti	0.8	0.0-10.5	289	0.6	0.1-6.5	242
Ce	46.5	13.7-61.2	27	40.7	22.6-55.4	26
Mn	9.2	1.0-20.7	61	7.2	0.8-18.5	74
Fe	3.6	0.3-24.0	159	3.2	1.7-12.1	73

When uranium was regressed against cerium, their molar ratio (U:Ce) ranged between 1:7-1:9 (Figure 4.36); the data shows good conformation of uranium and cerium. Microprobe analyses of the M1 profile (Table 4.6) indicate that a positive correlation ($P < 0.01$) exists between cerium and uranium (Figures 4.37 and 4.38). However, the molar stoichiometric ratio of U:Ce differs at M2, being much smaller at M1 (1:103).

TABLE 4.6 MEAN ELEMENTAL COMPOSITION (%) OF U-RICH ZONES IN MANGANESE OXY-HYDROXIDES AT M1 16 m (n=11) (ELECTRON MICROPROBE)

	Mean	Range	CV (%)
Al	3.9	0.8-10.6	79
Si	3.2	0.5-11.3	99
P	1.9	0.8-9.7	132
U	0.6	0.2-1.1	45
Ti	1.4	0.1-8.5	164
Ce	52.8	27.0-68.3	24
Mn	3.8	1.1-8.1	75
Fe	3.7	1.6-8.7	73

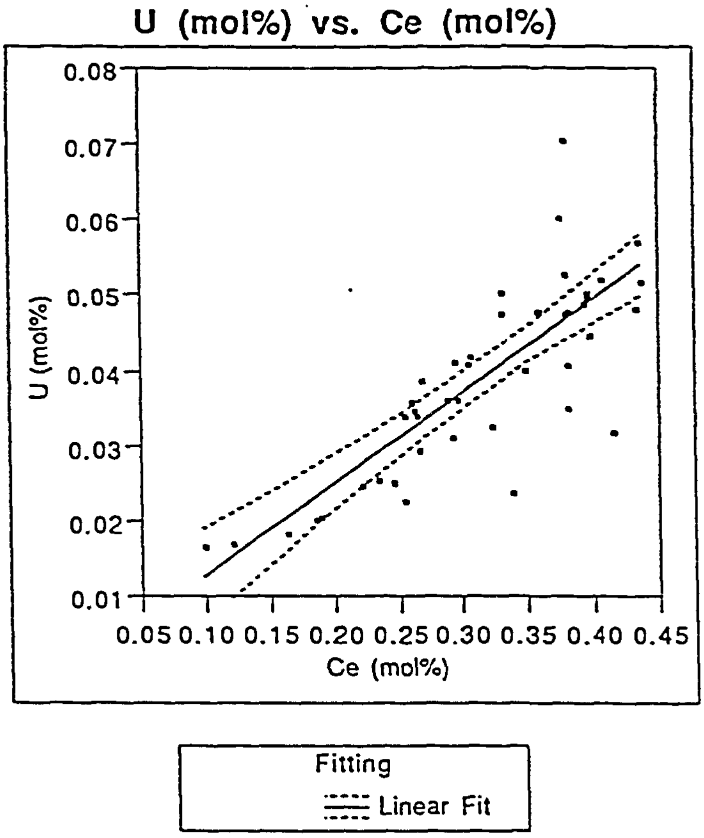

Linear Fit

Summary of Fit

Rsquare	0.667288
Root Mean Square Error	0.007338
Mean of Response	0.038963
Observations (or Sum Wgts)	44

Analysis of Variance

Source	DF	Sum of Squares	Mean Square	F Ratio
Model	1	0.00453594	0.004536	84.2351
Error	42	0.00226164	0.000054	Prob>F
C Total	43	0.00679758		0.0000

Parameter Estimates

Term	Estimate	Std Error	t Ratio	Prob>|t|
Intercept	0.0010168	0.00428	0.24	0.8134
Ce (mol%)	0.1208014	0.01316	9.18	0.0000

FIGURE 4.36 The relationship between uranium and cerium using combined data from manganese-rich zones at M2 8 m and 17 m

Correlation

Variable	P	U	Ce	Fe	Mn
P	1.0000	-0.4799	-0.6219	0.5820	-0.2507
U	-0.4799	1.0000	0.7683	-0.2875	0.0420
Ce	-0.6219	0.7683	1.0000	-0.4739	0.1927
Fe	0.5820	-0.2875	-0.4739	1.0000	-0.3690
Mn	-0.2507	0.0420	0.1927	-0.3690	1.0000

Scatter plots

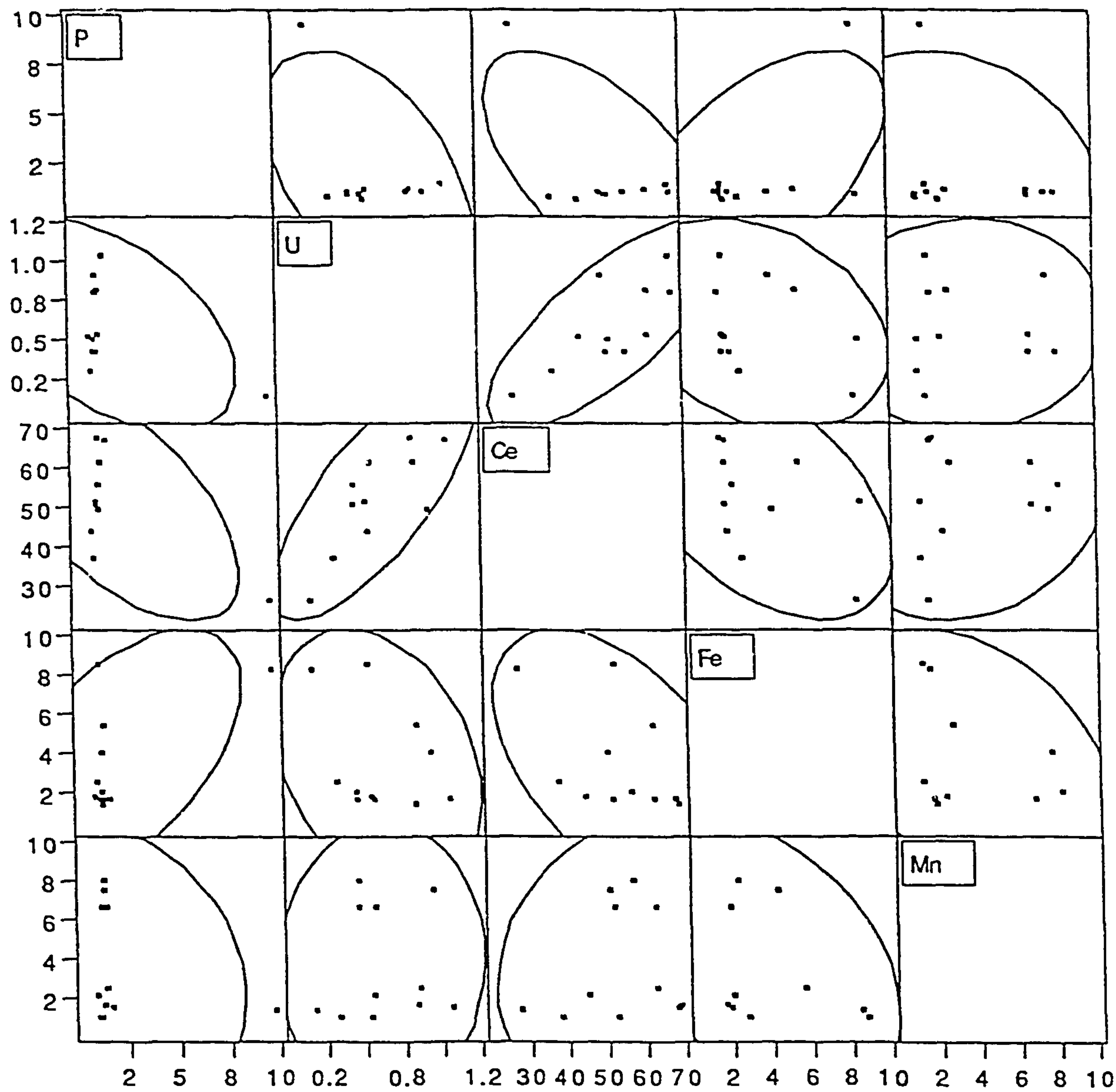

FIGURE 4.37 Correlation matrix and scatter plots of elements in a manganese-rich zone at M1 16 m

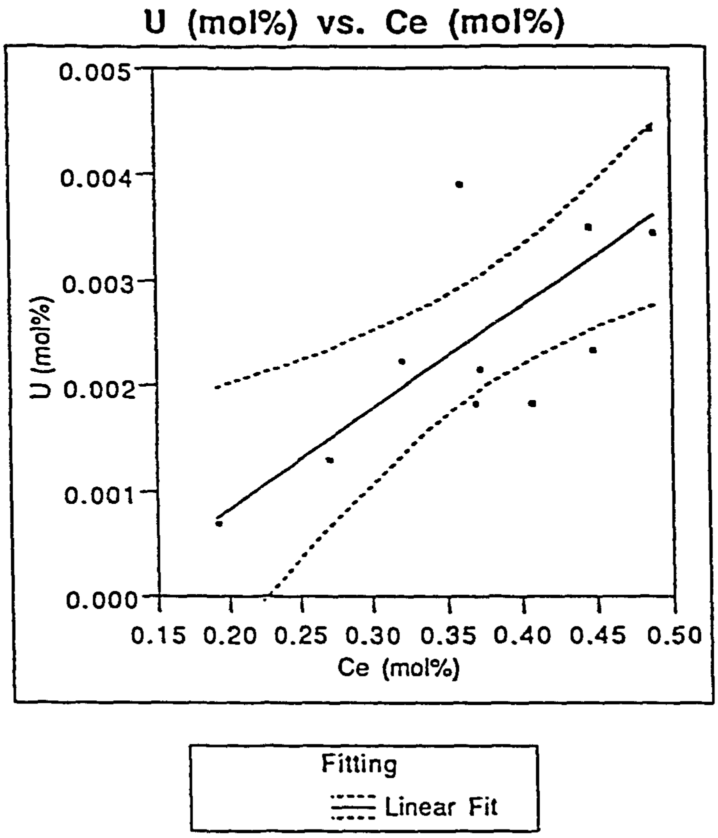

Linear Fit

Summary of Fit

Rsquare	0.590217
Root Mean Square Error	0.000779
Mean of Response	0.002538
Observations (or Sum Wgts)	11

Analysis of Variance

Source	DF	Sum of Squares	Mean Square	F Ratio
Model	1	0.00000786	0.000008	12.9628
Error	9	0.00000546	6e-7	Prob>F
C Total	10	0.00001332		0.0057

Parameter Estimates

Term	Estimate	Std Error	t Ratio	Prob>|t|
Intercept	-0.001127	0.00104	-1.08	0.3086
Ce (mol%)	0.0097185	0.0027	3.60	0.0057

FIGURE 4.38 The relationship between uranium and cerium in a manganese-rich zones at M1 16 m

Figure 4.39 shows a SEM secondary electron image of a manganese-rich area from M2 10 m, after treatment with strong hydrogen peroxide for two hours to remove amorphous manganese coatings. Prismatic rods and smaller (1-2 μm) individual globules or clusters of globules can be seen. Analysis of the rods by EDS showed them to be manganese- and aluminium-rich and devoid of uranium and cerium. X-ray diffraction has indicated that this phase is lithiophorite. Analysis of the globules by EDS showed them to be dominated by cerium and uranium.

The Ce/U globules have a composition different to that of published uranium or cerium containing minerals (Frondel, 1958; Vlasov, 1966; Cordfunke, 1969). TEM electron diffraction investigations of a ground sample from M2 10 m revealed that the composition of the Ce/U globules is consistent with a microcrystalline mixture of cerium and uranium oxides.

Iron and manganese oxy-hydroxides are not only amongst the most surface reactive of minerals with dissolved constituents in the regolith, but are also amongst its most transitory by virtue of the influence of pH and redox potential (Eh) on their solubilities. Within the weathered zone at Koongarra, the seasonal rainfall pattern influences Eh by its effect on the height of the watertable and the dissolved oxygen content of the groundwater. In addition, leaching of organic carbon from the soil to the groundwater may provide an energy source for heterotrophic bacteria, and could have a major effect on the kinetics of reduction of manganese and iron oxy-hydroxides. It is unclear whether the graphitic hanging wall unit provides a source of hydrocarbon which acts as a microbial energy source. Since uranium in the dispersion fan at Koongarra has been shown to be intimately associated with these potentially unstable or ephemeral fractions of the solid phase, uranium release from these fractions, its movement, and its subsequent redistribution by interaction with newly-formed and old oxy-hydroxide surfaces must be viewed as a dynamic process.

With decreasing Eh, cerium, manganese, and iron become reduced progressively in accordance with the electrochemical series (Weast, 1981). Reduced manganese ($MnO_2 + 4H^+ + 2e^- = Mn^{2+} + 2H_2O$; $E° = 1.24$ V) and iron ($Fe(OH)_3 + 3H^+ + e^- = Fe^{2+} + 3H_2O$; $E° = 0.93$ V), (Lindsay, 1979) are much more labile than their oxidised forms and some mobilisation will occur prior to their precipitation as oxy-hydroxides. Precipitation will occur in response to a falling water table, the invasion of more oxygen-rich water or a decline in microbial activity concurrent with that of a depleting organic substrate. Within the saturated zone, the principal dissolved form of cerium is likely to be Ce^{3+}, since the reduction of ceric occurs at a relatively high redox potential ($Ce^{4+} + e^- = Ce^{3+}$; $E^0 = 1.61$ V). Cerous complexes in aqueous solution mainly with carbonate at pH >7 (Cantrell & Byrne, 1987). Below pH 7, hydrated Ce^{3+} is probably the principal species in solution (de Baar et al, 1988). In a simple Ce-C-O-H system, it is important to note that CeO_2 is the dominant solid phase controlling solubility over a large part of the water stability field (Brookins, 1988). Based on the pH and Eh values observed in the weathered zone groundwater (6.0-7.5 and 100-250 mV respectively; Figure 4.2 in Volume 7 of this series), CeO_2 would be the major phase controlling cerium equilibrium concentrations in Koongarra groundwaters.

FIGURE 4.39 Secondary electron image of a manganese-rich area from M2 10 m (width of area in micrograph is 50 μm)

It has been shown that small but discrete zones of a cerium-rich phase, with a composition different to that of published uranium or cerium containing minerals Cordfunke, 1969; Vlasov, 1966), are intimately linked to uranium distribution in the vicinity of a manganese-rich phase. The ratio of uranium to cerium in the cerium-rich phase was nearly constant in the samples from hole M2 (U:Ce of 1:7 to 1:9 in M2 and 1:103 in M1). In addition, there appears little doubt that this cerium rich phase is an oxide, and that the association is based on a mixed solid solution of cerium and uranium oxides. It seems clear, however, that the formation of the Ce-U rich phase is related unequivocally to the distribution and occurrence of secondary manganese oxy-hydroxides. Parallels could be drawn here with rare earth enrichment of ferromanganese nodules in ocean floor sedimentation (Piper, 1974; lderfield et al, 1981; Calvert et al, 1987) and the role of ferromanganese-rich precipitates as scavengers of heavy metals and rare earths. Analysis of rare earth element concentrations in rock samples rich in manganese oxy-hydroxides (for example M3 10 m and 13 m, and M2 8 m), did not find anomalously high cerium concentrations, relative to PAAS rocks, either in absolute terms or relative to the other rare earth elements. However, neither lanthanum nor neodynium were detected by electron microprobe analysis.

The maximum proportion of the uranium associated with manganese oxides in a sample can be estimated using bulk and microprobe elemental analyses. At M2, 8 and 17 m depths, this was calculated to be about 0.96% and 1.5% respectively, based on assumptions:

(a) all the cerium in the samples was associated with manganese oxides

(b) that there was a constant ratio of Ce:U

(c) that all the uranium associated wiih manganese oxides was also associated with cerium.

The last two assumptions are supported by the microprobe analysis. At M1, the contribution of manganese oxides to the total uranium content was much smaller (<0.15% at 16 m depth). There is much less manganese in the weathered zone at M1 compared to at M2 and M3. o microprobe data has been collected for samples from M3, but the much greater amount of manganese at M3, suggests that it may be more important in the entrapment of radionuclides at that site than at M1 or M2. At DDH92, 18 m depth, about 2% of the total alpha activity was estimated to be associated with manganese oxides. Although the proportion of uranium entrapped by manganese oxides is small, this fraction of the uranium may be more labile than uranium associated with other solid phases.

In the case of iron oxy-hydroxides, the uranium concentration is relatively low (generally <4%) and the uranium appears to be distributed throughout the secondary iron depositions in a diffuse fashion. This suggests that a sorption process is the controlling mechanism for the initial association between U and oxy-hydroxide surfaces. This adsorbed uranium would become progressively occluded as further iron is deposited or or during transformations of the iron minerals. This mechansim would explain how adsorbed uranium becomes incorporated into iron-phases which are not extractable with TAO (see Section 6.2). Uranium is unlikely to replace iron in the crystal structures of iron-minerals (Gerth, 1987).

In summary, starting with U(VI), Ce(III), Fe(II) and Mn(II) in solution, with the onset of oxidising conditions iron oxy-hydroxide will be precipitated first, followed by manganese oxy-hydroxide then cerium oxide. Uranium will remain in the mobile oxidised form. Since the cerium phase was found only with manganese, it follows that the newly-precipitated manganese had an affinity for cerium and promoted its precipitation in the immediate vicinity. Since uranium is more strongly associated with cerium than with either manganese or iron, it follows that the newly-precipitated cerium had a stronger affinity for the uranium than uranium has with either iron or manganese.

4.5 Uranium-fissure Associations

The degree of uranium migration into the matrix from fissures was studied in rock showing various degrees of weathering. The changes in concentration of uranium with distance from fissures were estimated on the basis of

(a) electron microprobe line scans for uranium across fissures and uraninite veins,

(b) spot analyses at various distances from fissures,

(c) changes in α-track density moving away from fissures, and

(d) uranium assays of material sampled at various distances from fissures.

Unweathered rock

Figure 4.40 shows an EDS line profile for uranium across a uraninite veinlet within a chlorite vein from DDH119 55.6 m. The boundary of high uranium content was very abrupt between the chlorite and uraninite, and the chlorite in the vein only showed significant uranium where fissures or cracks occurred. This suggests that there was negligible penetration of uranium into the adjoining chlorite either at the time of uranium injection or post mineralisation, but some uranium may have migrated along fissures or cracks. Fine chlorite grains in veins appeared to be orientated such that there was a continuous plane of weakness at the centre of the vein, and this may have been the access pathway of the uranium which formed the veinlet.

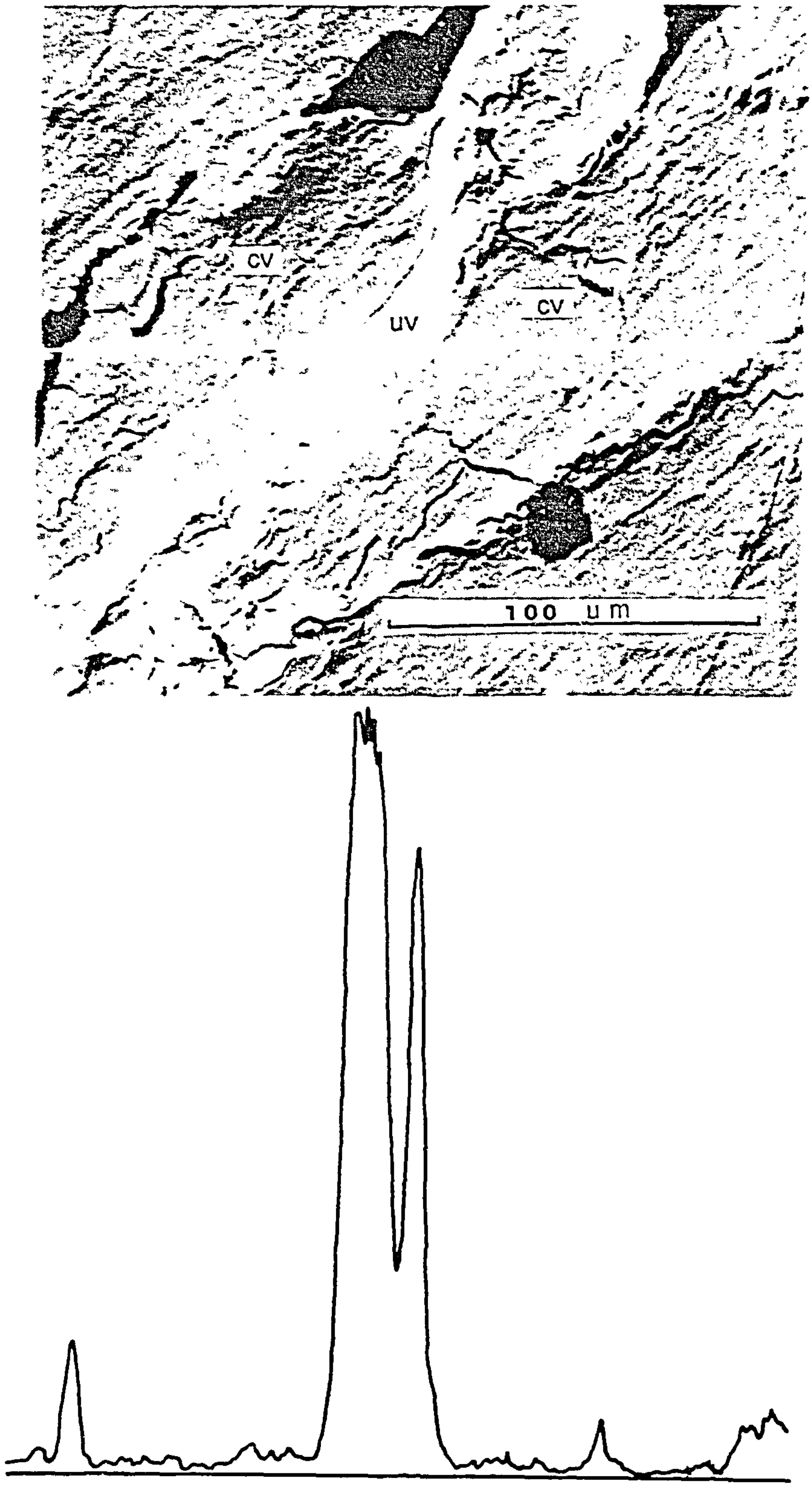

FIGURE 4.40 a) Back scattered electron image of a uraninite veinlet in a chlorite vein. b) Uranium X-ray profile across the uraninite veinlet (DDH119 55.6 m)

Figure 4.41 shows an EDS line profile for uranium across a fissure from the same sample (DDH119 55.6 m). The fissure was coated with rock alteration products on one side, and uraninite on both sides. This allowed a comparison of uranium penetration into rock alteration products and the unaltered quartz chlorite matrix. It was observed that very little uranium penetrated into the unaltered schist, while a significant amount was present in the secondary coating material. The thickness of the fissure coating was very variable, and even at the thickest point (about 60 μm) the uranium content of the coating was significantly higher than in the adjacent unaltered matrix, up to the coating/matrix boundary. There was very little iron in the coating material in unaltered areas of the section. These coatings probably contained a mixture of phases of varying crystallinity, resembling smectites and talc. The lack of visible signs of iron oxidation, and the low iron content of these coatings illustrates that such secondary clay minerals also contribute to the retardation of radionuclide migration.

The relationship between α-activity and distance from fissures with uraninite coatings was examined, using α-autoradiographs from samples containing unaltered quartz chlorite schist. A square ocelar mesh, with one hundred 25 μm cells was aligned along a fissure, and the number of α-tracks in the superimposed autoradiograph was recorded for each cell. Figure 4.42 shows the change in α-track density with distance from fissure surfaces, based on 10 mesh positions along two fissures in a thin section of sample DDH 119 55.6 m. Enhanced levels of α-activity were detected to a distance of about 150 μm. It can be seen in Figure 4.43 that α-track density was proportional to $\sqrt{\text{(distance)}}$ for approximately 180 μm.

This can be used as the distance of penetration of α-decaying radionuclides from a line source, and is the result of several processes including diffusion, sorption-desorption and α-recoil. The apparent diffusivity (D_a) incorporating the effects of all processes, can be estimated using the standard thermal diffusion equation (Crank, 1975):

$$C_X/C_0 = \mathrm{erfc}\ [(X/2)\ (D_a t)^{-0.5}]$$

where:

C_X = concentration at point x

C_0 = initial line source concentration

X = distance

D_a = apparent diffusivity

t = time

erfc is the complementary error function

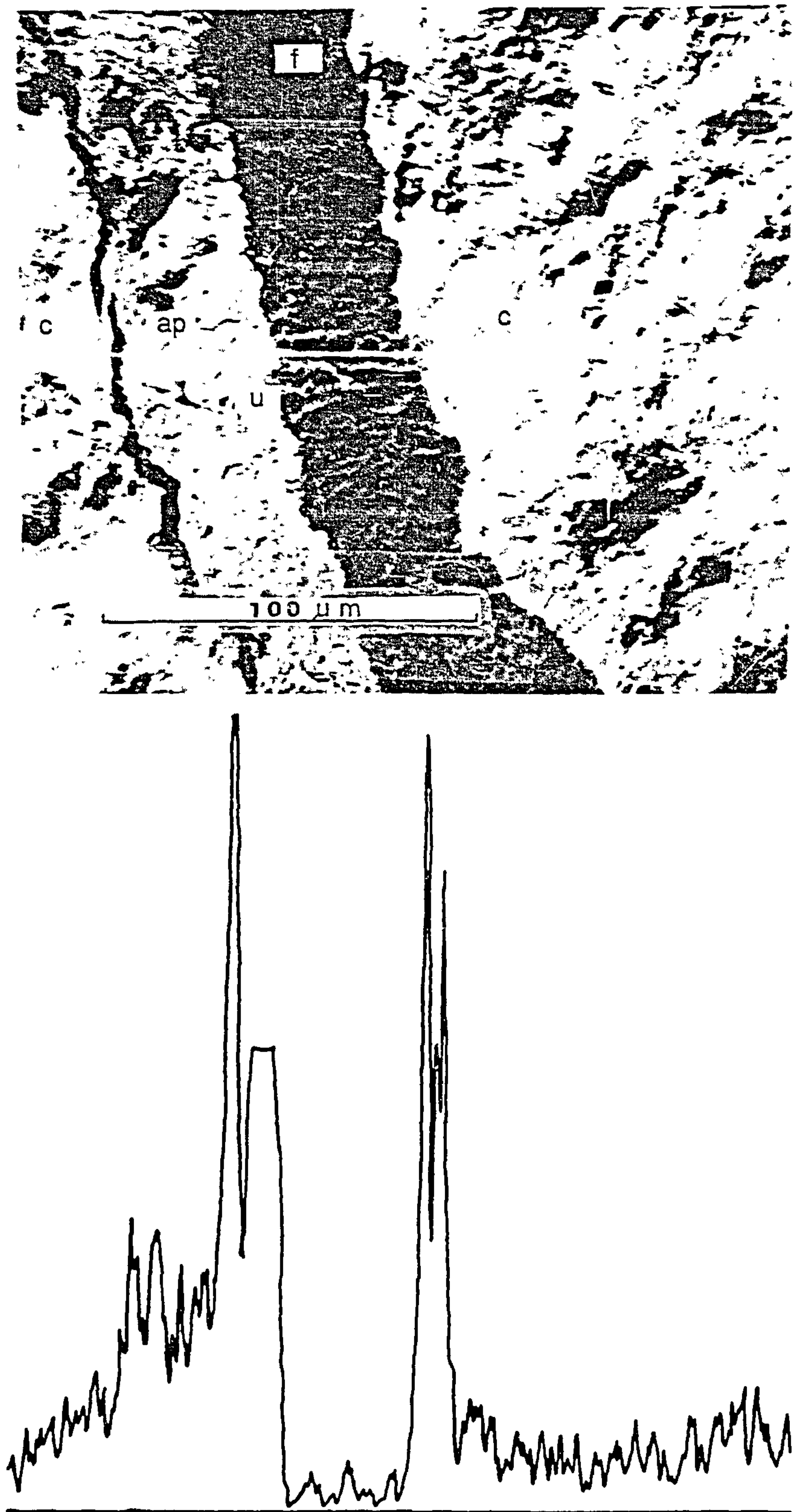

FIGURE 4.41 a) Back scattered electron image of a uraninite coated fissure through a chlorite matrix. b) Uranium X-ray profile across the fissure (DDH119 55.6 m)

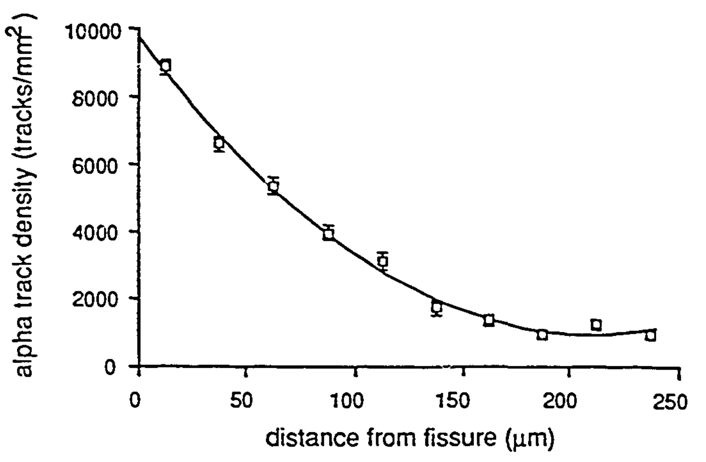

FIGURE 4.42 Plot of α-track density against distance from a fissure in unweathered chlorite schist (DDH119 55.6 m)

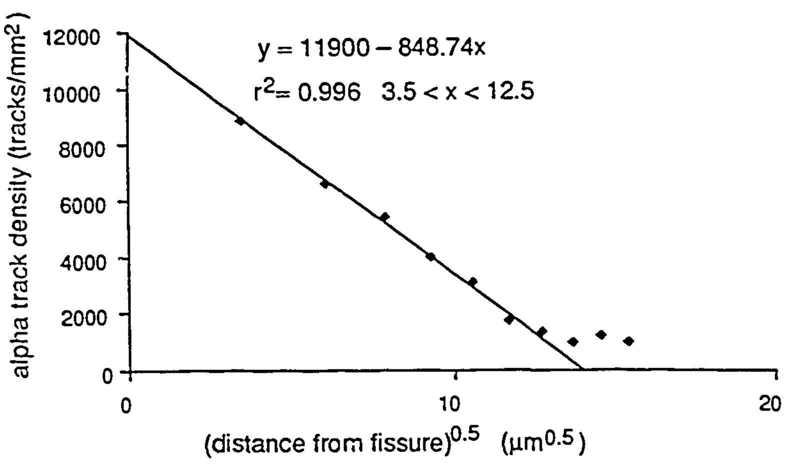

FIGURE 4.43 Plot of α-track density against √(distance) from a fissure in unweathered chlorite schist (DDH119 55.6 m)

For the current data it was assumed that

a) the track density at distance = 0 is equivalent to C_o,

b) t_o is approximately 10^8 years (the most recent period of uraninite formation suggested is 450 My BP (Snelling, 1989, and references cited therein)),

c) local uraninites supplied the equivalent of a constant line source since t = 0 and

d) the isotopic ratio of ^{238}U with its daughter elements, and other decay chain elements, was approximately constant with distance.

On the basis of these assumptions, D_a was calculated to be about 10^{-24} m^2/sec for uranium diffusion into unaltered, unfractured rock. The discontinuous nature of the coating on the fracture surfaces suggests that it did not protect the rock from contact with water. This value of D_a is smaller than values estimated by Shea (1984), for chlorite phases (10^{-22}-10^{-19} m^2/sec) in a study of individual grains, and below the range of values for granitoid rocks from experiments at a similar scale to the present experiments (10^{-19}-10^{-16} m^2/sec). This suggests that matrix diffusion into unweathered chlorite rock has been a minor factor in the retardation of uranium migration and is insignificant over the time scale of concern for nuclear waste repositories.

The α-track analyses indicated a greater penetration of uranium than the line scans, however this may be attributed to the greater sensitivity of α-autoradiography for uranium. Alternatively, other α-emitting members of the ^{238}U chain, such as ^{226}Ra, have preferentially migrated into the rock matrix. The apparent penetration, estimated by microprobe line scan, is about half the distance estimated by α-autoradiography, leading to a factor of four decrease in the D_a value. The given value is probably within an order of magnitude of the correct value, reflecting an approximate maximum D_a.

Weathered rock

In weathered rock samples, material adjacent to, or infilling fissures, generally contained much more uranium than the matrix. As previously mentioned, it appears that in weathered rock the spatial distribution of uranium is dependent upon the distribution of highly sorbing phases, such as iron and manganese oxides. It can therefore be suggested that associations of uranium with fissures are a result of redox properties at the fissure surfaces determining the distribution of sorbing phases.

Larger, millimetre sized samples were used when studying the U distribution near fissures in weathered rock so that variability resulting from the heterogeneous nature of sorbing phases would be minimised. The sample studied from DDH 86 12 m, was dominated by kaolinitic clay, yellow-orange in colour from a light goethitic stain, and contained a fissure approximately 1 mm wide which was almost entirely filled with a manganese-rich phase, cross-cutting the remnant schistosity. From XRD analysis and selective extractions on other samples, this phase was identified as lithiophorite, with a poorly crystalline component.

The manganese phase coating the fissure was sampled by scraping, then samples were taken from the uncovered rock surface, 0-1 mm from the fracture, then from ~1 mm, 1-3.5 mm, 3.5-7 mm, 7-10 mm and 10-13 mm from the fracture surface. The results of the uranium analyses are shown in Figure 4.44. While the results show a pattern for uranium reminiscent of a diffusion process, it is not possible to determine what the controlling mechanism is. The results could partially reflect the distribution of highly sorbing manganese or iron phases, which were observed to rapidly decrease moving into the rock. This would have the effect of concentrating uranium at the fissure surface, then under conditions leading to the dissolution of the manganese phase, the mobility of uranium could be enhanced.

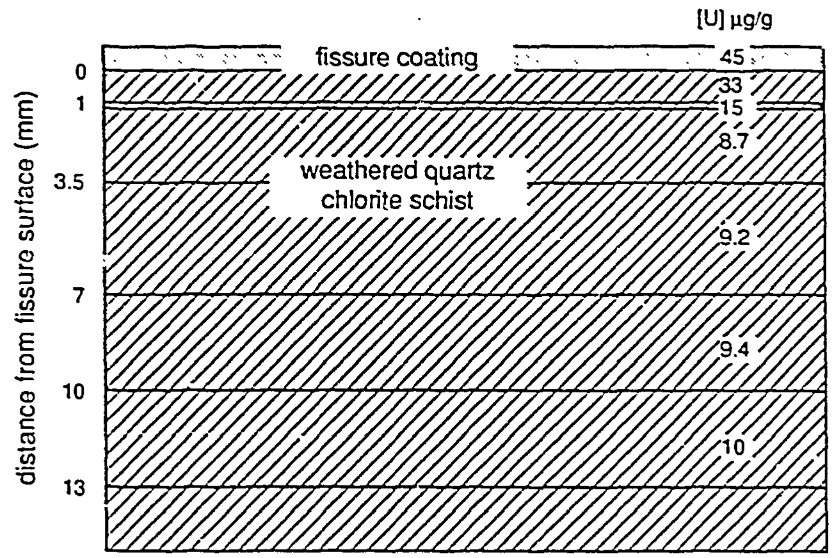

FIGURE 4.44 Uranium concentration in very weathered rock at various distances from a coated fracture (DDH86 12 m)

4.6 Summary

Multi-elemental analysis of bulk rock showed a number of relationships between elements, minerals and location. Elements can be classified into broad groups according to apparent element-mineral associations, leachability with weathering, and location at the site.

In the weathered zone, elements that were associated with iron oxides included U, P, As, Mn, Ni, V, Zr, and Cu. Elements that seemed to be associated with micas were Rb, F, Na and Ca. Lithium, Co, Ba, Y, and the rare earth elements, were associated with manganese oxides, particularly outside of the inner halo of alteration. Within manganese oxy-hydroxide phases, uranium appeared to be mainly associated with cerium. Within the secondary ore-body, uranium was correlated to phosphorus, and both elements followed variations in the iron oxide concentration. Down-gradient of the secondary ore body, uranium correlated to iron.

In the unweathered zone, some elements appeared to be concentrated in sulfide zones. These included S, Pb, Cu, La, Ce, Fe(III), Sc, V, Mn, Ca and P. Uranium was also concentrated in and adjacent to the graphitic hanging wall unit. Apatite was the major phosphorus containing phase in the unweathered zone. However, within the inner alteration halo, another source of phosphorus appeared to be present, and this may have influenced the formation of uranyl phosphates. There has been little penetration of uranium into the unaltered quartz chlorite matrix, from fissures. An apparent diffusivity was calculated to be about 10^{-24} m^2s^{-1}.

Some elements are very susceptible to leaching with weathering. These include U, Ca, S, Mn, Li and Mg. Elements that appeared to be removed from the weathered zone above the primary mineralisation, and deposited down-gradient were U, Mn, Li and possibly sulfur. Elements that appeared to be more immobile were Cu, Si, Cr, As, Zr, Al, Pb, Y, Ti, P and Ga. The change in the concentration of zirconium with weathering was used to estimate a rock mass loss and volume reduction of about 50% and 38% respectively.

The zone of primary mineralisation appears to be characterised by low lanthanum abundance, and relatively high, heavy rare earth element concentrations. Heavy rare earth elements were more readily leached than the light rare earth elements. There also appears to be a preferential entrapment of cerium into crystalline (non-extractable with TAO) phases.

The amount of TAO-extractable material, mainly Fe, Al, Mg, Mn and K, assumed to be present as amorphous accessible phases, appeared to increase with distance from the fault. The most highly extractable elements included Mn, Co, Cu, U, P, Pb and sometimes iron, with manganese being the most readily extractable. There was 5-17 mg/g extractable iron in the samples studied, corresponding to 7-29 mg/g ferrihydrite.

The electron microprobe and α-autoradiography study demonstrated the importance of the oxy-hydroxide fraction as a scavenger of uranium. The relationship between iron oxy-hydroxides and uranium appears to be of a diffuse nature, suggesting that sorption is the main initial mechanism of association. In addition, it was established that locally high concentrations of uranium within the dispersion zone are associated with cerium rich phases in a stoichiometric fashion. The distribution of cerium is closely related to the occurrence of manganese oxy-hydroxides. The concentration of cerium in the rock, however, was not anomalously high. The establishment of the chemical and mineralogical nature of the Ce-U association, together with an improved understanding of redox kinetics at Koongarra, is important to understand the dynamics of uranium movement and its redistribution.

5 URANIUM DISTRIBUTION

Uranium concentrations were obtained for rocks from various holes (see Figure 2.1) and depths. The uranium concentrations quoted in drilling logs (Noranda, unpublished) and data collected during this project, were used to draw contour maps of the distribution of uranium concentration in plan-view and cross-section. Uranium concentrations of samples analysed during the course of this project, are included in Appendix 1.

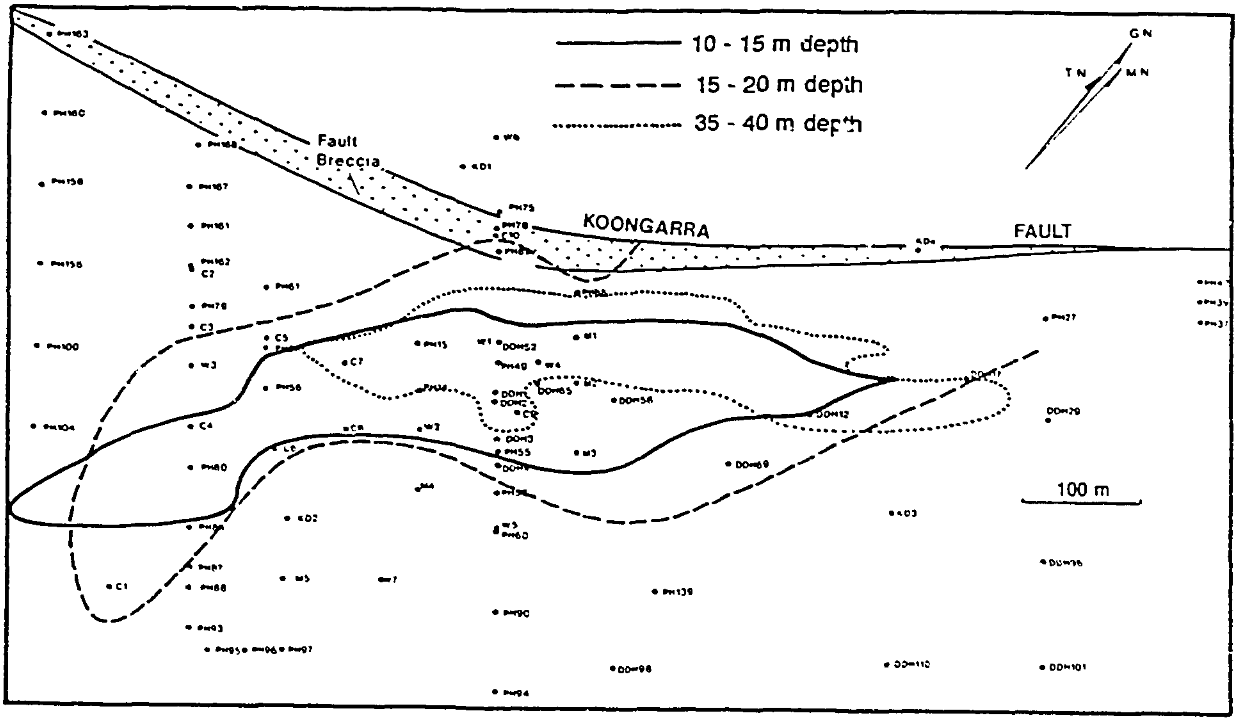

FIGURE 5.1 Contour lines of uranium concentration of 100 $\mu g/g$ at three depths

Figure 5.1 shows the 100 µg/g uranium concentration contour line in plan-view, for various depths; 35-40 m (unweathered zone); 15-20 m (deep weathered zone) and; 5-10 m (shallow weathered zone). Concentrations of uranium in excess of 100 µg/g in the unweathered rock were only detected in the vicinity of the ore body. The base of weathering was estimated from the drilling records for each hole, and from inspection of the core, and was operationally defined to be the depth at which fresh rock first occurred. It appears from the 100 µg/g contour lines, that the bulk of the apparent redistribution of uranium occurred in a SSW direction from the primary mineralisation. The maximum distance for which there was any increase in uranium concentration as a result of dispersion was not determined, but is certainly >300 m. The 100 µg/g uranium concentration contour deep in the weathered zone, near the base of weathering, is similar to that higher up in the weathered zone, which suggests that a large proportion of the mobilisation and entrapment of uranium may occur near or in the transition zone, at the early stages of weathering.

Figure 5.2 shows the contours of uranium concentration near the surface (0-5 m). The increase in uranium concentration is more widely spread at shallow depths than deep in the weathered schist, and more closely follows the topography (see Volume 4 of this series). Many holes which do not have increased uranium concentrations in the deep weathered zone, do have elevated uranium concentrations in the near surface. This suggests that shallow lateral transport has occurred, and that the uranium may have been transported a greater distance in this zone. While elevated uranium concentrations near the surface occur over a greater distance than in the general weathered zone, this component accounts for only a small proportion of the total redistributed uranium.

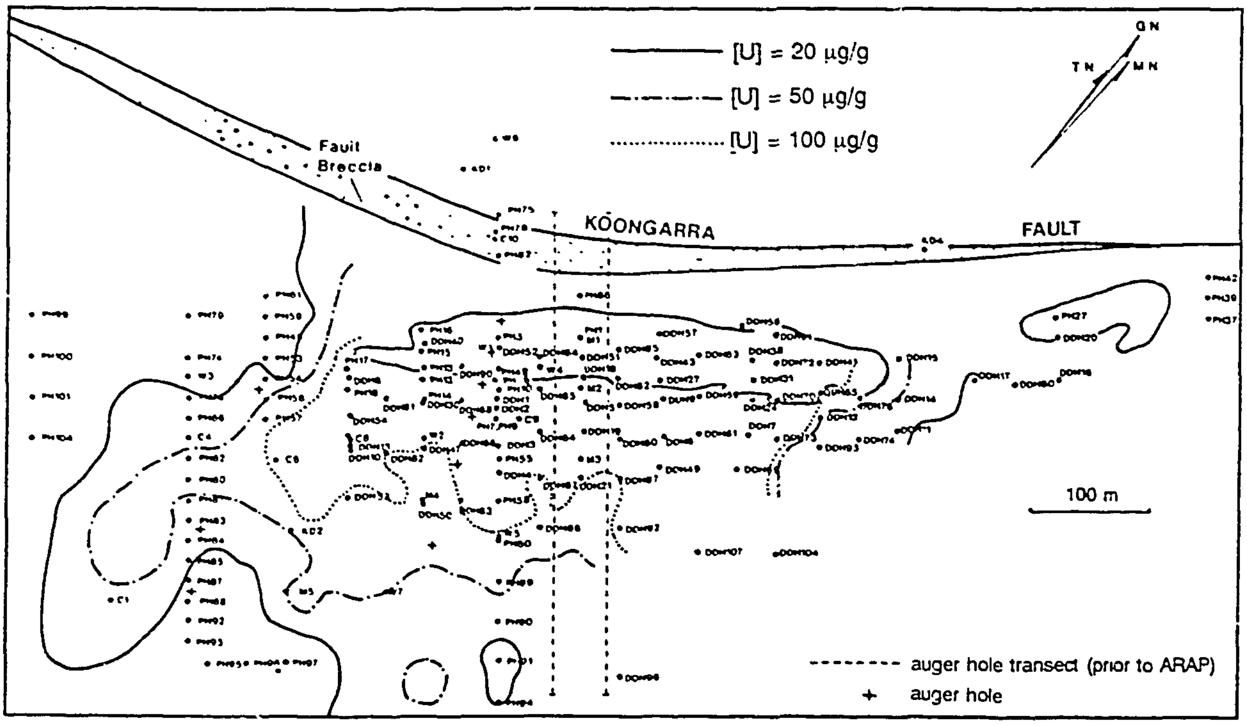

FIGURE 5.2 Contours of uranium concentration in the top 5 m

Figure 5.3 shows the uranium concentration contours for the cross-section from DDH52 to PH94 (Mine Grid Section 6109 mN, see Figure 5.1). The uranium distribution in cross-section 6170 mN is shown in Figure 2.2. These show that at the extremity of the uranium redistribution, most of the enrichment occurs near the surface. Outside of the zone of primary mineralisation, there is an abrupt uranium concentration boundary between the weathered and unweathered zones. This was the case for all holes outside the primary mineralised zone, and is evidence that the uranium found in the weathered zone SW-SSW of the primary deposit was indeed mobilised and deposited, and not simply inherited from the parent rock.

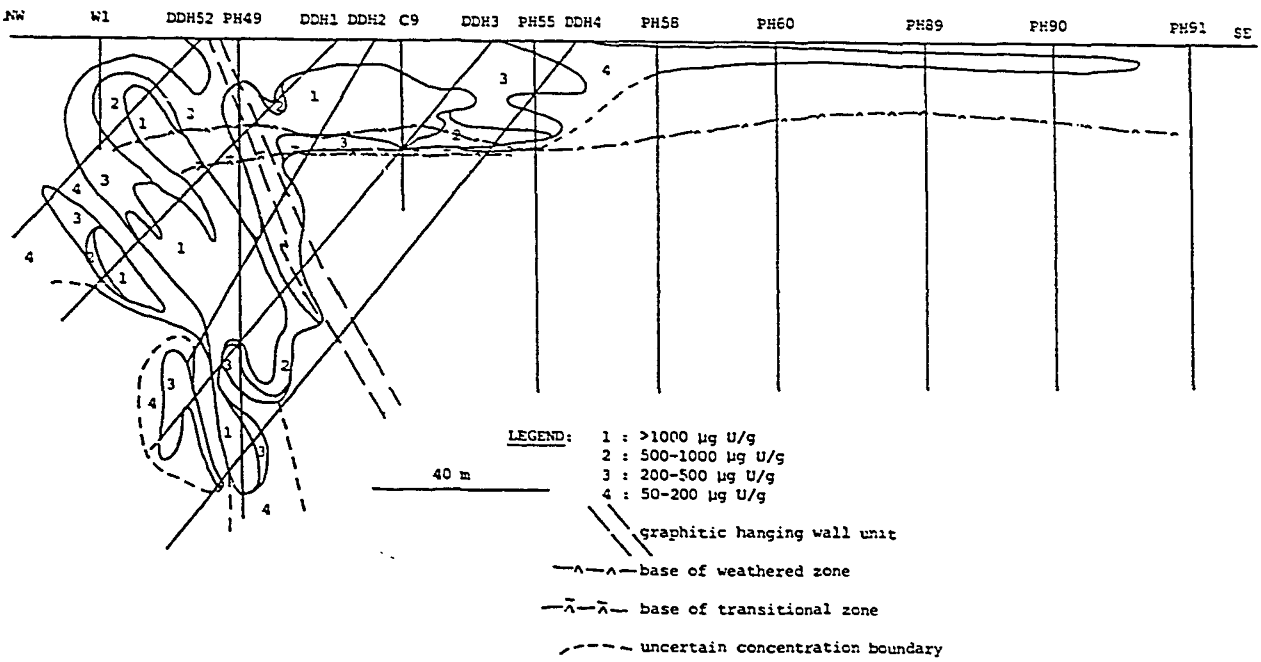

FIGURE 5.3 Contours of uranium concentration in cross section (section 6109)

The uranium concentration in the weathered zone was variable with depth for most holes in the dispersed uranium area. The depth of maximum uranium accumulation appears to decrease with increasing distance from the primary zone. This uneven distribution of uranium through the weathered zone suggests preferential pathways for uranium-bearing water, but may also be explained by variation of sorbing phases with depth.

The presence of elevated concentrations of uranium near the surface, with maximum values for some holes occurring in the top 3 m, suggests a shallow component to the uranium migration, possibly involving overland transport in runoff water during high intensity rainfall. In some cases, the maximum uranium concentration occurred near the base of the surficial sand deposits. It is possible that uranium-bearing waters occasionally travelled through the surficial sands, above the heavy, clayey B horizon. The surficial sands contain much less highly sorptive material, such as iron oxides, to impede the transport of uranium. A γ-ray survey of the site, by Emerson et al. (see Volume 4 of this series), which reflects gamma-ray production within approximately 60 cm of the ground surface, showed a similar pattern to the surficial uranium assays (Figure 5.4).

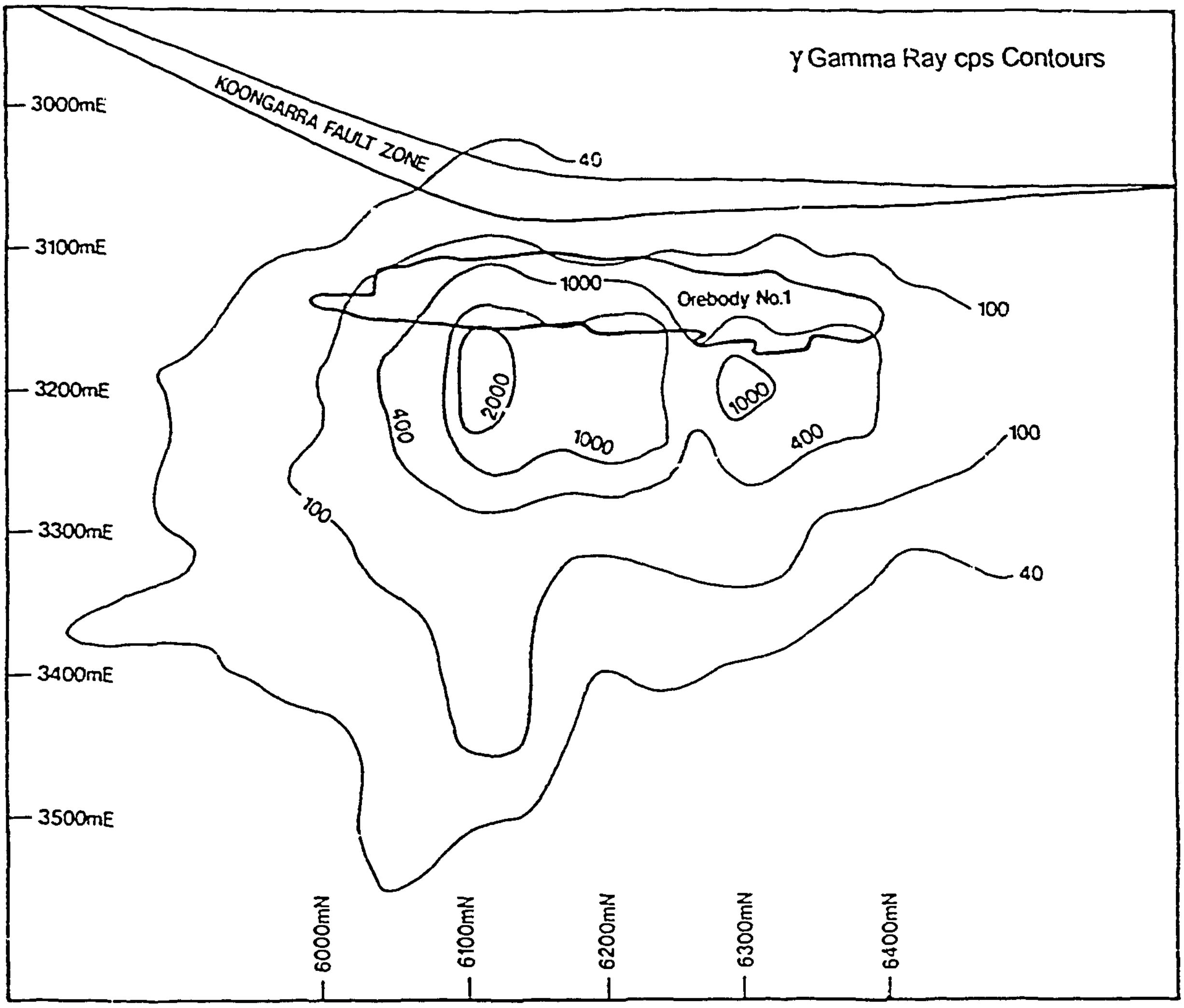

FIGURE 5.4 Gamma-Survey of the site (from Volume 4 of this series)

The pattern of uranium distribution in plan-view is similar to trends identified in the groundwater chemistry, as discussed in Volume 7. However, this did not correspond to the distribution of uranyl phosphate minerals, which was more towards the SE (Snelling, 1980a). Since the observed groundwater chemistry patterns pertain to current-day groundwater, and the groundwater chemistry required for the formation of the uranyl phosphate zone is different to that which currently prevails (see Volume 11 of this Series), it would appear that the uranyl phosphate zone was formed at an earlier period, with the SSW uranium dispersion occurring later and probably continuing at the present time (see Volume 12 of this Series).

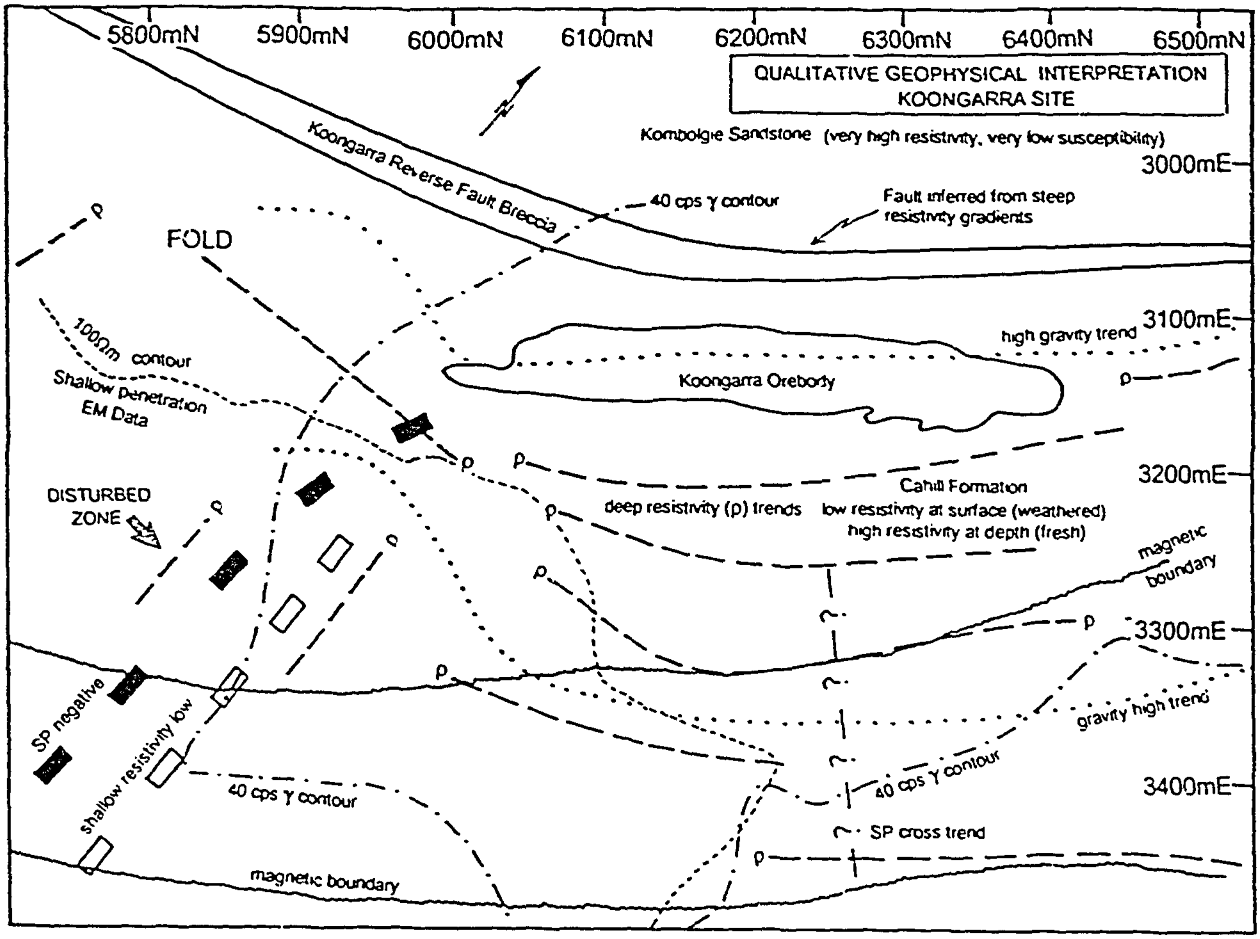

FIGURE 5.5 Summary of geophysical survey results (from Volume 4 of this series)

Figure 5.5 shows the summary of geophysical surveys conducted at the site (see Volume 4 of this Series for more details). Many of the geophysical parameters follow a similar pattern to that of the mobilised uranium concentrations.

6 URANIUM SERIES DISEQUILIBRIA

Samples of core and pulp material were analysed for uranium series disequilibria in laboratories at ANSTO and JAERI. Some samples were analysed prior to the commencement of the ARAP, and the results for these samples are included here for completeness. The degree of disequilibria has been determined for bulk whole rock, chemically defined phases (with two and five stage extraction schemes), mineralogically distinct zones and secondary uranium minerals. The isotopes most frequently considered were ^{238}U, ^{234}U and ^{230}Th, with some analyses of ^{235}U, ^{226}Ra, ^{210}Pb and ^{232}Th. Figure 6.1 shows in plan view, the location of holes from which samples were taken for uranium series analysis.

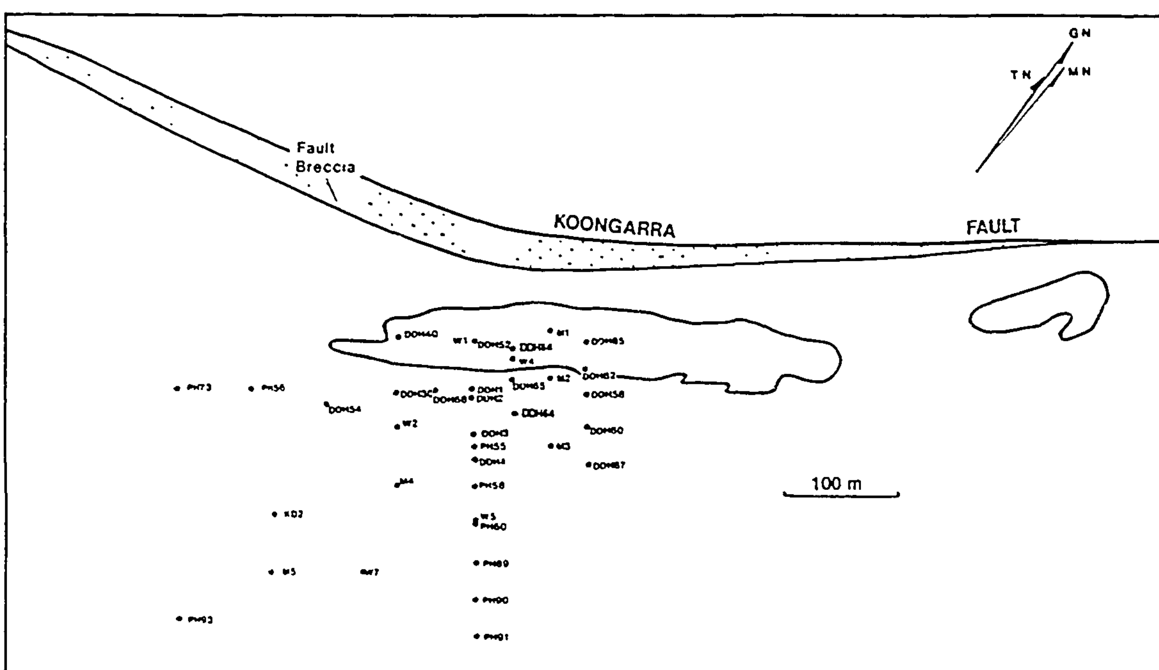

FIGURE 6.1 Location of holes sampled for uranium series analysis

6.1 Trends in Whole Rock

The earliest reported work on the disequilibria between uranium and its daughter nuclides at Koongarra was by Snelling and Dickson (1979), who compared uranium concentrations determined by delayed neutron activation with "gamma equivalent" uranium concentrations. This essentially gave a ratio of $^{238}U/^{226}Ra$, since the "gamma equivalent" uranium was an analysis of the short-lived ^{226}Ra daughters ^{214}Pb and ^{214}Bi. It was found that the massive primary ore zones were at, or near, radiometric equilibrium, but that disequilibria occurred in the low grade host wall rocks and in the weathered zone dispersion fan. In these zones there was an excess of ^{226}Ra (relative to uranium), but in the dispersion fan the ratio approached unity with distance from the primary ore along a probable direction of groundwater flow. This supports the proposition that the dispersion fan developed from a now leached upward extension of the No.1 orebody. An extension of this work by Dickson and Snelling (1980) used gamma spectrometry to measure individual isotopes. They postulated that ^{226}Ra, deposited in the transition zone, indicated upward flow of groundwater from reducing to more oxidising conditions, since radium may coprecipitate with newly formed iron and manganese oxides.

In an evaluation of soil lead isotope techniques for uranium exploration, Dickson et al. (1985) found that in the Koongarra region the ^{210}Pb content of soil was closely correlated to the ^{226}Ra content, which was often in great excess of ^{238}U. The ^{226}Ra excess appeared to have resulted from deposition of radium transported by water at or near the surface, apparently from the Koongarra fault zone, but probably originating from the Kombolgie sandstone. Radium-rich springs occur in the region, and often appear to source from sandstone outcrops (Pedersen et al 1980).

Disequilibria in unweathered samples

The disequilibria in 16 unweathered rock samples has been measured, and the results are included in Appendix 6. Generally, unweathered samples were in isotopic equilibrium, with activity ratios $^{234}U/^{238}U$ and $^{230}Th/^{234}U$ within 1σ of unity. Only three unweathered samples showed a deviation from unity by more than 2σ, and none by more than 3σ. It is unlikely that the unweathered rock experienced substantial uranium migration or deposition over the 100 ky timescale. Samples containing pitchblende, such as DDH2 38 m and 74 m, enabled the activity ratios to be determined with high precision. Both samples had $^{234}U/^{238}U$ and $^{230}Th/^{234}U$ activity ratios within 1σ of unity.

An excess of ^{226}Ra relative to uranium in unweathered rock was found by Snelling and Dickson (1979) and Dickson and Snelling (1980), in ore samples and particularly in host wall rocks with low uranium contents. This suggests some redistribution of radium in the unweathered environment.

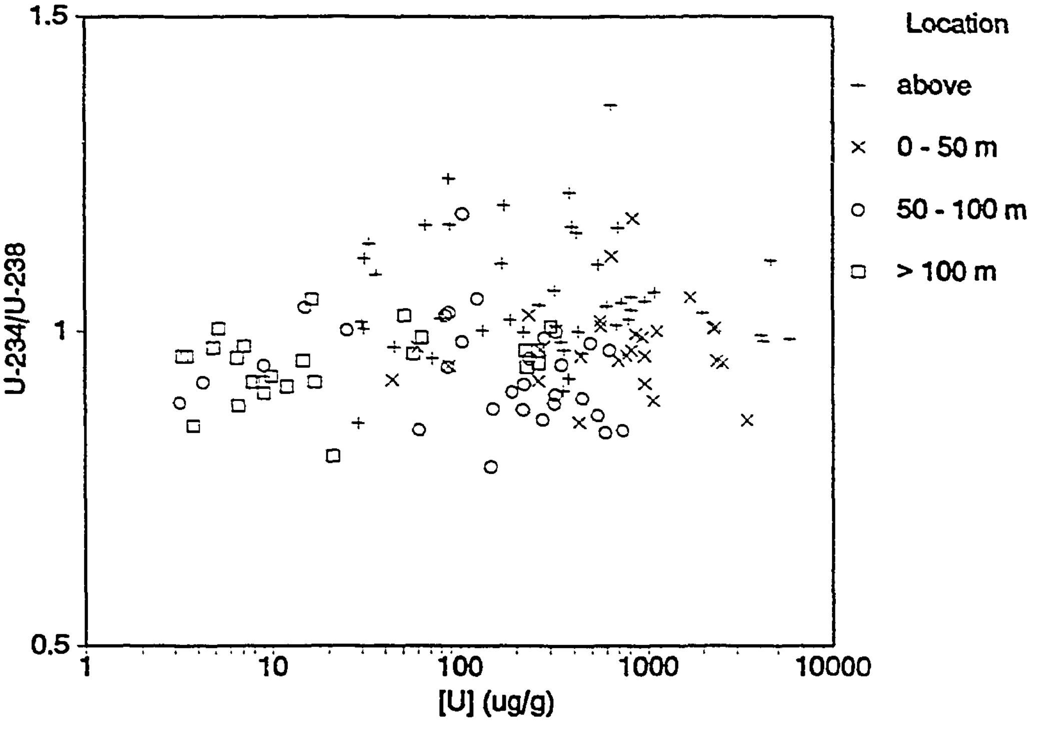

FIGURE 6.2 $^{234}U/^{238}U$ activity ratios in weathered rock versus uranium concentration. Location refers to position relative to the primary uranium mineralisation.

Disequilibria in weathered samples

Radionuclide concentrations and activity ratios determined by alpha spectrometry are included in Appendix 6. Figures 6.2 and 6.3 show the relationship between uranium content $^{234}U/^{238}U$ and $^{230}Th/^{234}U$ activity ratios respectively, for samples from the weathered zone. Distances from the primary mineralisation were determined according to the distance of the sample from the south easterly (down-gradient) boundary of primary mineralisation (Figure 6.1). It can be seen from the figures and Table 6.1 that samples taken from above the primary ore deposit tended to have ratios greater than unity, and samples from down-gradient generally had lower activity ratios, often below unity. This trend is most pronounced for the $^{234}U/^{238}U$ activity ratios. Samples with low uranium concentrations (<10 µg/g), from >100 m down-gradient, occasionally had activity ratios greater than unity. It is possible that these samples were not contacted by uranium bearing groundwaters from the primary mineralised zone, or that the authigenic $^{230}Th/^{234}U$ activity ratios swamped the affect of recently arrived uranium, or some leaching of uranium had recently occurred from this zone, leading to the observed values. Samples from >100 m from the primary zone appeared to show a trend of decreasing $^{230}Th/^{234}U$ activity ratio with increasing uranium content, possibly reflecting a greater recent allogenic component of uranium.

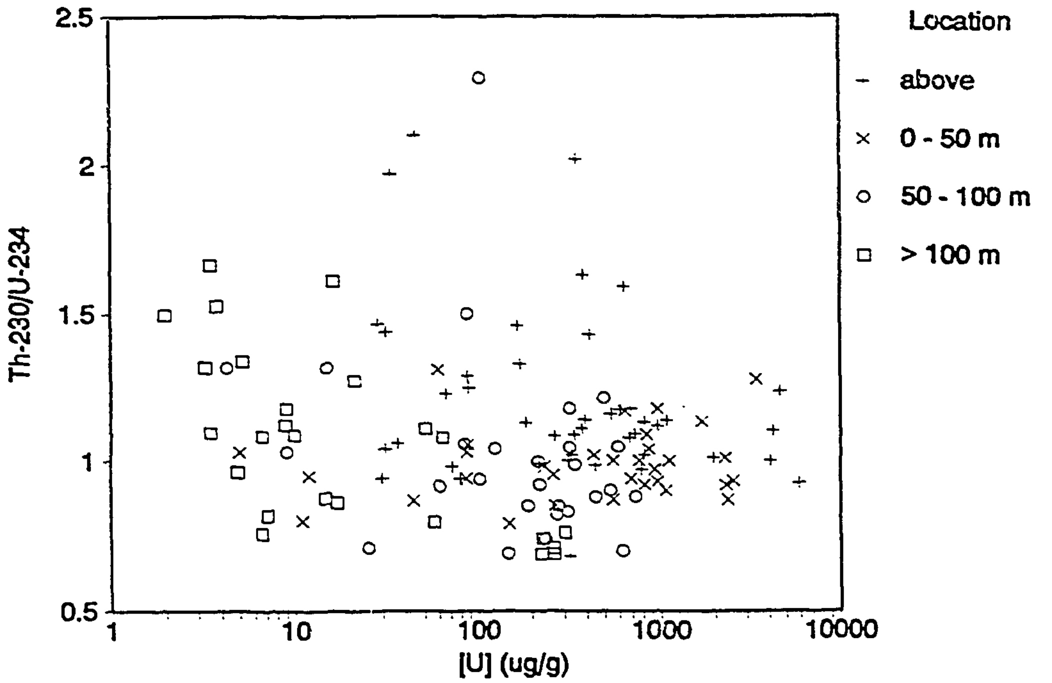

FIGURE 6.3 $^{230}Th/^{234}U$ activity ratios in whole rock versus uranium concentration. Location refers to position relative to the primary uranium mineralisation.

TABLE 6.1

AVERAGE VALUES FOR $^{234}U/^{238}U$ AND $^{230}Th/^{234}U$ ACTIVITY RATIOS IN WEATHERED ROCK

	Location*			
Activity Ratio	Above	0-50 m	50-100 m	>100 m
$^{234}U/^{238}U$	1.06 (0.10)**	0.98 (0.07)	0.93 (0.08)	0.95 (0.05)
$^{230}Th/^{234}U$	1.21 (0.30)	1.00 (0.12)	1.02 (0.32)	1.14 (0.42)

* lateral location of samples relative to primary mineralisation
** mean (standard deviation of mean)

Patterns in the $^{226}Ra/^{230}Th$ activity ratios are less clear. Figure 6.4 shows the pattern of $^{226}Ra/^{230}Th$ activity ratio against uranium content, and Figure 6.5 shows the pattern for distance from primary mineralisation for three depths in the weathered zone.

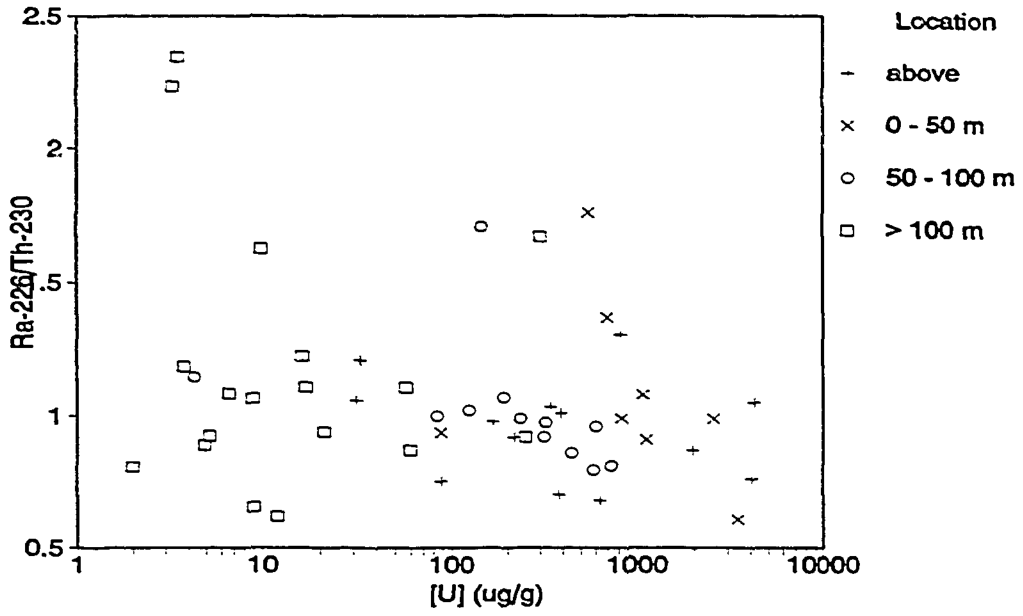

FIGURE 6.4 $^{226}Ra/^{230}Th$ activity ratios in whole rock versus uranium concentration.

The samples were allocated to depth categories according to their positions in the profile relative to the base of the surficial sand layer and the base of the weathered zone. The zones were classified as;

Shallow: within 2 m of the surficial sands and gravel,

Mid-weathered zone: between 2 m below the surficial sands and gravel and 2 m above the base of weathering.

Deep-weathered zone: within 2 m of the base of weathering, including partially weathered rock.

The depth of the surficial sands and the weathered zone were estimated from visual assessment of the core and pulp, and from the contours of surficial sand depth, the weathered zone isopach (Volume 2 of this series) and company drilling logs.

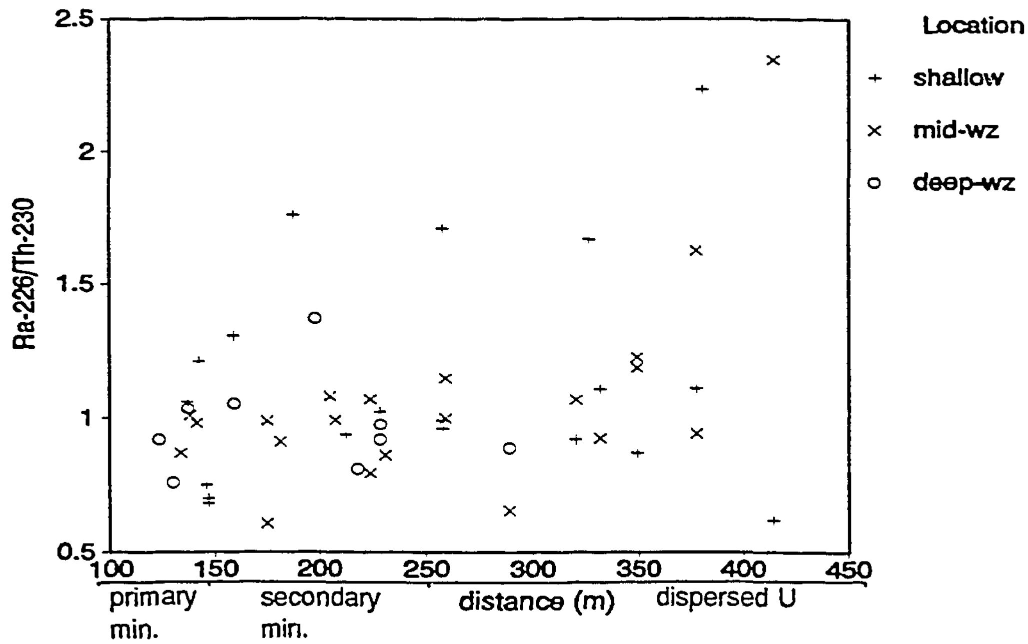

FIGURE 6.5 $^{226}Ra/^{230}Th$ activity ratios in whole rock samples plotted against distance from the 3000 mE mine gridline.

It appears that most of the samples had $^{226}Ra/^{230}Th$ activity ratios near to or below unity, suggesting a net leaching of radium from these weathered zone samples. No depositional site for this leached radium is clear from this data. While many samples had $^{226}Ra/^{230}Th$ activity ratios >1, particularly near surface samples, the degree of radium enrichment does not account for all the radium leached. Dickson and Snelling (1980) observed an approximate equilibrium between ^{226}Ra and ^{230}Th in weathered samples, and in one transition zone sample they found a large excess of ^{226}Ra. On the basis of this information, they postulated an upward movement of groundwater from unweathered reducing conditions, where radium would be expected to be mobile, to oxidising conditions, which cause the deposition of radium onto iron oxides and clays. However, of nine deep weathered zone samples analysed, only one showed a strong enrichment in ^{226}Ra.

Figure 6.6 shows the values of $^{230}Th/^{234}U$ activity ratio with distance from the primary mineralisation for samples from three depth intervals in the weathered zone. It appears that shallow and deep weathered zone samples have the strongest tendency towards low $^{230}Th/^{234}U$ activity ratios, which suggests that these zones may contain the most recently accumulated uranium relative to the authigenic component.

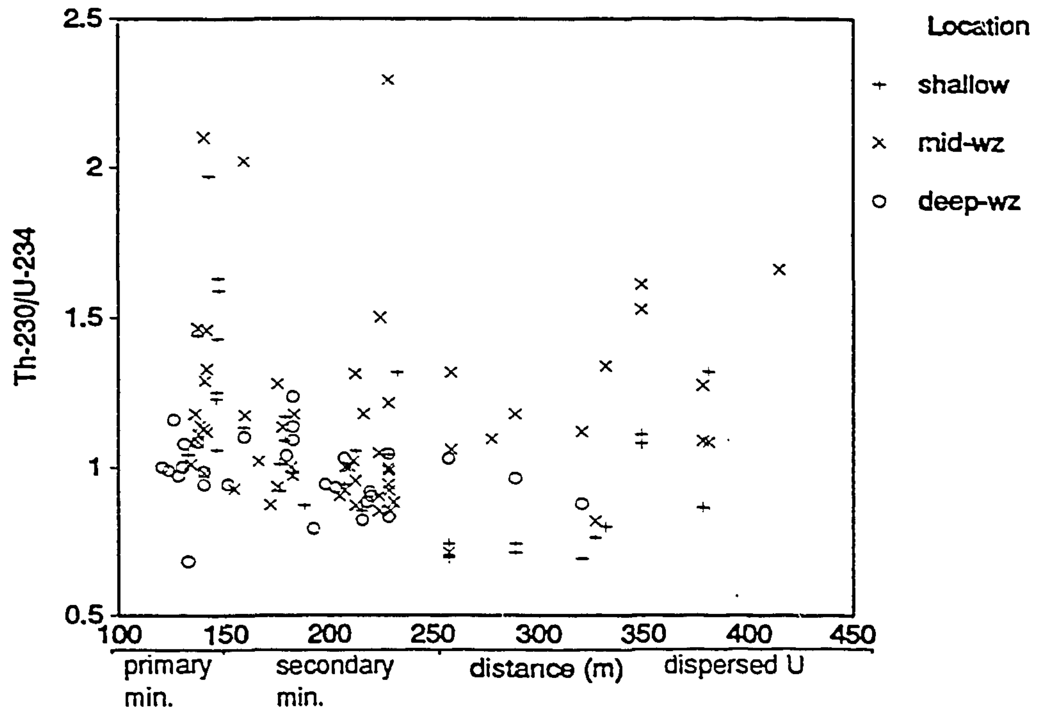

FIGURE 6.6 $^{230}Th/^{234}U$ activity ratios in whole rock plotted against distance from the 3000 mE mine gridline. Location refers to position in the weathered zone.

The effects of distance from the primary ore, and depth, on activity ratios are shown in Figure 6.7, a and b respectively. Samples from deep in the weathered zone, and from a distance of 50-100 m from the primary ore zone, tended to plot in the bottom left corner of the diagrams. Low activity ratios in this case suggest recent accumulation of uranium. Samples from greater than 100 m from the primary ore that showed uranium deposition were mainly from shallow depths. Samples from above the primary ore zone mostly plotted in the top right section, suggesting leaching of uranium.

The data suggest that leaching of uranium has occurred from the weathered zone above the present outline of primary mineralisation, which probably corresponds to a former upward extension of the primary ore. The $^{234}U/^{238}U$ activity ratio is below unity at sites of uranium deposition, and above unity where uranium was leached. This illustrates an apparent preferential mobility of ^{238}U, relative to ^{234}U, in the weathered zone of this deposit. The most pronounced, recent deposition of transported uranium occurs near the base of weathering, about 50-100 m down-gradient of the primary ore. Deposition of uranium further afield is most pronounced near the surface, within about 2 m of the base of the surficial sand deposits. The high $^{234}U/^{238}U$ and low $^{230}Th/^{234}U$ activity ratios in samples from near the surface suggest a more rapid transport system for uranium than deeper in the

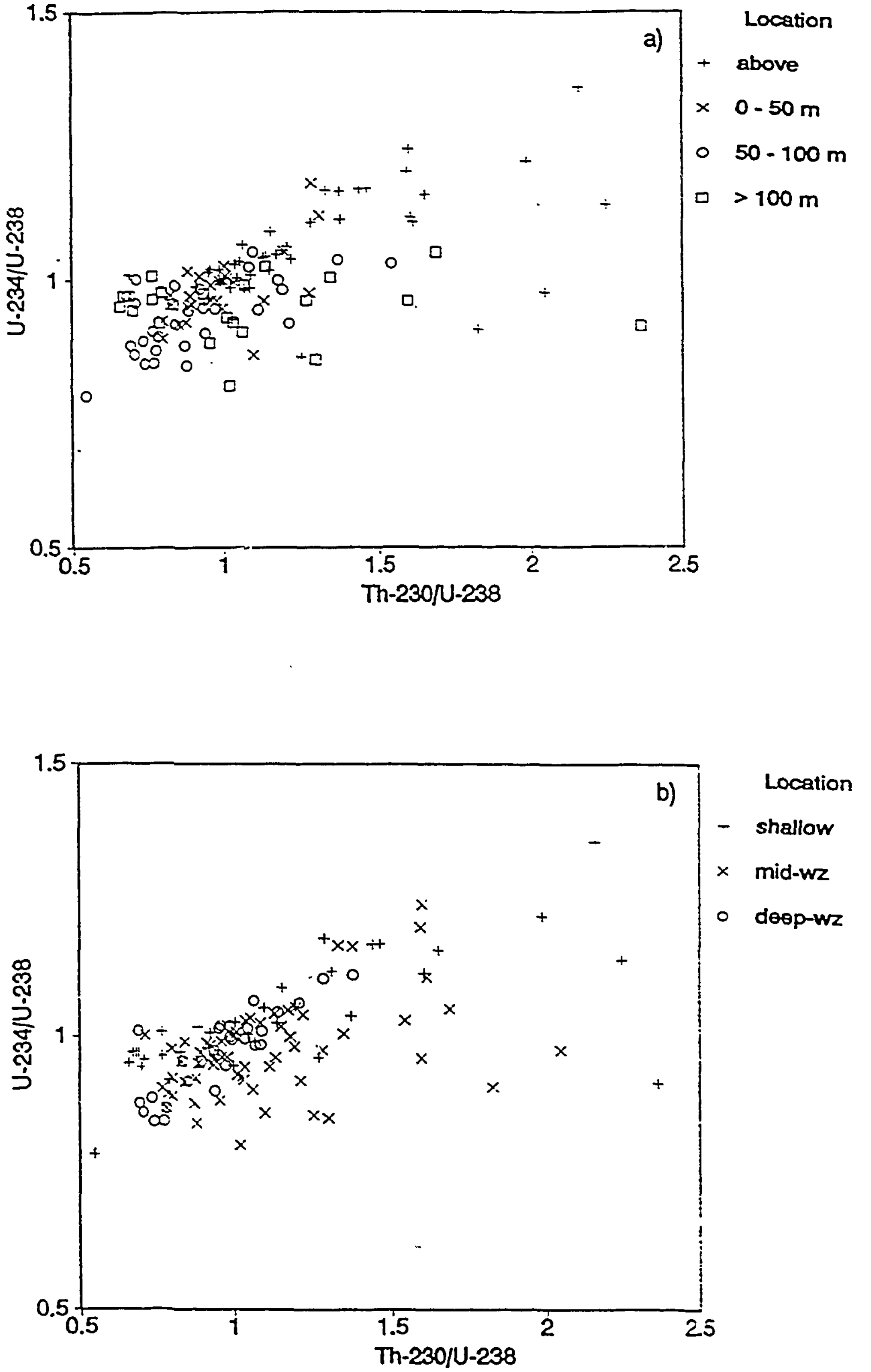

FIGURE 6.7 $^{234}U/^{238}U$ versus $^{230}Th/^{238}U$ in whole rock. Data points designated according to a) distance from primary mineralisation and b) depth

weathered zone (Osmond and Cowart, 1982), with insufficient time for fractionation processes, and/or different solid phase components less conducive to isotopic fractionation. Probable mechanisms for the development of this disequilibrium are discussed in Section 6.2, and in Volume 14 of this Series. An interpretation of bulk whole rock results is difficult, particularly for rock with low uranium content, because of the influence of authigenic components. Such samples are better dealt with by using extraction schemes, as discussed in Section 6.2.

Uranium series nuclides in rocks analysed by gamma spectrometry

Radionuclide concentrations and activity ratios determined using gamma spectrometry are included in Appendix 6. The results are similar to those determined by alpha spectrometry, with $^{230}Th/^{238}U$ activity ratios greater than unity in the upstream and less than unity in the down stream regions. Figure 6.8 shows a comparison of $^{230}Th/^{238}U$ activity ratios determined by α-and γ-spectrometry. There was generally good agreement between the two techniques (r^2=0.92), although γ-spectrometry tended to give a slightly higher ratio than α-spectrometry.

The results from sieved fractions of samples from PH73 13.5-15 m and 18.0-19.5 m revealed that the activity of the finer fractions was higher than the coarser fractions (see Appendix 6). This is probably due to mineral differences between the fractions, with the uranium being preferentially associated with finer minerals such as iron oxides and clays.

6.2 Trends in Chemically Defined Phases

6.2.1 Uranium and uranium series disequilibria in five chemically defined phases

Uranium concentrations and activity ratios for ^{238}U, ^{234}U and ^{230}Th in bulk rock samples have been investigated, to understand the timescale and processes involved for the uranium migration at Koongarra. However, the results obtained by bulk analysis are a composite value of the constituent minerals, which have different uranium concentrations, activity ratios and accessibilities to groundwater. Appendix 3 briefly reviews procedures developed to extract trace metals from specific phases of soil and sediment. Here the extraction procedures developed for soil chemistry were applied to the study of uranium series radionuclides in weathered rock, to identify the significant mineral phases in which isotopic disequilibrium has developed; details of the procedures were given. Before discussing the implications of disequilibrium in the various phases, it is necessary to discuss the effects of the extraction reagents on the minerals in the samples and the consistency and reproducibility of results from the extraction procedures.

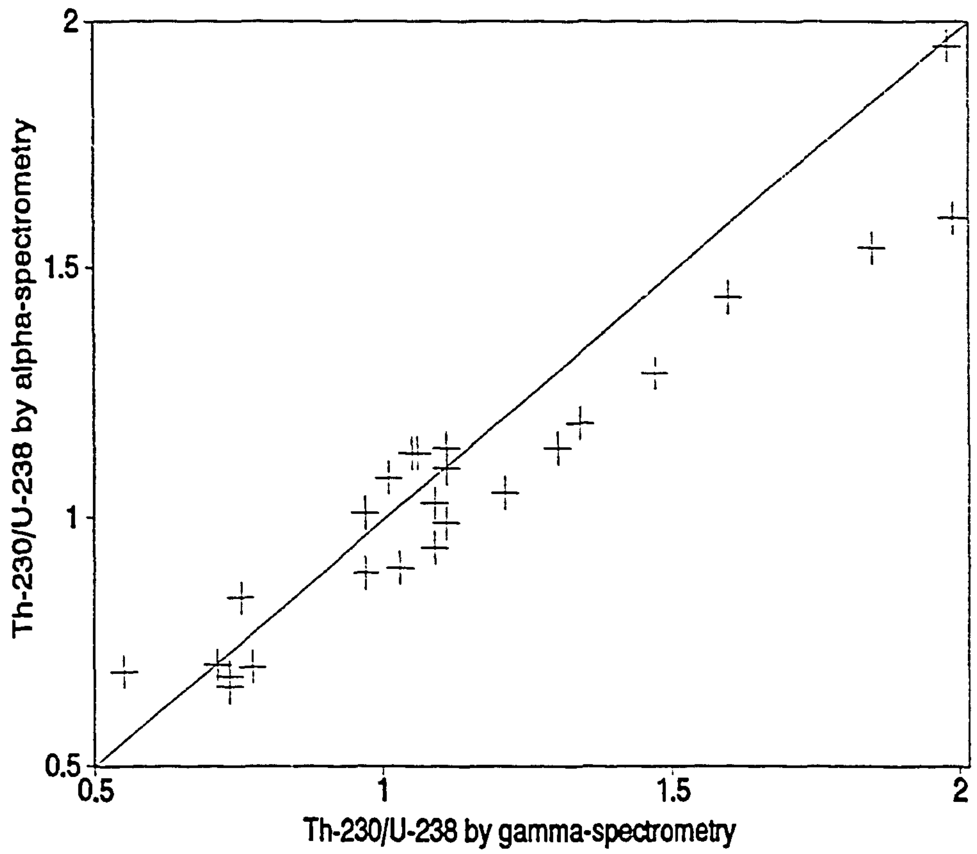

FIGURE 6.8 $^{230}Th/^{238}U$ Activity ratios determined by α- and γ-spectrometry

Reproducibility of results from sequential extractions

Duplicate analyses were carried out to check the reproducibility of the five stage extraction scheme using the sample DDH1 4.7 m (see Table 2.2). The percentages of total uranium removed by each extraction, applied sequentially, were; 31.8 and 31.5% by Morgan's reagent; 12.8 and 15.6% by Tamms acid oxalate (TAO) reagent; 47.5 and 46.5% by citrate dithionite bicarbonate (CDB) solution; 6.2 and 4.5% by 6M HCl and; 1.7 and 1.9% by digestion and fusion of the residual. Inconsistencies in the TAO and 6M HCl extraction steps probably result from a slight dissolution of the crystalline iron minerals by the TAO reagent, and an incomplete dissolution of the iron minerals by the CDB reagent, which would lead to an increase in the amount of uranium in the TAO and 6M HCl solutions respectively. Differences between the duplicates could also have resulted from slightly differing extraction conditions, such as the precise reaction time, filtration time and temperature. The most uranium rich fractions of the samples also gave the most reproducible results (Morgan's and CDB). The $^{234}U/^{238}U$ activity ratios were more consistent between duplicates than the percent uranium extracted or the $^{230}Th/^{234}U$ activity ratio, and were within 4% for each fraction. The $^{230}Th/^{234}U$ activity ratios were consistent within 10% except for the extraction with Morgan's reagent. Small amounts of weakly bound ^{230}Th was extracted using Morgan's reagent, and this amount varied considerably, probably being dependent upon the extraction conditions as discussed above.

Effect of extraction reagents on the mineral phases

The target minerals to be dissolved by each extractant used in this study are given below; additional information is provided in the review of sequential extraction schemes given in Appendix 3. However, X-ray diffraction patterns of residual material were collected after each step so that any mineralogical changes could be estimated, to ensure that the procedure used had the desired effect.

1. Adsorbed trace materials and carbonate minerals. No mineral phase appeared to be removed by extraction with Morgan's reagent (1 M sodium acetate/acetic acid, pH 5.0).

2. Amorphous phases of Fe (eg ferrihydrite), Al and Si, and secondary uranium minerals. Tamm (1922) used acid oxalate for dissolving amorphous phases and ferrihydrite. Chao and Zhou (1983) investigated the dissolution of amorphous and crystalline iron oxides by TAO, and reported the dissolution of 42% of natural and 73% of synthetic amorphous iron oxides, 17-20% of magnetite, and less than 1% of hematite and goethite after 4 hours reaction in darkness. Iron-rich chlorite, biotite and illite were also attacked by TAO solution (Mehra and Jackson, 1960). Random powder X-ray diffractograms of the sample DDH1 19.4-20.5 m (Figure 6.9) show the effect of the sequential extractions on the minerals present. It can be seen that sklodowskite was dissolved by TAO, as the peak for sklodowskite disappeared after treatment with TAO. Experiments conducted to study uranium adsorption onto ferrihydrite and hematite (see Volume 9 of this series), showed that ferrihydrite was completely dissolved by TAO extraction, and that the hematite appeared to be unaffected.

3. Crystalline iron oxides. Hematite (Mehra and Jackson, 1960) and goethite (Mehra and Jackson, 1960; Airey et al., 1985; Lowson et al., 1986) are dissolved by the citrate dithionite bicarbonate (CDB) reagent, while clay and quartz are not affected. X-ray diffraction analysis of extraction residues found this to be the case for the samples used in this study.

4. Clay and some refractory minerals. From XRD analysis, it was found that pitchblende, chlorite and some clay minerals (smectite and vermiculite) were dissolved, but quartz, mica and zeolite were not affected by the 6M HCl extraction step. It appears that kaolinite minerals were partially dissolved. Oxy-hydroxide layers of clay minerals appear to be affected by this extraction, with the leaching of contained elements. However, the skeletal structure of the clay minerals appear to remain intact. This extraction also dissolved any remaining iron oxide.

5. Remaining resistant minerals. Quartz, mica and zeolite were the remaining residual minerals which were dissolved in the digestion and fusion step.

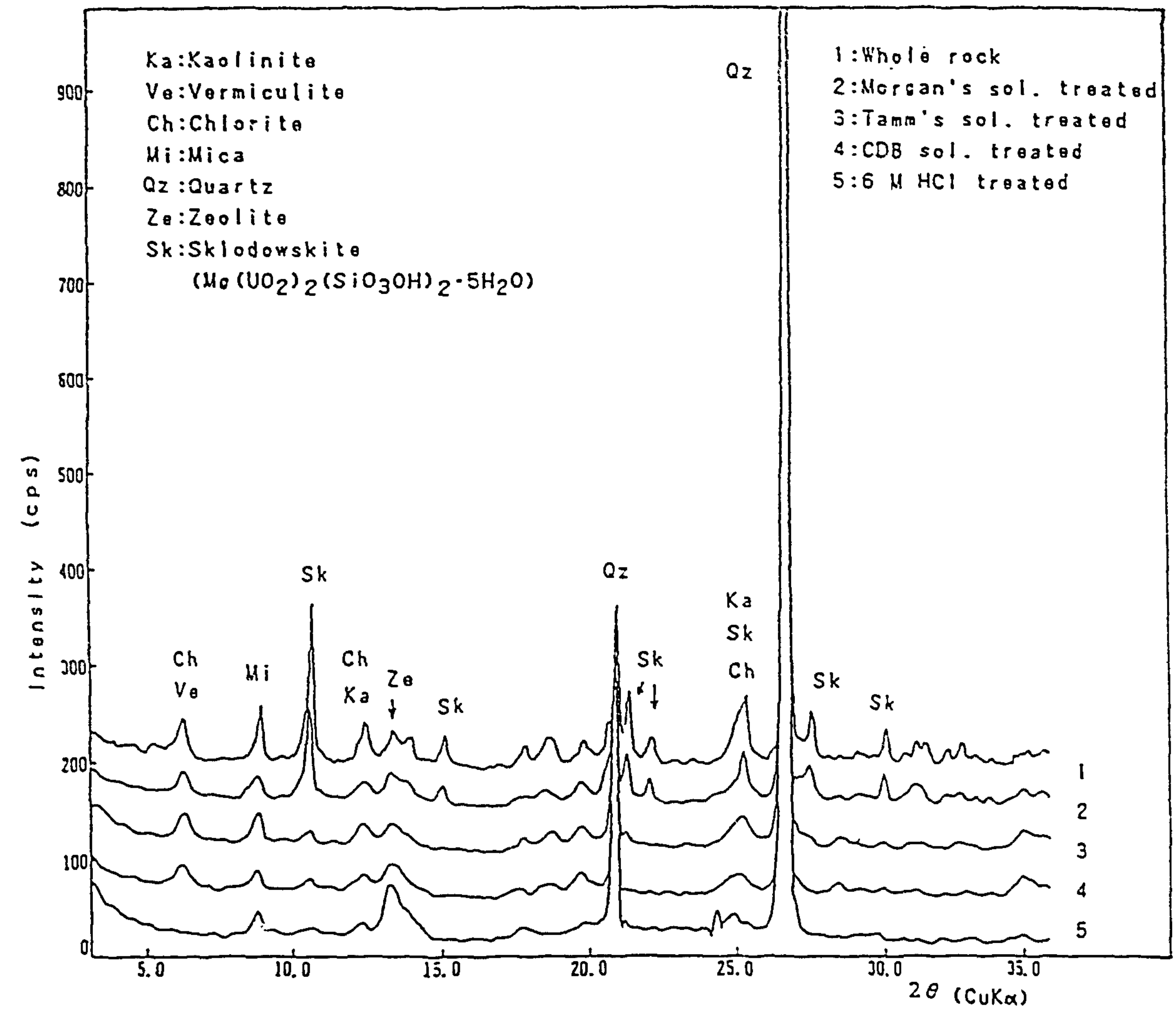

FIGURE 6.9 X-ray diffractograms of sample DDH1 19.4-20.5 m before and after each extraction step

Uranium distributions between minerals

The rock samples listed in Table 2.2 were analysed by the extraction procedure, and Table 6.2 and Figure 6.10 show the distribution of uranium in the extracted phases.

TABLE 6.2

DISTRIBUTION OF URANIUM AMONG EXTRACTED PHASES

Drill Hole	Depth (m)	Uranium Content (mg/kg)	Uranium Removed (%)				
			Morgan	TAO	CDB	6 M HCl	Fusion
DDH1	4.7	2270 (2.2)	31.5 (3.0)	15.6 (2.9)	46.5 (3.0)	4.5 (3.0)	1.9 (3.0)
	19.4-20.5	82300 (2.4)	20.5 (2.9)	72.0 (3.1)	1.3 (5.1)	6.2 (3.0)	0.04 (3.0)
DDH2	33.0-34.3	82500	13.7 (3.1)	7.7 (3.2)	5.3 (5.5)	69.8 (3.2)	3.5 (8.2)
DDH3	10.5-11.7	769 (3.3)	15.6 (2.7)	11.0 (2.9)	49.6 (2.6)	22.9 (2.6)	0.9 (3.3)
	16.3-17.5	965 (2.1)	21.5 (2.9)	6.9 (3.2)	59.6 (2.9)	11.1 (2.9)	0.9 (4.1)
DDH4	14.0-15.2	536 (2.4)	20.7 (3.1)	13.3 (3.5)	41.9 (3.0)	23.4 (3.2)	0.7 (4.2)
PH55	18.3-19.8	316 (2.2)	33.5 (3.0)	12.9 (3.3)	43.4 (3.0)	9.5 (2.8)	0.7 (6.5)
DDH54	13.5-15.0	963 (2.3)	15.0 (3.1)	8.5 (3.3)	71.7 (3.5)	3.7 (3.9)	1.1 (3.1)
PH56	13.5-15.0	323 (2.5)	16.1 (2.8)	5.0 (2.9)	75.7 (2.8)	1.9 (5.3)	1.3 (2.9)
DDH58	9.12	1700 (2.6)	35.2 (2.7)	10.7 (2.5)	47.7 (2.7)	4.0 (2.9)	2.4 (2.9)
	18.2	4620 (2.4)	23.0 (2.6)	18.7 (2.7)	54.3 (2.7)	3.6 (2.9)	0.4 (3.3)
	21.2	1090 (2.2)	24.5 (2.7)	8.3 (2.9)	57.8 (3.1)	6.6 (3.0)	2.8 (3.4)
	24.3	726 (2.4)	27.4 (2.7)	8.3 (2.9)	60.6 (2.7)	2.1 (3.4)	1.6 (3.8)
DDH87	24.3	61.4 (2.3)	25.3 (3.2)	8.4 (3.7)	54.3 (3.2)	6.7 (4.7)	53. (3.6)
DDH85	6.07	44.6 (2.2)	11.1 (3.0)	2.9 (4.3)	3.5 (7.1)	14.7 (3.1)	67.7 (2.5)
	9.12	377 (2.2	3.2 (2.4)	4.3 (2.4)	86.3 (2.3)	3.4 (3.6)	2.9 (5.7)
	15.2	186 (2.3)	11.8 (2.5)	6.9 (2.4)	70.4 (2.3)	3.9 (3.0)	7.0 (2.7)
	21.2	443 (2.5)	16.8 (2.3)	9.6 (2.3)	64.5 (2.2)	5.2 (2.6)	4.0 (2.5)
DDH62	9.12	605 (2.3)	25.1 (2.4)	7.7 (2.5)	62.7 (2.3)	1.8 (3.0)	2.7 (3.2)
	15.2	5907 (2.4)	14.9 (2.5)	38.1 (2.2)	45.5 (2.7)	1.3 (2.5)	0.26 (3.3)

The figures in parenthesis denote counting error (%).

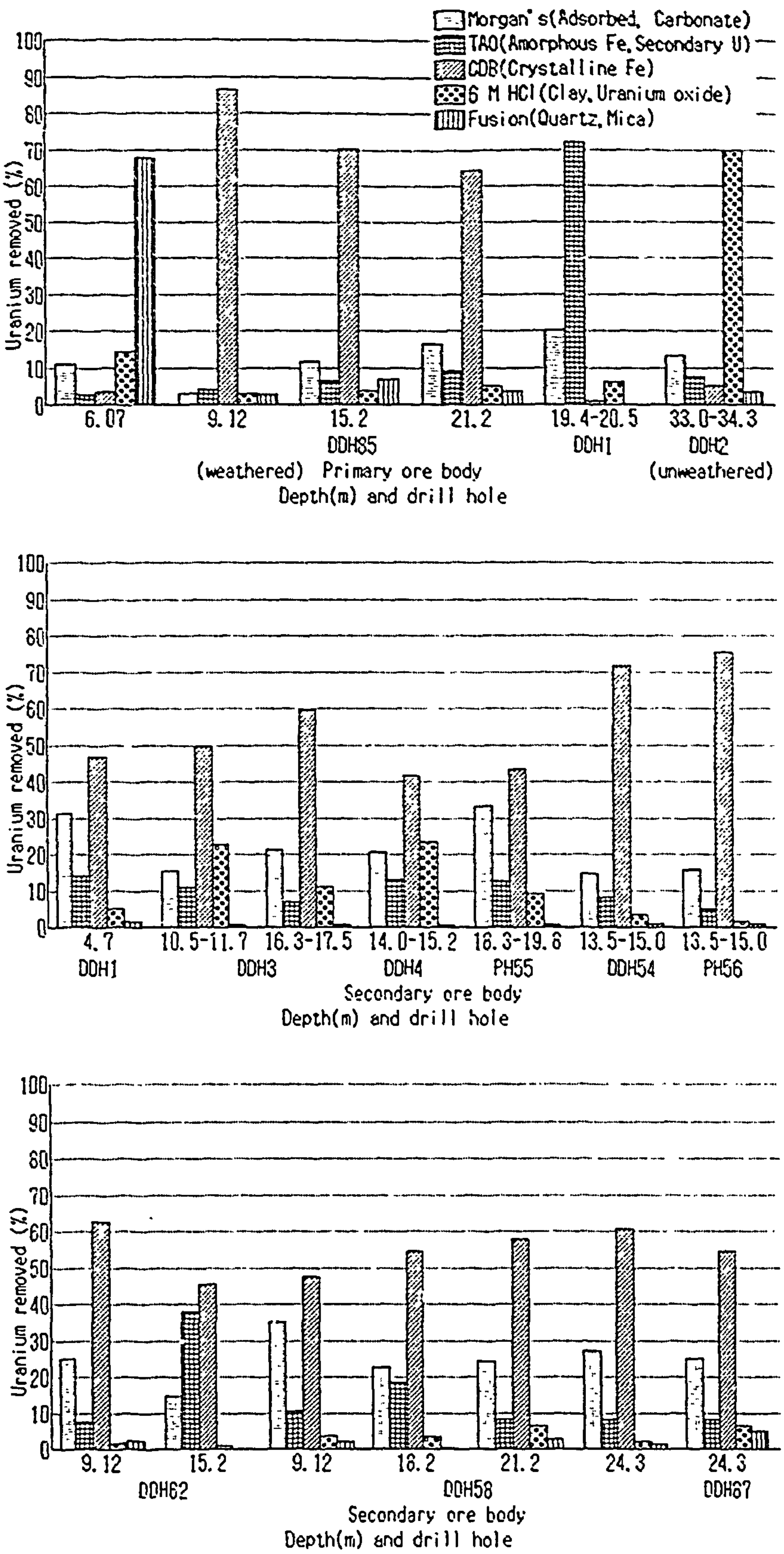

FIGURE 6.10 Distribution of uranium among extracted phases

In the shallow weathered zone of the primary orebody, most of the uranium was contained in the crystalline iron oxide fractions (42-60%), presumably owing partly to the high concentration of these minerals in the samples. Only the sample from DDH85 6.07 m had a high uranium content in the fusion fraction relative to the other fractions. The smaller amount of uranium in the crystalline iron oxide fraction may simply be due to the low concentration of iron oxides in this sample; no iron minerals were detected by XRD, and the colour of the sample was white.

In the mid- to deep-weathered zone of the primary orebody, 72% of the total uranium was incorporated in the TAO-extractable phases, including amorphous iron and secondary uranium minerals in the sample from DDH1 19.4-20.5 m. This sample contained uranyl silicates such as sklodowskite, which are soluble in TAO. Therefore, the large amount of uranium in the TAO fraction resulted from the dissolution of sklodowskite, and possibly other secondary uranium minerals.

In the unweathered primary orebody, 70% of the total uranium was found in the 6M HCl extraction from the sample from DDH2 33.0-34.3 m. Pitchblende was detected in this sample and is soluble in 6M HCl; it is likely that pitchblende was the main form of uranium in this sample.

In the secondary orebody, most of the uranium was contained in the CDB fraction (42-60%) for all weathered zone samples, presumably contained in the detected hematite and goethite.

The high fraction of uranium in TAO-extractable phases in the DDH62 15.2 m sample from the secondary orebody may result from the dissolution of secondary uranium minerals such as saleeite, although no uranium minerals were detected by XRD. Secondary minerals are dissolved by TAO, and the sample location was near to regions where secondary minerals have been observed.

Proportion of material dissolved by extractions

Table 6.3 shows the percent fraction of weight dissolved, and the uranium concentration of each mineral fraction. About 60-90% of sample weight was dissolved in the fusion step for each sample. The largest weight losses by TAO and 6M HCl were found for the DDH1 19.4-20.5 m and DDH2 33.0-34.3 m samples. These two samples contained sklodowskite and pitchblende respectively, and the dissolution of these minerals probably caused the greater weight loss.

TABLE 6.3

PERCENT OF MASS REMOVED BY EACH EXTRACTION STAGE

Drill Hole	Depth (m)	Uranium Content (mg/kg)	Percent mass dissolved (U concentration of extracted material (mg/kg))				
			Morgan	TAO	CDB	6 M HCl	Fusion
DDH1	19.4-20.5	82300 (2.4)*	5.1	7.6 (780000)	2.2 (49000)	19.5 (26000)	65.2 (50)
DDH2	33.0-34.3	82500 (2.2)	3.7	2.2 (290000)	2.1 (210000)	35.5 (162000)	57.1 (5100)
DDH58	9.12	1700 (2.6)	0.2	1.3 (14000)	15.5 (5230)	3.4 (2000)	79.6 (51)
	18.2	4620 (2.4)	0.6	1.3 (66000)	12.1 (21000)	6.2 (2700)	79.8 (23)
	21.2	1090 (2.2)	0.4	2.2 (4100)	7.6 (8300)	10.0 (720)	79.8 (38)
	24.3	726 (2.4)	1.0	1.1 (5500)	4.4 (10000)	5.6 (270)	87.9 (13)
DDH87	24.3	61.4 (2.3)	1.1	1.8 (290)	2.6 (1300)	18.3 (22)	76.2 (4.3)
DDH85	6.07	44.6 (2.3)	0.5	0.7 (180)	0.5 (310)	4.3 (150)	94.0 (32)
	9.12	377 (2.2)	0.6	2.0 (810)	17.3 (1880)	6.9 (190)	75.0 (15)
	15.2	186 (2.3)	0.8	1.3 (990)	8.6 (1500)	4.6 (160)	85.4 (15)
	21.2	443 (2.5)	2.1	1.3 (3300)	7.3 (3900)	22.9 (100)	69.0 (26)
DDH62	9.12	605 (2.3)	0.9	0.8 (5800)	10.7 (3500)	3.1 (350)	85.1 (19)
	15.2	5907 (2.4)	1.1	1.6 (140000)	6.8 (40000)	4.0 (1900)	87.1 (18)

* (% error)

Uranium concentrations in the extracted phases were calculated from the fraction of mass lost and the amount of uranium detected in each extraction (Table 6.3). Since trace materials and uranium adsorbed onto minerals are desorbed by the (initial) Morgan's reagent extraction, the uranium concentration in this fraction does not represent a particular phase, and the data is therefore not presented. The TAO fraction of the DDH1 19.4-20.5 m sample has approximately the same uranium concentration as sklodowskite. This is consistent with the suggestion that most of the uranium in this fraction of the sample is a result of the dissolution of sklodowskite.

The uranium concentration in the 6M HCl fraction of the DDH2 33.0-34.3 m sample (162000 mg/kg) was fairly low relative to pitchblende (869000 mg/kg), which was detected in this sample. If however the 6M HCl-extractable phases consisted of four times as much low uranium clay compared to pitchblende, then the uranium concentration expected in the 6M HCl fraction would be close to that observed. The TAO fraction of the DDH62 15.2 m sample was also rich in uranium (140000 mg/kg uranium). This high concentration suggests the presence of secondary uranium minerals, as it is unlikely that the amorphous phases could contain 14% uranium by mass, without the formation of uranium minerals.

Lead-210 distributions between minerals

Figure 6.11 shows the ^{210}Pb distribution between minerals measured by the sequential extraction procedure, coupled with gamma spectroscopy. The DDH85 6.07 m sample had a ^{210}Pb distribution similar to uranium (high in the fusion fraction). Other samples had different distributions of ^{210}Pb compared to uranium, with most of the ^{210}Pb occurring in the clay mineral fraction (6M HCl). There is a possibility of some reabsorption of lead leached from crystalline iron oxides onto clay minerals during the CDB extraction. The reabsorption of uranium and thorium during extractions is discussed later.

^{234}U/^{238}U activity ratios in chemically defined phases

The ^{234}U/^{238}U activity ratios of the extracted phases are shown in Figure 6.12 and Table 6.4. In the secondary orebody, the ^{234}U/^{238}U activity ratios in the residual minerals (possibly quartz) are significantly greater than unity (2.6-6.3). Sheng and Kuroda (1986) etched the surface of quartz sequentially by different concentrations of HCl or HF. Very high ^{234}U/^{238}U activity ratios were observed in the etching solution from the surface of the quartz. The mechanism proposed to explain these results was that enrichment of ^{234}U, relative to ^{238}U, occurs when ^{234}Th recoils into uranium-poor phases from an adjacent uranium-rich phase. If the uranium-poor phase is more isolated from leaching (e.g. by groundwater), then this would lead to preferential retention of ^{234}U. Therefore, the high ^{234}U/^{238}U activity ratios of resistant mineral phases in the secondary ore deposit of Koongarra probably developed through alpha recoil emplacement from adjacent uranium rich mineral phases and grain boundaries.

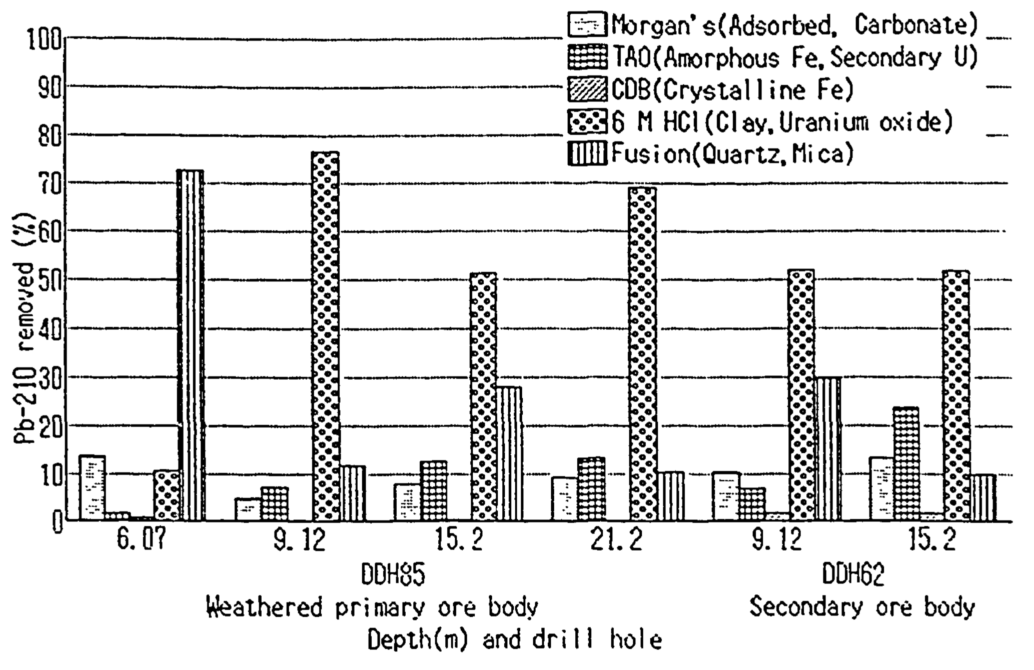

FIGURE 6.11 ^{210}Pb distribution between extracted phases

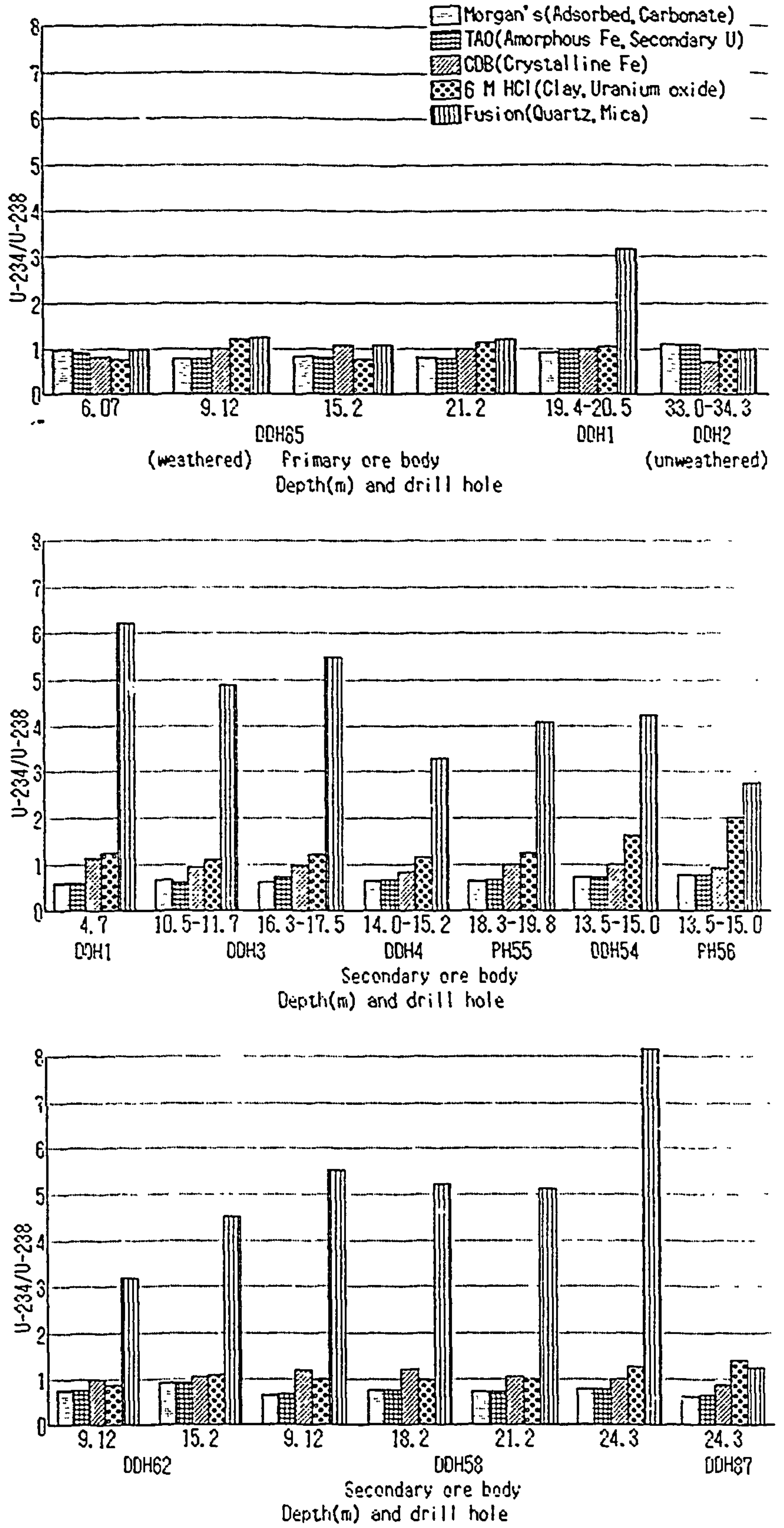

FIGURE 6.12 $^{234}U/^{238}U$ Activity ratios in extracted phases

TABLE 6.4

MEASURED $^{234}U/^{238}U$ ACTIVITY RATIO FOR EACH EXTRACTION

Drill Hole	Depth (m)	$^{234}U/^{238}U$ activity ratio of whole sample	$^{234}U/^{238}U$ activity ratio in extracted phases				
			Morgan	TAO	CDB	6 M HCl	Fusion
DDH1	4.7	1.004 (0.7)	0.605 (2.0)	0.616 (1.8)	1.134 (1.8)	1.210 (1.6)	6.145 (1.4)
	19.4-20.5	0.985 (1.1)	0.939 (0.9)	0.981 (0.9)	1.011 (6.0)	1.069 (1.3)	3.160 (1.1)
DDH2	33.0-34.3	0.999 (0.7)	1.105 (1.1)	1.113 (1.8)	0.715 (7.0)	0.980 (0.9)	1.000 (1.4)
DDH3	10.5-11.7	0.962 (1.6)	0.689 (1.3)	0.638 (2.2)	0.961 (1.3)	1.118 (1.2)	4.876 (2.4)
	16.3-17.5	0.917 (1.1)	0.641 (1.4)	0.730 (2.5)	0.984 (1.4)	1.216 (1.6)	5.500 (3.2)
DDH4	14.0-15.2	0.867 (1.5)	0.658 (1.2)	0.679 (2.9)	0.858 (1.3)	1.169 (2.0)	3.309 (3.7)
PH55	18.3-19.8	0.886 (0.9)	0.659 (1.8)	0.695 (2.6)	1.012 (1.7)	1.241 (1.5)	4.095 (6.3)
DDH54	13.5-15.0	0.961 (1.2)	0.728 (1.4)	0.738 (1.8)	0.994 (2.1)	1.617 (3.1)	4.233 (0.8)
PH56	13.5-15.0	1.000 (1.5)	0.787 (1.0)	0.782 (1.3)	0.931 (1.0)	2.018 (5.1)	2.776 (1.1)
DDH58	9.12	0.992 (1.6)	0.670 (0.9)	0.681 (0.8)	1.201 (1.0)	0.997 (1.9)	5.513 (1.2)
	18.2	1.037 (1.2)	0.763 (0.8)	0.761 (0.8)	1.221 (1.0)	0.983 (1.8)	5.236 (2.1)
	21.2	1.037 (1.1)	0.742 (0.8)	0.748 (1.5)	1.051 (1.5)	1.006 (1.4)	5.140 (2.0)
	24.3	0.980 (1.6)	0.777 (0.9)	0.795 (1.8)	1.003 (1.1)	1.274 (2.5)	8.189 (2.7)
DDH87	24.3	0.829 (1.2)	0.632 (1.8)	0.653 (3.2)	0.864 (1.0)	1.423 (4.8)	1.234 (3.0)
DDH85	6.07	0.926 (1.2)	0.987 (2.4)	0.930 (4.9)	0.809 (9.9)	0.759 (2.6)	0.985 (1.4)
	9.12	1.046 (0.7)	0.777 (1.5)	0.804 (1.7)	1.017 (0.9)	1.214 (1.7)	1.261 (1.9)
	15.2	1.051 (1.0)	0.843 (1.4)	0.828 (1.5)	1.079 (1.1)	0.764 (2.7)	1.077 (2.2)
	21.2	0.990 (1.5)	0.809 (1.1)	0.783 (1.3)	1.005 (0.9)	1.128 (1.3)	1.214 (1.5)

The figures in parenthesis denote counting error (%).

The $^{234}U/^{238}U$ activity ratios for the Morgan's and TAO extractions are similar, and are significantly below unity for all the samples in the secondary orebody (0.59-0.79 and 0.61-0.78 respectively). These values are consistent with values found for groundwater from this area (see Volume 7 of this series). Payne (1986) demonstrated that Morgan's solution extracted the uranium that was most exchangeable with the aqueous phase over short timescales, and Lowson et al (1986) suggested that the TAO-extractable uranium reached sorption equilibrium with the groundwater in natural systems. The results presented here also suggest a chemical equilibrium for uranium between the Morgan's and TAO-extractable fractions, and the groundwater.

The preferential leaching of ^{234}U from mineral phases of rock to liquid phases has been extensively investigated. It has been shown that alpha recoil damage of the mineral in the vicinity of the daughter ^{234}U renders the ^{234}U more accessible than ^{238}U to leaching by groundwater. However, this applies only to systems where the uranium is initially contained within the mineral phases. As has been discussed in Section 6.1, $^{234}U/^{238}U$ and $^{230}Th/^{234}U$ activity ratios of rock, up-gradient of the primary orebody, are greater than unity. Down-gradient, such as in the secondary orebody, the ratios tend to be below unity. Groundwater $^{234}U/^{238}U$ activity ratios were also lower in the secondary orebody compared to the primary ore zone (see Volume 7 of this series), and similar patterns have been observed for TAO only extractions, as discussed in Section 6.2.2. Low activity ratios possibly developed as a result of the location of most of the accessible uranium at grain boundaries, as opposed to within grains. This would result in an apparent preferential retardation of ^{234}U mobility relative to ^{238}U, owing to alpha recoil emplacement of ^{234}U.

Samples containing about 3% or more of their uranium in the fusion fraction, usually had low $^{234}U/^{238}U$ activity ratios in that fraction (<~1.3). These samples were either not fully weathered (DDH87 24.3 m, DDH2 33.0-34.3 m), or were from the zone of primary mineralisation. To develop strong disequilibrium between ^{234}U and ^{238}U in the resistant phases, it is necessary that the initial uranium concentration of these phases be low. In addition, the sample needs to be weathered, and contain uranium deposited after weathering.

Excess ^{234}U activity appears to be related to the concentration of uranium in the CDB fraction (crystalline iron oxides), as shown in Figure 6.13. In this case, the excess ^{234}U is the activity due to ^{234}U minus the activity from ^{238}U in Bq/g. Alpha-recoil emplacement of ^{234}Th into resistant minerals may occur if they are coated with iron oxides rich in uranium.

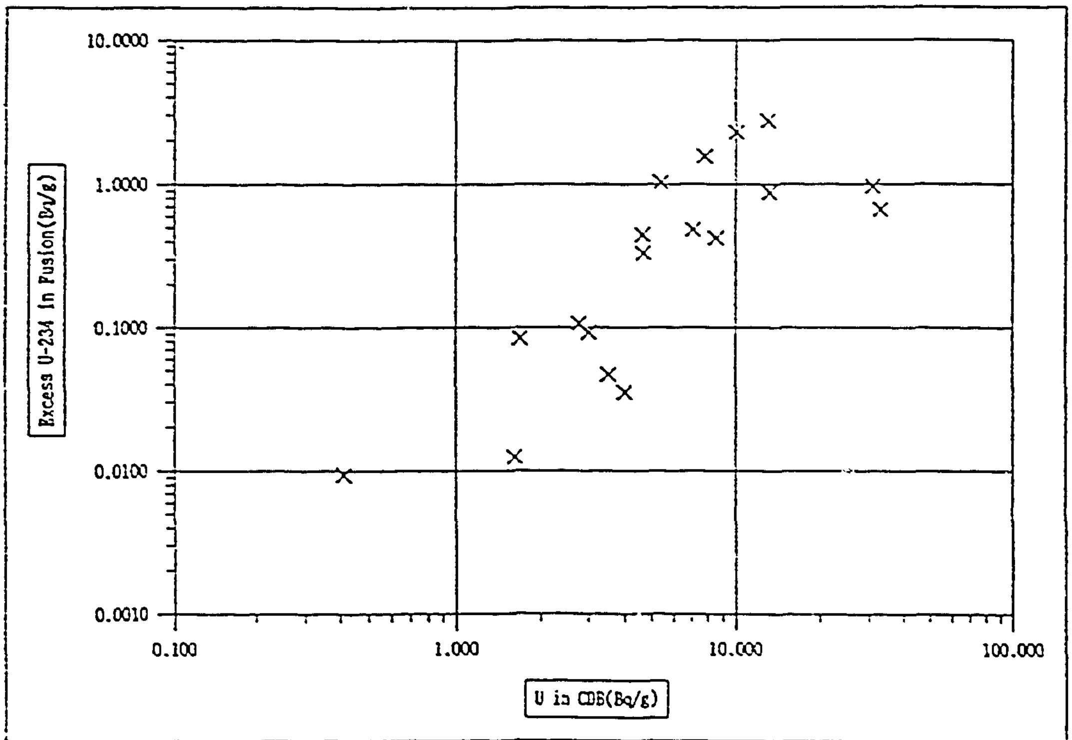

FIGURE 6.13 Excess ^{234}U in the fusion fractions (Bq/g) versus the uranium concentration in crystalline iron oxides (CDB fractions)

$^{230}Th/^{234}U$ Activity ratios between minerals

Sholkovitz (1989) noted some of the disadvantages of chemical leaching, by reporting that ^{152}Eu extracted from one phase readsorbed to another phase under some extraction conditions, included during extraction with Morgan's solution. Consequently, the extent of readsorption of uranium and thorium onto clay minerals during the extractions used in this study was examined prior to the analysis of the $^{230}Th/^{234}U$ activity ratio (Table 6.5). Pure chlorite (Nichika 16019-31-3) and smectite (Kunipia F) were treated separately with Morgan's, TAO and CDB solutions, containing ^{238}U and ^{229}Th tracers. The fraction of ^{238}U and ^{229}Th adsorbed onto the clay minerals and bottle surface were determined by measurement of the isotopes in solution. The activity of inherent ^{238}U in the minerals was negligible compared to the activity of the tracer.

Table 6.5 shows the extent of readsorption of uranium and thorium onto the clay minerals. The readsorption of uranium can be regarded as negligible. However, for thorium, a maximum of 20% readsorption onto the smectite was observed during the TAO extraction, and this must be considered in the discussion of $^{230}Th/^{234}U$ activity ratios obtained by this extraction procedure.

TABLE 6.5

ADSORPTION OF URANIUM AND THORIUM TO CLAY MINERALS DURING EXTRACTION

		% Activity adsorbed	
Reagent	Clay mineral	Uranium	Thorium
Morgans	Chlorite	2	12
	Smectite	0	8
	Blank	0	6
TAO	Chlorite	0	1
	Smectite	5	20
	Blank	0	1
CDB	Chlorite	0	1
	Smectite	0	0
	Blank	0	0

Table 6.6 and Figure 6.14 show the $^{230}Th/^{234}U$ activity ratios in the different phases determined by the extraction procedure. Remarkable disequilibrium is found in the CDB fraction of the DDH1 19.4-20.5 m sample, from the primary orebody near the base of weathering. The $^{230}Th/^{234}U$ activity ratios in the TAO and 6M HCl fractions of the DDH85 6.07 m sample are also much greater than unity. High $^{230}Th/^{234}U$ activity ratios in the weathered zone up-gradient of the primary ore zone indicate strong leaching of uranium has occurred.

TABLE 6.6

MEASURED $^{230}Th/^{234}U$ ACTIVITY RATIOS IN EXTRACTED PHASES

Drill Hole	Depth (m)	$^{230}Th/^{234}U$ activity ratio in whole sample	$^{230}Th/^{234}U$ activity ratio				
			Morgan	TAO	CDB	6 M HCl	Fusion
DDH1	4.7	1.01 (2.3)	0.053 (5.7)	0.779 (3.5)	1.263 (2.5)	1.036 (2.7)	1.057 (4.2)
	19.4-20.5	1.04 (2.9)	0.652 (2.4)	0.929 (3.5)	4.181 (5.3)	1.177 (1.7)	1.443 (1.6)
DDH2	33.0-34.3	0.99 (2.0)	0.399 (2.6)	1.719 (3.0)	1.391 (9.0)	0.927 (2.2)	1.092 (8.8)
DDH3	10.5-11.7	1.00 (4.0)	0.337 (7.6)	0.509 (4.6)	0.977 (2.9)	0.955 (2.7)	1.130 (5.7)
	16.3-17.5	0.93 (2.2)	0.062 (6.6)	0.913 (4.5)	1.062 (3.0)	1.038 (4.3)	1.205 (3.7)
DDH4	14.0-15.2	0.90 (2.1)	0.064 (9.4)	0.647 (4.0)	0.989 (4.0)	1.002 (2.8)	1.297 (5.2)
PH55	18.3-19.8	0.83 (2.4)	0.025 (9.6)	1.121 (4.4)	0.964 (2.9)	1.008 (2.5)	1.059 (6.7)
DDH54	13.5-15.0	1.178 (2.5)	0.068 (4.1)	1.847 (2.2)	1.225 (2.5)	1.423 (3.1)	1.463 (2.1)
PH56	13.5-15 0	1.179 (2.4)	0.151 (2.8)	2.249 (1.8)	1.282 (1.8)	1.474 (5.5)	1.339 (3.4)
DDH58	9.12	1.052 (3.8)	0.107 (2.7)	0.950 (1.4)	1.524 (1.8)	1.151 (2.5)	1.369 (4.2)
	18.2	1.063 (2.1)	0.150 (3.0)	0.978 (1.7)	1.384 (1.8)	1.244 (2.1)	1.648 (4.2)
	21.2	1.093 (1.5)	0.156 (2.4)	1.113 (2.6)	1.306 (2.0)	1.173 (2.5)	1.671 (2.7)
	24.3	1.098 (1.9)	0.133 (3.1)	0.952 (3.0)	1.230 (1.6)	1.598 (3.2)	1.976 (2.6)
DDH87	24.3	0.945 (1.9)	0.136 (5.8)	1.104 (4.4)	0.978 (3.1)	1.437 (4.9)	1.460 (5.2)
DDH85	6.07	2.193 (2.3)	1.347 (2.9)	7.000 (4.5)	2.270 (8.0)	6.005 (3.5)	1.492 (3.3)
	9.12	1.129 (1.3)	0.461 (2.7)	1.346 (2.2)	1.164 (1.6)	1.096 (3.8)	1.966 (23)
	15.2	1.124 (1.8)	0.200 (2.7)	1.538 (1.9)	1.164 (1.6)	2.042 (3.5)	1.328 (4.1)
	21.2	1.020 (1.9)	0.085 (3.3)	0.949 (1.9)	1.057 (1.4)	1.828 (2.4)	1.562 (2.9)
DDH62	9.12	1.011 (1.6)	0.102 (2.7)	0.953 (2.2)	1.184 (1.5)	1.611 (3.0)	1.417 (3.0)
	15.2	0.912 (1.4)	0.476 (2.2)	0.924 (1.3)	0.997 (2.5)	2.102 (1.8)	1.761 (2.6)

The figures in parenthesis denote counting error (%).

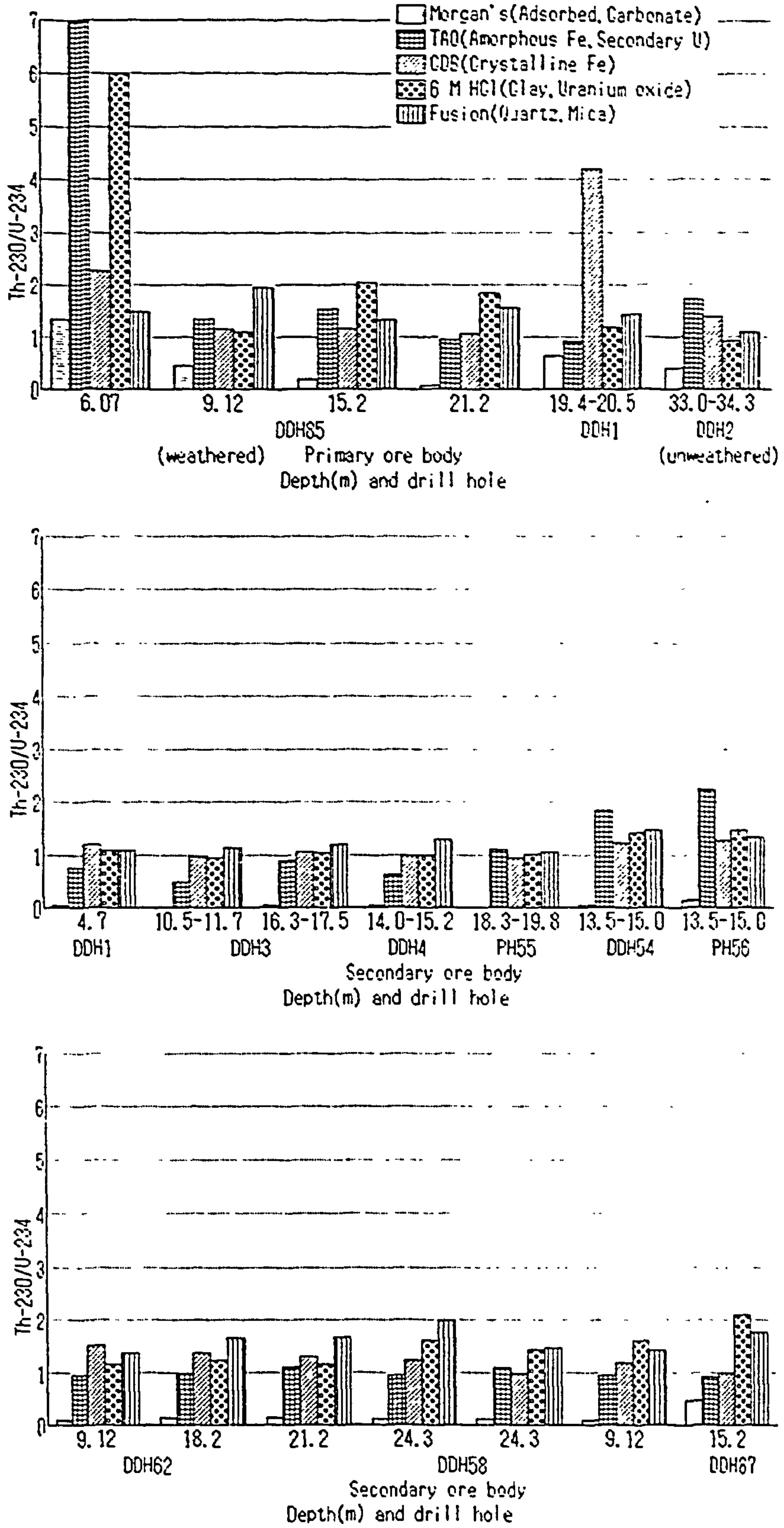

FIGURE 6.14 Measured $^{230}Th/^{234}U$ activity ratios in extracted phases

Mineral separation

Heavy liquid separation was used to separate mineral components of two samples according to their specific gravity. Combinations of tetrabromoethane and acetone were used to separate the minerals from samples (A) DDH68 14 m and (B) PH56 14 m into four density classes; (1) <2.63; (2) 2.63-2.77; (3) 2.77-2.93 and; (4) >2.93 g cm^{-3}. No material from PH56 14 m was found to be >2.92 g cm^{-3}. Further details of the methodology and mineralogical results are discussed in Volume 9 of this series. Each fraction was analysed by the sequential extraction procedure. This gave uranium concentrations and associated activity ratios in physically and chemically defined phases. Uranium distributions, and $^{234}U/^{238}U$ and $^{230}Th/^{234}U$ activity ratios are given in Table 6.7 and shown in Figure 6.15.

The mineral components of DDH68 14 m were not clearly separated by the heavy liquid procedure. X-ray diffraction analysis did show a lower quartz content and a higher kaolinite content in the heaviest fraction (A4) compared to the lighter fractions (A1, A2, A3). The minerals of PH56 14 m were more effectively separated, with the dominant mineral in each fraction being vermiculite in the lightest (B1), quartz in the middle fraction and illite in the heaviest fraction (B3). The patterns of dominant minerals in each density fraction do not follow the patterns of mineral densities, probably as a result of coagulation of mixed grains.

In the heaviest fraction from DDH68 14 m (A4), the uranium was less extractable by Morgan's reagent and more extractable by CDB than in the lighter fractions. For PH56 14 m, the extractability of the uranium by Morgan's reagent decreased with increasing specific gravity.

The $^{234}U/^{238}U$ activity ratio for fusion fractions from DDH68 14 m was smallest in the heaviest fraction (A4). In both DDH68 14 m and PH56 14 m samples, the $^{234}U/^{238}U$ activity ratio in the fusion fraction tended to decrease with increasing specific gravity. Similarly the contribution to the fusion fraction by quartz appeared to decrease with increasing specific gravity. The contribution of mica tended to increase, particularly in PH56 14 m. This suggests that ^{234}U enrichment is most pronounced in quartz, compared to in illite. Possibly illite contains more allogenic uranium, and therefore the activity ratio in illite could change less with the same amount of recoil input ^{234}U. However, A2 is the only DDH68 fraction with significant illite, yet has the highest ratio of the fusion extractions.

The activity ratio $^{230}Th/^{234}U$ was greater than 2 in the 6M HCl-extractable material of the heaviest fraction from DDH68 14 m (A4). This fraction was dominated by kaolinite, and there was a higher concentration of kaolinite in this sample than in PH56 14 m. In PH56 14 m, this ratio had a very different pattern between chemical phases in the heaviest fraction (B3), compared to the lighter fractions (B1, B2). This may be related to the greater relative abundance of illite in this fraction.

TABLE 6.7

RESULTS FOR MINERAL SEPARATION EXPERIMENTS

	DDH68 - 14 m				PH56 - 14 m		
	Specific Gravity						
	SG<2.63	2.63<SG<2.77	2.77<SG<2.93	2.93<SG	SG<2.63	2.63<SG<2.77	2.77<SG<2.93
% Weight	10.0	40.6	47.4	2.0	58.0	38.5	3.5
[U] Bq/g	6.08	15.2	28.5	47.5	4.55	2.14	4.19
% U Removed							
Morgan	35.3 (2.1)	32.7 (2.1)	31.9 (2.2)	25.2 (2.5)	17.6 (2.3)	15.6 (2.5)	8.2 (3.6)
TAO	19.9 (2.4)	18.4 (2.2)	19.0 (2.2)	18.5 (3.6)	6.4 (2.5)	5.9 (2.9)	5.6 (3.5)
CDB	41.9 (2.3)	45.7 (2.2)	45.2 (2.2)	53.2 (2.3)	72.9 (2.1)	74.9 (2.1)	74.5 (2.3)
6 M HCl	1.9 (2.9)	2.3 (2.6)	3.0 (2.7)	2.4 (2.7)	2.1 (5.0)	2.1 (6.3)	8.5 (4.0)
Fusion	0.94 (2.9)	0.87 (3.3)	0.87 (2.7)	0.64 (4.0)	1.1 (4.9)	1.5 (4.0)	3.2 (4.8)
$^{234}U/^{238}U$ AR							
Morgan	0.594 (0.8)	0.598 (0.7)	0.592 (0.9)	0.603 (2.2)	0.758 (1.4)	0.802 (1.7)	0.811 (4.3)
TAO	0.607 (1.7)	0.619 (1.1)	0.615 (1.1)	0.665 (4.6)	0.782 (2.2)	0.801 (2.7)	0.896 (4.1)
CDB	1.266 (1.3)	1.232 (1.1)	1.213 (1.0)	1.199 (1.1)	0.986 (0.6)	1.001 (0.6)	0.990 (1.4)
6 M HCl	1.972 (2.5)	1.595 (2.0)	1.425 (2.3)	1.078 (2.5)	2.180 (5.3)	2.066 (7.0)	1.024 (4.4)
Fusion	10.01 (2.0)	10.83 (1.9)	10.19 (1.2)	6.139 (3.4)	2.933 (4.5)	2.536 (3.7)	1.977 (5.0)
$^{230}Th/^{234}U$ AR							
Morgan	0.102 (2.9)	0.096 (2.8)	0.090 (2.9)	0.101 (7.3)	0.104 (5.0)	0.092 (6.9)	0.155 (12)
TAO	0.970 (2.2)	0.933 (1.4)	0.913 (1.4)	0.881 (4.7)	1.828 (2.3)	1.780 (3.3)	1.301 (4.0)
CDB	1.272 (1.5)	1.305 (1.4)	1.304 (1.2)	1.188 (1.3)	1.175 (1.0)	1.119 (1.3)	1.297 (1.5)
6 M HCl	1.696 (2.2)	1.596 (1.7)	1.578 (2.1)	2.010 (2.3)	1.430 (4.7)	1.313 (4.8)	1.430 (4.5)
Fusion	1.454 (5.2)	1.022 (3.8)	1.175 (4.7)	1.331 (4.2)	1.253 (5.5)	1.098 (8.7)	1.520 (8.8)

The figures in parentheses denote counting error (%).

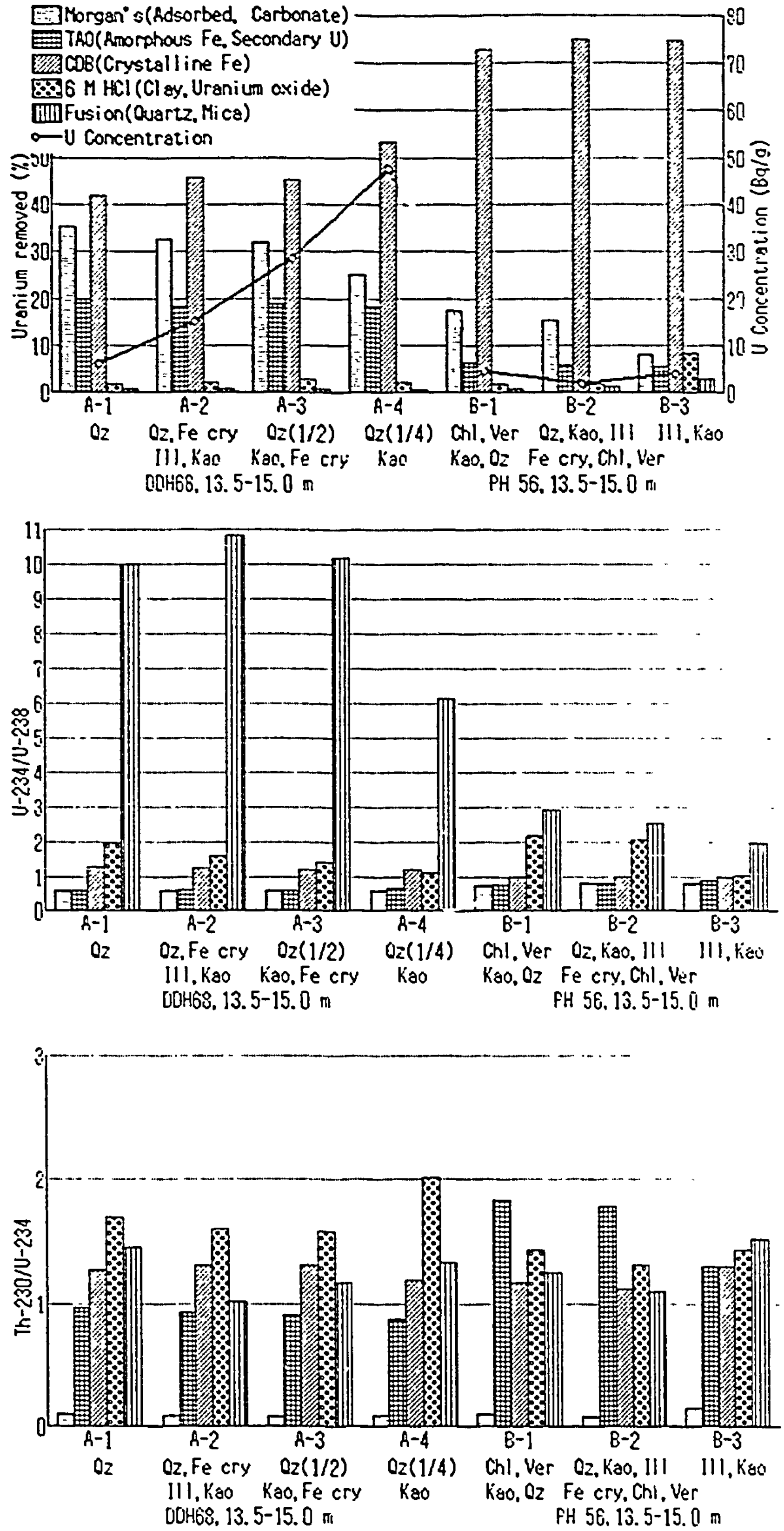

FIGURE 6.15 Uranium series results for chemical extractions of separates defined by specific gravity

Summary of 5-stage sequential extraction studies

The distribution of uranium between mineral phases, as determined by sequential extraction, can be explained on the basis of the mineral composition of the rock. In the secondary orebody (weathered), the CDB-extractable minerals (crystalline iron oxides) are the main mineral phases involved in uranium accumulation. Near the top of the unweathered zone of the primary orebody, TAO-extractable minerals (including secondary uranium minerals such as sklodowskite) are the mineral phases associated with uranium accumulations. In the primary orebody (unweathered), uranium was mainly 6M HCl-extractable, from uranium oxides such as pitchblende.

The $^{234}U/^{238}U$ activity ratios of Morgan's reagent and TAO-extractable phases (adsorbed, carbonate and amorphous iron phases) were less than unity and similar to that of the groundwater. This suggests that uranium in these phases is accessible to, and in approximate equilibrium with, the groundwater. More resistant minerals in the weathered rock, particularly quartz, are enriched in ^{234}U, probably by α-recoil. This illustrates a preferential retardation of ^{234}U mobility relative to ^{238}U.

High $^{230}Th/^{234}U$ activity ratios were found in some extraction fractions from very weathered samples up-gradient of the orebody. Strong leaching of uranium is likely to have occurred from these minerals at this location.

The results show that mineral alteration mechanisms, leading to strong fixation of radionuclides, as well as sorption, need to be considered in the evaluation of the long term migration behaviour of radionuclides in weathered rock.

6.2.2 Two stage dissolution system - estimates of accessible uranium-series isotopes

A two stage dissolution scheme was used to estimate the concentrations of uranium series isotopes in phases accessible to, and in equilibrium with, the groundwater. Extraction with TAO was used to estimate accessible uranium, and inaccessible uranium was estimated from the digestion of the TAO-extract residue. In addition, multi-stage extraction results were converted to two phases; TAO-extractable, which was the sum of Morgan's and TAO-extractable phases; and residual, which was the sum of CDB- and HCl-extractable phases and fusion of the residual. Uranium series disequilibria in accessible phases of the weathered zone at Koongarra was measured, to determine areas of accumulation and leaching of uranium, and their varying intensities. The data are presented in tabular form in Appendix 6. Much of the data presented in this section are used in Volume 14 of this series, for transport modelling.

Some general comments about the applicability of the technique to the estimation of accessible species at Koongarra and potential errors are appropriate. The term accessible implies species that are in isotopic equilibrium with the aqueous phase. The material may be trapped in recently formed minerals, that are sufficiently labile to allow exchange of constituents with groundwater over short timescales. If extractions with TAO are to be used as an indicator of accessible material, then the extraction should generate $^{234}U/^{238}U$ activity ratios similar to the groundwater, and to mild extractants such as Morgan's reagent. Also, samples separated by only a small distance should have similar $^{234}U/^{238}U$ activity ratios in TAO-extractable phases, assuming that the samples were in contact with the same groundwater. The dissolution of phases such as secondary uranium minerals, the possibility of readsorption during the extraction, and the reproducibility of the technique were considered in Section 6.2.1. Comparisons were made between $^{234}U/^{238}U$ activity ratios in Morgan's reagent extractions and TAO extractions. For each sample not containing uranium minerals, the $^{234}U/^{238}U$ activity ratios are similar in both fractions.

Local uniformity of $^{234}U/^{238}U$ activity ratios in TAO extracts

Examination of the data in Appendix 6 shows that the TAO extracts of many samples separated by small distances, had similar $^{234}U/^{238}U$ activity ratios. For example, four shallow samples from DDH52; 0-1.1 m, 1.9 m, 2.2-3.2 m and 5.8 m, which cover a distance of just over 8 m along the drill core, had activity ratios that lay between 0.915 and 0.889. The whole rock activity ratio was between 1.36 and 1.11. Other examples of samples close to one another (within about 10 m), showing similar $^{234}U/^{238}U$ activity ratios, include the 5.8-7 m samples from DDH3 and DDH4, and the 14-15.2 m samples from DDH3 and DDH4. Greater variability was observed at depth, but this may reflect variability in groundwater contact. It is therefore concluded that samples with similar mineral components and groundwater contact, for example those separated by distances of only about 1 m, have very similar $^{234}U/^{238}U$ activity ratios in TAO extracts. Analysis of subsamples, such as from M1 13 m, M3 13 m, and W2 14 m where strong iron oxide zoning was observed, showed significant variability in TAO-extractable components, particularly in the $^{230}Th/^{234}U$ activity ratio and uranium concentration. The most consistent parameter was the $^{234}U/^{238}U$ activity ratio.

Solubility of secondary uranium minerals in TAO

The dissolution of secondary minerals by TAO has been discussed in Section 6.2.1. It was found that sklodowskite was dissolved by TAO. Similarly Nightingale (1988a) found that saleeite is soluble in TAO. Such phases may approximate closed systems in which case they could not be rregarded as accessible. Consequently, samples were chosen only when no secondary uranium minerals could be seen. Noranda Australia company drill logs were consulted to see if any such minerals were observed in the vicinity of the analytical sample. Two samples were analysed that were known to contain traces of saleeite (DDH52 14-15.1 m and 18.3 m). The results given in Appendix 6 show that most of the uranium in the samples was TAO-extractable, giving 1350 and 3380 μg/g of TAO-extractable uranium. The $^{234}U/^{238}U$ activity ratios varied between 0.95 and 0.98 respectively. For samples from the same drill hole that contained less than 100 μg/g TAO-extractable uranium, the $^{234}U/^{238}U$ activity ratios varied between 0.65 and 0.92. Analyses of single crystals of saleeite from DDH52 (see Section 6.3) gave ratios close to unity. Therefore, saleeite in analytical samples is likely to result in ratios nearer to unity than the actual accessible phases. Caution needs to be exercised in the interpretation of data from samples containing more than about 1000 μg/g TAO-extractable uranium, due to the possible presence of secondary uranium minerals.

Readsorption of elements during TAO extraction

The effect of readsorption of uranium and thorium during extraction with various reagents, including TAO was discussed in Section 6.2.1. An illustration of the solubility of thorium in TAO is provided by the extraction of two samples known to contain secondary uranium minerals (DDH52 14-15.1 m and 18.3 m). It has been shown that saleeite is soluble in TAO, and that saleeite was the dominant source of uranium (and ^{230}Th) in these samples. The sample from DDH52 18.3 m contained the most saleeite and was close to secular equilibrium with $^{234}U/^{238}U$ and $^{230}Th/^{234}U$ activity ratios of 0.98 and 0.96 respectively. Since saleeite samples from this drill hole were in approximate secular equilibrium, see Section 6.3, the $^{230}Th/^{234}U$ activity ratio value of 0.96 suggests only a small to negligible error due to readsorption of thorium. Reabsorption of thorium onto smectite was seen to be a potential problem, however, smectite is present only in very small amounts at Koongarra.

Reproducibility of uranium and thorium in TAO extracts

Ten samples were studied for the reproducibility of parameters in TAO extracts and the results are included in Appendix 6. The samples were: DDH52 0-1.1 m, 9.7-10.8 m; DDH1 4.7 m; DDH3 14-15.2 m, 16.3-17.5 m; 21-22.2 m; PH56 13.5 m; PH58 1.5-3 m; PH60 6.1-7.6 m. The most reproducible parameter was the $^{234}U/^{238}U$ activity ratio, which generally varied only within 2σ (analytical uncertainty). This again suggests that TAO-extractable uranium represents a distinct phase. The amount of uranium extracted and the $^{230}Th/^{234}U$ activity ratio were not as reproducible. The difference between duplicates was 0-20% for the $^{230}Th/^{234}U$ activity ratios, and 0-15% for the uranium concentrations. This may be attributable to their greater sensitivity to variations in the extraction conditions, such as temperature (15-25°C) and filtration time (5-20 minutes).

Results of two stage dissolution procedure

Discussion of the results is presented in two parts:

a) discussion of a transect that runs perpendicular to the major fault, through the dispersion fan for about 500 m (DDH52-PH94, Mine Grid Section 6109 mN), and

b) a more general discussion about the distribution of accessible uranium series nuclides at Koongarra.

a) Disequilibria along Line Grid Section 6109 mN

Uranium concentrations and uranium series disequilibria, in accessible and inaccessible phases, were determined for 51 samples from the weathered zone along transect 6109 mN. The results for each sample are included in Appendix 6. The variables considered here are:

- the concentrations of ^{238}U and ^{232}Th,
- the activity ratios of ^{238}U, ^{234}U, ^{230}Th and ^{226}Ra,
- accessible and inaccessible phases,
- the position and depth of the sample in the transect.

Unless stated otherwise, comments refer only to weathered samples unlikely to contain secondary uranium minerals.

Uranium and thorium concentrations

The proportion of uranium extractable by TAO was very variable, with 10-73% of the uranium extractable. While there was no clear trend with position, it did appear that samples from DDH52 (primary mineralisation) tended to have a lower proportion of extractable uranium, particularly shallow and mid-weathered zone samples. This would be expected if this hole is through a leached zone, since accessible uranium is likely to be leached first. The distribution of uranium concentrations in both accessible and inaccessible phases approximately followed bulk uranium concentrations. A small but significant amount of ^{232}Th was detected in the accessible fractions. The amounts of ^{232}Th appeared to be unrelated to the distribution of uranium, and were probably more related to the distribution accessory minerals such as monazite.

Activity ratio $^{234}U/^{238}U$

The values for $^{234}U/^{238}U$ activity ratios are shown in Figures 6.16 and 6.17 for accessible and inaccessible phases respectively. The $^{234}U/^{238}U$ activity ratios were generally less than unity in the extracts and greater than unity in the residual phases. The $^{234}U/^{238}U$ activity ratios in the extracts suggest a preferential accessibility, leading to a preferential mobility, of ^{238}U. This is in agreement with the observed $^{234}U/^{238}U$ activity ratios below unity in the groundwater (see Volume 7 of this series). The proposed explanation for this phenomena is α-recoil of the daughter ^{234}Th, into inaccessible phases after alpha decay of ^{238}U situated adjacent to these phases, such as at sorption sites.

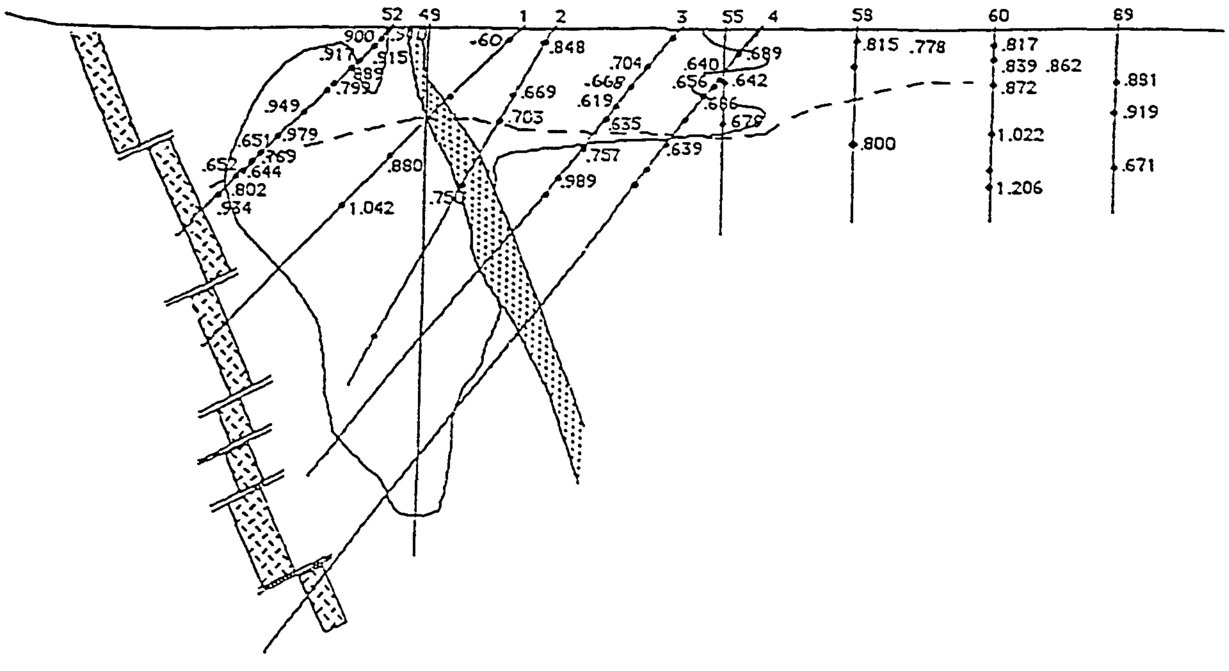

FIGURE 6.16 $^{234}U/^{238}U$ activity ratios in TAO extractable (accessible) phases

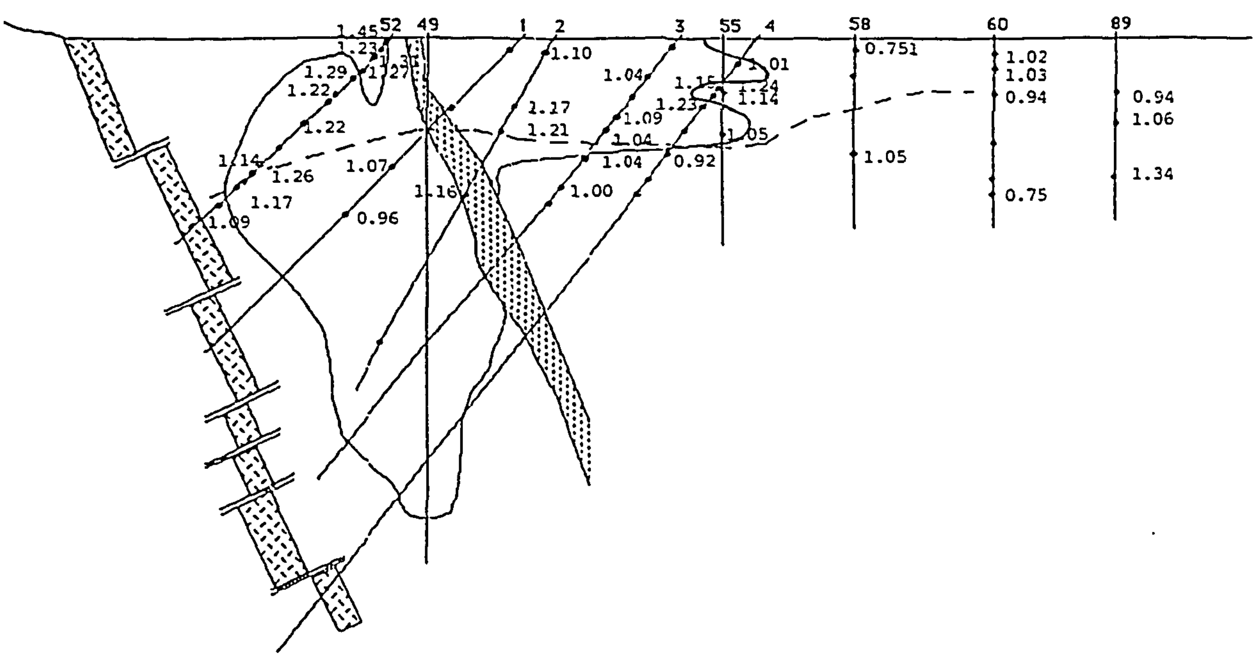

FIGURE 6.17 $^{234}U/^{238}U$ activity ratios in TAO-residual (inaccessible) phases

The highest $^{234}U/^{238}U$ activity ratios for accessible phases were observed above the primary mineralisation, near the top of DDH52, and in barren zones down-gradient of the dispersion fan. Unweathered samples also tended to give high values. It is likely that the high values at the top of DDH52 reflect intense leaching of uranium, and the barren zones down-gradient of the dispersion fan were possibly not contacted by groundwater that had passed through the uranium mineralisation. Lowest $^{234}U/^{238}U$ activity ratio values occurred within the dispersion fan, just down-gradient of the primary ore zone. The trend of accessible $^{234}U/^{238}U$ with distance from the fault is shown in Figure 6.18, for three depths.

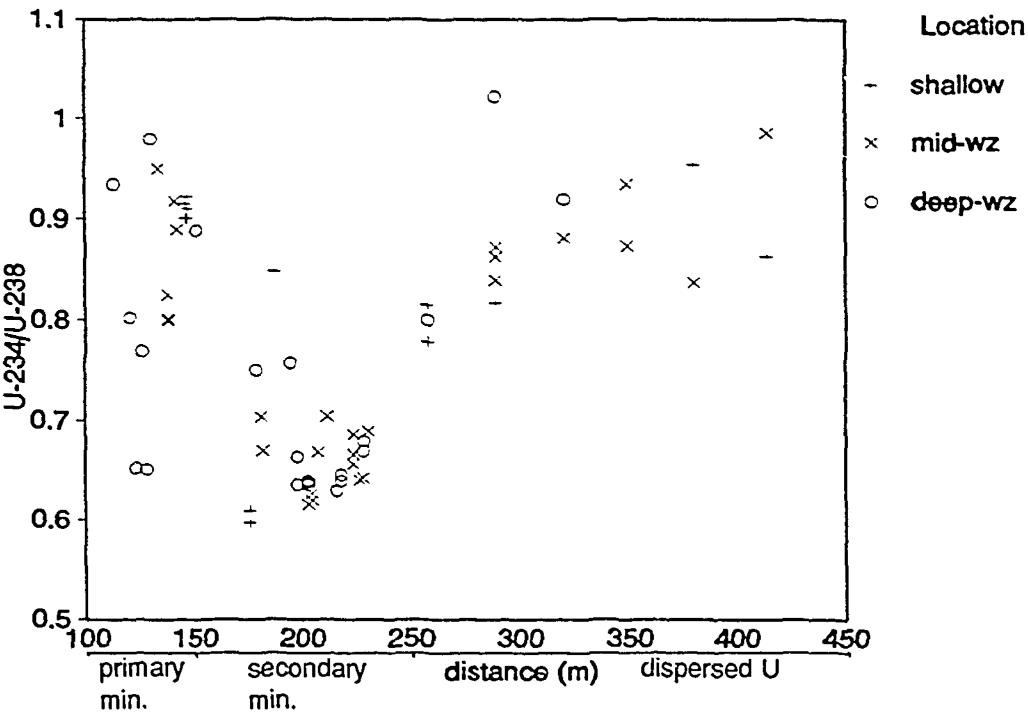

FIGURE 6.18 $^{234}U/^{238}U$ activity ratios in TAO-extractable (accessible) phases along the 6109 mN mine grid line (from 3000 mE). Location refers to position in the weathered zone.

Activity ratio $^{230}Th/^{234}U$

Figure 6.19 shows the $^{230}Th/^{234}U$ activity ratios for accessible phases. The $^{230}Th/^{234}U$ activity ratios were generally less than unity, and lower than the ratios in the residual phases, as was the case for $^{234}U/^{238}U$. Again the ratio was highest near the top of DDH52, and high below ~5 m at PH60 and PH89, down-gradient of the dispersion fan. Particularly low values, of about 0.4 or less, occurred near the surface at DDH1, DDH2, PH58, and PH60. Low values also occurred near the base of weathering along the dispersion fan. The low values suggest that these areas experienced recent accumulation of uranium. This ratio seems to be a minimum down-gradient of the primary mineralisation, particularly in samples deep in the weathered zone, near the base of weathering. Near the surface, $^{230}Th/^{234}U$ activity ratios were lowest downslope of the primary mineralisation, and were higher than for other depths near to the fault. This pattern is similar to that for the $^{234}U/^{238}U$ activity ratio.

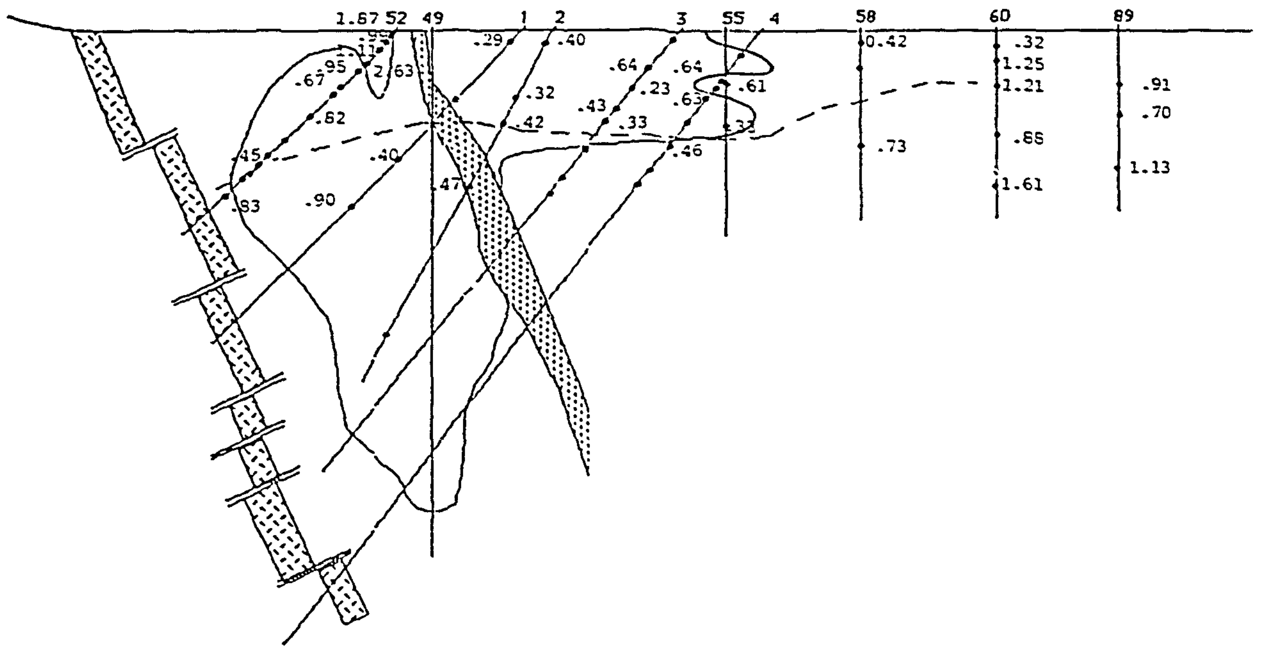

FIGURE 6.19 $^{230}Th/^{234}U$ activity ratios in TAO-extractable (accessible) phases in cross-section 6109 mN.

The accessible phase (TAO-extractable) $^{234}U/^{238}U$ and $^{230}Th/^{238}U$ activity ratios are plotted in Figure 6.20 to recognise and group samples where accumulation or leaching of uranium has occurred. The data points appear to cluster into groups of like samples, which correspond to zones of different leaching/accumulation intensity. The zones were allocated numbers and their position in cross-section is shown in Figure 6.21.

Zone 1 in Figure 6.21 represents the area of most intensive recent accumulation of uranium, with ^{238}U accumulating preferentially to ^{234}U. Zone 2 is probably similar to Zone 1, but with less intense accumulation. Zone 3 in the near surface is probably an area of rapid accumulation, but with less preferential accumulation of ^{238}U. Zone 4 is ambiguous, but may represent areas with slight net leaching of uranium, while Zone 5 is where the most intensive leaching of uranium has occurred.

Most rapid recent accumulation seems to have occurred near the centre of the dispersion fan and near the base of weathering to the leading edge of the fan. It is possible that near the base of the weathered zone, corresponding to the early

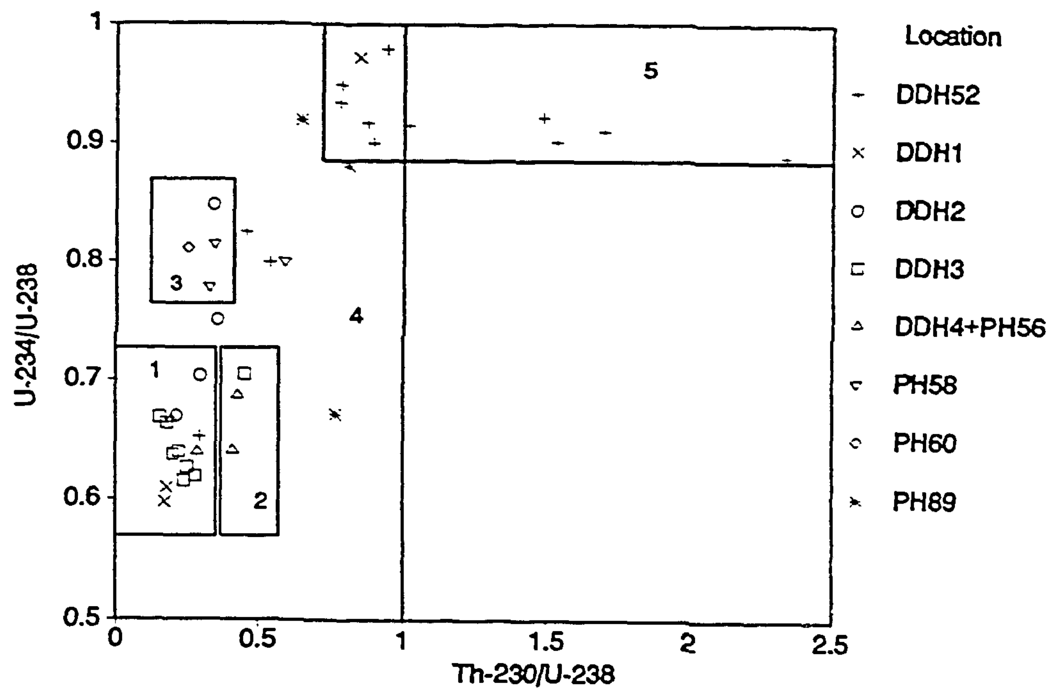

FIGURE 6.20 $^{234}U/^{238}U$ versus $^{230}Th/^{238}U$ in TAO-extracts, from grid line transect 6109N, showing source drill hole and disequilibrium zones (see text for explanation).

stages of weathering, there is preferential movement of uranium bearing water.

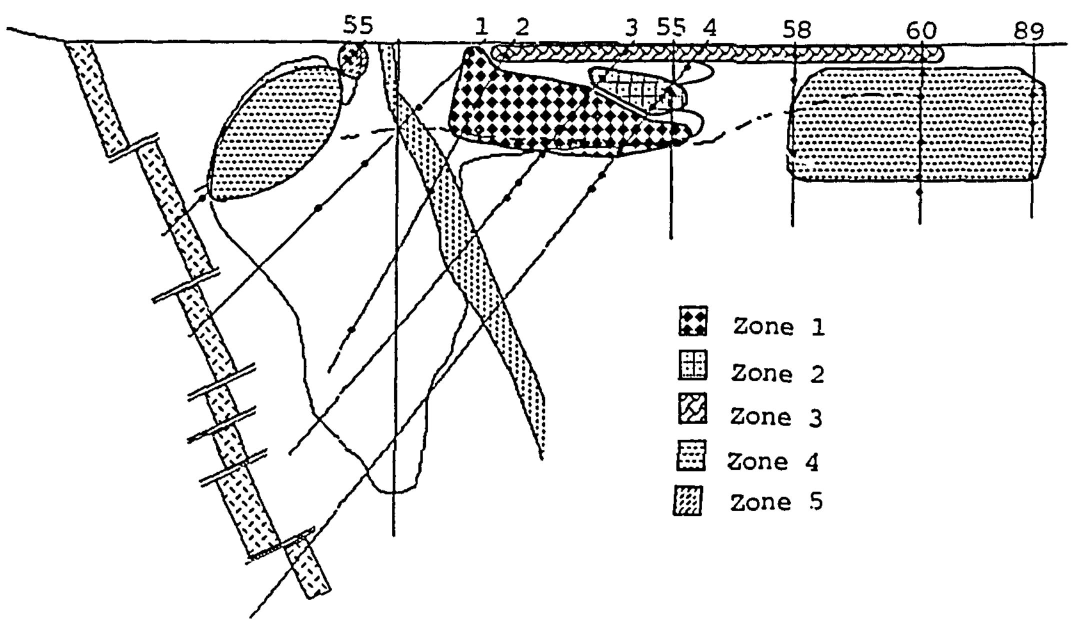

FIGURE 6.21 Disequilibrium zones in cross-section 6109 mN (see text for explanation.

Rapid entrapment of uranium by newly formed secondary minerals, such as ferrihydrite, and a greater accessibility of water to the rock matrix may occur at the early stages of weathering. This highlights the potential importance of the early stages of weathering in the migration of radionuclides. The near surface, near to the fault, appears to be the most intensely leached zone, while down-gradient, the near surface appears to have experienced recent accumulation of uranium without the preferential retardation of ^{234}U. This may reflect a more rapid transport system than deeper in the weathered zone, through a less sorbing matrix.

b) Disequilibria over the whole site

Here, results for samples from holes covering the whole site will be discussed to give the overall pattern. The holes from which samples were analysed are shown in Figure 6.1. The samples have been placed into 3 depth categories:

Shallow: within 2 m of surficial deposits of sands and gravel.

Mid-weathered zone: between 2 m below the surficial deposits and 2 m above the transition zone.

Deep-weathered zone : within 2 m of the transition zone, including partially weathered rock.

A distance parameter is also included for some presentations and is based on the minimum distance of the sample from the (Mine Grid) 3000 mE line along a line passing through the primary ore zone.

<u>Fraction of accessible uranium</u>

The percentage of uranium extracted from each sample by TAO is shown in Figure 6.22.

It can be seen that a large range of results were obtained, but some trends may be present. There appears to be a lesser percentage of accessible uranium above the primary ore zone in the first 100 m down-gradient. Above the primary ore zone there also appears to be a greater proportion of accessible uranium in samples near the base of weathering, than in shallow or mid-weathered zone samples. This would be expected if these areas were zones of uranium leaching, in that accessible phases would be removed first. Down-gradient of the primary ore zone generally between about 20-60% of the uranium was extractable, with no clear depth or distance pattern.

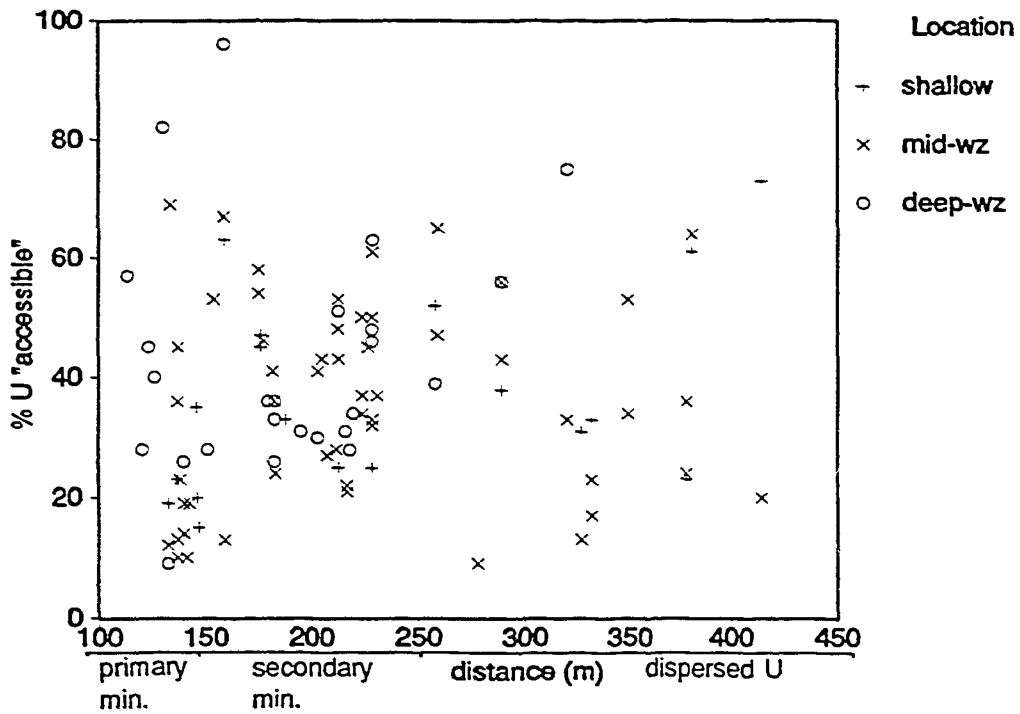

FIGURE 6.22 Percent of total uranium in TAO-extractable (accessible) phases versus distance from the 3000 m East gridline. Location refers to position in the weathered zone.

Activity ratio $^{234}U/^{238}U$

The distribution of $^{234}U/^{238}U$ activity ratios with distance and depth is shown in Figure 6.23 and the isotope ratio data is summarised in Table 6.8. Generally the samples had accessible (TAO-extractable) $^{234}U/^{238}U$ activity ratios less than unity and less than those in the residual phases. The activity ratio in accessible phases was lowest about 0-100 m down-gradient of the primary mineralisation, particularly within the dispersion fan. The accessible $^{234}U/^{238}U$ activity ratio appeared to decrease with distance from the up-gradient boundary of primary mineralisation with a minimum at about 60 m down-gradient of the SE boundary. Further down-gradient, the activity ratio appeared to rise again. It must be remembered that the samples presented in the figure are not from a straight line traverse, and that other aspects of sample location in addition to distance may be important.

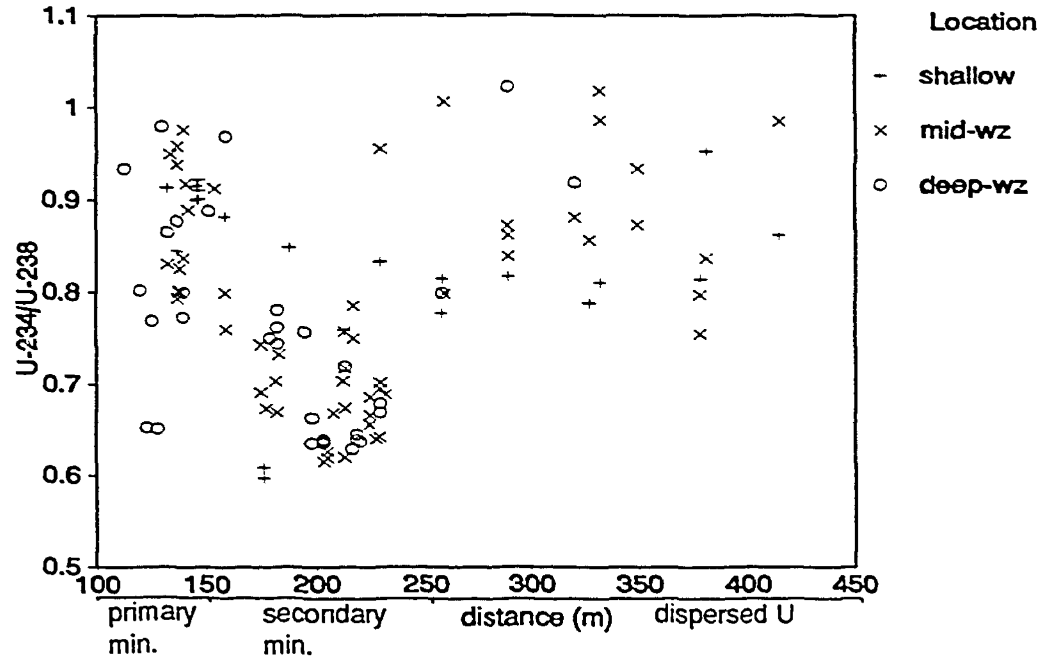

FIGURE 6.23 $^{234}U/^{238}U$ activity ratios in TAO-extractable (accessible) phases, versus distance from the 3000 mE mine grid line.

Activity ratio $^{230}Th/^{234}U$

The $^{230}Th/^{234}U$ activity ratio (Figure 6.24 and Table 6.8) shows a similar pattern with distance as the $^{234}U/^{238}U$ activity ratio, displaying a minimum for samples from 0-60 m down-gradient from the primary mineralisation. As previously mentioned, additional factors to the sample distance may be important, particularly for samples greater than 100 m from the primary ore. Some interesting depth patterns can be seen in this data. For example, shallow samples gave lower accessible activity ratios than deeper samples for holes PH93, M5, PH60, W7, and PH58 (see Figure 6.1). All these holes are >90 m from the primary mineralisation, and this suggests that recent deposition within and near the surficial deposits has occurred more extensively than in the general weathered zone. In many samples with low $^{230}Th/^{234}U$ activity ratios (suggesting recent deposition of uranium), less than half of the uranium was not TAO extractable. This suggests that transformation processes have occurred in which the uranium is entrapped.

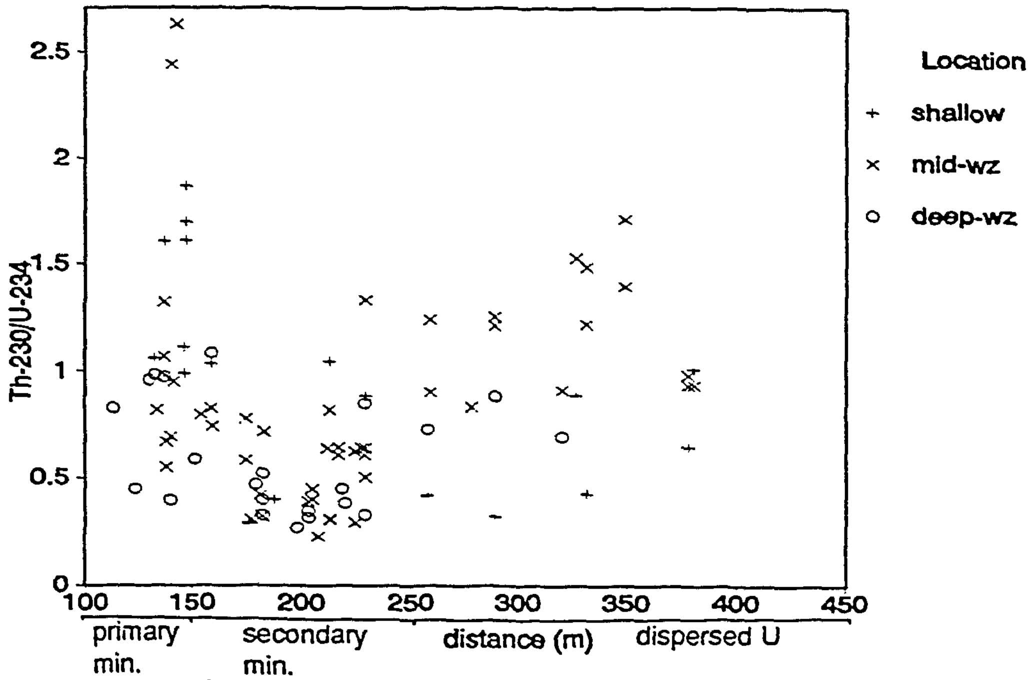

FIGURE 6.24 $^{230}Th/^{234}U$ activity ratios in TAO-extractable (accessible) phases versus distance from the 3000 m E mine grid line.

TABLE 6.8

SUMMARY OF ALL TAO-EXTRACTABLE (ACCESSIBLE) ISOTOPE DATA

	$^{234}U/^{238}U$		$^{230}Th/^{234}U$	
Location	No. of cases	Mean (s.d)	No. of cases	Mean (s.d)
*	37	0.853 (0.083)	32	1.021 (0.548)
0-50 m*	27	0.682(0.061)	23	0.459 (0.213)
50-100 m*	23	0.731 (0.098)	18	0.658 (0.284)
>100 m*	22	0.903 (0.132)	21	1.214 (0.712)
shallow	21	0.832 (0.093)	21	1.003(0.677)
mid-weathered zone	57	0.803 (0.140)	51	0.919 (0.593)
deep-weathered zone	33	0.760 (0.118)	22	0.602 (0.265)

* position relative to the primary mineralisation

Figure 6.25 shows $^{234}U/^{238}U$ versus $^{230}Th/^{238}U$ activity ratios for the accessible data, excluding data from the 6109 mN transect. The data points are denoted according to a) distance, and b) depth. Most samples from above the primary zone contained high activity ratios, suggesting leaching, while some samples showing depositional characteristics were from near the base of weathering.

Samples within 50 m of the primary mineralisation demonstrate uranium deposition, particularly in the mid-weathered zone. Near the leading edge of the dispersion fan, up to 100 m down-gradient, there appeared to be uranium deposition within the mid-and deep-weathered zone (PH56, M3, DDH87). Samples from the weathered zone at M4 do not show obvious recent accumulation of uranium.

Greater than 100 m from the primary ore the pattern becomes more complicated. At M5 and W7, only shallow samples showed activity ratios indicative of uranium accumulation. At PH93, samples from the mid-weathered zone showed possible slight accumulation of uranium, while accumulation near the surface was more pronounced.

Along Section 6109 mN, shallow samples showed clear accumulation at least to PH60. Bulk data suggests accumulation at shallow depths for PH89, but not for PH90. Disequilibria suggesting possibly slight accumulation deeper in the weathered zone occurs to PH89, but is less dramatic than at shallow depths.

Uranium appears to have been leached from above the present primary mineralisation, possibly from previous zones of primary mineralisation, particularly from shallow depths. Accumulation of uranium appears to have occurred throughout the weathered zone, particularly near the base of weathering, to the leading edge of the dispersion fan, up to about 80 m from primary mineralisation. Beyond the dispersion fan, most pronounced accumulation appears to have occurred near the surface, probably following topographic features, S-SW of the orebody. Slight deep weathered zone accumulation may have occurred at PH93, but not in the vicinity of W7, M5 and M4.

6.3 Uranium Series Disequilibria in Secondary Uranium Minerals

The results of a series of measurements of the $^{234}U/^{238}U$, $^{230}Th/^{234}U$ and $^{227}Ac/^{235}U$ activity ratios on a number of secondary uranium mineral crystals are shown in Table 6.9. In all cases, the crystals in each case were assumed to be saleeite, although identification was made only visually. Saleeite is a common mineral in the Alligator Rivers region and arises from the weathering of uranium orebodies containing magnesium-rich chlorites.

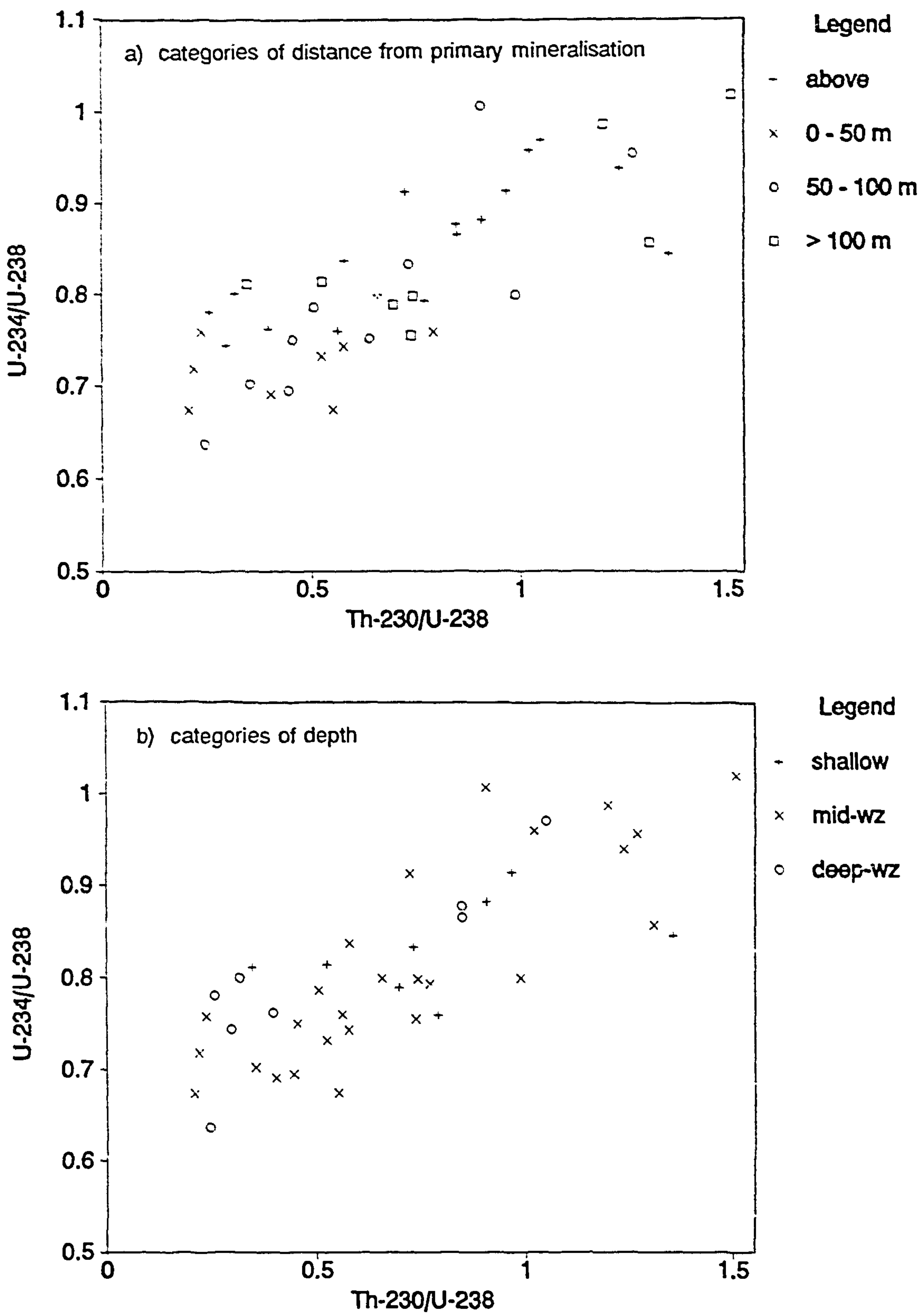

FIGURE 6.25 $^{234}U/^{238}U$ versus $^{230}Th/^{238}U$ for TAO-extractable (accessible) phases for all samples excluding those from section 6109 mN

TABLE 6.9

URANIUM CONCENTRATIONS AND ACTIVITY RATIOS OF CRYSTALS OF SECONDARY URANIUM MINERALS

Hole/depth		[U] (% w/w)	$^{234}U/^{238}U$	$^{230}Th/^{234}U$	$^{227}Ac/^{235}U$
DDH52 20 m	(a)	53	1.006(.015)	0.965(.030)	
	(b)	50	0.999(.005)	1.234(.017)	1.001(.034)
	(c)	44	1.001(.008)	0.992(.027)	
DDH84 22 m			0.997(.015)	1.049(.030)	
DDH84 29 m	(a)	35	1.002(.012)	1.050(.026)	
	(b)		1.005(.007)		
DDH65 27 m			1.077(.015)	0.780(.020)	
DDH65 29 m	(a)	40	1.075(.011)	0.840(.020)	
	(b)	41	1.029(.008)	0.871(.016)	0.887(.030)
	(c)	46	1.078(.010)	0.827(.010)	
DDH64 27 m	(a)	44	0.785(.010)	0.143(.005)	
	(b)		0.793(.009)		
	(c)	48	0.785(.008)	0.334(.009)	0.517(.036)
	(d)	52	0.795(.009)	0.416(.012)	0.635(.021)
DDH64 29 m		48	0.844(.010)	0.632(.015)	0.79(.04)

The uranium content of these crystals ranged from 35 to 52% by mass compared to a stoichiometric composition of 52% for saleeite. Due to the small size of some crystals it was not always possible to isolate a pure sample that was free of the surrounding material. This may have accounted for the composition of only 35% measured in one crystal. The crystals may also have consisted of either autunite or torbernite, the calcium and copper analogues of saleeite. The samples from DDH52 20 m were large cleavage crystals from a vein approximately 1 cm wide. The other samples were scrapings of coatings, smeared along schistosity planes and surfaces.

The location of each drill hole is in indicated in Figure 6.1. Holes DDH52 and DDH84 intersect a zone of net uranium leaching, while DDH65 and DDH64 lie close to DDH3 and DDH4 respectively, in a parallel section. DDH64 is located in the area defined as the secondary dispersion fan.

It was hoped that these measurements would give some indication of the *isotopic* signature of the local groundwater uranium in the past million years. Recent crystallisation of the uranium from solution (in the absence of thorium) would be indicated by a low $^{230}Th/^{234}U$ activity ratio and facilitate dating by the uranium series method. The ages of these crystals have been estimated using an open system model, which is described in Volume 14 of this series. Like thorium, protactinium is unlikely to be present at the onset of crystallisation due to its low solubility and low mobility. With its short half-life (27 years), ^{227}Ac is assumed to acquire equilibrium with its parent ^{231}Pa at a rate that is fast compared to its rate of leaching by groundwaters. The $^{227}Ac/^{235}U$ activity ratio was easily measured in these samples and it offered an indirect method of measuring the $^{231}Pa/^{235}U$ activity ratio.

Minerals from DDH52 and DDH84

Drill holes DDH52 and DDH84 are located near the up-gradient edge of the zone of primary mineralisation. Three crystals from a depth of 20 m in DDH52, and two crystals from DDH84 at 27 and 29 m, were analysed. In each case the $^{234}U/^{238}U$ activity ratio was determined with high precision and found to be very close to the equilibrium value of unity. A similar result was found for the crystals from the two depths in DDH84. The $^{230}Th/^{234}U$ activity ratio in two of the DDH52 crystals was within 2 σ of unity, while the third gave a value of 1.23. This suggested that while uranium accumulation may have occurred in three of the crystals the other had incurred a net uranium loss. If the three crystals near secular equilibrium are considered individually, then the activity ratios suggest either that they were formed by "in situ" alteration of a primary mineral or that they crystallised from solution after which there was sufficient time for ^{230}Th to come close to equilibrium. The former is an important consideration since DDH52 and DDH84 are thought to intersect a previous upward extension of the primary orebody, and extensive "in situ" alteration of primary minerals is believed to have occurred even below the zone of weathering. It is suggested that this zone consisted of weathered and leached primary ore.

The large difference in the $^{230}Th/^{234}U$ activity ratios of the crystals from DDH52 20 m suggests that there has been exchange of uranium between neighbouring crystals, with ^{230}Th remaining at its point of generation. The close similarity in the $^{234}U/^{238}U$ activity ratios between the crystals supports this view. The mean age of these crystals is unlikely to be less than 500 ky, since any "in situ" alteration of primary minerals would probably have occurred prior to or during the onset of weathering.

The $^{227}Ac/^{235}U$ activity ratio in the second crystal from DDH52 20 m (Table 6.9) shows ^{227}Ac to be close to equilibrium with its parent ^{235}U. Since ^{227}Ac and ^{231}Pa, like ^{230}Th, are considered to be relatively immobile, one would expect an excess of ^{230}Th to be accompanied by a slightly smaller excess of these two nuclides (the half-life of ^{231}Pa is about half that of ^{230}Th). The $^{227}Ac/^{235}U$ activity ratio of unity therefore appears to disagree the high $^{230}Th/^{234}U$ activity ratio.

Minerals from DDH65

Three crystals from DDH65 29.0 m and one from 27 m were analysed. The $^{234}U/^{238}U$ activity ratio varied between 1.029 and 1.078 (Table 6.8). The $^{230}Th/^{234}U$ activity ratios varied between 0.780 and 0.871. These values appear to be at odds with the general pattern of disequilibria at the deposit since they suggest that crystal formation arose by deposition of uranium that was marginally enriched in ^{234}U. The $^{234}U/^{238}U$ values in the four samples were similar, but the lowest activity ratio was separated from the other two by greater than 2σ. This difference is difficult to explain but it does suggest that only limited exchange of uranium has taken place between surrounding crystals.

The $^{227}Ac/^{235}U$ activity ratio was also measured from one crystal, giving a value of 0.887, similar to the $^{230}Th/^{234}U$ activity ratio of 0.871. The two ratios still appear to be discordant with respect to the simultaneous radiometric ingrowth of ^{230}Th and ^{231}Pa. The measured value of the $^{227}Ac/^{230}Th$ activity ratio was about 0.05, approximately the secular equilibrium value. Such a situation could have arisen by the very recent incorporation of further uranium by a crystal that had previously acquired secular equilibrium. There is a strong argument for measuring both the $^{230}Th/^{234}U$ and the $^{227}Ac/^{235}U$ activity ratios to see if they indicate with a single depositional event.

Since the DDH65 crystals came from 27 m and 29 m depths, which is close to the weathering horizon, the explanation for the high $^{234}U/^{238}U$ activity ratios may lie in the possibility that they formed by the upward passage of groundwater through a fracture originating within the primary orebody. Deep aquifers are commonly enriched in ^{234}U (Osmond and Cowart, 1976) and the fracture may well have facilitated the passage of such water. The $^{234}U/^{238}U$ activity ratio in groundwater from near the base of weathering, taken from W4 24 m (the nearest well available), was 1.21. Groundwaters from this location are the only waters from the weathered zone with $^{234}U/^{238}U$ activity ratios above unity. Groundwater from the unweathered zone had an activity ratio above unity at several locations (see Volume 7 of this series). The material surrounding the crystal had the appearance of being only partially weathered. The influence of surface aquifers at this depth may therefore have been very limited. However in the absence of further data on core samples from this drillhole it is not possible to speculate further on their origin.

Minerals from DDH64

Crystals from DDH64 were of greatest interest since they were located within a zone of known uranium accumulation and it was therefore anticipated that they may have formed quite recently. Four different crystals were analysed from a depth range of 26.5-26.8 m. All gave the same $^{234}U/^{238}U$ activity ratio of 0.79 (to within a 2% margin) but the $^{230}Th/^{234}U$ activity ratio varied from 0.14 to 0.42, indicating different ages. Such low $^{234}U/^{238}U$ activity ratios suggest that crystallisation was indeed quite recent. The $^{227}Ac/^{235}U$ activity ratio (and hence the $^{231}Pa/^{235}U$ activity ratio) was measured in two of these crystals and found to lie between the $^{230}Th/^{234}U$ activity ratio and unity. This is an expected correlation since the half-life of ^{231}Pa (33 ky) is about half that of ^{230}Th and it therefore equilibrates at twice the rate with its parent ^{235}U.

An additional crystal from DDH64 was selected from a depth of 29.0 m. This was found to have $^{234}U/^{238}U$ and $^{230}Th/^{234}U$ activity ratios of 0.84 and 0.63 respectively, slightly higher than those from the 26.5-26.8 m depth. This clearly points to a greater age, although the source of the uranium may have been the same as that which gave rise to crystals from the 26.5-26.8 m depth range. The $^{227}Ac/^{235}U$ activity ratio in this crystal was measured to be 0.79. Again this is concordant with the $^{230}Th/^{234}U$ activity ratio.

Multi-stage dissolution of saleeite crystals

Saleeite crystals, possibly single crystals, from DDH65 27 m and DDH84 22 m were leached with 0.1M, 1M and 6M HCl sequentially to dissolve the uranium minerals from the surface to the centre. Table 6.10 shows the extraction

TABLE 6.10

PROPORTION OF URANIUM AND ACTIVITY RATIOS IN SEQUENTIALLY LEACHED FRACTIONS OF TWO SALEEITE CRYSTALS

Hole/depth	Reagent	Time (min)	% U dissolved	$^{234}U/^{238}U$	$^{230}Th/^{234}U$
DDH65 27 m	0.1M HCl	1	1.1	1.074	0.184
	0.1M HCl	9	5.2	1.099	0.199
	1M HCl	5	33.3	1.088	0.633
	1M HCl	1	13.0	1.072	0.803
	6M HCl	30	47.4	1.068	0.958
	12M HCl	> 5 days	0.01	1.012	1.324
DDH84 22 m	1M HCl	1	30.6	0.988	0.914
	1M HCl	1	17.3	1.033	0.839
	1M HCl	1	9.1	0.988	1.045
	1M HCl	1	8.2	1.039	1.009
	6M HCl	30	34.7	0.982	1.292
	12M HCl	> 5 days	0.004	1.094	2.143

conditions, uranium activity, and $^{234}U/^{238}U$ and $^{230}Th/^{234}U$ activity ratios. About 30% of the crystal from DDH84 22 m was dissolved by 1M HCl in 1 minute. This was followed by a dramatic decrease in the dissolution rate. This may have been due to a decrease in the surface area of the crystal in the first minute. The $^{234}U/^{238}U$ activity ratio was similar in all the dissolution steps, and was close to unity. In the 0.1M HCl-extractable fractions, the $^{230}Th/^{234}U$ activity ratio was very low. The $^{230}Th/^{234}U$ activity ratio increased with leaching time with 1M HCl, and this may reflect an increase in age with distance into the crystal. It is likely that the 6M HCl step dissolved the remaining saleeite, and that the 12M HCl step dissolved any resistant impurities.

Summary results for secondary uranium minerals

Saleeite crystals from the weathered primary ore zone had $^{230}Th/^{234}U$ activity ratios greater than unity, while down-gradient $^{230}Th/^{234}U$ activity ratios were less than unity. This indicates significant differences in their periods of formation.

The crystals from DDH64 were occupying small veins within the weathered schist. It is therefore likely that the influx of uranium-rich water through these veins gave rise to crystal formation followed by ingrowth of ^{230}Th and ^{231}Pa. Closer examination of individual crystals within such a vein may well indicate that their activity ratios are closely related to their locations.

The crystals from DDH64 were a rare example of quite recent mineralisation resulting from deposition of uranium that was depleted by over 20% in ^{234}U. They showed the same trends in their $^{234}U/^{238}U$ and $^{230}Th/^{234}U$ activity ratios as core and pulp samples from the secondary dispersion fan. In contrast, crystals from DDH65 apparently arose by deposition of uranium that was slightly enriched in ^{234}U.

The variability of the $^{230}Th/^{234}U$ activity ratio and the consistency of the $^{234}U/^{238}U$ activity ratio between crystals in close proximity suggests that they are behaving as dynamic systems, exchanging with dissolved uranium. If this were the case then strong leaching conditions would lead to rapid remobilisation of the uranium with subsequent mineralisation in a down-flow location or dispersion within adsorptive components of the host rock. It would appear that penetration of groundwater has been sufficient only to cause very local migration of uranium. The high uranium concentration in each crystal may have caused considerable radiation damage by recoiling nuclei. This may enhance their solubility and encourage the formation of new sites of precipitation.

The DDH65 and DDH64 crystals almost certainly formed by deposition of uranium, the former from ^{234}U-enriched uranium, the latter from ^{234}U-depleted uranium. However it could not be proved whether the DDH52 crystals were "in situ" alteration products or arose by accumulation of uranium within a vein.

Since the crystals from DDH64 originated by an influx of uranium, this raises the question of whether it was transported and subsequently precipitated as the phosphate complex or whether the phosphate combined with uranium at the present location. As these samples were close to the weathering horizon, the latter possibility seems plausible, since the influx of uranium may have coincided with the release of phosphate from newly weathered apatite. Therefore, the location of secondary mineral crystals may be as much a consequence of the original location and form of apatite as the of the degree of penetration of uranium-rich water. Dall'Aglio et al. (1974) discussed the geochemical processes giving rise to the precipitation of autunite (calcium uranyl phosphate). In one case, they noted that circulating water containing appreciable uranium had pervaded a region not previously subject to groundwater penetration. Precipitation of autunite had then occurred by way of a lowering of the alkalinity of the water, thereby increasing the activity of UO_2^{2+}. In the case of the DDH64 mineralisation, it is suggested that precipitation of saleeite arose when sudden weathering of the rock liberated phosphate from apatite. Dall'Aglio et al. (1974) also pointed out that precipitation of uranyl species was all the more likely when the carbonate concentration was very low. This could occur with the development of unsaturated conditions.

Sequential dissolution of saleeite crystals gave $^{230}Th/^{234}U$ activity ratios which tended to increase with leaching, indicative that the core of the crystals may be older than the skin.

6.4 Summary

In the unweathered zone, the ore material and the host rock were at approximate secular equilibrium, except for a small apparent depletion of ^{226}Ra. While there appears to have been negligible redistribution of uranium in the unweathered zone over the last few hundred thousand years, some mobility of radium is likely. It has been suggested that ^{226}Ra may be relatively mobile in the unweathered zone, but is removed from solution on contact with more oxidising conditions.

In the weathered rock, above the primary mineralised zone, high $^{230}Th/^{234}U$ activity ratios indicate strong recent leaching of uranium. In these leached areas the $^{234}U/^{238}U$ activity ratios are high, above unity in the bulk rock and near unity in the accessible phases. This indicates a preferential mobility of ^{238}U relative to ^{234}U. The most intensely leached samples came from near the surface, near the up flow boundary of the primary ore.

The most intense recent accumulation of uranium appears to have occurred about 0-50 m from the down flow boundary of primary ore, particularly near the base of weathering. This highlights the importance of the early stages of weathering to the migration and retardation of uranium. Uranium deposition samples, giving low $^{230}Th/^{234}U$ activity ratios, also contained low $^{234}U/^{238}U$ activity ratios. Further than about 50 m down-gradient, both activity ratios tend to increase with distance.

At distances greater than about 100 m from the primary ore, deposition of uranium is most pronounced in the near surface. In the shallow zones, low $^{230}Th/^{234}U$ activity ratios were associated with higher $^{234}U/^{238}U$ activity ratios than depositional samples deeper in the weathered zone. Three explanations are offered; firstly, different sources may be supplying the uranium, with the shallow material receiving uranium from the most intensely leached sources with higher $^{234}U/^{238}U$ values; secondly, a faster flowing system may be involved, perhaps seasonally and; thirdly, the solid substrates are probably different, with the coarser shallow material being less conducive to isotopic fractionation.

A scenario for the development of disequilibria between ^{234}U and ^{238}U is proposed. The onset of weathering conditions may have caused the rapid dissolution of the primary uranium minerals, resulting in the congruent liberation of ^{238}U and ^{234}U. This may have been followed by preferential entrapment of ^{234}U from solution and accessible sites, by various processes, including α-recoil and mechanisms involving the chemistry of ^{234}Th. This would have resulted in a preferential mobility of ^{238}U, leading to high $^{234}U/^{238}U$ activity ratios in leached samples and low ratios in depositional samples down-gradient.

Greater than about 50 m down-gradient, where the uranium content of groundwater and accessible phases is low, uranium mobilised from the primary ore makes a smaller contribution to the total accessible uranium. It is likely that slowly dissolving minerals that contain uranium, such as zircon and monazite, would be preferentially leached of ^{234}U relative to ^{238}U, consequently increasing the $^{234}U/^{238}U$ activity ratio of the accessible uranium. It is proposed that these phases make an increasingly significant contribution to the accessible uranium with distance from the primary ore zone.

In general it appears that where the uranium content in accessible phases is high, then the accessible (or solution) $^{234}U/^{238}U$ activity ratio will tend to decrease with time or distance due to preferential retardation of ^{234}U. However, where the accessible phase uranium content is low, and a major source of the accessible uranium is resistant minerals, then the accessible $^{234}U/^{238}U$ activity ratio will tend to increase owing to preferential leaching of ^{234}U.

Sequential extraction data showed that most of the uranium in the dispersion fan was accessible or entrapped by crystalline iron oxides, with the crystalline phases containing the higher $^{234}U/^{238}U$ activity ratios. This indicates a mechanism of isotopic fractionation involving iron oxides. The highest activity ratios came from resistant phases with low uranium contents (after extraction with hot 6M HCl), such as quartz and muscovite. The high ratios in these essentially chemically inert phases suggests that α-recoil emplacement of ^{234}Th occurrs at Koongarra. Other mechanisms may also be operating to reduce the mobility of ^{234}U, such as rapid, strong and specific adsorption of ^{234}Th, preferential entrapment of ^{234}Th by transforming iron oxides, and preferential migration of ^{234}Th into inaccessible sites (eg. by diffusion). Processes related to the chemistry of ^{234}Th do, however, need to be rapid, since ^{234}Th has a half life of only 22 days.

Further Work

Further extraction experiments on pure minerals are needed to clarify the relationships between extraction reagents and mineral dissolution. Similarly, further tracer adsorption and extraction experiments could be undertaken. Complete physical mineral separation is needed to clarify the relationships between uranium distributions and minerals, and to identify the mineral phases predominantly responsible for uranium adsorption. The location of excess ^{234}U in quartz could also be determined; if α-recoil is the dominant mechanism, most of the excess ^{234}U should be located near the quartz surface.

Further concentration and isotopic data for rock and groundwater sampled from the same location is required to more clearly understand uranium migration at Koongarra. Additional work on multi-stage dissolution of single uranium mineral crystals could determine whether mineralisation occurred in one or several periods. Other techniques, such as secondary ion mass spectrometry (SIMS) may also provide useful information.

Laboratory experiments are required to assist in elucidating the mechanisms involved in the development of uranium series disequilibria, particularly between ^{234}U and ^{238}U. This should include transformation experiments to study the relative occlusion of uranium and thorium by iron oxides as they become increasingly crystalline.

7 PARTITIONING OF URANIUM AND THORIUM BETWEEN ROCKS AND GROUNDWATER

Introduction

The partition coefficient (P) for a radionuclide bound by a solid phase is defined as follows:

$$P = \frac{\text{amount of radionuclide bound by solid per unit mass}}{\text{amount of radionuclide in solution per unit volume}}$$

The distribution coefficient (K_d) is defined similarly to P, except that it refers strictly to adsorbed species only. The relationship between P and K_d is not straightforward; P is generally an overestimate of K_d, although may also be an underestimate. The distribution ratio (R_d) is defined similarly to K_d, and is more appropriate in cases where equilibrium may not be achieved such as laboratory experiments. In this report, various P terms (functionally defined partition coefficients) will be used, but it should be noted that sorption equilibrium is not implied by these terms. The units of K_d and P are mL/g, although dimensionless K_d values have been reported where both numerator and denominator are expressed per unit mass. In-situ approaches to distribution coefficients have several limitations to their applicability (see McKinley and Alexander 1992), with the main concern being the potential overestimation of retardation of contaminant migration. By presenting several approaches for a range of groundwaters and substrates, it is hoped that such limitations can be identified.

In this report, partition coefficient (P) values for ^{238}U and ^{230}Th in the Koongarra system will be discussed. This survey will not include the results of laboratory sorption experiments undertaken as part of the ARAP program (Volume 13 of this series). Groundwater concentrations and $^{234}U/^{238}U$ activity ratios have been compared to those in bulk rock, and when data are available, in accessible phases of the solid material from or near the groundwater sampling position. Comparisons between groundwater and entrained particles have also been made. Details about the chemistry of the groundwater are given in Volume 7 of this series, and the positions of boreholes sampled are shown in Figure 2.1.

Partitioning of ^{230}Th between groundwater and bulk rock

Table 7.1 shows a comparison of ^{230}Th concentrations in groundwaters and nearby core samples. Thorium concentrations for groundwaters, and reported values for solid-phase (crushed rock) samples from the vicinity of the water sampling location were compared. The resulting bulk partition values (P_B = total rock/groundwater) were extremely high (4×10^5 to 2×10^9 mL/g), reflecting the levels of dissolved ^{230}Th in these groundwaters, which bordered on detection limits. The spread of values was attributed to the heterogeneity of the distribution of ^{230}Th in the bulk rock. A potentially large proportion of the rock ^{230}Th may not have been accessible to the groundwater, however, the high P_B values for thorium were considered to demonstrate its immobility in the Koongarra system as is commonly the case in geological systems. The potential of a colloidal component to the groundwater phase is given discussed in Volume 7 of this series.

TABLE 7.1

COMPARISON OF ^{230}Th ACTIVITY IN GROUNDWATER AND ROCK (ASSUMING APPROXIMATE ISOTOPIC EQUILIBRIUM IN THE ROCK)

Hole/Depth (m)	^{230}Th water (dpm/L)	[U] rock (μg/g)	^{230}Th rock (dpm/g)	P_B ^{230}Th (mL/g)
PH14 <26	0.0014 (.0011)*	~500	~370	~2.6×10^{8}
PH14 <30	0.0034 (.0011)	~500	~370	~1.1×10^{8}
PH49 28-30	0.050 (.005)	~6000	~4450	~8.9×10^{7}
PH49 44-46	0.036 (.006)	~810	~600	~1.7×10^{7}
PH55 40-42	0.001 (.005)	3	2.2	2.2×10^{6}
PH56 26-28	<0.0017	32	24	$>1.4\times10^{7}$
PH61 43-45	0.0024 (.0022)	8	6	2.5×10^{6}
PH88 38-40	0.0055 (.0017)	4	3	5.5×10^{5}
PH94 40-42	0.0052 (.0012)	3	2.2	4.2×10^{5}
PH96 <26	0.0114 (.0025)	2	1.5	1.7×10^{5}

* values in parentheses are analytical errors (1σ)

Partitioning of ^{230}Th and ^{238}U between groundwater and entrained particles

Table 7.2 shows particle partition values (P_P) obtained for particles entrained in groundwater when boreholes PH14 and PH49 at Koongarra were sampled using a submersible pump. The particles were retained on prefilters with pore sizes of 5 µm and 1 µm, dividing the particles into two size ranges > 5µm and 1-5 µm respectively. The filtered groundwater and the particles were analysed for their uranium and thorium content, giving an opportunity to measure P_P values for geological material in contact with a groundwater with a known radionuclide content. The resulting P_P values for ^{238}U were in the range 3.7-6.5 $\times$ 10^4 mL/g. This relatively small range was considered to be evidence that the distribution of uranium in the system may be governed by sorption interactions. The P_P values for ^{230}Th were much higher and more variable, between 7.3 $\times$ 10^7 and 1.6 $\times$ 10^9 mL/g. Two important points need to be made about this data set:-

a) The ^{238}U and ^{230}Th contents of the particles were determined by a total digestion of the particles. Therefore the calculated P_p values are higher than would be if only surface bound Th and U were considered. See Table 7.3 discussed below.

b) The groundwater particles sampled in this experiment had much higher contents of amorphous (coating) minerals than a typical (bulk) rock sample from Koongarra, observed using SEM.

TABLE 7.2

^{238}U AND ^{230}Th PARTITION COEFFICIENTS FOR GROUNDWATER AND ENTRAINED PARTICLES

	Hole	^{238}U dpm/g	P_p ^{238}U mL/g	^{230}Th dpm/g	P_p ^{230}Th mL/g
Particles >5 μm	PH14 (a)	3300	5.1×10^4	696	7.3×10^7
	PH14 (b)	5700	3.7×10^4	664	1.8×10^8
	PH49	6000	4.5×10^4	3700	1.2×10^9
Particles 1-5 μm	PH14 (a)	3000	4.6×10^4	770	8.0×10^7
	PH14 (b)	10000	6.5×10^4	330	8.9×10^7
	PH49	6700	5.0×10^4	5200	1.6×10^9

In Table 7.3 the partition ratios for weak acid (0.5M HCl)-extractable phases on the particles entrained in the groundwater were estimated. The filters carrying the particles were leached with 0.5M HCl for 2-3 days, after a short initial period of heating to 70°C. This may better represent material accessible to interactions with the groundwater than a bulk analysis. The data differ from those in Table 7.2, which were obtained by digestion of the particles. The P_{PA} values in Table 7.3 are somewhat lower than the P_p values in Table 2, in the range 2.6-6.5 $\times$ 10^4 mL/g for ^{238}U, and 2.4 $\times$ 10^6 to 1.1 $\times$ 10^9 mL/g for ^{230}Th. The $^{234}U/^{238}U$ activity ratios of the acid-extractable phases of these particles was consistent with these phases containing radionuclides adsorbed from the groundwater, whereas the data obtained by total digestion included some radionuclides in inaccessible phases.

TABLE 7.3

^{238}U AND ^{230}Th PARTITION COEFFICIENTS (P_{PA}) FOR ACID-EXTRACTABLE MATERIAL OF ENTRAINED GROUNDWATER PARTICLES

Hole	[^{238}U] acid leach dpm/g	P_{PA} ^{238}U mL/g	[^{230}Th] acid leach dpm/g	P_{PA} ^{230}Th mL/g
Particles >5 μm				
PH14 a	2470	3.7×10^4	23.2	2.4×10^5
PH14 b	3990	2.6×10^4	80.7	2.2×10^7
PH49	3820	1.9×10^4	1270	4.0×10^8
Particles 1-5 μm				
PH14 a	2500	3.8×10^4	313	3.3×10^7
PH14 b	9940	6.5×10^4	53	1.4×10^7
PH49	5630	4.2×10^4	3390	1.1×10^9

Partitioning of ^{238}U between groundwater and <10 μm particles

The fine fraction of the solid phase probably dominates the sorption characteristics of the weathered rock. The fine particle fraction (nominally below 10 μm size) was separated from three weathered samples to study the partitioning of uranium between this fraction and the groundwater (Table 7.4). Laboratory sorption experiments have been carried out using these fractions, and the separation procedure and particles are described in Volume 13 of this Series. For W1 and W2 samples, which are from the weathered zone, the fine fraction makes up a substantial proportion of the mass and the surface area of the samples. The C8 sample is probably less representative of the bulk solid phase which is only partially weathered at the sample depth.

Table 7.4 gives P_{PB} (bulk particle partition coefficient) values for uranium obtained after a total digestion of the samples. The P_{PB} values are between 5.1×10^3 and 1.1×10^5 mL/g. Also presented are P_{PA} values for accessible phases only, as estimated by extraction with TAO reagent (see section 6.2 and 2.4). Here the data fall into the narrow range 2.7×10^3 to 1.4×10^4 mL/g.

TABLE 7.4

^{238}U PARTITION COEFFICIENT (P_{PB}) FOR GROUNDWATER AND <10 μm PARTICLES FROM CORE

Sample	[^{238}U] particles ($\mu g/g$)	[^{238}U] water ($\mu g/L$)	Partition coefficient
Total digestion of particles			P_{PB} (mL/g)
W1 13-15 m	356	3.2-8.8	4.0×10^4-1.1×10^5
W2 13-15 m	426	16-83	5.1×10^3-2.6×10^4
C8 25 m	45	2.3	2×10^4
Accessible phases (TAO-extractable)			P_{PA} (mL/g)
W1 13-15 m	43	3.2-8.8	4.9×10^3-1.4×10^4
W2 13-15 m	225	16-83	2.7×10^3-1.4×10^4
C8 25 m	23	2.3	1×10^4

Partitioning of uranium between groundwater and bulk rock

Averaged bulk rock ^{238}U contents compared with groundwater from the same borehole/depth are shown in Table 7.5. The bulk partition coefficients (P_B) were estimated only for points where the occurrence of uranium minerals was unlikely. This was done to minimise the inclusion of very large amounts of uranium not accessible to the groundwater. The range of P_B values for this data set is from 1.0×10^3 to 5.2×10^4 mL/g. Figure 7.1 shows a plot of uranium concentrations in the groundwater against those in the bulk rock. While there is a trend of increasing groundwater uranium with increasing concentration in the rock, the spread in some places is over an order of magnitude. The PH bores are cased through the weathered zone and are only open in the unweathered zone. Therefore, for the PH holes in this table, the data is obtained in barren rock underlying the dispersion fan. This limits its usefulness for the weathered zone where both groundwater and solid phase concentrations may be orders of magnitude higher and the rock may have totally different sorption characteristics. Nonetheless, they are an indication of likely P_B values at Koongarra.

TABLE 7.5

BULK PARTITION COEFFICIENT (P_B) BASES ON TOTAL ROCK URANIUM CONCENTRATIONS

Hole/depth	[U] Rock	[U] Water	P_B mL/g
PH56 43-45	7	7	1.0×10^3
W2 14	46	43.4	1.1×10^3
W2 24	100	85	1.2×10^3
PH61 43-45	6	3.47	1.7×10^3
PH58 25-27	4	1.82	2.2×10^3
W5 24	3	1.3	2.3×10^3
PH61 26-28	8	3.44	2.3×10^3
PH88 38-40	8	3.14	2.5×10^3
W4 14	1418	441	3.2×10^3
PH56 26-28	32	9.69	3.3×10^3
PH55 40-42	4	1.02	3.9×10^3
PH58 38-40	3	0.76	3.9×10^3
PH49 44-46	809	199	4.1×10^3
W1 24	250	60.4	4.1×10^3
W3 24	9.2	1.6	5.8×10^3
W7 13	7.1	1	7.1×10^3
PH96 26	2	0.28	7.1×10^3
W7 24	3	0.42	7.1×10^3
PH94 40-42	3	0.38	7.9×10^3
PH88 28-30	22	2.52	8.7×10^3
W5 13	3.5	0.4	8.8×10^3
PH55 26-28	5	0.5	1.0×10^4
PH94 26-28	2	0.2	1.0×10^4
PH14 21	670	65	1.0×10^4
W3 14	60	5.5	1.1×10^4
PH80 20	89	7.8	1.1×10^4
W4 24	5441	348	1.6×10^4
FH14 26	548	31	1.8×10^4
W1 13	278	6.2	4.5×10^4

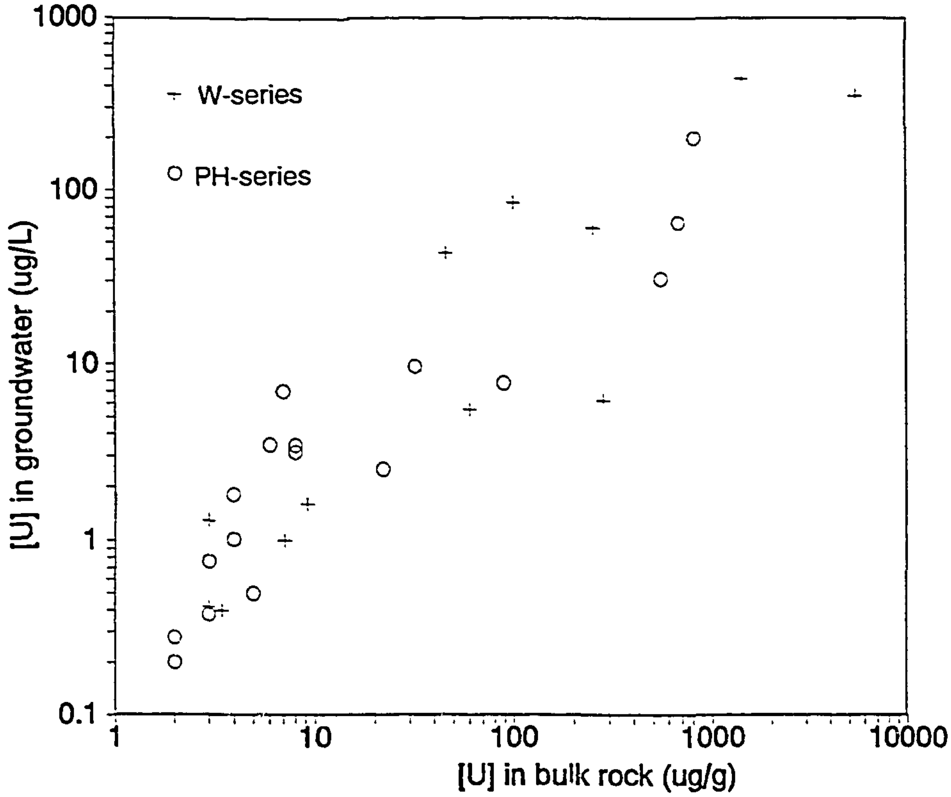

FIGURE 7.1 Comparison of uranium concentrations in groundwater and rock .

The data for the W-holes is not subject to this limitation, as they were constructed for the purpose of obtaining water and core samples from the same location within the dispersion fan. Hence, the data for the W-holes probably provides the best distribution data so far obtained at Koongarra. The P_B values for W-series holes were distributed evenly within the range for the PH-series holes.

Andrews and Kay (1983) suggested that the degree of disequilibrium between ^{234}U and ^{238}U is dependent upon the uranium concentration of the rock relative to the groundwater, a comparison which can be expressed as a partition coefficient. Figure 7.2 shows the relationship between $^{234}U/^{238}U$ activity ratio in the groundwater and the bulk rock partition coefficient (P_B). There appears to be a trend of decreasing activity ratio with decreasing P_B for samples taken from near the base of weathering (B-depth, 24 m). The activity ratio in samples from the mid-weathered zone (A-depth, 14 m) did not appear to be affected by P_B, and this was also the case for unweathered zone samples (not shown). These data suggest that, where the concentration of uranium in the groundwater is high compared to that

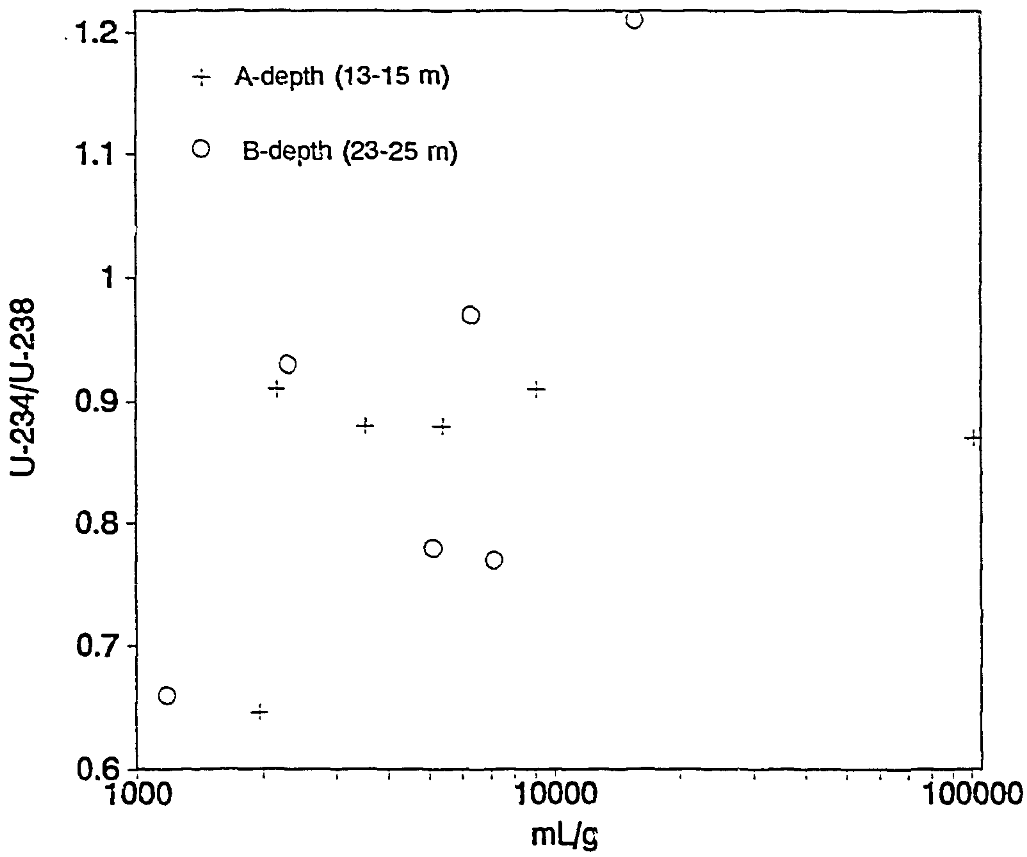

FIGURE 7.2 $^{234}U/^{238}U$ versus P_B for W-series holes (A-depth = 14 m, B-depth = 24 m)

in the partially weathered rock (P_B approximately $<10^4$ mL/g), $^{234}U/^{238}U$ activity ratios less than unity may develop.

Partitioning of ^{238}U between groundwater and rock accessible phases

It is also possible to compare the groundwater with different chemically defined phases of the solid substrate, to determine if the $^{234}U/^{238}U$ activity of a particular component of the solid material reflects an interaction with the groundwater. Table 7.6 shows this comparison. Tamms acid oxalate (TAO) extraction was used to estimate the amount of uranium accessible for interaction with the groundwater (see Sections 2.4 and 6.2). The comparisons could only be made where the rock sample was weathered and contained no uranium minerals, hence, there were only five points suitable for this comparison. However, there does appear to be a strong relationship between concentrations of uranium in groundwater and accessible phases of the rock. The accessible partition coefficient (P_A) was in the range 4.6×10^2 to 1.0×10^3 ml/g total rock, and was significantly lower than the P_B or P_P. values. The $^{234}U/^{238}U$ activity ratios in the accessible phases were close to those in the corresponding groundwater, giving confidence that exchange between the solute and the accessible solid phases is occurring. The greatest discrepancy between groundwater and accessible phases was from a sample from W5, which appears to be in a zone unrelated to the orebody. The nature and the extent of the exchange between solids and liquids cannot, however, be determined from this data, and other mechanisms as well as sorption may be operating. It is possible however that sorption will be the controlling mechanism.

TABLE 7.6

COMPARISON OF URANIUM CONCENTRATION AND ACTIVITY RATIO BETWEEN BULK ROCK, ACCESSIBLE PHASES (TAO-EXTRACTABLE) AND GROUNDWATER

Hole/ depth (m)	Total rock		TAO-extractable		Water		
	[U] (μg/g)	$^{234}U/^{238}U$	[U] (μg/g)	$^{234}U/^{238}U$	[U] (μg/L)	$^{234}U/^{238}U$	P_A (mL/g)
W1 24	250	1.0	28	0.86	60	0.78	460
W2 14	46	0.86	21	0.67	43	0.65	480
W4 14	1418	0.91	239	0.80	441	0.81	540
W5 13	3.5	0.94	0.3	1.4	0.4	0.88	800
W7 13	7.1	0.98	1.0	0.86	1.0	0.88	1000

While only five data points are available, there does appear to be a linearity between uranium concentrations in the groundwater and accessible phases of the rock. The accessible phase partition coefficient (P_A) was almost constant over a large range of uranium concentrations, mineral components, and groundwater chemistry. This, together with the similar $^{234}U/^{238}U$ activity ratios in groundwater and accessible phases, suggests exchange between the two phases. In Section 3.2 it was suggested that very different mineralogical groups had similar amounts of TAO-extractable iron, but with very different amounts of crystalline iron oxides.

Conclusions

A large number of measurements have become available in the course of this study, and this has allowed several different approaches to the description of partitioning of uranium between solid and solute phases. All data should be assessed with regard to whether it refers to the bulk rock, fractionated core, fine particles in groundwater and whether it is for a chemical extraction of accessible phases or a total digestion. The various P values are summarised in Table 7.7.

The choice of appropriate values for modelling studies is left to the individual modellers, bearing in mind that bulk rock data or data for more sorptive fine particles or accessible phases could lead to different results. The use of bulk rock data unambiguously overestimates the partitioning of material onto the solid phases, so a more realistic value may be obtained using chemical extractions. However the specificity of these schemes for the target phases is uncertain. Nonetheless, the data tend to indicate that the variations from one sampling point to another are the major cause of the variability in "P" values obtained.

If the data are considered as a whole, a reasonable "P" value for ^{238}U might be in the range 1×10^3 to 2×10^4 mL/g. Comparing accessible (TAO-extractable) phase data with groundwater suggests a much lower partition ratio, with values lying in the range 5×10^2 to 1×10^3 mL/g.

The much lower P_A than P_B values may result from the non-inclusion of crystalline material, and lower P_A than P_P values from the inclusion of material with much lower surface area/mass ratios, and hence a dilution effect. The corresponding value for ^{230}Th is unquestionably much higher; about 8×10^7 mL/g might be a reasonable estimate.

TABLE 7.7

SUMMARY TABLE OF PARTITION COEFFICIENTS

	Range of observed values (mL/g)	
Partition Coefficient	^{238}U	^{230}Th
Bulk rock (P_B)	1×10^3-5×10^4	2×10^5-3×10^8
Bulk rock accessible phases (P_{PA})	5×10^2-1×10^3	
Particles <10 μm, bulk (P_{PB})	5×10^3-1×10^5	
Particles <10 μm, accessible (P_{PA})	3×10^3-5×10^4	
Particles in groundwater, bulk (P_{PB})	4×10^4-7×10^4	7×10^7-2×10^9
Particles in groundwater, accessible (P_{PA})	2×10^4-7×10^4	2×10^6-1×10^9

8 DISCUSSION AND CONCLUSIONS

The chemistry and mineralogy of rock and soil at Koongarra have been investigated with the aim of gaining understanding about the migration of radionuclides. Of central interest was the mobility and retardation of uranium over long timescales. In addition, data was collected to provide a geochemical framework of the Koongarra system. This was necessary for the application, testing and development of transport and geochemical models, and to allow a realistic evaluation of the transferability of the results.

Data were collected to clarify the scale of the redistribution of uranium from the primary ore body. Leaching and deposition of uranium are strongly linked to the weathering process. Uranium concentrations in the weathered and transition zones are high compared to the unweathered parent material for at least 300 m from the source. The direction of the plume appears to be mainly toward the south-south west, and corresponds well with many hydrochemical and geophysical parameters. The most important zones of enrichment appear to be near the base of weathering, and in the very shallow zone. The shallow component appears to be more wide spread than the deeper component, but it accounts for only a small proportion of the mobilised uranium.

The main mineral constituents of the host schists are quartz, chlorite and muscovite. Small amounts of graphite, sulfides, garnets, feldspars and remnant biotite also occur, particularly outside of the primary ore zone. The abundance of the major rock constituents vary spatially over the site, however, zones of generally similar mineralogy can be delineated. Within the primary ore zone, the nature of the chlorite is mainly magnesium-rich. Outside of this inner halo of hydrothermal alteration, iron-rich chlorite tends to dominate. Differences in type and structure of the chlorite probably resulted from differences in the intensity of hydrothermal alteration, possibly reflecting conditions of ore genesis. The forms and abundances of the mineral constituents greatly affect weathering processes, final products, groundwater chemistry and radionuclide-mineral interactions.

Weathering of the schist has occurred to a depth of approximately 25 m over the site, with the deepest weathering near to the Koongarra fault which separates the schist and the Kombolgie Sandstone. From concentration profiles of zirconium, it appears that with weathering there has been a loss of rock mass of approximately 50%, and a reduction in rock volume of around 38% in the primary and secondary ore zones. Most of these reductions appear to have occurred in the early stages of weathering. Further down-gradient the trends were unclear. In the weathered zone above the primary ore body, kaolinite is the only clay mineral present in significant quantities. Near the base of weathering, there is a thin layer of partially weathered rock containing vermiculite. Down-gradient, where the degree of hydrothermal alteration of the rock is less, smectite also becomes a significant component of the weathered zone. The proportion of clay size material (<2 μm) is much higher in the weathered primary ore zone than down-gradient, and the weathered primary ore contains less gravel. These observations indicate that the intensity of weathering and alteration decreases with distance from the fault.

The iron oxides detected at Koongarra are goethite, hematite and ferrihydrite. Of the crystalline iron oxides, goethite appears to be generally the most abundant, with the hematite content highest in the weathered primary ore zone. The iron oxides occur as fissure and remnant schistosity coatings, dispersed clay coatings, and nodules, and these different forms probably play different roles in the capture and storage of otherwise mobile species. The abundance of iron oxides is very variable, with occasional bands of bleached clay juxtaposed with iron rich bands. Differences in iron content between different mineralogical zones over the site, appear to be mainly accounted for by differences in the amounts of crystalline iron oxides. Assuming all the crystalline iron in the weathered zone is present as goethite, then the concentration of goethite is 2-19%. The concentration of ferrihydrite, estimated by extraction with Tamms acid oxalate (TAO), is between 7 and 29 mg/g, making up an average of about 10% of the total iron. Lithiophorite is the only manganese mineral identified in the weathered zone, and mainly occurs coating fissures and remnant schistosity. Manganese, and to a lesser extent amorphous iron phases, appear to have been leached from the weathered primary ore zone, and deposited down-gradient. Up to 3% of the weathered rock in the dispersion fan was manganese oxide, of which 47% was TAO-extractable. This demonstrates the potential transitory nature of this material. Coatings of iron- and manganese oxy-hydroxides on pore and fissure surfaces are well placed for contact with migrating species.

Areas of depletion and enrichment of elements of interest were identified. The concentration and distribution of elements, potentially geochemically significant to radionuclide migration, were determined and associations between various elements, and between elements and minerals were examined; in the unweathered rock, uranium appears to be associated with a few trace elements, but not with any major rock forming elements. There has been very little penetration of uranium into the quartz chlorite matrix from fissures; an apparent diffusivity of 10^{-24} m^2s^{-1} was estimated, however, there appears to be greater penetration and adsorption of uranium into secondary phases, such as smectite and talc, which periodically coat the surfaces of fissures.

In the weathered zone of the secondary ore body, uranium is correlated with phosphorus, and the uranyl phosphate mineral saleeite has been detected, particularly near the base of weathering. Further down-gradient, uranium is correlated with iron and iron oxide associated elements. The concentrations of phosphorus within the secondary orebody are not significantly greater than elsewhere. This suggests that a the formation of uranyl phosphates is not explained by a phosphate concentration anomaly. The main source of phosphorus at Koongarra is fluorapatite. However, within the inner halo of alteration, a non-apatite source of phosphorus is also present.

The area of primary mineralisation is characterised by marked relative enrichment of heavy rare earth elements, compared to the regional host rock. The heavy rare earth elements were also those most accessible to the groundwater (TAO-extractable), and may therefore be preferentially transported. Cerium appears to be preferentially taken up into inaccessible phases, compared to other rare earth elements, probably into oxides of iron and manganese. Monazite and zircon are probably the major rare earth element sources in the host rock, while uraninite may be a source rich in the heavy rare earth elements. The high heavy rare earth content associated with the primary mineralisation may reflect a high concentration of carbonate in the uranium-bearing fluids involved in ore genesis.

The association of uranium with mineral phases was studied using various microscopic and chemical techniques. In the weathered zone, uranium appears to be associated with secondary oxides of iron and manganese, and its distribution is determined by the distribution of these phases. Phase selective extraction schemes showed that the uranium in the weathered zone is mainly either accessible to the groundwater (adsorbed or associated with amorphous phases, 10-73%), or entrapped within crystalline iron oxides (<27-82%). The relationship with iron oxy-hydroxide appears to be of a diffuse nature, suggesting sorption as the initial mechanism for association. Near the base of weathering in the dispersion fan, uranium was strongly associated with red iron oxides, likely to be ferrihydrite or hematite. However, in the centre of the weathered zone, uranium was most strongly associated with yellow, goethitic phases. This may reflect an aging of the iron oxides, with the early association with uranium being retained. Within manganese phases, uranium is almost exclusively associated with hot spots containing a cerium oxide or hydroxide phase. This cerium phase occurs as small spheres, approximately 2 μm in diameter, and is probably a microcrystalline mixture of cerium and uranium oxides. The mechanism for the cerium-uranium association is not clear, but probably involves a redox interaction between manganese and cerium, followed by sorption of uranium onto the cerium phase. Anomalously high concentrations of cerium were not found in the Koongarra rock. Lithium, barium and cobalt are also strongly associated with manganese phases. In the dispersion fan, up to 2% of the uranium in the weathered zone was estimated to be associated with manganese phases, with the remainder accounted for by iron oxides. Since uranium in the dispersion fan at Koongarra is intimately associated with these potentially unstable or ephemeral fractions of the solid phase, uranium release from these fractions, its movement, and its subsequent redistribution by interaction with newly-formed and old oxy-hydroxide surfaces must be viewed as a dynamic process.

Uranium series disequilibria has been extensively examined, particularly in the weathered zone of Koongarra. In the unweathered zone, the ore material and the host rock were at approximately secular equilibrium, except for a small apparent depletion of ^{226}Ra. In the weathered rock, above the primary mineralised zone, high ^{230}Th/^{234}U activity ratios indicate strong recent leaching of uranium. In these leached areas, the ^{234}U/^{238}U activity ratios are high, above unity in the bulk rock and near unity in the accessible phases (TAO-extractable). This indicates a preferential mobility of ^{238}U relative to ^{234}U. The most intensely leached samples came from near the surface, near the up-gradient boundary of the primary ore. The most intense recent accumulation of uranium appears to have occurred about 0-50 m from the down-gradient boundary of primary ore, particularly near the base of weathering. This highlights the importance of the early stages of weathering to the migration and retardation of uranium. Uranium deposition samples having low $^{230}Th/^{234}U$ activity ratios, also contained low $^{234}U/^{238}U$ activity ratios. Beyond about 50 m down-gradient, both activity ratios tend to increase with distance. At distances greater than about 100 m from the primary ore, deposition of uranium seems to have occurred particularly SSW of the deposit, and is most pronounced near the surface.

A scenario for the development of disequilibria between ^{234}U and ^{238}U is proposed. The onset of weathering conditions causes the rapid dissolution of the primary uranium minerals, resulting in the congruent liberation of ^{238}U and ^{234}U. This is followed by preferential entrapment of ^{234}U from solution and accessible sites which results in an apparent preferential mobility of ^{238}U. This leads to high $^{234}U/^{238}U$ activity ratios in leached samples and low ratios in depositional samples down-gradient. Beyond about 50 m down-gradient, uranium mobilised from the primary ore makes a smaller contribution to the total accessible uranium. It is likely that slowly dissolving minerals that contain uranium, such as zircon and monazite, would preferentially leach ^{234}U relative to ^{238}U, resulting in higher $^{234}U/^{238}U$ activity ratios of the accessible (TAO-extractable) and groundwater uranium. It is suggested that where the uranium content in accessible phases is high, the accessible (or solution) $^{234}U/^{238}U$ activity ratio will generally tend to decrease with time or distance due to preferential retardation of ^{234}U.

Sequential extraction data showed that the highest $^{234}U/^{238}U$ activity ratios came from resistant phases with low uranium contents, such as quartz and muscovite. The amount of excess ^{234}U appeared to be related to the amount of uranium present in the crystalline iron oxide phases. Iron oxides were frequently observed coating minerals. The high activity ratios in the resistant phases suggest that α-recoil emplacement of ^{234}Th is a significant process occurring at Koongarra. Other mechanisms may also be operating to reduce the mobility of ^{234}U.

Saleeite crystals from the weathered primary ore zone had $^{234}U/^{238}U$ and $^{230}Th/^{234}U$ activity ratios greater than unity, while crystals from down-gradient had $^{230}Th/^{234}U$ activity ratios below unity. This indicates significant differences in the time of formation, with the down-gradient crystals being much younger. At one deposition site, the crystals had $^{234}U/^{238}U$ activity ratios less than unity, suggesting formation from groundwater depleted in ^{234}U. At another deposition site, saleeite had $^{234}U/^{238}U$ activity ratios above unity, suggesting formation from groundwater enriched in ^{234}U. The difference is likely to be due to different sources of groundwater, with the high activity ratio site receiving water from a deeper and less weathered aquifer. This was supported by activity ratios measured in groundwater from the two sites.

Estimates of the partitioning of ^{238}U and ^{230}Th between groundwaters and solid phases were made using several approaches. The best agreement between the uranium isotope ratios for the solid phase and the groundwater was with the TAO-extractable fraction (accessible or amorphous material) of the weathered rock. This suggests that this extraction removes material accessible to exchange with the groundwater. Partition coefficients of 0.5-1 $\times$ 10^3 mL/g were calculated by using the TAO-extractable uranium; bulk rock data gave partition coefficients of 1-45 $\times$ 10^3 mL/g. Near the base of weathering, there appears to be a trend of increasing $^{234}U/^{238}U$ activity ratio in the groundwater with increasing partitioning of uranium onto the rock. This suggests that when the uranium content of the groundwater is high relative to the partially weathered rock, development of $^{234}U/^{238}U$ activity ratios less than unity may occur in the groundwater.

In summary, considerable information has been gathered on the migration of uranium at Koongarra. Generally applicable data has been collected on: the importance of the early stages of weathering in radionuclide transport; the behaviour of uranium in weathered environments; the development of isotopic disequilibria under weathering conditions, the behaviour of rare earth elements, and the associations of uranium with mineral phases.

9 REFERENCES

Airey, P.L., Roman, D., Golian, C., Short, S., Nightingale, T., Lowson, R.T. and Calf, G. E. (1982) Radionuclide migration around uranium ore bodies analogues of radioactive waste repositories. United States Nuclear Regulatory Commission Contract NRC-04-81-172, Annual Report 1981-82, Australian Atomic Energy Commission Report AAEC/C29.

Airey, P.L., Roman, D., Golian, C., Short, S., Nightingale, T., Lowson, R.T., Calf, G. E., Davey, B.G., Gray, D.G., Ellis, J and Shirvington, P.J. (1983) Radionuclide migration around uranium ore bodies analogues of radioactive waste repositories. United States Nuclear Regulatory Commission Contract NRC-04-81-172, Annual Report 1982-83, Australian Atomic Energy Commission Report AAEC/C40.

Airey, P.L., Roman, D., Golian, C., Short, S., Nightingale, T., Payne, T., Lowson, R. T., Duerden, P., Davey, B.G., Gray, D.J. and Ivanovich, M. (1985) Radioactive migration around uranium ore bodies analogues of radioactive waste repositories. United States Nuclear Regulatory Commission Contract NRC-04-81-172, Annual Report 1983-84, Australian Atomic Energy Commission Report AAEC/C45.

Andrews, J.N. and Kay, R.L.F. (1978) The evolution of enhanced uranium activity ratios for dissolved uranium and groundwater dating. Proceedings of 4th Int. Conference on Geochronology, Denver, pp.11-13.

Andrews, J.N. and Kay, R.L.F. (1983) The U contents and $^{234}U/^{238}U$ activity ratios of dissolved uranium in groundwaters from some Triassic sandstones in England. Isot. Geosci. 1: 101-117.

Anthony, P.J. (1975) Nabarlek uranium deposit. In C.L. Knight (Ed.) Economic geology of Australia and Papua New Guinea, Australas. Inst. Min. Metall., Monograph series 5, 1. Metals, 304-308.

Asikainen, M. (1981) State of disequilibrium between ^{238}U, ^{234}U, ^{226}U and ^{222}Rn in groundwater from bedrock. Geochim. Cosmochim. Acta 41: 1200-1206.

Barnhisel, R.I. and Bertsch, P.M. (1989) Chlorites and Hydroxy-Interlayed Vermiculite and Smectite. In Dixon, J.B. and Weed, S.B. (eds.), Minerals in soil environments. Soil Science Society of America, Madison. pp. 729-788.

de Barr, J.W, German, C.R., Elderfield, H. and van Gaans, P. (1988) Rare earth element distributions in anoxic waters at Cariaco Trench. Geochim. Cosmochim. Acta 52: 1203-1219.

Belzile, N. and Tessier, A. (1990) Interactions between arsenic and iron oxyhydroxides in lacustrine sediments. Geochim. Cosmochim. Acta 54: 103-109.

Brindley, G.W. and Brown, G. (1980) Crystal structures of clay minerals and their X-ray identification. Mineralogical Society Monograph 5, London.

Brookins, D.G. (1988) Eh-pH diagrams for geochemistry. Springer-Verlag, Berlin.

Calvert, K.J., Piper, D.Z. and Baedecker, P.A. (1987) Geochemistry of the rare earth elements in ferromanganese nodules from DOMES site A, northern equatorial Pacific. Geochim. Cosmochim. Acta 51: 2231-2338.

Cantrell, K.J. and Byrne, R.H. (1987) Rare earth element complexation by carbonate and oxalate ions. Geochim. Cosmochim. Acta 51: 597-605.

Carl, C. (1985) Investigations of uranium series disequilibria as a means to study the transport mechanism of uranium in sandstone samples during weathering. Proceedings of International Meeting on Concentration Mechanisms of Uranium in Geological Environments, Nancy (October 1985), pp.299-304.

Carl, C. and Meyer, M. (1984) α-Spectrometric investigations of radioactive disequilibrium in early precambrian quartz pebble conglomerates. J. Radioanal. Nucl. Chem. (articles) 81: 235-246.
Chalov, P.I. (1959) Isotopic ratio of $^{234}U/^{238}U$ in some secondary minerals. Geochem. Int. 2: 203-210.

Chalov, P.I., Tuzova, T.V. and Musin, Y.A. (1964) The $^{234}U/^{238}U$ activity ratio in natural waters and its use in geochronology. Geochem. Int. 1: 402-408.

Chau, T.T and Zhou, L. (1983) Extraction techniques for selective dissolution of amorphous iron oxides from soils and sediments. Soil Sci. Soc. Am. J. 47: 225-232.

Cherdyntsev, V.V., (1968) English Translation of Uran-234 Atomizdat, Moscow. Uranium-234. Israel Program for Scientific Translations, Jerusalem (1971).

Childs, C.W. (1975) Composition of iron-manganese concentrations from some New Zealand soils. Geoderma 13: 141-152.

Childs, C.W. and Leslie, D.M. (1977) Inter-element relationships in iron-manganese concretions from a catenary sequence of yellow-grey earth soils in loess. Soil Sci. 123: 369-375.

Chopin, G.R. (1988) Humics and radionuclide migration. Radiochim. Acta 44/45: 23-28.

Christian, C.S. and Stewart, G.A. (1952) Survey of the Katherine/Darwin region 1946. Commonwealth Scientific and Industrial Research Organisation, Australian Land Resource Series. 1.

Coffin, D.E. (1961) A method for the determination of free iron in soils. Can. J. Soil Sci. 43:7-17.

Colombo, C., Buondonno, A., Violante, A. and Torrent, J. (1991) The contrasting of goethite and hematite on phosphate sorption and desorption by terre rosse. Z. Pflanzenernahr. Bodenk. 154: 301-305.

Cordfunke, E.P.H. (1969) The chemistry of uranium including its applications in nuclear technology. Elsevier, Amsterdam.

Crank, J. (1975) The mathematics of diffusion. 2nd Edn. Oxford Press, London.

Crowther, D.L., Dillard, J.G. and Murray, J.W. (1983) The mechanism of Co(II) oxidation on synthetic birnessite. Geochim. Cosmochim. Acta 47: 1399-1403.

Dall'Aglio, M., Gragnani, R. and Locardi, E. (1974) Geochemical factors controlling the formation of the secondary minerals of uranium. Proceedings of a Symposium on Formation of Uranium Ore Deposits, Athens (May 1974), pp.33-48. ISBN 92-0-040274-7.

Deer, W.A., Howie, R.A. and Zussman, J. (1983) An introduction to the rock forming minerals. Longman Group, Essex.

Dervin, J. and Faucherre, J. (1973) Study of carbonate complexes of thorium and Ce(III): Solubility and nature of the complex ions in solution. Bull. Soc. Chim. France 1973: 2930-2933.

Dickson, B.L., Gulson, B.L. and Snelling, A.A. (1985) Evaluation of lead isotopic measurements for uranium exploration, Koongarra area, Northern Territory, Australia. J. Geochem. Explor. 24: 81-102.

Dickson, B.L. and Snelling, A.A. (1980) Movements of uranium and daughter isotopes in the Koongarra uranium deposit. In Ferguson, J. and Goleby, A.B. (eds.), Uranium in the Pine Creek Geosyncline. International Atomic Energy Agency, Vienna. pp. 499-507.

Donelly, T.H. and Ferguson, J. (1980)A stable isotope study of three deposits in the Alligator Rivers Uranium Field, N.T. In Ferguson, J. and Goleby, A.B. (eds.), Uranium in the Pine Creek Geosyncline. International Atomic Energy Agency, Vienna. pp. 397-406.

Elderfield, H., Hawkesworth, C.J., Greaves, M.J. and Calvert, S.E. (1981) Rare earth element geochemistryof oceanic ferromanganese nodules and associated sediments. Geochim. Cosmochim. Acta 45: 513-528.

Ellis, W.R. and Wall, T. (1982) Use of particle track analysis to measure fissile particle size distributions in contaminated soils. Nucl. Instrum. Methods 200: 411-415.

Eupene, G.S., Fee, P.H. and Colville, R.G. (1975) Ranger One uranium deposits.
In C.L. Knight (Ed.) Economic geology of Australia and Papua New Guinea, Australas. Inst. Min. Metall., Monograph series 5, 1. Metals, 308-317.

Ewers, Y. and Ferguson, J. (1980) Mineralogy of the Jabiluka, Ranger, Koongarra, and Nabarlek uranium deposits. In Ferguson, J. and Goleby, A.B. (eds.) Uranium in the Pine Creek Geosyncline. International Atomic Energy Agency, Vienna. pp. 363-374.

Eyal, Y. (1982) Isotopic fractionation of thorium and uranium upon leaching of monazite. In W. Lutze (ed), The scientific basis for radioactive waste management. Volume V. (pp.399-408. (Elsevier).

Eyal, Y. and Fleischer, R.L. (1985a) Timescale of natural annealing in radioactive minerals affects retardation of radiation-damage-induced leaching. Nature 314: 518-520.

Eyal, Y. and Fleischer, R.L. (1985b) Preferential leaching and the age of radiation damage from alpha decay in minerals. Geochim. Cosmochim. Acta 49: 1155-1164.

Eyal, Y. and Kaufman, A. (1982) Alpha recoil damage in monazite: preferential dissolution of the radiogenic actinide isotopes. Nucl. Technol. 58: 77-83.

Ferguson, J. and Winer, P. (1980) Pine Creek geosyncline: statistical treatment of whole rock chemical data. In Ferguson, J. and Goleby, A.B. (eds.) Uranium in the Pine Creek Geosyncline. International Atomic Energy Agency, Vienna. pp. 191-208.

Fitzpatrick, E.A. (1984) Micromorphology of soils. Chapman & Hall, London.

Fitzpatrick, R.W., Le Roux, J. and Schwertmann, U. (1978) Amorphous and crystalline titanium and iron-titanium oxides in synthetic preparations, at near ambient conditions, and in soil clays. Clays Clay Miner. 26: 189-201.

Foy, M.F. and Pedersen, C.P. (1975) Koongarra uranium deposit. In Economic geology of Australia and Papua New Guinea. 1. Metals. Australas. Inst. Min. Metall., Monograph series 5, Melbourne. pp. 317-321.

Frondel, C. (1958) Systematic mineralogy of uranium and thorium. Geological Survey Bulletin 1064. United States Government Printing Office, Washington.

Gerth, J. (1987) Role of iron oxides in the retention of trace metals and radionuclides. Australian Institute of Nuclear Science and Engineering Research Fellowship Project, Final Report.

Ghaleb, B., Hillaire-Marcel, C., Causse, C., Gariepy, C. and Vallieres, S. (1990) Fractionation and recycling of U and Th isotopes in a semi-arid endoreic depression of Central Syria. Geochim. Cosmochim. Acta 54: 1025-1035.

Gill, J.B. and Williams, R.W. (1990) Th-isotope and U-series studies of subduction - related volcanic rocks. Geochim. Cosmochim. Acta 54: 1427-1442.

Gleadow, A.J.W. and Lowring, J.F. (1974) The effect of weathering on fission track dating. Earth Planet. Sci. Lett. 22: 163-168.

Gray, D. (1986) The Geochemistry of Uranium and Thorium During Weathering of Chloritic Schists at the Alligator Rivers Uranium Province, N.T., Australia. PhD Thesis, The University of Sydney.

Gueniot, B., Guillet, B. and Souchier, B. (1982) Uranium fixation on the surface of iron oxyhydroxide in placic horizons of hydromorphic soils: one example of stagnogley in the chrystalline Vosges Mountains (France) C. R. Acad. Sci. Ser. 2. 251: 31-36.

Guthrie, V. (1991) Determination of recent ^{238}U, ^{234}U and ^{230}Th mobility in granitic rocks: application of a natural analogue to the high-level waste repository environment. Appl. Geochem., 6: 63-74.

Hansen, R.O. (1970) Radioactivity of a California terrace soil. Soil Sci., 110, 31-36.

Hansen, R.O. and Huntingdon. G.L (1969) Thorium movements in morainal soils of the High Sierra, California. Soil Sci. 108: 257-265.

Hansen, R.O. and Stout, P.R. (1968) Isotopic distributions of uranium and thorium in soils. Soil Sci. 105: 44-50.

Harter, R.D. (1979) Adsorption of copper and lead by Ap and B2 horizons of several north eastern United States soils. Soil Sci. Soc. Am. J. 43: 679-683.

Hashimoto, T., Kido, K. and Sotabayashi, T. (1981) Ranges of α-recoil ^{234}Th atoms in uranium oxides. J. Inorg. Nucl. Chem. 43: 2233-2238.

Hashimoto, T., Aoyagi, Y., Kudo, H. and Sotobayashi, T. (1985) Range calculation of alpha-recoil atoms in some minerals using LSS-theory. J. Radioanal. Nucl. Chem. 90: 415-438.

Hegge, M.R., Mosher, D.V., Eupene, G.S. and Anthony, P.J. (1980) Geological setting of the East Alligator uranium deposits and prospects. In Ferguson, J. and Goleby, A.B. (eds.) Uranium in the Pine Creek Geosyncline. International Atomic Energy Agency, Vienna. pp. 259-272.

Hey, M.H. (1954) A review of the chlorites. Mineral. Magazine 30: 277-300.

Hsu, P.H. (1965) Fixation of phosphate by aluminium and iron in acidic soils. Soil Sci. 99: 398-401.

Ivanovich, M. and Harmon, R.S (eds.) (1982) Uranium Series Disequilibria: Application to Environmental Problems in the Earth Sciences. Clarendon Press, Oxford.

Kabata-Pendias, A. and Pendias, H. (1984) Trace Elements in Soils and Plants. CRC Press, Boca Raton.

Kigoshi, K. (1971) Alpha-recoil of thorium-234: dissolution into water and the uranium-234/uranium-238 disequilibrium in nature. Science 173: 47-48.

Kolodny, Y. and Kaplan, I.E. (1970) Uranium isotopes in seafloor phosphorites. Geochim. Cosmochim. Acta 34: 3-24.

Koons, R.D., Helmke, P.A. and Jackson, M.L. (1980) Association of trace elements with iron oxides during rock weathering. Soil Sci. Soc. Am. Proc. 44: 155-159.

Kronfield, J., Gradsztajn, E., Muller, H.W., Radin, J., Yaniv, A. and Zach, R. (1974) Uranium deposition and ^{234}Th alpha recoil : an explanation for extreme ^{234}U/^{238}U fractionation within the trinity aquifer. Earth. Planet. Sci. Lett. 21: 327-330.

Langmuir, D. and Herman, J.S. (1980) The mobility of thorium in natural waters at low temperatures. Geochim. Cosmochim. Acta 44: 1753-1766.

Latham, A.G. and Schwarcz, H.P. (1987) The relative mobility of U, Th and Ra isotopesin the weathered zones of the Eye-Dashwa Lakes granite pluton, north western Ontario, Canada. Geochim. Cosmochim. Acta 51: 2787-2793.

Laul, J.C. and Smith, M.R. (1988) Disequilibrium study of natural radionuclides of uranium and thorium series in cores and briny groundwaters from Palo Duro Basin, Texas. Radioact. Waste Manage Nucl Fuel 11(2): 169-225.

Levinson, A.A. and Coetzee, G.L., (1978) Implications of disequilibrium in exploration for uranium ores in the surficial environment using radiometric techniques - a review. Miner. Sci. Eng 10: 19-27.

Levinson, A.A., Bland, C.J. and Lively, R.S. (1982) Exploration for U ore deposits. In Ivanovich, M. and Harmon, R.S. (Eds.) Uranium Series Disequilibrium: Applications to Environmental Problems. Clarendon Press Oxford. pp:167-180.

Lindsay, W.L. (1979) Chemical Equilibria in Soils. Wiley, New York.

Lively, R.S., Harmon, R.S., Levinson, A.A. and Bland, G.J., (1979) Disequilibrium in the ^{238}U series in samples from Yeelirrie, Western Australia. J. Geochem. Explor. 12: 57-64.

Longworth, G., Ivanovich and Wilkins, M.A. (1989) Uranium series disequilibrium studies at the Broubster analogue site, progress report April 1988 - March 1989. UK Department of the Environment, report No. DOE/RW/89.100.

Lowson, R.T., Reid, P.D., Sarbutt, J.V., McIntyre, M.G., Bowdler, R.J., Short, S.A., Wong, H., Palmer, von Gunten, H. (1992) Uranium, thorium and radium isotope profiles of aqueous and mineral phases in a lateritic weathered zone. Report to the final meeting of the IAEA on nuclear techniques in the study of pollutant transport in the environment: Interaction of solutes with geological media (methodological aspects), Vienna, June 1992.

Lowson, R.T., Short, S.A., Davey, B.G. and Gray, D.J. (1986) ^{234}U/^{238}U and ^{230}Th/^{234}U activity ratios in mineral phases of a lateritic weathered zone. Geochim. Cosmochim. Acta 50: 1697-1702.

Maya, L. (1982) Sorbed uranium(VI) species on hydrous titania, zirconia and silica gel. Radiochim. Acta 31: 147-151.

McKeague, J.A., Damman, A.W.H. and Heringa, P.K. (1968) Iron-manganese and other pans in some soils of Newfoundland. Can. J. Soil Sci. 48: 243-253.

McKeague, J.A. and Day, J H. (1966) Dithionite-and oxalate-extractable Fe and Al as aids in differentiating various classes of soils. Can. J. Soil Sci. 46: 13-22.

McKenzie, R.M. (1975) An electron microprobe study of the relationships between heavy metals and manganese and iron in soils and ocean floor nodules. Aust. J. Soil Res. 13: 177-188.
McKenzie, R.M. (1989) Manganese oxides and hydroxides. In Minerals in Soil Environments. 2nd Edn. Dixon, J.B. and Weed, S.B. (eds.) Soil Science Society of America, Madison. pp. 439-465.

McKinley, I.G. and Alexander, W.R. (1992) Constraints on the applicability of "in-situ distribution coefficient" values. J. Environ. Radioact. 15: 19-34.

McLennan, S.M. and Taylor, S.R. (1979) Rare earth element mobility associated with uranium mineralisation. Nature 282: 247-250.

McLennan, S.M. and Taylor, S.R. (1980) Rare earth elements in sedimentary rocks, granites and uranium deposits of the Pine Creek Geosyncline. In Ferguson, J. and Goleby, A.B. (eds.) Uranium in the Pine Creek Geosyncline, International Atomic Energy Agency, Vienna. pp. 175-190.

Means, J.J., Crerar, D.A., Borcshi, M.P. and Duguid, J.O. (1978) Adsorption of Co and selected actinides by Mn and Fe oxides in soils and sediments., Geochim. Cosmochim. Acta 42: 1763-1773.

Mehra, O.P. and Jackson, M. (1960) Iron oxide removal from soils and clays by a dithionite-citrate system buffered with sodium bicarbonate. Proceedings of 7th Int. Conf. on Clays and Clay Minerals, 1958, Washington D.C., Monograph No.5, 317-327.

Mendelovici, E. and Sagarzazu, A. (1991) Characteristics of products from the acid ammonium oxalate treatment of manganese minerals. Clays Clay Miner. 39: 246-269

Milnes, A.R. and Fitzpatrick, R.W. (1989) Titanium and zirconium minerals. In Minerals in Soil Environments. 2nd Edn. Dixon, A. R. and Weed, S.B. (eds.) Soil Science Society of America, Madison. pp. 1131-1205.

Morgan, M.F. (1935) The universal soil testing systems. Connecticut Agricultural Experiment Station Bulletin, 372.

Murakami, T. and Isobe, H. (1990) Alteration of chlorite and its relevance to the uranium redistribution in the vicinity of the ore deposit at Koongarra, Northern Territory, Australia. Proceedings of Geoval-90 Symposium, 14-18 May, Stockholm, Sweden.

Nash, J.T. and Frishman, D. (1983) Chemical data and statistical interpretations for rocks and ores from the Ranger uranium mine N.T., Australia. United States Department of the Interior Geological Survey, Open-File Report 83-239.

Needham, R.S. and Stuart-Smith, P.G. (1976) The Cahill formation host to uranium deposits if the Alligator Rivers uranium field, Australia. BMR J. Aust. Geol. Geophys 1: 321-333.

Nightingale, T.J. (1988a) Measurement of activity ratios of uranium series nuclides in sections of rock bordering a fracture. In P. Duerden (Ed.) Radionuclide migration around uranium ore bodies - analogue of radioactive waste repositories, annual report 1986-1987, Contract NRC-04-81-172, Australian Nuclear Science and Technology Organisation, Ansto/C72 pp: 67-75.

Nightingale, T.J. (1988b) A study of uranium mobilisation at the Koongarra deposit using U-234/U-238 and Th-230/U-234 ratios. In P. Duerden (Ed.), Radionuclide migration around uranium ore bodies - analogue of radioactive waste repositories, annual report 1986-1987, Contract NRC-04-81-172, Australian Nuclear Science and Technology Organisation, Ansto/C72 pp: 37-62.

Noranda (1978) Koongarra Project: Draft Environmental Impact Statement Appendices. Noranda Australia Limited, Melbourne.

Noranda (unpublished) Drilling logs for Koongarra drill holes. Noranda Australia Limited, Melbourne.

Osmond, J.K. (1980) Uranium disequilibrium in hydrologic studies. In Fritz, P. and Fontes, J.Ch. (eds.) Handbook of environmental isotope geochemistry, pp. 259-282.

Osmond, J.K. and Cowart, J.B. (1976) The theory and uses of natural uranium isotopic variations in hydrology. At. Energy Rev. 14: 621-679.

Osmond, J.K., and Cowart, J.B. (1982) Natural uranium and thorium series disequilibrium : new approaches tc geochernical problems. Nucl. Sci. Appl. (B) 1, 303-355.

Pea, F. and Torrent, J. (1984) Relationships between phosphate sorption and iron oxides in alfisols from a river terrace sequence of mediterranean Spain. Geoderma 33: 283-296.

Pedersen, C.P. (1978) The geology of the Koongarra deposits including investigations of contained elements. In Koongarra project: Draft environmental impact statement, Noranda Australia Ltd, Melbourne, Appendix 5.

Pedersen, C.P., Dunbier, J., Gingrich, J.E. (1980) Experience with the track etch method for uranium exploration in Northern Australia. In Ferguson, J and Goleby, A.B. (eds.) Uranium in the Pine Creek Geosyncline, IAEA, Vienna 351-356.

Petit, J., Langevin, Y. and Dran, J. (1985a) Radiation-enhanced release of uranium from accessory minerals in crystaline rocks. Geochim. Cosmochim. Acta 49: 871-876.

Petit, J-C, Langevin, Y. and Dran, J-C (1985b) $^{234}U/^{238}U$ isotopic disequilibrium in nature: Theoretical reassessment of proposed models. Bull. Mineral. 108: 745-753.

Piper, D.Z. (1974) Rare earth elements in ferromanganese nodules and other marine phases. Geochim. Cosmochim. Acta 42: 1007-1022.

Rosholt, J.N. (1961a) Uranium migration and geochemistry of uranium deposits in sandstone above, at and below the water table; Part 1: calculation of apparent dates of uranium migration in deposits above and at the water table. Econ. Geol. 56: 1392-1403.

Rosholt, J.N. (1961b) Late pleistocene and recent accumulation of uranium in groundwater saturated sandstone deposits. Econ. Geol. 56: 423-430.

Rosholt, J.N. (1980) Uranium and thorium disquilibrium in zeolitically altered rock. Nucl. Tech., 51, 143-146.

Rosholt, J.N. (1982) Mobilization and weathering. In Ivanovich, M. and Harmon, R. S. (eds.) Uranium series disequilibrium: applications to environmental problems. Clarendon Press, Oxford. pp: 167-180.

Rosholt, J.N. (1983) Isotopic composition of uranium and thorium in crystalline rocks. J. Geophys. Res. 88: 7315-7330.

Rosholt, J.N., Shields, W.R. and Garner, E.L. (1963) Isotope fractionation of uranium in sandstone. Science 139: 224-226.

Rosholt, J.N., Garner, E.L. and Shields, W.R. (1964) Fractionation of uranium isotopes and daughter products in the weathered granite and uranium-bearing sandstone, Wind River Basin, Wyoming. U.S. Geological Survey Prof. Paper 501-B: 84-87.

Rosholt, J.N., Doe, B.R. and Tatsumoto, M. (1966) Evolution of isotopic composition of uranium and thorium in soil profiles. Geol. Soc. Am. Bull., 77, 987-1044.

Ruzicka, V. and Littlejohn, A.L. (1982) Mode of occurrence of secondary radionuclide-bearing minerals in natural argillized rocks: a preliminary report related to a barrier clay in nuclear waste disposal. Paper - Geological Survey of Canada 82-1A: 247-259.

Sakanoue, M. and Komura, K. (1971) Anomalously high $^{234}U/^{238}U$ ratios in a natural sample. Nature Phys. Sci. 233: 80-81.

Schwertmann, U. and Taylor, R.M. (1989) Iron oxides. In Dixon, J.B. and Weed, S.B. (eds.) Minerals in Soil Environments. 2nd Edn., Soil Science Society of America, Madison, p. 379-438.

Schwarcz, H.P., Gascoyne, M. and Ford, D.C. (1982) Uranium series disequilibrium studies of granitic rocks. Chem. Geol. 36: 87-102.

Scott, R.D., MacKenzie, A.B., Ben-Shaben, Y.A., Hooker, P.J. and Houston, C.M. (1991) Uranium transport and retardation at the Needle's Eye natural analogue site, South Western Scotland. Radiochim. Acta, 52/53: 357-365.

Shea, M. (1984) Uranium migration at some hydrothermal veins near Marysvale Utah: a natural analog for waste isolation. In McVay, G. L. (Ed.), The scientific basis for nuclear waste management VII. North Holland Publishing, New York. pp. 186-193.

Shirvington, P.J. (1980a) $^{234}U/^{238}U$ activity ratios in clay as a function of distance from primary ore. In Uranium in the Pine Creek Geosyncline. Ferguson, J. and Goleby, A.B. (eds.), International Atomic Energy Agency, Vienna. pp. 509-519.

Shirvington, P.J. (1980b) $^{238}U/^{234}U$ disequilibrium as a measure of uranium migration in clay over the past 250 000 years. Underground Disposal of Radioactive Wastes Volume II, IAEA/NEA symposium proceedings, pp 239-252.

Shirvington, P.J. (1983) Fixation of radionuclides in the ^{238}U decay series in the vicinity of mineralized zones: I. The Austatom Uranium Project, Northern Territory, Australia. Geochim. Cosmochim. Acta 47: 403-412.

Short, S.A. (1988) Chemical Transport of Uranium and Thorium in the Alligator Rivers Uranium Province, Northern Territory, Australia. PhD Thesis, The University of Wollongong.

Short, S.A., Lowson, R.T., Ellis, J. and Price, D.M. (1989) Thorium-uranium disequilibrium dating of Late Quatemary ferruginous concretions and rinds. Geochim. Cosmochim. Acta 53: 1379-1389.

Sholkovitz, E.R. (1989) Artifacts associated with the chemical leaching of sediments for rare earth elements. Chem. Geol. 77: 618-621.

Sidhu, P.S., Sehgal, M.K., Sinha, M.K. and Randhawa, N.S. (1977) Composition and mineralogy of iron-manganese concretions from some soils of the Indo-Gangetic plain in northwest India. Geoderma 18: 241-249.

Sill. C.W. (1977) Determination of thorium and uranium isotopes in ores and mill tailings by alpha spectrometry. Anal. Chem. 49: 618-621.

Snelling, A.A. (1980a) A Geochemical Study of the Koongarra Uranium Deposit, Northern Territory, Australia. PhD Thesis, The University of Sydney.

Snelling, A.A. (1980b) Uraninite and its alteration products, Koongarra uranium deposit. In Ferguson, J. and Goleby, A.B. (eds.), Uranium in the Pine Creek Geosyncline. International Atomic Energy Agency, Vienna pp. 487-498.

Snelling, A.A. (1984) A soil geochemistry orientation survey for uranium at Koongarra, Northern Territory. Journal of Geochemical Exploration 22: 83-99.

Snelling, A.A. (1989) Koongarra uranium deposits. In Hughes, F. E. (Ed.), The Geology of the Mineral Deposits of Australia and Papua New Guinea. The Australasian Institute of Mining and Metallurgy, Melbourne. Monograph 14.

Snelling, A.A. and Dickson, B.L. (1979) Uranium/daughter disequilibrium in the Koongarra uranium deposit, Australia. Miner. Deposita 14: 109-118.

Speer, J.A., Solberg, T.N. and Becker, S.W. (1981) Petrography of the uranium-bearing minerals of the Liberty Hall Pluton, South Carolina: phase assemblages and migration of uranium in granitoid rocks. Econ. Geol. 76: 2162-2175.

Stewart, G.A. (1956) Soils of the Katherine/Darwin region, Northern Territory. Commonwealth Scientific and Industrial Research Organisation, Australian Soil Publications. 6.

Story, R., Galloway, R.W., McAlpine, J.R., Aldrick, J.M. and Williams, M.A.J. (1976) Lands of the Alligator Rivers area, Northern Territory. Commonwealth Scientific and Industrial Research Organisation, Australian Land Research Series. 38.

Szabo, B.J. (1982) Extreme fractionation of $^{234}U/^{238}U$ and $^{230}Th/^{234}U$ in spring waters, sediments, and fossils of the Pomme de Terre Valley, Southwestern Missouri. Geochim. Cosmochim. Acta 46: 1675-1679.

Szabo, B.J. and Rosholt, J.N. (1982) Surficial Continental Sediments. In Ivanovich, M. and Harmon, R.S. (eds.) Uranium series disequilibria: Application to environmental problems. pp.246-267. (Clarendon Press, Oxford).

Tamm, O. (1922) Um besta dotdtmring ow oorganiska komponenterna i markens gelkomplex. Medd. Statens Skogsforsokanst. 19: 384-404.

Tamm, O. (1934) Uber die Oxalatmethode in der chemischen Bodenanalyse (oxalate method in chemical extraction of soils) Medd. Statens Skogsforsokanst. 27: 1-20.

Taylor, R.M. (1968) The association of manganese and cobalt in soils - further observations. Journal of Soil Sci. 19: 77-80.

Taylor, R.M., McKenzie, R.M. and Norrish, K. (1964) The mineralogy and chemistry of manganese in some Australian soils. Aust. J. Soil Res. 2: 235-248.

Taylor, S.R. and McLennan, S.M. (1985) The continental crust: Its composition and evolution, an examination of the geochemical record preserved in sedimentary rocks. Blackwell Scientific, Oxford.

Tessier, A., Campbell, P.G.C. and Bisson, M. (1979) Sequential extraction procedure for the speciation of particulate trace metals. Anal. Chem. 51: 844-851.

Ticknor, K.V., Vandergraaf, T.T. and Kamineni, D.C. (1989) Radionuclide sorption on primary and fracture-filling minerals from the east Bull Lake pluton, Massey, Ontario, Canada. Appl. Geochem. 4: 163-176.

Toulhoat, P. and Beaucaire, C. (1991) Comparison between lead isotopes, $^{234}U/^{238}U$ activity ratio and saturation index in hydrogeochemical exploration for concealed uranium deposits. J. Geochem. Explor., 41: 181-196.

Tucker, D.C. (1975) Wall Rock Alteration at the Koongarra Uranium Deposit. MSc Thesis, James Cook University of North Queensland.

Venkataramani, B. and Gupta, A.R. (1991) Effect of anions on the sorption of uranyl ions on hydrous oxides: application of the surface hydrolysis model. Colloids Surf. 53: 1-19.

Vlasov, K.A. (1966) Geochemistry and mineralogy of rare elements and genetic types of their deposits. In Mineralogy of rare elements, Volume 2, K.A. Vlasov (ed.) Israel program for scientific translations, Jerusalem, pp: 249-266.

Weast, R.C. (Ed) (1981) Handbook of chemistry and physics. 61st edition, CRC Press, Florida.

Weaver, C.E. (1976) The nature of TiO_2 in kaolinite. Clays Clay Miner. 24: 215-218.

Wells, M.R. (1979) Soils studies in Magela Creek catchment. Part 1. Land Conservation Unit, Territory Parks and Wildlife Commission, Darwin. Report L.C. 79/1A.

White, L.A., Findlater, P.A., Van Cuylenburg, H.R.M. and Hall, I.R. (1982) Soil studies in the eastern sector of the Nourlangie Creek catchment 1979. Land Conservation Unit, Conservation Commission, Darwin. Report LC 82/3.

Yamashita, H., Ozawa, Y., Nakajima, F. and Murata, T. (1980) The collection of uranium from sea water with hydrous metal oxide. II. The mechanism of uranium adsorption on hydrous titanium(IV) oxide. Bull. Chem. Soc. Jpn 53: 1-5.

Zielinski, R.A., Bush, C.A. and Rosholt, J.N. (1986a) Uranium series disequilibrium in a young surficial uranium deposit, northeastern Washington, U.S.A.. Appl. Geochem. 1: 503-511.

Zielinski, R.A., Bush, C.A., Spengler, R.W. and Szabo, B.J. (1986b) Rock-water interaction in ash-flow tuffs (Yucca Mountain, Nevada, USA) - the record from uranium studies. Uranium 2: 361-386.

Zielinski, R.A., Lindsey, D.A. and Rosholt, J.N. (1980) The distribution and mobility of uranium in glassy and zeolitized tuff, Keg Mountain area, Utah, U.S.A. Chem. Geol. 29: 139-162.

APPENDIX 1 SAMPLE DESCRIPTIONS AND ANALYSES UNDERTAKEN

Hole (Lab.)	Depth	Zone	Description	Analyses	[U] (μg/g)
DDH1 (J)	2.2	2	weathered	γ, α	641
DDH1 (J,A)	4.7	2	weathered	5Ex, XRD, α	$2.3\ 10^3$
DDH1 (A)	9.3	2	weathered	α	$2.4\ 10^3$
DDH1 (J,A)	19.4-20.5	1	transition	5Ex, XRD, α	$82.3\ 10^3$
DDH2 (A)	13.2-14.5	2	weathered	2Ex, α	$1.1\ 10^3$
DDH2 (J)	33.0-34.3	1	unweathered	5Ex, XRD, α	$82.5\ 10^3$
DDH3 (A)	8.2-9.3	1	weathered	α	559
DDH3 (J)	10.5-11.7	2	weathered	5Ex, XRD, α, γ	820
DDH3 (J)	16.3-17.5	2	weathered	5Ex, XRD, α	965
DDH3 (J)	33.3	3	unweathered	γ, α	11
DDH3 (PNC)	68.6	1	unweathered	α	331
DDH4 (A)	3.5-4.7	2	weathered	α	15
DDH4 (J)	7.7	2	weathered	γ, α	280
DDH4 (A)	8.2-9.3	2	weathered	α	221
DDH4 (J)	13.3	2	weathered	γ, α	88
DDH4 (J,A)	14.0-15.3	2	weathered	5Ex, 2Ex, XRD, α	$0.6\ 10^3$
DDH4 (2)	18.7-19.8	2	weathered	α	536
DDH4 (J)	23.6	2	transition	γ, α	274
DDH30 (J)	7.5-9.0	2	weathered	γ	
DDH30 (J)	13.5-15.0	2	weathered	γ	
DDH30 (J)	22.5-24.0	2	transition	γ	
DDH40 (PNC)	19.5	1	weathered	α	356
DDH40 (PNC)	25.5	1	transition	α	56
DDH52 (J)	2.2	1	weathered	γ, α	36
DDH52 (J)	6.9	1	weathered	γ, α	173
DDH52 (A)	7.8	1	weathered	α	88
DDH52 (J)	17.3	1	weathered	α	678
DDH52 (A)	20	1	weathered	2Ex, α	792
DDH52 (A)	22.3	1	weathered	2Ex, α	543
DDH54 (J)	3.0-6.0	4(SW)	weathered	γ	
DDH54 (J)	13.5-15.0	4(SW)	weathered	5Ex, XRD, γ, α	963
DDH54 (J)	22.5-24.0	4(SW)	transition	γ	
DDH58 (J)	9.1	2	weathered	5Ex, XRD, γ, α	$1.7\ 10^3$
DDH58 (J)	18.2	2	weathered	5Ex, XRD, γ, α	$4.6\ 10^3$

Hole (Lab.)	Depth	Zone	Description	Analyses	[U] (μg/g)
DDH58 (J)	21.2	2	transition	5Ex, XRD, γ, α	1.1 10^3
DDH58 (J)	24.3	1	transition	5Ex, XRD, γ, α	726
DDH58 (J)	30.4	1	unweathered graphite	γ	
DDH60 (J)	9.1	2	weathered	γ	
DDH60 (J)	18.2	2	weathered	γ	
DDH60 (J)	21.2	2	transition	γ, α	150
DDH60 (J)	27.3	3	unweathered	α	4.7
DDH62 (J)	9.1	2	weathered	5Ex, γ, α	605
DDH62 (J)	15.2	2	weathered	5Ex, γ, α	5.9 10^3
DDH62 (J)	21.2	1	transition	γ	
DDH65 (J)	7.5-9.0	2	weathered	γ	
DDH65 (J)	13.5-15.0	2	weathered	γ	
DDH65 (J)	22.5-24.0	2	transition	γ	
DDH68 (J)	7.5-9.0	2	weathered	γ	
DDH68 (J)	13.5-15.0	2	weathered	γ	
DDH68 (J)	22.5-24.0	2	transition	γ	
DDH85 (J)	6.1	1	weathered	5Ex, γ, α	45
DDH85 (J)	9.1	1	weathered	5Ex, γ, α	377
DDH85 (J)	12.2	1	weathered	γ, α	72
DDH85 (J)	15.2	1	weathered	5Ex, γ, α	186
DDH85 (J)	18.2	1	weathered	γ	
DDH85 (J)	21.2	1	weathered	5Ex, γ, α	446
DDH87 (J)	6.1	2	weathered	γ	
DDH87 (J)	18.2	2	weathered	γ	
DDH87 (J)	24.3	3	transition	5Ex, XRD, γ, α	61
DDH92 (A,SU)	18	4(SE)	weathered	TS, XRD	
DDH92 (A,SU)	123	3	unweathered	TS, XRD	
DDH119 (A,SU)	56	1	unweathered	TS, XRD	
PH55 (A)	7.6	2	weathered	α	103
PH55 (A)	13.7-15.2	2	weathered	2Ex, α	217
PH55 (J)	18.3-19.8	2	weathered	5Ex, XRD, α	316
PH56 (J)	6.0-7.5	4(SW)	weathered	γ	
PH56 (J)	13.5-15.0	4 (SW)	weathered	5Ex, XRD, γ, α	323
PH56 (J)	18.0-19.5	4 (SW)	weathered	γ	
PH58 (J,A)	1.5-3.0	4(SE)	weathered	2Ex, γ, α	

Hole (Lab.)	Depth	Zone	Description	Analyses	[U] (μg/g)
PH60 (J)	1.5-3.0	4(SE)	weathered	γ, α	261
PH60 (A)	6.1-7.6	4(SE)	weathered	2Ex, α	6.5
PH60 (A)	10.7-12.2	4(SE)	weathered	2Ex, α	9.0
PH60 (A)	19.8	4(SE)	transition	2Ex, α	4.9
PH60 (A)	30.5	4(SE)	unweathered	2Ex, α	6.6
PH73 (J)	6.0-7.5	4(SW)	weathered	γ	
PH73 (J)	13.5-15.0	4(SW)	weathered	γ	
PH73 (J)	18.0-19.5	4(SW)	weathered	γ	
PH89 (J)	3.0-4.6	4(SE)	weathered	γ, α	263
PH89 (A)	9.1-10.7	4(SE)	weathered	2Ex, α	8.9
PH89 (A)	15.2	4(SE)	transition	2Ex, α	14.6
PH89 (A)	29	4(SE)	unweathered	2Ex, α	2
PH90 (J,A)	3.0-4.6	4(SE)	weathered	γ, α	60
PH90 (A)	10.7	4(SE)	weathered	2Ex, α	16
PH90 (A)	15.2	4(SE)	weathered	2Ex, α	3.8
PH91 (A)	9.2	4(SE)	weathered	2Ex, α	3.3
PH91 (A)	13.7	4(SE)	weathered	2Ex, α	6.6
PH93 (A)	6.1	4(S)	weathered	2Ex, α	17
PH93 (A)	3.6	4(S)	weathered	2Ex, α	9.9
PH93 (A)	13.7	4(S)	weathered	2Ex, α	21
PH94 (A)	9.2	4(SE)	weathered	2Ex, α	12
PH94 (A)	13.7	4 (SE)	weathered	2Ex, α	3.5
KD2	6.0-7.0	4(S)	weathered	γ	
KD2	13.0-14.0	4(S)	weathered	γ	
KD2	19.0-20.0	4(S)	weathered	γ	
M1 (A,SU)	3	1	weathered	S, E, XRD, TS, P	
M1 (A)	5	1	weathered	2Ex, α	31
M1 (A,SU)	7	1	weathered	S, E, XRD, TS, P	
M1 (A,SU)	9	1	weathered	S, E, XRD, TS, P	
M1 (A,SU)	13	1	weathered	S, E, XRD, 2Ex, α, TS, P	
M1 (A,SU)	16	1	weathered	S, E, XRD, TS, P	
M1 (A,SU)	19	1	weathered	E, XRD, 2Ex, α, TS, P	
M1 (SU)	21	1	weathered	TS, P	
M1 (A)	23	1	transition	E, XRD	

Hole (Lab.)	Depth	Zone	Description	Analyses	[U] (μg/g)
M1 (A)	27	1	unweathered	E, XRD	
M1 (A)	31	1	unweathered	E, XRD	
M1 (A)	37	1	unweathered	E, XRD	
M1 (A)	43	1	unweathered	E, XRD	
M1 (A)	49	1	unweathered	E, XRD	
M2 (A,SU)	3	2	weathered	S, E, XRD, TS, P	
M2 (A,SU)	8	2	weathered	E, XRD, TS, P	
M2 (A)	10	2	weathered	2Ex, α	2.4 10^3
M2 (A,SU)	13	2	weathered	S, E, XRD, TS, P	
M2 (A)	14	2	weathered	2Ex, α	3.4 10^3
M2 (A,SU)	17	2	weathered	S, E, XRD, TS, P	
M2 (A,SU)	21	2	weathered	E, XRD, TS, P	
M2 (A,SU)	25	2	transition	S, E, XRD, TS, P	
M2 (A)	32	3	transition	E, XRD	
M2 (A)	36	3	unweathered	E, XRD	
M2 (A)	42	3	unweathered	E, XRD	
M2 (A)	48	1	unweathered	E, XRD	
M3 (A,SU)	4	2	weathered	E, XRD, 2Ex, α, TS, P	
M3 (A,SU)	7	2	weathered	E, XRD, TS, P	
M3 (A,SU)	10	2	weathered	E, XRD, TS, P	
M3 (A,SU)	13	2	weathered	S, E, XRD, 2Ex, α, TS, P	
M3 (A)	15	2	weathered	S, E, XRD	
M3 (A)	20	2	transition	E, XRD	
M3 (A)	26	2	transition	E, XRD	
M3 (A)	32	2	unweathered	E, XRD	
M4 (A)	11	4(S)	weathered	2Ex, α	4.3
M4 (A)	15	4(S)	weathered	2Ex, α	8.4
M5 (A)	5	4(S)	weathered	2Ex, α	57
M5 (A)	11	4(S)	weathered	2Ex, α	5.2
M5 (A)	15	4(S)	weathered	2Ex, α	7.9
W1 (A)	3	1	weathered	2Ex, α	31
W1 (A)	13	1	weathered	2Ex, α	
W1 (A)	24	1	weathered	2Ex, α	322
W2 (A)	5.2	2	weathered	2Ex, α	89

Hole (Lab.)	Depth	Zone	Description	Analyses	[U] (μg/g)
W2 (A)	14	2	weathered	S, 2Ex, α, M, E	
W4 (A)	5	1	weathered	2Ex, α	820
W4 (A)	14	1	weathered	2Ex, α	354
W4 (A)	24	1	transition	2Ex, α	$4.2\ 10^3$
W5 (A)	13	4(SE)	weathered	2Ex, α	3.5
W7 (A)	4	4(S)	weathered	2Ex, α	304
W7 (A)	13	4(S)	weathered	2Ex, α	7.1

α	=	alpha-spectrometry
γ	=	gamma-spectrometry
2Ex	=	2 phase dissolution
5Ex	=	5 phase dissolution
S	=	subsampled
XRD	=	x-ray diffraction
M	=	Mössbauer spectroscopy
E	=	elemental analysis
TS	=	thin section analysis
P	=	particle size analysis
J	=	JAERI
A	=	Ansto
PNC	=	Power Reactor and Nuclear Fuel Development Corporation of Japan
SU	=	Sydney University, Soil Science Dept.

Zones

1	=	primary mineralised zone
2	=	dispersion fan
3	=	under fan
4	=	outside fan (direction)

APPENDIX 2

MÖSSBAUER SPECTROSCOPIC ANALYSIS

J D Cashion and L J Brown
Department of Physics, Monash University

Introduction

Iron oxides have been found to be of great importance in the retention of radionuclides in the Koongarra weathered rock. Consequently, the nature of these iron oxide phases is of great interest, but remains poorly understood. Methods such as X-ray diffraction are useful only for highly crystalline phases, and since the importance of ferrihydrite in sorption has been widely hypothesised, other techniques are required to study the poorly crystalline phases.

A sample to be used for sorption experiments was subsampled for different phases of iron oxides (W2-14 m). It was noticed that in general, the sample was a red colour, but that throughout the core ran bands of clayey material, up to about 1 cm thick. These bands were white and grey to black, and were much wetter than the bulk of the sample. These gleyed bands were flanked by yellow to orange material, up to 1 cm thick, followed by the red material which made up the bulk of the sample. Each phase was carefully sampled separately for Mössbauer spectroscopic analysis.

Room temperature Mössbauer spectra were initially made on each of the samples. Liquid nitrogen temperature measurements were then made and compared with those from the room temperature measurements.

Measurements at room temperature

This section covers the analysis by Mössbauer spectroscopy of three subsamples supplied from the core sample W2 14 m:

#1 Grey/white/black material
#2 Orange/yellow material
#3 Red material

A room temperature Mössbauer spectrum was run for each of the samples using approximately 180 mg of specimen. The normal technique of crushing the sample to ensure a uniform loading in the sample holder could not be used because of the texture of the material. Consequently, the sample was squashed into the holder to try and achieve a uniform thickness. If this is not done, there is not necessarily a simple proportional relation between the areas of the absorption peaks and the amount of material in that phase. We consider that reasonable consistency in thickness was achieved.

Table A2.1 gives the parameters used and the resulting spectra are given in Figure A2.1. The parameters listed in the table are:

∂ - isomer shift in mm/s
Δ - quadrupole splitting in mm/s
ε - effective quadrupole splitting in the field (= $\Delta/4$) in mm/s
H - hyperfine magnetic field in kOe
A - area in % (= proportion of iron in this phase)

TABLE A2.1

PARAMETERS FOR ROOM TEMPERATURE RUNS

Sample	Field 1				Doublet 1			Doublet 2			Gaussian	
	∂	ε	H	A%	∂	Δ	A%	∂	Δ	A%	∂	A%
grey					.38	.59	51.5	1.08	2.20	48.5		
yellow	.35	-.12	295	42	.37	.65	26.2	1.11	2.41	5.2	.53	26.4
red					.36	.64	79.9				.36	20.1

Sample 1 - white to black

Two doublets were observed from this sample. Doublet 1 is from ferric iron probably in an environment of an octahedron of oxygen atoms. The splitting of ferrihydrite is normally 0.8 mm/s in poorly crystalline material (2 XRD line) and reduces to less than 0.7 mm/s in better crystallised samples (6 XRD line). Comparison of the line positions for this phase in the three spectra show that in this one the fitted position of the left hand line is moved to the right by 0.4 mm/s due to the difficulty for the program in fitting the two overlapping peaks. We believe that this subspectrum is due to well-crystallised ferrihydrite but low temperature spectra would be required to confirm this.

The second doublet is from ferrous iron and since there are a rather large number of compounds with parameters in this region we have not tried a literature search to identify it. It is not from to siderite which was one of the compounds suggested. The quadrupole splitting of siderite is 1.8 mm/s at room temperature which is outside the error limits of this fit. It may be result from iron in an aluminosilicate in which case one may expect that there should probably a further subspectrum due to ferric iron in the aluminosilicate. This would further effect the fitting of the parameters for the ferrihydrite. However, the relatively large proportion of the iron in this phase (almost half of the total) suggest that it is probably from a substituted phase unless that phase constitutes the majority of the sample. Since we do not know the approximate analysis of the sample we cannot draw further conclusions on this point. However our tentative conclusion is that it is probably a mineral species and could be related to siderite, but is not siderite itself.

Sample 2 - yellow to orange

The spectrum of this sample shows both of the doublets which appeared in the spectrum of sample 1, but with the ferrous component considerably reduced. A new broad component has appeared from a ferric iron phase which is magnetically relaxing. This component has been fitted with the sum of a sextet for the better resolved part and a gaussian for the remainder. However, this is really an approximation to the correct relaxation line shape which we have not attempted to fit. This component is almost certainly from superparamagnetism which occurs in very fine particle material (<10 nm) for which the volume-dependent anisotropy energy becomes comparable with the thermal energy, kT, and the entire magnetisation vector of the particle flips between the different easy directions at a rate comparable with the nuclear Larmor precession frequency. For this to occur at room temperature, the most likely candidate is goethite, but a low temperature spectrum would be required to confirm this. It cannot be due to either lepidocrocite or ferrihydrite, which both have ordering temperatures below room temperature. It is unlikely to be from hematite because it is quite difficult to obtain superparamagnetic hematite under natural conditions, although it is obtainable synthetically.

Sample 3 - red

The spectrum of this sample, somewhat unexpectedly, shows an almost clean doublet with the parameters of the phase attributed to ferrihydrite. It is poorly fitted with a single doublet as evidenced by the line not reaching up in to the experimental points in the centre. This is a characteristic of ferrihydrite, in which there is a distribution of both quadrupole splittings and isomer shifts due to the different local coordination of the iron atoms. As with the other samples, a low temperature spectrum is really required to definitely confirm the ferrihydrite phase. A very small trace of the ferrous phase is visible at 2.3 mm/s but this has not been fitted.

Conclusions

It is clear that the analyses presented here are not entirely in accord with the descriptions of the samples, as supplied. There is certainly a gradation in oxidation in the three samples, but not a gradation in weathering. Sample 2 follows naturally from sample 1 by oxidation and weathering, but sample 3 does not follow simply from sample 2 except by dissolution of the assumed goethite phase. It could, however, come directly from sample 1 by oxidation and subsequent breakup of the ferrous phase. Note that the size of the ferrous phase doublet indicates that there is no possibility of a mix-up in the samples.

These comments suggest a slightly different interpretation of the three samples, with both samples 2 and 3 being derived separately from sample 1. The ferrihydrite phase is quite sensitive to small changes in temperature and pH, which decide whether it will travel down the path to goethite or to hematite, but the two paths cannot be altered once the route is chosen. It is thus very likely from its colour, that sample 3 will eventually become hematite but it is unlikely that it is yet hematite unless the particle size is less than 8 nm. A low temperature spectrum would quickly confirm this.

Measurements at liquid nitrogen temperature

The same samples were used as for the room temperature experiments described above. These have been stored at room temperature and there is no reason to expect faster oxidation of these samples than for the original material in the containers supplied. Table A2.2 gives the spectral parameters for the liquid nitrogen runs. Figure A2.2 shows the spectra.

TABLE A2.2

PARAMETERS FOR LIQUID NITROGEN TEMPERATURE RUNS

Sample	Field 1				Field 2				Doublet 1			Doublet 2		
	∂	ε	H	A%	∂	ε	H	A%	∂	Δ	A %	∂	Δ	A%
grey	.48	-.12	480	14.4					.47	.52	59	1.19	2.57	26.6
yellow	.47	-.12	458	28.2	.48	-.13	466	40.5	.46	.57	26	1.20	2.64	5.3
red	.47	-.12	480	24.6	.47	-.13	454	36.7	.47	.77	37	1.23	2.87	1.4

Sample 1 - white to black

The room temperature spectrum of this sample consisted of two doublets, one from an Fe^{3+} species and the other from an Fe^{2+} species. The Fe^{3+} species was assigned to well-crystallised ferrihydrite as the most likely interpretation, but it was emphasised that low temperature spectra would be required to confirm this.

The liquid nitrogen spectrum shows the appearance of a sextet containing 14.4% of the area. The lines are quite broad, indicating either poor crystallinity or some aluminium substitution and the hyperfine field is slightly less than that expected for pure goethite (500kOe), but either of the two imperfections described would account for the difference. The quadrupole splitting and isomer shift both agree with the literature values for goethite.

The surprising feature is that the quadrupole splitting of the principal doublet has decreased slightly. Since the quadrupole splitting of goethite in the (super) paramagnetic state is 0.48 mm/s and that of ferrihydrite is higher than this, we would have expected that the transfer of intensity due to goethite from the doublet to the sextet would have resulted in an increase in the doublet splitting if all the doublet remaining at 78°K is from ferrihydrite. This raises the possibility that the remaining doublet is not from ferrihydrite and a spectrum at liquid helium temperature, when the material should also produce a sextet, should resolve the matter. The lack of sensitivity in distinguishing the different iron (III) oxides and oxyhydroxides is due that fact that all of them have the same nearest neighbour configuration of an iron atom surrounded by a (slightly distorted) octahedron of oxygen atoms.

The quadrupole splitting of the Fe^{2+} species has increased slightly on reduction of temperature. This is common in Fe^{2-} species and is due to the depopulation of the crystal field split levels and consequent increase in $<J_z^2>$ of the Fe 3d shell. There is also a reduction in the area of the Fe_{2+} component from 48.5% at room temperature to 26.6% at 78°K. This is a result of the very small particle size of the other constituents, which reduces their Debye temperature and hence makes their Debye-Waller factor (recoilless fraction) more dependent on temperature in the regime used. Thus as the absolute intensity of the absorption from these two components increases, then the relative intensity of the Fe^{2+} phase absorption will decrease. This is also consistent with the assignment of the Fe^{2+} phase to a well-crystallised mineral species.

Since the areas at low temperature are a more reliable estimate of the relative volume fraction of the phase in the material, we estimate the composition to be:

Fe^{2+} mineral phase	2%
Goethite, very fine particle	at least 14%
Ferrihydrite or other oxide/oxyhydroxide	59%

Sample 2 - yellow to orange

The room temperature spectrum of this sample showed two doublets from an Fe^{3+} oxide/oxyhydroxide and the Fe^{2+} mineral species and a contribution from goethite which was partly relaxing. The 78°K spectrum showed the same three components, with the goethite now being fully ordered although still having slightly broad lines. The quadrupole splitting of the oxide/ oxyhydroxide component had reduced slightly as for the above sample, but the reason for this is not clear.

The estimates for the percentages of the phases present agree very well:

	RT	78°K
Fe^{2+} species	5.2%	5.3%
Goethite	68.6%	68.7%
Ferrihydrite or oxyhydroxide	26.2%	26.0%

Sample 3- red

The room temperature spectrum of this sample showed a clean doublet which was tentatively interpreted as being ferrihydrite, and a weak line (1% intensity) from the Fe^{2+} phase. However the spectrum at 78°K shows that over 60% of the intensity has moved out into a sextet structure, which is not consistent with ferrihydrite for which even the most crystalline samples do not order until just below liquid nitrogen temperatures. The mean quadrupole splitting of the remaining doublet has also increased as the temperature decreased, consistent with the removal of a phase from the doublet intensity which had a quadrupole splitting smaller than the mean. The parameters of this remaining doublet phase are more consistent with that of ferrihydrite than the parameters of the first two samples.

The sextet phase would appear to be principally or possibly entirely from goethite although the lines are broad with a strong asymmetry towards the inner sides of the lines which could mask another component with a slightly smaller hyperfine field. Combining the results of the two spectra we estimate the composition to be:

Fe^{2+} phase	1.4%
Goethite	61%
Ferrihydrite	38%

However a further spectrum at liquid helium temperature would be necessary to distinguish the ferric phases. At this temperature the goethite spectrum should sharpen up and the ferrihydrite should become ordered and produce a sextet structure with a characteristic line shape and a smaller hyperfine field than for goethite.

Conclusions

These results indicate how difficult it is to unambiguously interpret a single Mössbauer spectrum of an unknown set of ferric oxy-hydroxides. Only in the case of Sample 2 is the interpretation of the two spectra consistent and even there the assignment of the ferrihydrite phase is not definite. However we would expect further spectra at liquid helium to resolve the issue.

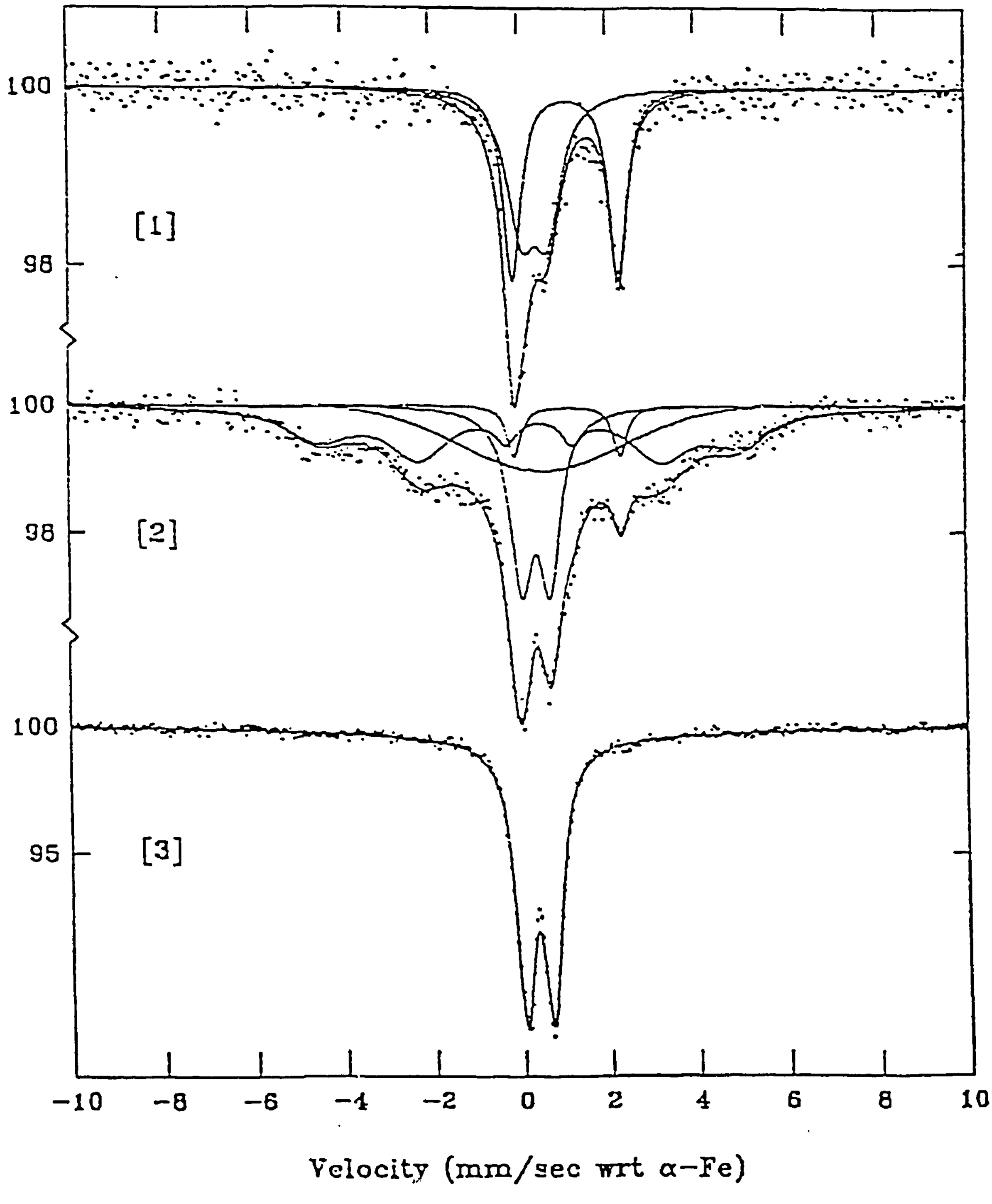

[1] White to black
[2] Orange yellow
[3] Red

FIGURE A2.1 Mössbauer spectra at room temperature

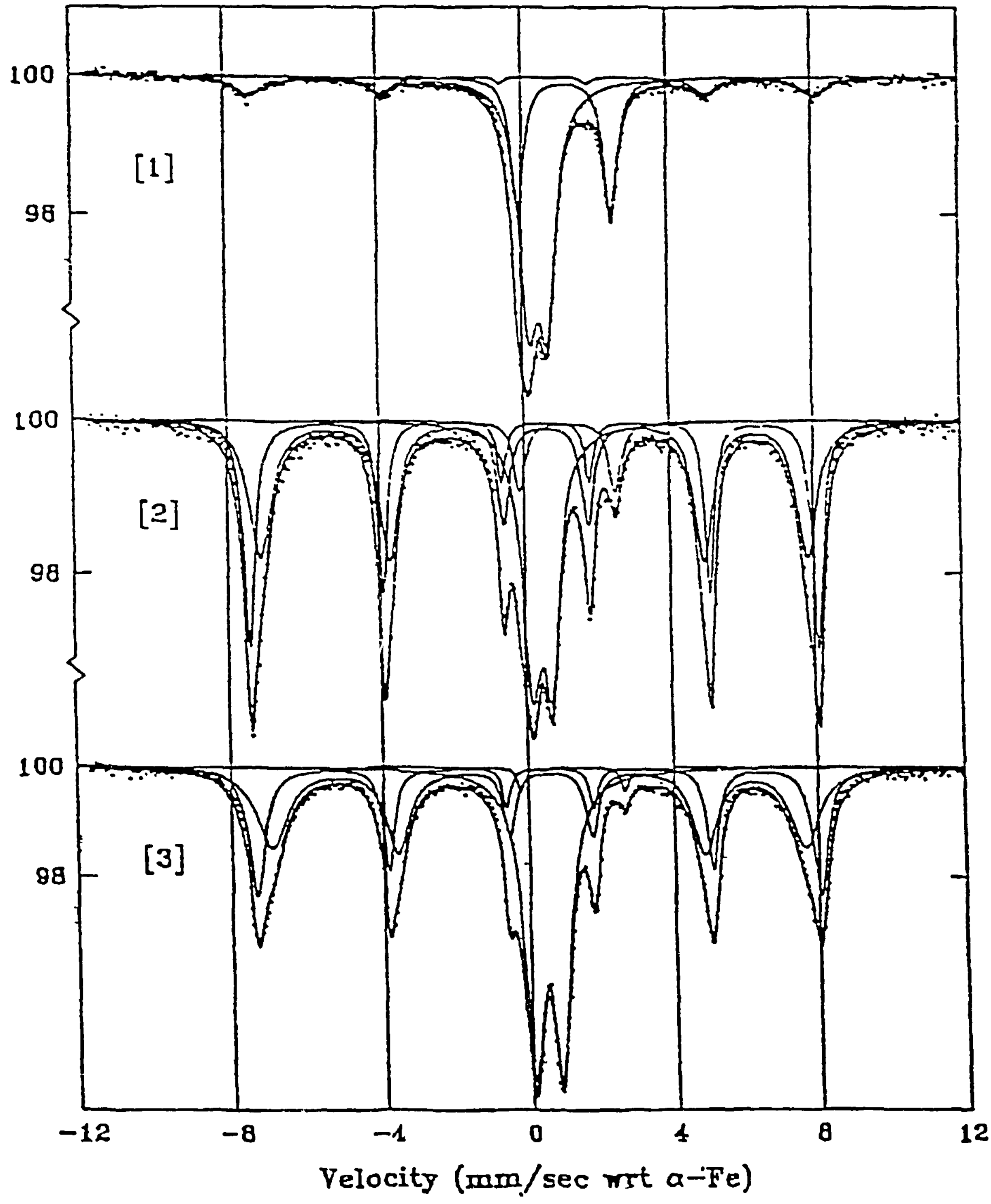

[1] White to black
[2] Orange yellow
[3] Red

FIGURE A2.2 Mössbauer spectra at liquid nitrogen temperature

APPENDIX 3

USE OF SEQUENTIAL, PHASE SELECTIVE EXTRACTION SCHEMES

Aims of extraction schemes

Many selective phase extraction schemes have been described in the literature, each one tailored to suit the particular requirements and constraints of the investigation. The diversity not only of schemes but also of different substrates makes intercomparison difficult. However, the review presented here will discuss the array of possible schemes in relation to their practicality and suitability for the present study. Although it is unlikely that any single extraction scheme could be accepted as a standard for use on all possible substrates, most schemes tend to concentrate on the distribution of metal species in five general forms;

Exchangeable metal species

Organically bound metals

Metals associated with carbonates

Metals associated with iron and manganese oxides and oxy-hydroxides

Metals in chemically resistant minerals

In this study, it was felt that the organically bound components would be insignificant, and these will therefore not be discussed further.

Exchangeable and weakly bound metal species

Typically a pH neutral solution of a chemically inert salt such as $MgCl_2$ has been used as the electrolyte to replace bound exchangeable metal species. Tessier et al. (1979), Shuman (1979) and Nirel et al. (1985) used $MgCl_2$, while Shuman (1985) used 1 M $Mg(NO_3)_2$, also at pH 7.0. Several authors have used 1 M ammonium acetate at pH ~8.2, including Rapin et al. (1983), Tessier et al. (1979) and Salomons and Forstner (1980).

Metals associated with carbonates

A 1 M sodium acetate solution buffered at pH 5.0 with acetic acid is commonly employed for the purpose of dissolving carbonate phases, while leaving phases such as ferrihydrite intact. Early work on this extracting solution was done by Morgan (1935), and it has become known as Morgan's reagent. Grossman and Millet (1961) reported no change in the organic carbon and free iron concentrations in non- calcareous soil samples after being in contact with this solution for nine weeks. Tessier et al. (1979) studied the effectiveness of this reagent in dissolving calcium from the carbonate fraction of marine sediments and found that dissolution was complete after a period of about 4 hours at room temperature. This treatment was also recommended by Nirel et al. (1986), Rapin et al. (1983) and Forstner et al. (1981). Schwertmann (1979) also recommended it for similar use with clay-containing substrates.

The fact that Morgan's reagent was used for the extraction of heavy metals warrants its possible application to substrates containing uranium, thorium and other actinides. In particular the fact that the solution is slightly acidic and contains acetate, a potentially complexing ion, suggests that it may be more effective in retaining these nuclides in solution than magnesium chloride solution.

Tessier et al. (1979) reported that the apparent levels of Cu, Ni, Pb and Zn in the carbonate-bound fraction (i.e. in the extract of Morgan's reagent) were well in excess of those expected for dolomite, on the basis of available information on trace metal contents. They proposed that this was due to a partial extraction of specifically adsorbed trace metals by the $MgCl_2$ solution, the preceding reagent in the extraction scheme. The same considerations may well apply to uranium. Several autnors have shown that uranium tends to adsorb very strongly onto the substrate at pH values above 5.0. For example Hsi and Langmuir (1985) demonstrated this using both ferrihydrite and goethite as the substrate (see also Volume 13 of this series). From this point of view Morgan's reagent, which is buffered at pH 5.0, would appear to be an excellent reagent for removing specifically adsorbed uranium, but less so for thorium. Therefore, in this study, Morgan's reagent was used to extract both the adsorbed and the carbonate-bound components. This minimised the ambiguity of readsorption of uranium during extraction with a less aggressive reagent.

Metals associated with iron and manganese oxides

Oxides of iron and manganese are known to play an important part in the adsorption of metal species in both soils and sediments. The dissolution of amorphous phases, or those with short order crystallinity such as ferrihydrite, is commonly achieved using a solution of ammonium oxalate buffered with oxalic acid. This method was reported by Tamm (1922 and 1934) and the reagent will be referred to as "Tamms acid oxalate (TAO)". In order to make it more selective towards less crystalline iron oxides and oxy-hydroxides, Schwertmann (1964) proposed a modification. It was found that in the absence of light at pH ~3 the dissolution of the crystalline oxides was greatly reduced. McKeague and Day (1966) found that 0.2 M ammonium oxalate solution, buffered at pH ~3.0 with oxalic acid and also used in the dark, was highly selective towards the "amorphous" iron oxy-hydroxides. Pawluk (1972) tested the repeated effect of the TAO extraction and found that the second and third treatments were capable of completely dissolving the crystalline oxides goethite and lepidocrocite.

Dissolution of crystalline iron oxides

Dissolution of crystalline iron oxides is normally achieved by a combination of a reducing agent and a complexing agent. In early studies of iron oxides their dissolution was achieved by simply reducing the iron(III) with a solution of sodium dithionite, thereby liberating the more soluble iron(II) species. This technique was described by Mackenzie (1954) and was later employed by Taylor (1959) and Norrish and Taylor (1961) who used it to study the aluminium content of soil goethites. Mehra and Jackson (1960) proposed a modification to this procedure whereby sodium citrate was added to the solution as a complexing agent and sodium bicarbonate was employed to buffer it at pH ~7.3. Coffin (1961) showed good reproducibility with the citrate dithionite bicarbonate (CDB) reagent with regard to the quantities of iron and aluminium extracted.

Arshad et al. (1972) examined the effect of the TAO and CDB reagents on a selection of trioctahedral layer silicates and found that the release of cations from these minerals increased with decreasing particle size, becoming significant in the < 2μm fraction. This was attributed in part to the exposure of fresh surfaces during grinding. They concluded that the TAO extraction removed an appreciable amount of iron and aluminium from trioctahedral layer silicates while the CDB extraction removed a slightly smaller amount.

Dudas and Howard (1971) investigated the effect of the TAO and CDB treatments on crystalline and clay mineral components and reported some structural alteration of nontronite but more by the TAO reagent than by the CDB. The TAO reagent was found to cause little or no structural alteration of biotite and interstratified vermiculite-mica. Pawluk (1972) compared the effects of repeated extractions with the TAO and CDB reagents. Crystalline iron oxides were found to be removed after several extractions with the TAO reagent. XRD reflections for goethite and lepidocrocite were found to be partially removed after the second TAO extraction and completely removed after the third. A single CDB extraction was found to remove nearly all reflections associated with crystalline oxides but they also showed some removal of iron that was more closely associated with clays. Schwertmann (1979) recommended the CDB treatment for use within a sequential extraction scheme for samples containing clay minerals, proposing two successive extractions for samples containing "well- crystallised" or greater amounts of iron oxides. It was pointed out that considerable amounts of aluminium were commonly found in the extract, which were attributed either to the dissolution of free alumina or to isomorphous substitution of aluminium within natural goethites. The latter was first proposed by Norrish and Taylor (1961).

Lowson et al. (1986) employed both the TAO and CDB treatments within a sequential extraction scheme for the purpose of studying the distribution of uranium and thorium isotopes in mineral phases of a lateritic weathered zone. The TAO reagent was used to dissolve "amorphous" iron and aluminium oxides while the CDB treatment removed crystalline oxides. X-ray diffraction analysis demonstrated that while the TAO treatment had no effect on goethite, the CDB treatment appeared to completely dissolve it. Quartz and clay mineral reflections were unaffected by either treatment. Since the samples were taken from the Ranger uranium deposit, located within a few kilometres of the Koongarra deposit, these results were highly relevant to the present study, in which samples of similar mineralogy were examined.

Michel (1984) used a single CDB extraction to measure amount of uranium and thorium associated with secondary phases in isovolumetrically weathered granites. Up to 81% of the total thorium and 23% of total uranium were found to be dissolved in this treatment. Little attention however was paid to the selectivity of the extractant. These results, and those of Lowson et al. (1986), demonstrated that both elements had appreciable solubility in the CDB reagent. The fact that thorium tends to form stable complexes with oxo-ligands would tend to favour the use of the TAO and CDB reagents. Langmuir and Herman (1980) extensively reviewed data on thorium complexation, and reported that it formed strong complexes with oxalate and citrate.

In this study, extraction with TAO was used as either the first or the second extraction. Where TAO was used as the first extraction, it was assumed that metals that were either adsorbed, carbonate-bound or associated with amorphous phases of iron and aluminium would be removed. This extraction was used to define the material accessible for interaction with the groundwater. Where TAO was used as the second extractant, it followed an extraction with Morgan's reagent. Citrate dithionite bicarbonate was used to extract material contained in crystalline iron oxides, and followed extraction with TAO.

A 6 M HCl extraction step was also included for some samples, aimed at dissolving clay minerals, any residual iron oxides, and primary uranium minerals where present, before the digestion of residual minerals (Yanase et al., 1991).

References

Arshad, M.A., St. Arnaud, R.J. and Huang, P.M. (1972) Dissolution of trioctahedral layer silicates by ammonium oxalate, sodium dithionite-citrate-bicarbonate and potassium pyrophosphate. Can. J. Soil Sci. 52: 19-26.

Coffin, D.E (1961) A method for the determination of free iron in soils. Can. J. Soil Sci. 43: 7-17.

Dudas, M.J. and Howard, M.E. (1971) Effect of dissolution treatments on standard soils and clays. Soil Sci. Soc. Amer. Proc. 35: 134-140.

Forstner, U., Calmano, W., Conradt, K., Jaksch, H., Schimkus, C. and Schoer, J. (1981) Chemical speciation of heavy metals in solid waste material by sequential extraction. Int. Conf. on Heavy Metals in the Environment, Amsterdam, September 1981, CEC/WHO, pp.698-704.

Grossman, R.B. and Millet, J.C. (1961) Carbonate removal from soils by a modification of the acetate buffer method. Soil Sci. Soc. Am. Proc. 25: 325-326.

Hsi, C.D. and Langmuir, D. (1985) Adsorption of uranyl onto ferric oxyhydroxides: application of the surface complexation site-binding model. Geochim. Cosmochim. Acta 49: 1931-1941.

Langmuir, D. and Herman, J.S. (1980) The mobility of thorium in natural waters at low temperatures. Geochim. Cosmochim. Acta 44:1753-1766.

Lowson, R.T., Short, S.A., Davey, B.G. and Gray, D.J. (1986) $^{234}U/^{238}U$ and $^{230}Th/^{234}U$ activity ratios in mineral phases of a lateritic weathered zone. Geochim. Cosmochim. Acta 50: 1697-1702.

MacKenzie, R.C. (1954) Free iron oxide removal from soils. J. Soil Sci. 5: 167-172.

McKeague, J.A. and Day, J.H. (1966) Dithionite-and oxalate-extractable Fe and Al as aids in differentiating various classes of soils. Can. J. Soil Sci. 46: 13-22.

Mehra, O.P. and Jackson, M. (1960) Iron oxide removal from soils and clays by a dithionite-citrate system buffered with sodium bicarbonate. Proceedings of 7th Int. Conf. on Clays and Clay Minerals, 1958: Washington D.C., Monograph No.5: 317-327.

Michel, J. (1984) Redistribution of uranium and thorium series nuclides during isovolumetric weathering of granite. Geochim. Cosmochim. Acta 48: 1249-1255.

Morgan, M.F. (1935) The universal soil testing systems. Connecticut Agricultural Experiment Station Bulletin pp. 372.

Nirel, P., Thomas, A.J. and Martin, J.M. (1985) A critical evaluation of sequential extraction techniques. In Seminar on speciation of fission and activation products in the environment. Oxford, April 1985.

Norrish, K. and Taylor, R.M. (1961) The isomorphous replacement of iron by aluminium in soil goethites. J. Soil Sci. 12: 294-306.

Pawluk, S. (1972) Measurement of crystalline and amorphous iron oxides. Can. J. Soil Sci. 52: 119-123.

Rapin, F., Nembrini, G.P., Forstner, U and Garcia, J.I. (1983) Heavy metals in marine sediment phases determined by sequential extraction and their interaction with interstitial water. Environ. Technol. Lett. 4: 387-396.

Robinson, G.D. (1985) Sequential chemical extractions and metal partitioning in hydrous Mn-Fe oxide coatings: reagent choice and substrate composition affect results. Chem. Geol. 47: 97-112.

Salomons, W. and Foerstner, U. (1980) Trace metal analysis on polluted sediments. Part II. Evaluation of environmental impact. Environ. Technol. Lett. 1: 506-517

Schwertmann, U. (1979) Dissolution Methods. In H. Van Olphen & J.J.Fripiat (eds) Data handbook for clay minerals and other non-metallic minerals, prepared under the auspices of the OECD and the Clay Minerals Society, Pergamon Press, Oxford. pp.163-172.

Shuman, L.M. (1979) Zinc, manganese and copper in soil fractions. Soil Sci. 127: 10-17.

Shuman, L.M. (1985) Fractionation method for soil microelements. Soil Sci. 140: 11-22.

Tamm, O. (1922) Um besta dotdtmring ow oorganiska komponenterna i markens gelkomplex. Medd. Statens Skogsforsokanst 19: 384-404.

Tamm, O. (1934) Uber die Oxalatmethode in der chemischen Bodenanalyse (oxalate method in chemical extraction of soils). Medd. Statens Skogsforsokanst. 27: 1-20.

Taylor, R.M. (1959) Amorphous iron oxides in soils. J. Soil Sci. 10: 309- 315.

Tessier, A., Campbell, P.G.C. and Bisson, M. (1979) Sequential extraction procedure for the speciation of particulate trace metals. Anal. Chem. 51: 844-851.

Yanase, N., Nightingale, T., Payne, T. and Duerden, P. (1991) Uranium distribution in mineral phases of rock sequential extraction procedure. Radiochim. Acta 52/53: 387-393.

APPENDIX 4
ELEMENT CONCENTRATIONS IN WHOLE ROCK SAMPLES
(μg/g unless otherwise stated)

A4.1 Samples Analysed During the ARAP (determined by PIXE/PIGME unless otherwise stated)

	M1 3	M1 3	M1 7	M1 7	M1 9	M1 9	M1 13	M1 13	M1 16	M1 16
	gen.	red	white	red	white	red	white	brown	gen.	orange
F	225	251	143	141	132	168	379	544	237	226
Li	10.2	<10	12.4	<10	23.3	13.2	14.2	20.7	42.8	51.1
Na	164	130	122	110	105	83.8	289	466	99.1	104
Al (mg/g)	115	93	89	69.2	105	69.3	115	138	123	146
Mg (mg/g)	<4.0	<4.0	<4.0	<4.0	<4.0	<4.0	<4.0	4.4	<4.0	<4.0
Si (mg/g)	281	329	401	344	374	229	379	252	241	246
S	<200	<200	<200	<200	<200	<200	<200	<200	<200	<200
K (mg/g)	0.89	0.62	0.7	0.51	0.26	0.11	18.9	21.7	0.492	0.27
Ca	<45	<45	<45	<45	59.2	<45	108	112	<45	<45
Ti (mg/g)	2.43	1.84	2.52	2.14	3.21	2.66	2.55	3.89	4.34	3.3
V	202	292		180		267		62.2	124	132
Cr	146	218	254	197	199	562	214	106	407	311
Mn	<20	<20	<20	<20	<20	<20	33.9	20	47.8	<20
Fe (mg/g)	88	114	12.9	103	8.96	204	6.83	115	121	127
Ni	38.3	39.9	42.7	54.4	35.4	80.3	34.1	68.1	143	268
Cu	<4	5.6	7.6	8	<4	10.3	14.2	16.2	27.8	36.1
Zn	5.4	8	10.6	20.7	14	37.1	27.3	64	102	186
Ga	53.1	46.7	36.7	35.4	29.5	24.7	24.8	37.7	53.7	72.3
As	6.5	10.7	<2.6	3.3	<2.6	27.5	<2.6	4.7	10.9	14.1
Rb	<13	<13	<13	8.8	<13	<13	90.5	117	<13	<13
Y	26.2	19.6	8.6	9.6	34.7	41.4	47.1	66.2	50.1	38.2
Zr	288	302	200	167	521	321	332	318	412	306
Pb	23.3	21.4	<22	55.2	23.4	24.7	<22	120	101	56.9
U	28.3	25.4	31.2	143	30.8	247	21.2	265	462	548
U (DNAA)	25.5	30.7	36.8	184	32.8	299	29.1	266	517	544
P (XRF)	176	-	161	761	148	2073	137	973	1350	-
Oxide (%)	94.3	104	105	101	102	90.4	107	99.8	91.8	97.8

	M1 19	M1 23	M1 27	M1 31	M1 37	M1 43	M1 49	M2 3	M2 3	M2 3
								<2mm	>2mm	<2 µm
F	431	648	749	632	754	752	441	247	101	489
Li	198	119	126	102	129	107	53.8	16.7	<10	72
Na	7605	142	152	67.1	388	308	337	254	161	409
Al (mg/g)	84.6	70.7	76.8	70.7	84.8	74.1	53.4	101	31	189
Mg (mg/g)	43.8	71.4	88.1	81.5	88.4	59.6	46.9	<4	<4	8.1
Si (mg/g)	289	311	279	299	285	323	365	298	432	245
S	<200	<200	<200	<200	<200	<200	<200	<200	<200	<200
K (mg/g)	0.441	2.63	1.17	0.939	5.5	10.1	6.03	8.31	3.1	8 63
Ca	208	862	860	903	1180	848	466	83.1	61.2	267
Ti (mg/g)	2.17	2.31	2.51	2.17	3.82	2.05	1.46	4.82	1.64	3.75
V	193	126	178	203	177	120	114	123	88.9	47.4
Cr	221	182	157	141	192	167	173	519	579	156
Mn	351	323	263	301	343	804	262	2407	1629	444
Fe (mg/g)	78.2	72	73.3	67.4	67.6	58.8	43.9	104	79.8	49.7
Ni	498	137	173	161	167	119	92.2	93.7	51.3	169
Cu	64.5	<4	70.7	<4	<4	<4	<4	452	320	447
Zn	295	85.5	75.2	120	68.8	59.5	65.7	52.5	15.6	228
Ga	34.9	35.5	37.8	36	44	32.8	21.7	23.1	11.3	53.5
As	6.2	2.8	11.5	9	5.6	<2.6	<2.6	7.6	4.5	3.6
Rb		14.6	34.1	22.3	27.4	54	31.8	39.1	21.2	52.5
Y	37.1	43.1	31.1	28.6	13.4	14.5	17.1	41.7	24.5	25.5
Zr	382	213	129	215	195	152	415	107	99.2	111
Pb	145	233	254	286	237	103	79.2	751	471	236
U	317	512	1481	1061	581	344	526	401	296	182
U (DNAA)	353	553	1394	1237	663	373	676	438	349	-
P (XRF)	605	519	575	438	504	370	323	275	319	-
Oxide (%)	96.1	102	99.6	101	102	103	103	99	110	98.1

	M2 8	M2 13	M2 13	M2 13	M2 17	M2 17	M2 21	M2 25	M2 25	M2 25
	<2mm	<2mm	100-45µ	<2 µm	<2mm	>2mm	<2mm	<2mm	>2mm	<2 µm
F	324	438	587	453	353	68.5	474	511	499	760
Li	81.1	36	44.2	53.8	48.5	13.9	79.5	82.6	71.1	131
Na	362	615	1571	382	440	147	613	404	221	329
Al (mg/g)	116	124	166	158	113	18.1	125	90.9	74.6	130
Mg (mg/g)	<4	<4	<4	10.8	4.9	<4	16.3	40.6	44.5	74.6
Si (mg/g)	307	252	265	193	302	483	273	296	332	173
S	<200	<200	<200	<200	<200	<200	<200	454	<200	<200
K (mg/g)	28.6	36.8	54.4	24.4	30.8	4.55	33.2	18	12.7	18.8
Ca	106	116	335	320	140	72.5	180	306	69.9	350
Ti (mg/g)	5.77	6.2	6.53	1.89	6.13	0.84	8.93	5.79	4.43	1.83
V	54	130	232	151	111	34.1	223	152	115	208
Cr	287	843	173	249	338	652	532	446	403	260
Mn	3922	541	581	296	612	306	1045	914	587	876
Fe (mg/g)	93.3	86.4	64	130	79.2	22.4	91.8	100	85.8	150
Ni	330	74	59.5	218	157	63.2	340	122	98.5	214
Cu	647	260	216	1825	394	100	97.2	153	10.4	1148
Zn	105	83.1	69.6	973	112	23.3	602	297	157	1624
Ga	10.4	21	37.9	35	18.3	<3.5	24.4	19.3	19.8	27.1
As	6.8	<2.6	<2.6	6.5	<2.6	<2.6	3.6	3.5	<2.6	<2.6
Rb	147	165	198	154	173	30.7	162	93.4	73.4	111
Y	10.1	12.8	13.4	28.6	23.2	<5	18.1	14.7	13.1	2.9
Zr	152	135	146	98.4	240	16.7	205	152	91.4	59.5
Pb	159	<22	<22	<22	<22	<22	<22	<22	<22	32.2
U	1858	1246	720	1470	1462	336	1221	488	188	743
U (DNAA)	1912	1169	-	-	1545	399	1248	525	212	-
P (XRF)	429	322	446	-	550	245	343	522	406	-
Oxide (%)	105	95.1	105	93.9	102	111	103	104	106	97.1

	M2 32	M2 36	M2 42	M2 48	M3 4	M3 7	M3 10	M3 13	M3 13	M3 13
								gen.	white	yellow
F	465	663	532	491	269	615	571	440	410	393
Li	62.7	48.4	31.6	47.9	70.7	83.8	270	87.6	87.8	83.9
Na	257	116	97.2	183	122	143	283	288	214	176
Al (mg/g)	66.3	50.3	45.8	41.2	61.7	90.1	108	93	119	105
Mg (mg/g)	33.2	50	39.1	34.1	4.4	15.8	10.3	14.6	9.4	8.2
Si (mg/g)	365	325	278	361	272	280	254	278	349	267
S	930	10186	14776	17428	<200	<200	<200	<200	<200	<200
K (mg/g)	17	0.733	0.357	5.18	0.576	15.4	11	14.8	14.4	9.15
Ca	898	8443	1907	3489	129	105	183	120	145	95.5
Ti (mg/g)	3.22	2.48	2.14	2.03	1.54	15.9	5.64	7.94	8.33	10.4
V	92.8	85.5	121	256	62	164	71.1	162	43.8	230
Cr	376	205	1486	267	347	213	247	287	373	429
Mn	823	530	463	223	1649	2212	17376	2952	319	1073
Fe (mg/g)	58.7	103	121	51.7	196	123	128	120	30.6	154
Ni	73.4	49.9	91.4	160	53.8	57	75	103	48.4	95.3
Cu	183	24.2	96.7	917	275	<4	8.3	19.9	11.4	35.7
Zn	114	169	83.8	70.1	64.4	70.7	80.2	71.4	38	79.8
Ga	12.1	13	15.8	37.9	8.3	18.7	15.4	14.7	23.3	23.3
As	3.6	9.4	31.3	78.3	5.4	<2.6	<2.6	3.4	<2.6	<2.6
Rb	83.3	<13	<13	313	<13	112	88.2	105	81.2	65.6
Y	9.9	14	22.2	77.7	22.9	63	34	29.1	22.8	31.1
Zr	91.9	88.3	71.4	50.8	33.7	296	161	159	179	213
Pb	<22	289	1144	10122	<22	<22	<22	<22	<22	<22
U	349	62.5	<30	14364	103	117	262	345	148	585
U (DNAA)	373	94	11.3	16712	125	117	292	382	151	619
P (XRF)	356	1132	703	1285	138	199	218	481	157	-
Oxide (%)	107	103	91.6	99.1	97.4	101	96.1	98.9	106	102

	M3 13	M3 15	M3 15	M3 20	M3 26	M3 32	W2 14	W2 14	W2 14	W2 14
	black	soft	hard				gen.	grey	orange	red
F	301	174	110	172	311	722	345	785	536	294
Li	309	62.7	31	51.4	47.3	63	59.3	66.2	<10	129
Na	236	196	152	249	218	112	1582	6354	3725	387
Al (mg/g)	76.4	62.9	25.1	34.9	51.5	83.7	75.1	138	111	79.8
Mg (mg/g)	10	8.4		6.6	23.9	64	15	25.5	21.6	26.5
Si (mg/g)	325	303	414	411	344	237	391	249	216	239
S	<200	<200	<200	<200	341	339	<200	<200	<200	<200
K (mg/g)	6.85	0.514	0.437	4.25	5.35	10.3	17.6	2.11	6.3	2.62
Ca	201	157	112	216	489	3153	468	1951	1121	288
Ti (mg/g)	2.85	1.61	1.71	2.57	3.83	15.3	2.58	1.99	5.12	12.6
V	128	105	54.2	43.5	61.8	234	124	381	480	273
Cr	310	200	250	282	291	130	701	463	447	135
Mn	14457	386	218	1237	1184	1312	1538	366	186	1533
Fe (mg/g)	104	165	112	81.7	106	130	65.8	61.3	108	147
Ni	313	59.8	49.2	58.5	56.4	41.4	52.5	51.8	51.7	73
Cu	9.1	50.2	43.5	78.5	152	30.1	39	29.2	46.9	48.7
Zn	69.9	87.6	60.1	51.8	54.1	230	97.2	279	184	181
Ga	8.7	29.7	11.7	4.6	7.1	19.1	19.2	68.7	58.1	20
As	<2.6	33.8	17.1	6.2	5.4	<2.6	6.3	1.6	6.2	5.4
Rb	49.9	30.4	27.1	27.1	26.5	51.2	118	12	45.1	25.7
Y	11.1	17.7	20	12.7	17.8	59.5	10.4	18.8	19	32
Zr	103	45.9	51.7	47.9	116	303	35	59.5	85.6	152
Pb	<22	<22	<22	<22	<22	<22	52.8	141	117	25.5
U	430	412	290	276	208	<30	165	71.4	290	297
U (DNAA)	479	480	346	337	244	20.6	-	-	-	-
P (XRF)	-	345	363	379	399	826	-	-	-	-
Oxide (%)	101	101	109	108	103	99	112	93.7	87.6	93

	W1 3	W1 13 <10μm	W1 13	W1 24	W2 14 <10μm	W2 14	W2 5	W3 4	W3 14	W3 24	W4 5
F	151	448	282	231	417	345	372	76.2	438	616	162
Li	<10	14.3	19.4	155	148	47.4	104	10	106	96.9	28.1
Na	192	255	231	58.4	603	669	27.8	33	96.4	80.4	86.4
Al(mg/g)	107	158.3	96.3	85.3	133	95.5	87.1	29	90.3	79.2	40.9
Mg(mg/g)	<4	6.14	2.23	20.9	21.4	16.4	29.6	<4	45.1	67	<4
Si(mg/g)	217	216	248	218	195	299	210	341	196	194	342
S	<100	<100	<100	<100	<100	<100	112	111	<100	<100	140
Cl	329	250	152	421	766	96.2	427	239	347	212	226
K(mg/g)	3.63	27.2	19.3	5.31	7.45	32.7	1.48	0.6	3.86	4.65	7.28
Ca	60	338	245	236	383	331	97.6	57.9	87.2	755	141
Ti(mg/g)	3.45	4.37	3.31	4.26	1.49	0.17	8.79	1.67	4.16	4.67	2.17
V	141	203	131	307	431	<25	347	194	178	199	342
Cr	99.6	50.5	125	177	90.5	261	106	221	123	181	267
Mn	<15	<15	<15	639	391	691	422	<15	686	1345	151
Fe(mg/g)	72.5	86.5	67.7	65	115	35	110	68.3	85.7	97.2	23.6
Co	84.2	134	82.9	316	91.2	54	112	61.9	113	107	70.5
Ni	117	213	146	973	44.7	23.5	53.4	9.6	52.4	54	108
Cu	6	8.6	10	0.7	89	24.6	48.8	24.4	32.4	6.6	309
Zn	11.6	82	44.4	432	236	71.6	158	8.2	203	262	66.3
Ga	61.2	50.6	30.5	41.8	51.7	21.3	17.2	5.5	23.7	21.8	33.4
Rb	<15	70	32.2	<15	<15	180	<15	<15	<15	<15	22.4
Y	19.6	34.4	46.3	147	30.4	<10	74.2	<10	<10	<10	<10
Zr	164	85.2	522	122	60	<10	183	10	30.2	24.1	19
Nb	14.1	5.3	5.4	6.8	<5	5.3	<5	70.6	164	149	87.8
Mo	<10	<10	<10	<10	<10	<10	<10	<10	<10	<10	<10
Ru	18.3	<15	<15	20	42.3	<15	30.3	<15	<15	<15	<15
Rh	<15	<15	<15	<15	20.5	<15	<15	16.5	21.6	21.5	<10
Ag	88.7	<10	18.6	14.2	<10	<10	11.6	<10	<10	<10	28.4
Ba	<10	<10	<10	<10	<10	294	<10	<10	<10	11.9	<10
Pb	38.7	59.8	38.9	154	415	11.1	1.7	24.1	11.6	4.3	1041
Th	43	53.4	53.7	26.7	23.9	<20	<20	<20	22.4	32.8	<20
U	<20	389	304	307	459	45.9	84	20	66.9	<20	748
U(DNAA)	27.7	363	278	250	-	46.1	73.1	16.8	59.5	9.2	720
P(XRF)	177	1133	833	481		154	434	278	302	271	239

	W4 14	W4 24	W5 14	W7 4	W7 13 <10μm	W7 13	M2 13 <10μm	M2 24 <10μm	C1 5	C1 13	C1 23
F	193	459	732	142	336	390	412	674	135	434	558
Li	128	144	52.8	28.4	152	105	52.3	174	43.6	82	75.7
Na	47.5	119	780	82.1	167	93.7	399	213	56.8	66.1	94.4
Al(mg/g)	99	70.7	91.2	49.4	143	94	148	123	48.4	78.3	73
Mg(mg/g)	8.33	50.7	30.7	<4	27.3	22.2	<4	57.5	6.2	42.9	53.2
Si(mg/g)	202	217	246	246	206	206	183	178	258	198	205
S	128	208	<100	<100	<100	<100	<100	1220	<100	<100	<100
Cl	306	333	47.7	240	467	435	300	210	270	412	285
K(mg/g)	2.34	6.49	39.7	1.8	13.9	11	27.6	19.3	4.6	10.3	9.5
Ca	103	1792	957	33	196	262	266	426	99.2	220	378
Ti(mg/g)	3.32	2.85	4.94	4.2	2.7	16.2	7.2	2.7	4.5	9.3	6
V	790	398	173	403	332	605	310	253	191	358	205
Cr	99.7	145	202	250	173	121	617	221	312	238	171
Mn	242	508	830	<15	503	430	651	1300	485	1160	1027
Fe(mg/g)	67.2	52.2	57.4	159	89.9	114	130	127	64	113	87.6
Co	160	128	90.6	80.9	104	115	171	200	77	122	87.5
Ni	346	152	30.9	23.6	27.3	28.9	98.1	407	23.8	62.6	48
Cu	22.9	3.2	47.9	28.9	98.5	201	436	731	10.5	54	75
Zn	387	137	103	17.6	62.9	105	128	737	45.7	121	132
Ga	59.5	47.8	12	19.2	25.3	20.4	22.5	19.8	10	15	11.6
Rb	<15	103	188	<15	<15	<15	76.3	<15	<15	<15	<15
Y	<10	<10	<10	<10	<10	43	<10	<10	<10	<10	<10
Zr	73.9	24.6	26.5	<10	34.8	70.3	47.3	32.8	30.7	38.3	42.4
Nb	206	214	216	163	98	318	237	71.9	168	246	128
Mo	<10	<10	14.3	<10	10	11.8	14.3	<10	<10	<10	<5
Ru	22.5	46.9	<15	<15	<15	<15	21.5	23	<15	<15	<15
Rh	39.1	48.3	17	27.1	<15	24.6	25.2	34.9	<15	32.7	<15
Ag	44.5	108	<10	12.7	<10	<10	63.4	27.7	<10	17.7	<15
Ba	77.6	<10	<10	<10	10.1	12.6	<10	<10	<10	<10	<10
Pb	1302	1527	10.2	68.9	<10	<10	14.9	21.1	13	<10	<10
Th	55.4	40.4	32.5	34.8	<20	<20	61	34.3	25.5	28.1	<20
U	1820	5139	<20	360	<20	<20	2220	994	71.9	225	101
U(DNAA)	1418	3330	3.5	301		6.6			74	205	95.5
P(XRF)		418	267	460		618					

	C1 39	C4 5	C4 13	C4 23	C4 39	C6 5	C6 13	C6 23	C6 39	C7 5	C7 13
F	637	146	185	473	533	194	271	556	702	212	157
Li	33.6	14.1	102	90.5	33.3	31.5	77.5	47.1	59.6	17.6	58.2
Na	55.6	59.6	107	178	<50	517	102	81.2	<50	107	114
Al(mg/g)	50.2	80.7	84.7	70.8	54.8	87.9	83.6	69.7	76.4	93.5	87.2
Mg(mg/g)	48.8	<4	13.5	52.6	53	<4	15.7	57.6	90.2	4	<4
Si(mg/g)	246	200	193	201	209	226	182	198	151	216	224
S	3670	<105	<105	<105	1830	<105	<105	434	<105	<105	112
Cl	67.8	368	443	366	180	325	390	171	226	291	322
K(mg/g)	6.8	1.5	4.4	7.2	0.2	10.7	7.4	7.1	4.1	6	4.9
Ca	2815	59.4	148	205	2191	152	230	1696	1923	124	123
Ti(mg/g)	2.4	11.5	6.6	6.2	2.3	6.2	10.5	6.6	10.7	5.8	5.9
V	127	365	384	207	423	250	199	198	421	239	227
Cr	304	251	343	220	369	173	128	171	111	158	123
Mn	1053	122	904	599	1172	254	559	877	1457	22.4	628
Fe(mg/g)	91.9	106	119	77.4	128	112	125	100	110	109	94.6
Co	77.7	82.1	159	107	94.7	107	118	130	170	80.5	185
Ni	17.9	43.4	68.5	66.7	46.7	48.3	<10	26.8	49.6	66.2	146
Cu	76.9	13.3	36.9	10.4	29.8	14.1	20.7	10.7	3.5	55.1	10.7
Zn	84.6	43.1	276	188	199	47.1	235	215	434	57.6	170
Ga	4.7	14.7	18.2	20.6	11.9	21.4	22.3	17.6	19.8	19.9	22.7
Rb											
Y	21	30.7	28.8	22.1	12.7	33.3	167	28.4	38.7	26	23.8
Zr	136	161	203	150	76.9	164	517	143	176	126	168
Nb	<5	<5	<5	<5	<5	8.1	9.9	10.8	6.3	<5	<5
Mo							<10	<10	<10	<10	<10
Ru	35.4	<15	36.8	<15	35.7	25.8	16.8	49.5	29.6	21.5	<15
Rh	<15	<15	36.7	<15	<15	<15	<15	<15	<15	<15	35.6
Ag							11	18	11.2	11.5	<10
Ba											
Pb	13.7	10.9	<10	<10	41.4	25	20	11.2	16.1	97.4	12.9
Th	22.7	30.8	28	22.1	20.7	31.8	48.9	31	21.2	10	53.7
U	<20	157	721	230	15.8	113	132	<20	20	326	987
U(DNAA)	4	115	611	195	8.8	109	114	8.3	2.4	271	877
P(XRF)		263	497	288	484	239	727	361	334	268	518

	C7 23	C7 39	C8 5	C8 13	C8 23	C8 39	C8 25 <10μm	M4 5	M4 13	M4 23	M4 39
F	693	806	406	506	357	550	802	324	441	274	688
Li	88.8	105	58.2	70.9	95.2	119	139	66.1	63.4	51.7	62.4
Na	62.5	<50	<50	1016	120	274	98.5	83.9	<50	190	182
Al(mg/g)	78.9	87.5	74.6	90.1	57.3	92.6	103	67.5	82.2	57.9	81.3
Mg(mg/g)	76.2	91.7	46.1	39.7	44	90.6	116	27.1	49	30.2	69
Si(mg/g)	205	298	188	238	239	159	152	216	199	234	218
S	<105	3874	<105	<105	<105	133	400	<105	<105	766	437
Cl	216	114	383	301	340	351	350	506	433	297	205
K(mg/g)	5.6	0.06	0.3	19.3	3.6	4.9	0.5	1.9	9.2	9.7	9.2
Ca	981	2443	38.3	238	223	584	394	71.8	334.3	564	2590
Ti(mg/g)	4.1	5.8	10.2	4.4	2.9	5.8	4	10.5	9.9	10.8	12.1
V	161	344	342	142	83	184	359	524	379	257	285
Cr	212	231	284	227	183	271	70	62	107	119	107
Mn	686	743	510	268	346	816	1068	1023	1355	910	872
Fe(mg/g)	84.7	112	140	60.9	73.1	112	131	108	113	88.3	114
Co	122	139	172	122	98.4	234	207	131	135	113	130
Ni	121	138	90.8	63.2	41.6	150	99.4	52	20.4	17.2	9.9
Cu	4.6	38.3	6.4	9	48.6	3.2	13.5	47.2	32.9	59.6	225
Zn	174	176	151	71.6	95.2	104	310	139	99.9	73	206
Ga	27.8	28.9	24.6	18.6	8.9	32.4	19.2	11.5	17.4	10.2	13.2
Rb			<15	36.1	<15	<15	<15	<15	<15		
Y	13.5	24.2	41.4	44.8	22.8	28.2	25.8	45.7	50.6		
Zr	127	130	308	168	103	142	107	227	174		
Nb	<5	<5	<5	12.3	<5	<5	<5	<5	6.2		
Mo	<10	<10	<10	<10	<10	<10	<10	<10	<10		
Ru	<15	28.8	<15	<15	<15	22.7	44.3	<15	29.1		
Rh	<15	<15	<15	<15	<15	<15	<15	<15	<15		
Ag	<10	18	10.4	<10	13.9	<10	<10	<10	13		
Ba											
Pb	10	322	57.7	<10	<10	<10	15.2	11.4	12	34.3	86.1
Th	32.8	30.6	59.4	26.8	24.2	28.1	14.5	14.4	21	102	355
U	89.3	334	241	45.6	59.3	<20	39.8	66.4	<20	<20	<20
U(DNAA)	79.6	294	212.3	47.1	34.6	9.7		45.9	4.1	5	8.8
P(XRF)	322	501	264	234	246	180		334	469	356	714

A4.2 Rare Earth Element Concentrations in Bulk Rock Samples (determined by INAA)

Sample	M1 3	M1 3	M1 7	M1 7	M1 9	M1 9	M1 13	M1 13	M1 16	M1 16
	red	gen.	red	white	red	white	brown	white	gen.	orange
La	8.77	10.9	0.37	4.10	1.50	11.6	82.7	97.8	2.25	3.02
Ce	14.7	18.7	8.20	9.00	32.2	27.0	162	199	69.1	61.3
Nd	6.30	6.50	0.74	2.00	9.30	6.20	51.7	67.8	42.1	39.0
Sm	1.09	1.47				1.70	5.69	12.8		
Eu	0.34	0.41	0.29	0.22	0.63	0.42	1.36	1.20	0.60	0.54
Tb	0.21	0.26	0.19	0.14	1.62	0.84	2.34	1.94	0.78	0.66
Dy	3.33	3.55	2.63	2.21	7.15	5.76	13.2	10.2	7.26	7.94
Yb	1.90	2.23	1.38	1.33	4.26	3.81	7.67	5.25	4.80	4.40
Lu	0.34	0.40	0.20	0.24	<0.85	0.62	1.35	0.82	0.75	0.72
Th	27.4	26.7	19.7	13.3	30.7	31.8	52.8	44.5	37.6	31.8
U	28.9	27.3	208	37.3	290	34.3	278	29.7	326	392

Sample	M1 19	M1 23	M1 27	M1 31	M1 37	M1 43	M1 49	M2 3	M2 3	M2 8
								<2 mm	>2 mm	<2mm
La	6.63	<0.78	<0.82	<0.94	<0.9	2.00	<2.1	29.7	13.1	<6.2
Ce	40.9	59.6	<7.1	17.0	11.2	27.7	6.40	75.0	44.0	92.0
Nd	28.5	33.0	<60	<14	<11	1.80	<16	16.0	5.80	<47
Sm										
Eu	0.60	0.73	0.20	0.90	0.49	0.29	0.38	1.15	0.78	1.12
Tb	0.62	0.77	0.18	0.79	0.48	0.33	0.56	1.29	0.64	0.75
Dy	5.66	9.43	9.66	8.29	4.13	2.76	3.59	5.90	3.59	4.86
Yb	2.75	3.65	1.99	3.16	2.32	1.64	2.21	3.41	2.24	2.25
Lu	0.41	<0.53	0.45	0.48	0.38	0.28	0.34	0.60	0.31	0.43
Th	19.2	19.4	2.94	18.7	20.4	16.8	14.3	14.6	9.05	17.9
U	230	363	1376	1238	681	360	700	467	384	2073

Sample	M2 13	M2 13	M2 17	M2 17	M2 21	M2 25	M2 25	M2 32	M2 36	M2 42
	<2 mm	45-100μ	<2 mm	>2 mm	<2 mm	<2 mm	>2 mm			
La	15.60	16.00	15.40	6.30	24.80	3.30	1.60	19.00	17.20	14.69
Ce	98.0	75.0	104	36.0	108	36.0	15.3	61.0	34.7	28.9
Nd	1.20	<29	<63	<18	8.20	<14	<6.3	9.20	8.50	10.5
Sm										2.14
Eu	0.94	0.70	0.94	0.24	1.20	0.39	0.19	0.58	0.52	0.46
Tb	0.69	0.67	0.89	0.20	0.85	0.32	<0.37	0.43	0.56	0.57
Dy	3.96	3.51	4.70	0.90	4.67	2.13	1.41	1.93	2.17	2.62
Yb	2.79	2.85	2.88	0.56	3.38	1.73	1.13	1.57	1.63	1.86
Lu	0.50	0.52	0.56	0.13	0.66	0.31	0.11	0.30	0.26	0.36
Th	18.0	13.8	16.5	2.32	15.2	10.8	9.70	10.2	10.9	12.4
U	1299	840	1589	403	1311	540	226	407	101	11.0

Sample	M2 48	M3 4	M3 7	M3 10	M3 13	M3 13	M3 13	M3 13	M3 15	M3 15
					yellow	white	gen.	black	hard	soft
La	5090	23.1	43.4	60.0	28.0	34.8	32.0	2.80	22.0	<9.6
Ce	1900	34.9	130	138	76.5	58.8	60.2	48.0	1.70	23.0
Nd	302	16.9	42.3	37.6	18.0	17.9	7.90	<18	<0.73	<26
Sm	119		6.08			0.96				
Eu	2.87	0.78	2.43	1.46	1.63	1.16	1.32	0.81	0.44	0.52
Tb	6.27	0.53	2.79	1.03	1.50	0.64	0.92	<0.57	<0.5	<0.59
Dy	28.8	2.34	11.3	<60	6.91	4.06	4.27	<8.1	2.50	2.60
Yb	13.0	1.45	8.70	3.56	4.11	3.42	3.23	2.22	1.94	1.89
Lu		0.27	1.70	0.58	0.76	0.62	0.55	0.30	0.32	0.34
Th	5.96	5.91	14.8	19.1	12.8	12.0	10.5	9.09	7.28	6.08
U	13830	135	130	302	683	167	417	526	378	485

Sample	M3 20	M3 26	M3 32	M3 38.5	AAS[1]	PAAS[2]	Chond[3]	NAS[4]	SDO-1[5]	
La	12.1	31.1	36.9	30.5	12.6	38.0	0.32	32.0	36.0	
Ce	43.0	76.0	79.4	51.6	26.8	80.0	0.81	73.0	64.0	
Nd	9.30	22.0	34.1	24.5	13.0	32.0	0.60	33.0	35.0	
Sm			8.65	6.38	2.78	5.60	0.19	5.70	7.50	
Eu	0.56	1.08	1.90	1.37	0.92	1.10	0.07	1.20	1.20	
Tb	0.36	0.58	3.46	1.03	0.48	0.77	0.05	0.90	1.10	
Dy	2.23	3.36	9.00	6.66	2.93	4.40	0.33	5.80	6.90	
Yb	1.61	2.56	7.65	4.99	1.79	2.80	0.21	3.10	3.40	
Lu	0.26	0.47	1.23	0.67				0.48	0.00	
Th	6.01	7.54	14.7	8.32		2.85	4.70			
U	334	248	20.4			0.63	1.00			

1 AAS = Archeaen Australian Shales (McLennan and Taylor, 1980)
2 PAAS = Post Archeaen Australian Shales (McLennan and Taylor, 1980)
3 Chond. = Chondrite
4 NAS = North American Shale (Leventhal, 1990)
5 SDO-1 = Black Shale standard (Leventhal, 1990)

A4.3 Sample Analysed Prior to ARAP

Data reported by Ferguson and Winer (1980) *

HOLE	DDH49	DDH49	DDH49	DDH49	DDH49	DDH49	DDH49	DDH49	DDH49	DDH49
DEPTH (m)	155.5	148.8	4.5	32	39.9	43.3	88.4	95	106.4	137.2
DESC.	K ss	K qite	w m st	w l st	m q c st	g b m q st	p q c st	h c qite	q-c st	br c qite
% SiO_2	92.25	93.07	66.15	54.53	53.4	60.35	60.43	67.35	57.22	68.71
% TiO_2	0.06	0.06	0.59	0.69	0.62	0.92	0.52	0.25	0.34	0.42
% Al_2O_3	1.65	1.73	10.47	16.19	14.62	18.91	10.55	9.53	13.9	12.98
% Fe_2O_3	0.99	1.05	11.09	1.35	2.13	2.85	2.87	2.48	3.32	1.8
% FeO	0.45		0.07	6.74	4.32	3.91	6.07	3.53	5.03	1.62
% MnO	0.01	0.02	0.17	0.06	0.05	0.04	0.04	0.04	0.08	0.03
% MgO	3.04	2.84	1.98	10.72	13.39	5.76	10.89	9.97	10.96	6.34
% CaO	0.04	0.05	0.04	0.06	0.21	0.18	0.35	0.14	0.18	0.33
% Na_2O	0.08	0.02		0.04	0.04	0.16	0.01	0.03	0.06	0.03
% K_2O	0.05	0.03	0.18	1.75	1.52	3.81	0.07	0.11	0.88	1.66
% P_2O_5	0.01	0.01	0.08	0.04	0.15	0.07	0.23	0.06	0.08	0.2
% S	0.02	0.03	0.04	0.11	0.57	0.45	0.62	0.05	0.08	0.04
% CO_2	0.05	0.1	0.05	0.05		0.05	0.05	0.1	0.05	0.05
Ba (µg/g)	4		318	270	87	357	9	26	65	79
Rb (µg/g)			6	59	52	104	2	3	40	33
Sr (µg/g)	3	2	4	6	18	17	4		3	5
Pb (µg/g)			35	6	7	7	137	40	20	68
Th (µg/g)	5	4	10	16	14	12	10	13	25	7
U (µg/g)	2		215	122	4	3	23	486	235	719
Zr (µg/g)	157	95	92	109	112	160	108	107	188	87
Nb (µg/g)			9	10	9	10	5	10	13	14
Y (µg/g)		3	32	17	18	20	9	6	26	5
La (µg/g)	9	14		14	36	22			17	
Ce (µg/g)	24	29	67	36	68	42	14	7	36	10
Li (µg/g)	7	8	69	87	102	47	69	71	91	76
Cs (µg/g)			4	5	4	6	4	3	4	5
Sc (µg/g)		3	29	24	17	25	15	14	15	23
V (µg/g)	5	14	240	233	222	151	312	159	118	317
Co (µg/g)		5	30	29	29	35	46	37	40	16
Ni (µg/g)	6	11	42	63	39	54	101	92	74	114
Cu (µg/g)	2	3	102	94	433	1041	210	24	10	8
Zn (µg/g)	7	23	77	64	35	46	90	61	55	38
Ga (µg/g)	2	2	14	22	19	23	23	30	27	63
Be (µg/g)		1	4	5	4	5	3	3	5	3
As (µg/g)			2							
Mo (µg/g)		2	3		7	6	6	2	4	
Sn (µg/g)	5		4	3		3	4	4	4	3
Hf (µg/g)	4	4		7	2	8	9	5	8	5
W (µg/g)		4	3		3	2				
F (µg/g)	380	280	340	800	1200	770	730	540	810	460
Cl (µg/g)		20	50	20	60		30	20		100

HOLE	DDH49	DDH49	DDH49	DDH49	DDH49	DDH49	DDH21	DDH21	DDH21	DDH21
DEPTH (m)	40.5	100.9?	126.2	138.4	114.6	82.9	21.3	55.5	78	84.1
DESC.	g py c q st	m q c st	m h c q st	br c q st	q c st	gr c q st	w l st	p g c m st	ca m c st	gr q c st
% SiO2	65.86	61.45	60.28	65.8	46.61	63.96	55.14	63.67	58.98	59.73
% TiO2	0.28	0.2	0.37	0.31	0.61	0.33	0.81	0.56	0.6	0.38
% Al2O3	7.26	13.14	14.46	12.1	17.28	9.11	11.88	13.51	15.26	8
% Fe2O3	5.82	2.27	1.94	2.01	3	3.23	19.3	3.42	1.44	14.33
% FeO	7.79	4.14	5.82	4.21	6.42	4.46	0.2	5.95	6.87	
% MnO	0.17	0.05	0.11	0.06	0.06	0.04	0.11	0.11	0.06	0.07
% MgO	3.86	11.36	9.13	8.57	15.86	9.16	2.15	4.22	7.21	7.82
% CaO	0.7	0.09	0.17	0.21	0.2	0.3	0.05	0.38	0.14	0.44
% Na2O	0.02	0.07	0.06	0.01	0.03	0.02	0.03	0.04	0.04	0.02
% K2O	0.1	0.55	1.46	0.98	0.83	0.01	0.97	2.55	2.3	0.04
% P2O5	0.18	0.06	0.12	0.14	0.13	0.22	0.14	0.11	0.06	0.29
% S	7.65	0.03	0.02	0.02	0.02	2.1	0.06	0.57	0.13	1.61
% CO2	0.1	0.1	0.1	0.1	0.05	0.05	0.05	0.05	0.05	0.05
Ba (μg/g)	12	46	80	75	32	28	201	331	131	
Rb (μg/g)	5	15	71	32	33		58	86	101	2
Sr (μg/g)			2	3		2	3	13	5	3
Pb (μg/g)	21	166	9	42	32	2060	7	7	3	298
Th (μg/g)	11	29	23	18	29	23	12	12	16	11
U (μg/g)	6	1250	59	850	156	2799	508	3	5	11
Zr (μg/g)	64	211	200	180	270	110	152	101	143	90
Nb (μg/g)	5	23	14	18	13	39	14	8	10	6
Y (μg/g)	20	26	23	20	18	33	29	16	22	4
La (μg/g)	23	4	23	12	2	3	42	34	26	2
Ce (μg/g)	42	8	51	33	8	13	100	64	58	17
Li (μg/g)	38	88	84	75	105	52	69	29	49	26
Cs (μg/g)	0	0					9	7	7	3
Sc (μg/g)	8	12	12	10	18	18	35	16	25	13
V (μg/g)	145	128	72	81	126	317	285	186	225	260
Co (μg/g)							24	13	25	62
Ni (μg/g)	41	90	52	64	109	113	28	36	46	70
Cu (μg/g)	262	58	25	12	12	474	79	49	8	61
Zn (μg/g)	55	56	52	62	91	62	71	126	94	228
Ga (μg/g)	11	35	25	27	47	30	14	16	17	14
Be (μg/g)	0	0					3	3	3	2
As (μg/g)										
Mo (μg/g)	13						8	6	6	16
Sn (μg/g)				2	4		2	3	3	3
Hf (μg/g)	2	5	4	4	5	3	3	6	8	2
W (μg/g)	4		6	4						
F (μg/g)	480	660	800	600	760	620	450	660	740	730
Cl (μg/g)							110		40	50

HOLE	DDH21	DDH21	DDH21	DDH21	DDH5	DDH5	DDH5	DDH5	DDH5	DDH5
DEPTH (m)	91.4	96	123.8	129.9	33.5	41.6	47.6	51.5	64.6	79.3
DESC.	m q c st	m q c st	m q c st	q h c st	gr m q c st	m q c st	c m q st	h m c q st	br h m c q st	c m q st
% SiO2	66.75	54.98	67.98	59.89	64.16	61	66.86	65.72	67.25	64.14
% TiO2		0.32	0.23	0.36	0.36	0.34	0.2	0.29	0.22	0.26
% Al2O3	8.64	14.43	13.88	13.59	7.61	15.43	13.32	13.03	11.07	12.6
% Fe2O3	3.45	2.41	1.35	1.94	13.57	2.32	2.57	2.66	4.93	2.8
% FeO	3.76	5.73	2.5	5.96		3.44	2.28	1.24	1.66	2.97
% MnO	0.04	0.07	0.05	0.08	0.1	0.06	0.05	0.05	0.18	0.04
% MgO	6.65	13.01	6.25	10.1	6.91	8.56	6.87	7.77	6.31	8.06
% CaO	0.44	0.29	0.1	0.16	0.4	0.19	0.17	0.24	0.1	0.1
% Na2O		0.03	0.06	0.02		0.07	0.05	0.06	0.01	0.04
% K2O	0.3	0.45	2.19	0.99	0.15	1.68	1.6	1.5	0.9	1.33
% P2O5	0.29	0.38	0.06	0.13	0.25	0.12	0.23	0.13	0.05	0.09
% S	0.59	0.06	0.04	0.05	1.1	0.03	0.03	0.03	0.02	0.02
% CO2	0.05	0.05	0.05	0.05	0.05				0.05	0.05
Ba (μg/g)	39	39	199	57	27	116	117	170	123	165
Rb (μg/g)	3	9	80	54	2	67	55	60	5	40
Sr (μg/g)	4	3	3	3	4	5	3	4	3	3
Pb (μg/g)	6082	360	14	24	2863	183	424	542	610	88
Th (μg/g)	3	17	27	23	6	30	25	24	21	21
U (μg/g)	1732	920	67	192	983	1111	2771	3414	6704	849
Zr (μg/g)	119	177	181	260	80	231	183	217	165	141
Nb (μg/g)	29	19	8	11	16	22	36	42	63	14
Y (μg/g)		6	15	15		20	33	34	28	24
La (μg/g)			13	8	34	11	27	7		2
Ce (μg/g)	29	13	34	29	89	50	65	28	24	8
Li (μg/g)	60	83	59	78	29	111	103	122	72	62
Cs (μg/g)	2	3	5	4	4	6	12	11	9	5
Sc (μg/g)	20	25	11	11	18	15	19	23	26	18
V (μg/g)	431	415	107	124	234	110	104	185	311	209
Co (μg/g)	33	50	20	37	23	39	19	21	43	27
Ni (μg/g)	89	145	47	62	29	63	47	69	53	68
Cu (μg/g)	402	179	17	6	13	14	20	23	179	5
Zn (μg/g)	63	158	38	53	88	92	39	31	127	51
Ga (μg/g)	41	51	33	23	16	28	25	35	26	33
Be (μg/g)	2	3	3	4	2	6	4	4	3	3
As (μg/g)					15	16	7	5	12	
Mo (μg/g)	4	3	8	7			30	14	31	2
Sn (μg/g)	3	5	5	3	2	5	5	5	17	4
Hf (μg/g)			7	10	2	8	7	7		6
W (μg/g)		3				4	12	5	7	2
F (μg/g)	490	660	640	660	580	810	610	680	520	700
Cl (μg/g)	150	50				210	80	60	30	30

* Ferguson, J. and Winer, P. (1980) Pine Creek geosyncline: statistical treatment of whole rock chemical data. In Ferguson, J. and Goleby, A.B. (eds.) Uranium in the Pine Creek Geosyncline. International Atomic Energy

HOLE	DDH5	DDH5	DDH5	DDH5	DDH5	HDH3	HDH3	QDH2	QDH2	DDH48
DEPTH (m)	84.3	57.6	66.9	70.1	90.4	453.4	399.6	117.4	115.8	30.8
DESC.	h m q c st	c m q st	br c qite	br c m q st	c h q m st	gt gn	t-begtpe	b gt gn	am (Z)	am (Z)
% SiO_2	65.98	70.74	52.28	73.48	62.01	74.66	71.54	55.95	51.67	43.87
% TiO_2	0.55	0.26	0.51	0.44	0.55	0.01	0.02	0.78	1.52	4.18
% Al_2O_3	15.89	10.73	16.9	12.67	15.75	13.92	14.21	19.4	13.95	11.19
% Fe_2O_3	2.29	1.21	3.71	1.29	3.24	0.18	0.19	1.42	1.57	6.29
% FeO	1.57	3.65	5.93	2.51	1.8	0.89	0.54	7.1	11.56	13.96
% MnO	0.03	0.06	0.2	0.08	0.03	0.05	0.03	0.15	0.23	0.17
% MgO	5.23	7.53	9.95	3.28	7.36	0.33	2.11	4.32	6.8	7.4
% CaO	0.21	0.11	0.22	0.16	0.25	0.63	0.75	1.21	7.26	6.68
% Na_2O	0.03	0.05	0.08	0.05	0.09	3.08	3.37	2.2	0.91	0.96
% K_2O	3.58	0.99	2.19	3.05	2.95	5.79	5.01	4.23	1.64	0.82
% P_2O_5	0.17	0.09	0.16	0.12	0.18	0.11	0.11	0.07	0.21	0.26
% S	0.02	0.02	0.02	0.02	0.06	0.11	0.02	0.15	0.08	0.01
% CO_2	0.1	0.05	0.05	0.05	0.05	0.15	0.05	0.2	0 1	0.05
Ba (µg/g)	188	43	147	221	97	421	60	528	373	166
Rb (µg/g)	149	41	77	163	85	89	142	150	59	16
Sr (µg/g)	4	2		3		125	46	165	100	55
Pb (µg/g)	96	26	154	34	44	75	62	70	9	10
Th (µg/g)	21	19	23	18	19	6	3	13	3	5
U (µg/g)	925	170	2542	205	277	14	8	6		2
Zr (µg/g)	166	163	198	159	209	66	18	176	143	150
Nb (µg/g)	15	10	36	10	13		2	8	6	6
Y (µg/g)	22	16	34	15	13	13	14	13	31	42
La (µg/g)		18	2	2		8		27	17	20
Ce (µg/g)	7	41	10	9	10	20	12	63	59	55
Li (µg/g)	54	94	54	23	58	9	15	26	16	15
Cs (µg/g)	5					2	10	11		
Sc (µg/g)	19	8	13	11	16	8	3	20	36	66
V (µg/g)	199	61	284	94	162	9	5	247	522	1741
Co (µg/g)	4					4	3	30	50	60
Ni (µg/g)	35	40	63	30	51	3	3	60	44	34
Cu (µg/g)	7	11	5	5	4	39	10	61	37	59
Zn (µg/g)	38	35	378	52	34	17	16	194	91	148
Ga (µg/g)	29	21	38	22	60	12	13	26	19	19
Be (µg/g)	5					2	8	13	2	2
As (µg/g)	2							9		
Mo (µg/g)	2		2	5		4	3	7	8	8
Sn (µg/g)	16		40	38	3				2	
Hf (µg/g)	7	5	5	4	5	3	3	6	5	4
W (µg/g)	6	4	6	9	4	2	2			
F (µg/g)	720	560	1000	840	1000	40	150	720	610	570
Cl (µg/g)	40					90	80	50	60	50

* Ferguson, J. and Winer, P. (1980) Pine Creek geosyncline: statistical treatment of whole rock chemical data. In Ferguson, J. and Goleby, A.B. (eds.) Uranium in the Pine Creek Geosyncline. International Atomic Energy Agency, Vienna. pp. 191-208.

Data Reported by Tucker (1975) **

HOLE	DDH98	DDH98	DDH98	DDH98	DDH92	DDH92	DDH92	DDH92	DDH87	DDH87
DEPTH (m)	47	78	88	121	28	28	31	93	30	45
DESC.	st	st	am	c pe	g st	g (sub)	st	c st	g st	g st
% SiO2	57.8	58.7	44.2	58.9	57.8	35.6	64.5	55.6	65.4	66.4
% TiO2	0.63	0.8	2.93	0.05	0.39	0.15	0.42	0.66	0.59	0.32
% Al2O3	18.55	17.78	12.8	14.9	12.7	19.48	15.95	16.38	14.88	6.78
% Fe2O3	9.05	8.4	17	7.1	18	34.6	6.45	9.75	7	14.75
% MnO	0.04	0.04	0.14	0.07	0.12	0.35	0.03	0.04	0.06	0.18
% MgO	5.55	4.68	13.1	9.65	5.9	2.05	3.75	10.62	3.9	4.62
% CaO	0.22	0.15	0.95	0.3	1.31	5.78	0.1	0.15	0.22	0.73
% Na2O	0.16	0.2	0.3	0.05	0.03	0.05	0.14	0.08	0.1	0.02
% K2O	3.72	4.43	0.45	0.87	0.87	0.06	4.05	1.8	3.17	0.08
Rb (µg/g)	140	160	40	245	80		130	110	90	10
Sr (µg/g)	22	30	8	10	5		25	10	10	8
U (µg/g)	7	9	5	12	6		14	6	5	5
Th (µg/g)	10	8	7	5	17		17	17	14	10
Pb (µg/g)	7	5	6	5	7		9	9	6	21
Cu (µg/g)	11	8	6	9	460		37	55	54	174
Co (µg/g)	33	28	55	38	15		20	45	23	19
Ni (µg/g)	38	53	15	9	40		34	75	32	42
V (µg/g)	83	95	91	5	45		77	100	75	173
Vol % Mins.										
Q	32	17	22	46	35		33	12	37	47
M	21	33		6	2		36	15	13	
B	2	4			28		4		8	11
C	19	21	73	46	10		19	73	20	17
Ser. Feld	27	25		2	10		7		18	
G					15				3	15
H										
access.			5						1	10
SG (g/cm3)	2.8	2.8	2.87	2.71	2.88		2.76	2.77	2.8	2.87

** Tucker, D.C. (1975) Wall Rock Alteration at the Koongarra Uranium Deposit. MSc Thesis, James Cook University of North Queensland.

HOLE	DDH87	DDH87	DDH87	DDH87	DDH87	DDH101	DDH101	DDH101	DDH101	DDH101
DEPTH (m)	67	69	72	73	95	38	52	64	80	123
DESC.	g st	gr c br	grc br	c st	st	st	st	pe	st	am
% SiO2	69.9	67.2	58.9	58.9	56.8	74	63.3	75.8	69	45.2
% TiO2	0.26	0.32	0.53	0.53	0.42	0.38	0.57	0.05	0.5	4.43
% Al2O3	6.14	5.76	14.04	14.04	15.8	12.75	17.7	15.1	15.9	12.32
% Fe2O3	5.8	5.08	4.9	7.9	8.25	4.33	6.57	0.5	6.05	17.35
% MnO	0.01	0.06	0.04	0.04	0.04	0.06	0.08	0.01	0.05	0.07
% MgO	7.38	4.5	6.02	6.02	12.9	2.75	3.8	0.5	2.9	14
% CaO	0.37	0.49	0.26	0.26	0.22	0.13	0.13	0.23	0.15	0.57
% Na2O	0.04	0.07	0.04	0.04	0.02	0.36	0.25	3.66	0.33	0.08
% K2O	0.05	0.05	1.74	1.74	1.33	4.18	4.67	3.55	4.17	0.22
Rb (μg/g)	10	15	47	24	90	97	133	335	116	28
Sr (μg/g)	8	5	5	5	5	24	21	21	25	10
U (μg/g)	9	27500	23000	7000	108	11	5	5	7	5
Th (μg/g)	75	165	33	30	50	12	20	5	12	8
Pb (μg/g)	3770	19600	2820	643	9	8	5	5	5	5
Cu (μg/g)	1370	940	2760	152	6	10	9	119	61	19
Co (μg/g)	36	57	26	53	50	17	26	5	18	54
Ni (μg/g)	66	66	74	98	103	21	33	28	28	21
V (μg/g)	363	436	558	306	57	49	70	18	57	379
Vol % Mins.										
Q	60				29	47	43	32	36	14
M						16	33	16	33	
B					9	16	11		17	5
C	35				62	4	1	1	1	70
Ser. Feld						18	11	51	13	4
G										
H										
access.	5						1			8
SG (g/cm3)	2.69				2.74	2.71	2.78	2.66	2.76	2.85

HOLE	DDH101	DDH101	DDH96	DDH96	DDH75	DDH75	DDH75	DDH29	DDH29	DDH110
DEPTH (m)	129	216	32	136	106	101	110	80	87	21
	g st	g st	am	c st	g st	st	am	st	am	st
% SiO2	62.5	58.85	47	66.1	60.6	55.8	43.2	54.9	35.5	81.6
% TiO2	0.5	0.39	0.42	0.61	0.61	0.35	2.13	0.23	2.05	0.23
% Al2O3	16.78	13.1	15.88	15.88	19.2	13.4	16.74	14.8	16.06	9.46
% Fe2O3	6.05	7.05	10	4.58	3.83	7.8	10.45	7.53	14.65	2.87
% MnO	0.03	0.08	0.18	0.03	0.02	0.04	0.05	0.06	0.13	0.03
% MgO	5.5	13.5	15.8	6.25	6.9	15.3	17.9	16	19.9	1.9
% CaO	0.1	0.2	3.58	0.19	0.11	0.42	0.5	0.11	0.47	0.11
% Na2O	0.31	0.02	0.54	0.11	0.22	0.08	0.07	0.13	0.06	1.52
% K2O	3.22	0.38	3	3.22	4.03	0.05	0.77	0.27	0.05	2.11
Rb (µg/g)	75	16	90	62	83	5	27	11	5	101
Sr (µg/g)	32	5	60	30	15	5	7	5	5	20
U (µg/g)	5	750	5	325	430	465	19	645	480	5
Th (µg/g)	20	26	5	64	28	30	13	19	5	7
Pb (µg/g)	13	72	5	1210	47	105	9	85	53	5
Cu (µg/g)	5	7	31	26	5	11	10	99	16	5
Co (µg/g)	27	55	57	34	25	69	73	51	107	21
Ni (µg/g)	36	132	177	69	47	119	131	174	166	19
V (µg/g)	87	107	217	252	175	173	436	428	502	68
Vol % Mins.										
Q	41	46			26		9	27	5	56
M	34				23					11
B	20	15								7
C	4	39			51		87	73	91	1
Ser. Feld										25
G	1									
H										
access.							4		4	
SG (g/cm3)	2.79	2.75	2.82	2.77	2.72	2.7	2.75	2.71	2.76	2.67

HOLE	DDH110	DDH110	DDH110	DDH105	DDH73	DDH73	DDH73	DDH70	DDH70	DDH48
DEPTH (m)	58	63	77	131	39	59	89	40	42	24
	st	am	g st	c peg	c st	g st	c st	g st	st	am
% SiO2	75	44.9	58.8	56.4	58.8	69.5	61.4	53.9	51.7	44
% TiO2	0.46	0.5	0.72	0.1	0.65	0.27	0.27	0.57	0.23	3.32
% Al2O3	13.4	16.5	17.12	13.1	14.4	6.34	14.24	17.12	12.52	11.04
% Fe2O3	4.58	12.45	9.75	7.8	7.8	10	6.58	6.58	6.58	21.58
% MnO	0.05	0.06	0.44	0.04	0.04	0.03	0.02	0.04	0.02	0.17
% MgO	3.3	16.7	5.9	14.63	11.2	8.1	9.3	10.8	19.5	6.9
% CaO	0.11	0.11	0.28	0.2	0.1	0.35	0.1	0.1	0.13	7.48
% Na2O	0.32	0.09	0.23	0.07	0.12	0.07	0.14	0.1	0.07	1.54
% K2O	2.93	1.54	3	0.28	1.34	0.05	2.32	1.8	0.05	0.77
Rb (µg/g)	50	35	108	32	33	5	85	52	5	21
Sr (µg/g)	12	2	50	5	8	11	5	5	5	55
U (µg/g)	5	5	6	12	20	13	1100	2100	65	5
Th (µg/g)	11	5	14	5	19	23	31	22	10	8
Pb (µg/g)	5	5	21	5	5	233	123	108	20	5
Cu (µg/g)	7	10	29	6	30	44	11	19	197	38
Co (µg/g)	10	62	39	53	47	44	39	46	59	43
Ni (µg/g)	17	153	63	66	94	58	84	95	62	49
V (µg/g)	22	257	91	5	148	211	196	257	177	1201
Vol % Mins.										
Q	62		39	57	48	27	22	16	29	8
M	13		18	2	14		63	14		
B	9		19		17	9	4	1		
C	1		9	36	19	45	8	64	69	4
Ser. Feld	16		5		1					8
G			9							
H										73
access.			1	4		19	2	5	2	7
SG (g/cm3)	2.72	2.77	2.83	2.74	2.73	2.3	2.79	2.7	2.64	3.13

HOLE	DDH58	DDH60	DDH60	DDH60	DDH60	DDH60	DDH60
DEPTH (m)	42	45	46	49	59	64	68
	c st	gr f st	u	c st	st	c st	c st
% SiO2	62.1	79.1	28.2	61	70.2	62.1	65.4
% TiO2	0.18	0.23	0.27	0.42	0.16	0.26	0.39
% Al2O3	12.26	5.06	6.25	14.04	13.64	7.54	7.52
% Fe2O3	6.4	4.85	6.1	6.25	3.7	15.2	7.3
% MnO	0.06	0.03	0.18	0.06	0.05	0.07	0.05
% MgO	11.62	4.62	4	9.24	6.38	5.42	6.9
% CaO	0.1	0.37	1.17	0.26	0.1	0.3	0.44
% Na2O	0.62	0.02	0.05	0.02	0.03	0.03	0.09
% K2O	0.25	0.08	0.1	1.13	1.98	0.05	0.05
Rb (μg/g)	24	6	5	20	78	5	5
Sr (μg/g)	5	5	5	5	5	5	2
U (μg/g)	4050	3950	50000	13000	165	23	14000
Th (μg/g)	28	52	270	30	31	12	103
Pb (μg/g)	500	2870	50000	1590	42	290	6600
Cu (μg/g)	40	207	236	564	9	434	1180
Co (μg/g)	44	28	5	45	24	21	38
Ni (μg/g)	85	54	30	113	48	447	94
V (μg/g)	162	239	334	545	113	169	543
Vol % Mins.							
Q							
M							
B							
C							
Ser. Feld							
G							
H							
access.							
SG (g/cm3)							

LEGEND

Z = Zamu dolerite
am = amphibolite
Nan = Nanambu complex
gn = gneiss
gt = granite
gr = graphite
ca = carbonaceous
l = limonitic
w = weathered
br = brecciated
py = pyrite
qite = quartzite
h = hematite
m, M = muscovite
q, Q = quartz
c, C = chlorite
st = schist

g, G = garnet
b, B = biotite
p = porphory
K = Kombolgie
ss = sandstone
H = hornblende
access = accessory minerals
SG = specific gravity
t = tourmaline
be = bearing
pe = pegmatite
f, F = feldspar
u = uraninite ore
ser = sericite

APPENDIX 5

ELEMENT CONCENTRATIONS IN CHEMICALLY DEFINED PHASES

A5.1 Concentration of Elements in Whole Samples and TAO Extracts

Concentrations of elements in whole samples (mg/g) (from Nightingale 1983*)

Hole	Depth	Al	Mg	Fe	Mn	Ti	K	U	Zr
DDH52	0-1.5	32	0.5	51	0.05	1.4	0.37	0.64	0.13
	3-3.6	9.6	0.6	8.3	-	0.2	0.04	0.09	
	8.22	96	0.5	5.4	0.02	1.4	3.1	0.03	
	9.6	52	18	320	0.08	0.8	2.4	0.97	
	9.75	71	0.7	68	0.06	1.3	1.8	0.17	
	13.7-15	58	1.7	33	0.02	1	-	0.39	0.13
	20-21.3	65	4	46	0.06	1.8	0.49	1.97	
	35.4	75	5.5	29	0.7	2.8	20	0.22	
	49-50.3	59	44	44	0.13	1.7	5.6	0.21	0.13
DDH1	49-50.3	60	46	38	-	2.1	9.3	0.21	
DDH2	3-3.7	32	1.3	72	0.08	1.4	2.7	0.56	0.04
	3-3.7	31	1.1	84	0.09	1.3	3	0.56	
	15-16.7	85	8.8	85	0.06	4.1	11	1.12	
	20-21.3	76	14	56	0.4	4.8	15	0.86	
DDH3	7.6-9	78	7.4	118	0.14	12	0.7	0.27	
	18.3-20	81	9.7	79	1.2	10	6.5	1.07	
	29-30.3	66	18	58	0.47	3.5	16	0.7	
	36.6-38	55	66	62	0.5	2.6	3.3	0.09	
DDH4	18.3-20	62	18	104	1.2	12	-	0.19	
	27.4-29	72	22	91	1	14	0.1	0.73	0.25
	36.6-38	79	85	138	1.7	8.3	0.37	0.007	
	36.6-38	82	89	147	1.8	8.4	0.63	0.007	
PH55	18.3-20	48	14	78	0.78	11	4.4	0.32	

Element concentrations in TAO extracts (mg/g) (from Nightingale, 1988*)

Hole	Depth	Al	Mg	Fe	Si	Mn	U
DDH52	0-1.5	1.9	0.063	3.9	0.44	0.037	0.098
	0-1.5	1.7	0.056	3.7	0.41	0.038	
	0-1.5	1.5	0.033	1.5	0.33	0.042	
	8.22	3.4	0.045	0.35		0.002	0.006
	9.75	1.3	0.16	0.86		0.008	0.017
	13.7-15	0.77	0.37	0.67	0.44		0.09
	13.7-15	0.83	0.37	1.2	0.41		
	13.7-15	0.68	0.32	1.2	0.37		
	20-21.3	2.1	0.7	3.6	0.86	0.018	1.35
	35.4	1.4	0.055	0.96		0.029	0.098
	39.6	1.5	1.3	2	1.8	0.041	0.088
DDH1	49-50.3	2.1	2.5	3	1.3	0.06	0.103
DDH2	3-3.7	2.6	0.34	10.9	1.6	0.08	0.183
	20-21.3	2.7	2.3	3.5	1.6		0.31
DDH3	7.6-9	0.72	2.7	1.2	0.42	0.87	0.12
	18.3-20	2.9	3.5	3.5	0.91	0.59	0.456
	18.3-20	2.3	3.3	1.4	0.72	0.48	
DDH4	27.4-29	5.2	7.5	6.2	3.8	0.32	0.207

* Nightingale T.J. (1988) Redistribution of Uranium Series Radionuclides during Weathering of the Koongarra Uranium Deposit, Northern Territory. MSc Thesis, The University of Sydney

A5.2 Element Concentrations in TAO Extracts (T) and Residuals (R) (µg/g of whole sample, unless otherwise stated)

extract	T	R	T	R	T	R	T	R	T	R
hole	PH55	PH55	PH55	PH55	PH58	PH58	PH60	PH60	PH60	PH60
depth	14.4	14.4	31.2	31.2	2.2	2.2	6.8	6.8	11.5	11.5
V	49	145	235	188	6		12	97	13	72
Cr	45	331	142	446	1		69	221	68	279
Mn(mg/g)	1.6	1.3	0.7	1.2	0.6		1.9	0.3	0.1	0.3
Co	39	48	29	45	34		4	15	4	21
Ni	19	52	31	28	2		8	42	9	34
Cu	7	28	12	25	2		5	19	8	14
Zn	68	209	128	248	2		7	100	34	141
Br	5.0		27.5	4.1	2.0		2.3	11.5	3.2	9.9
Se		3.3	0.3					1.8		0.8
Rb	2	17	7	7	1		2	90	3	103
Sr	1.0	3.6	0.9	4.3	0.2		0.5	10.1	0.6	8.2
Zr	2	234	3	312	1		7	183	6	141
Mo	1.1	2.7	1.9	1.8	0.2		0.7	1.4	0.9	0.8
Ba	130	92	5	10	8		29	397	16	242
La	1.1	17.3	0.6	15.0	1.0		1.0	39.1	1.2	33.5
Ce	3.6	45.5	1.2	36.2	4.7		1.8	86.7	2.7	75.0
Nd	1.4	22.4	0.8	19.1	1.4		0.8	33.5	1.2	29.5
Sm	0.4	5.9	0.3	5.7	0.3		0.2	6.7	0.3	5.3
Pb	2	10	1	17	17		4	8	3	7
Th	1	8	2	6	1		1	11	2	10
U	118	81	2	2	76		2	3	4	4
B	1	3729	7	768	nd	nd	3	1891	3	957
Na	126	2751	178	576	52	116	63	3010	78	1811
Mg(mg/g)	8.4	11.1	30.6	27.1	0.1	0.3	3.3	19.3	3.0	20.6
Si(mg/g)	3		3		0		1		1	
P	66	1083	602	477	27	301	79	90	101	91
K(mg/g)	0.6	3.3	1.2	1.3	0.1	0.8	0.6	23.2	0.8	19.4
Ca	89	524	326	2658	33	71	41	203	121	262
Fe(mg/g)	16.6	93.9	76.1	51.6	1.3	51.4	8.2	40.7	9.4	37.0
Al(mg/g)	11.3	61.2	42.2	34.1	2.1	21.5	2.9	84.6	3.7	76.6
Ti	47	12372	53	17655	10	2032	43	3225	25	2749

extract	T	R	T	R	T	R	T	R	T	R
hole	PH60	PH60	PH60	PH60	PH89	PH89	PH89	PH89	PH89	PH89
depth	20.5	20.5	29.7	29.7	9.8	9.8	16.0	16.0	29.7	29.7
V	14	50	9	107	5	71	20	33	22	167
Cr	80	417	43	291	48	224	154	571	53	454
Mn(mg/g)	0.1	0.3	0.1	0.9	0.2	0.3	0.1	0.2	0.1	0.7
Co	4	15	4	25	3	12	6	7	5	38
Ni	10	30	10	40	6	31	23	40	18	130
Cu	6	14	8	14	7	25	7	11	3	18
Zn	13	104	36	134	8	52	18	41	29	104
Br	4.2		3.3		2.6	15.9	6.6	3.0	7.6	0.2
Se		0.9	0.2			1.0	0.6	3.3		1.0
Rb	3	95	10	137	1	100	1	26	3	81
Sr	0.3	13.9	0.3	22.0	0.4	17.1	1.1	16.4	0.4	20.1
Zr	6	152	3	310	4	142	1	40	1	91
Mo	1.0	1.0	0.6	3.8	0.6	1.0	1.4	1.6	0.4	0.9
Ba	20	391	36	642	35	475	26	81	9	205
La	1.0	32.1	0.9	40.2	0.8	34.5	1.1	6.6	0.3	12.9
Ce	1.9	73.3	1.8	93.2	1.9	78.7	2.0	13.9	0.6	29.9
Nd	0.9	27.5	0.8	35.0	0.8	29.3	1.2	6.0	0.3	13.3
Sm	0.2	4.8	0.2	5.0	0.2	5.3	0.2	1.2	0.1	2.6
Pb	4	12	3	18	1	8	1	6	1	5
Th	2	8	2	10	1	10	0	2	1	4
U	3	2	1	2	3	6	9	3	1	1
B	2	3074	4	4589	2	1995	2	7	4	4236
Na	86	3516	198	5949	52	2838	75	271	124	3538
Mg(mg/g)	3.8	18.8	4.7	nd	2.0	19.2	3.6	8.8	9.5	64.0
Si(mg/g)	1		2		1		1		2	
P	295	122	344	77	30	153	78	66	188	106
K(mg/g)	1.2	26.6	2.9	39.3	0.4	31.2	0.5	6.9	0.8	19.1
Ca	24	851	24	1301	20	107	87	77	87	988
Fe(mg/g)	10.9	28.7	8.6	43.2	4.6	35.4	12.1	15.6	9.9	70.2
Al(mg/g)	4.9	68.4	7.6	105.0	1.9	84.0	4.1	27.4	8.1	88.7
Ti	48	2722	115	4042	20	2752	25	1366	48	3287

extract	T	R	T	R	T	R	T	R	T	R
hole	PH90	PH90	PH90	PH90	PH91	PH91	PH91	PH91	PH93	PH93
depth	11.5	11.5	16.0	16.0	9.9	9.9	14.4	14.4	9.9	9.9
V	21	59	11	73	11	26	25	52	14	109
Cr	67	336	55	278	101	348	85	337	56	320
Mn(mg/g)	0.2	0.2	0.1	0.2	0.1	0.1	0.7	0.3	0.6	0.5
Co	3	10	4	14	2	4	4	8	13	15
Ni	7	31	8	56	10	15	12	23	9	39
Cu	7	16	4	12	2	0	99	166	4	7
Zn	0	34	2	46	1	25	7	49	7	96
Br	1.3		1.9	9.7		13.3	2.3	26.2	0.2	2.1
Se	0.2	1.1		0.6	0.4		0.1	1.8	0.4	0.6
Rb	1	58	1	73	1	33	4	68	2	122
Sr	0.5	10.6	2.7	18.3	0.2	7.5	0.7	9.8	0.5	16.7
Zr	3	98	1	353	3	339	4	106	2	159
Mo	0.7	2.0	0.4	2.2	1.1	2.2	1.0	2.3	0.6	1.6
Ba	32	283	16	353	19	117	55	284	95	605
La	1.4	20.9	0.8	25.5	1.0	13.3	1.2	20.6	6.6	34.2
Ce	1.7	49.1	1.4	56.8	1.2	29.8	2.4	47.7	13.0	80.9
Nd	1.3	19.5	1.1	22.2	0.7	12.4	1.4	17.7	6.2	29.5
Sm	0.3	3.6	0.3	4.3	0.1	2.2	0.3	3.1	1.2	5.4
Pb	1	4	1	5	1	3	4	6	2	8
Th	1	6	1	8	1	4	1	7	4	14
U	7	7	1	2	2	1	4	2	3	8
B	nd	1575	nd	2354	nd	822	nd	2012	nd	1037
Na	78	3044	51	4630	nd	1773	nd	2834	78	5393
Mg(mg/g)	2.9	13.6	3.9	22.2	1.5	5.2	3.6	11.0	0.7	3.7
Si(mg/g)	2		2		2		3		1	
P	35	62	38	0	25	6	84	111	67	387
K(mg/g)	0.5	18.7	0.5	24.6	0.5	9.7	0.8	16	0.7	27.4
Ca	0	193	0	356	0	928	0	360	12	168
Fe(mg/g)	13.2	26.7	8.0	32.9	9.0	9.6	14.5	23.1	12.3	61.9
Al(mg/g)	3.7	55.4	3.4	67.3	2.6	26.2	5.2	46.8	3.6	106.0
Ti	50	1971	39	2580	58	1276	114	2000	84	3091

extract	T	R	T	R	T	R	T	R	T	R
hole	PH93	PH93	PH94	PH94	PH94	PH94	DDH4	DDH4	DDH4	DDH4
depth	14.4	14.4	9.9	9.9	14.4	14.4	11.1	11.1	21.1	21.1
V	24	108	12	23	9	71	25	234	44	258
Cr	65	239	106	375	67	333	7	199	44	338
Mn(mg/g)	1.1	0.6	0.2	0.1	0.1	0.2	0.4	0.6	0.1	0.5
Co	17	18	5	4	3	9	21	36	11	35
Ni	11	36	12	23	8	34	8	53	12	47
Cu	5	17	7	6	9	27	7	25	1	6
Zn	29	166	9	34		39	33	254	100	421
Br	0.9	1.3		16.6	0.9	6.7	3.2		7.2	4.3
Se	1.0		0.1	1.0	0.6	0.6	0.2	2.0	0.2	1.3
Rb	4	73	2	23	2	136	1	9	1	1
Sr	0.6	5.5	9.2	30.1	0.6	13.3	0.4	3.6	0.3	2.1
Zr	3	223	5	355	5	721	0	240	0	890
Mo	0.6	36.2	1.4	3.0	0.7	3.3	0.2	2.1	0.3	2.6
Ba	220	190	48	105	9	348	20	61	1	16
La	9.9	33.4	7.8	21.6	0.6	35.5	0.3	23.3	0.5	22.2
Ce	12.2	82.2	18.9	37.6	1.0	75.2	1.0	59.6	0.7	62.8
Nd	10.1	37.5	7.7	19.1	0.7	28.7	0.4	30.7	0.6	35.6
Sm	2.0	8.0	1.6	3.3	0.1	4.6	0.1	8.1	0.2	7.2
Pb	2	4	6	11	1	10	2	9	1	12
Th	3	10	7	5	0	13	0	9	0	9
U	4	16	8	4	1	2	74	144	201	412
B	nd	1678	nd	2212	nd	2826	3	5117	2	7183
Na	62	3650	1764	3345	0	5304	87	3989	96	5564
Mg(mg/g)	1.1	4.0	1.8	3.6	2.4	12.4	5.8	14.3	10.5	15.0
Si(mg/g)	2		2		2		2		3	
P	65	639	12	0	81	112	47	1095	34	740
K(mg/g)	0.6	11.1	0.5	6.3	0.7	29.6	0.2	2.1	0.1	1.2
Ca	12	148	0	1248	0	254	55	356	44	398
Fe(mg/g)	13.0	87.7	11.1	13.6	9.7	31.4	6.2	115	17.5	122
Al(mg/g)	4.4	66.3	3.9	49.2	3.1	84.0	5.8	75.4	0.0	99.9
Ti	62	7947	61	1281	49	2480	28	12753	89	12489

extract	T	R	T	R	T	R	T	R	T	R	T	R
hole	M2	M2	M2	M2	M4	M4	M4	M4	M5	M5	M5	M5
depth	10.0	10.0	14.0	14.0	11.0	11.0	15.0	15.0	11.0	11.0	15.0	15.0
V	18	130	22	119	20	248	17	231	15	156	16	150
Cr	31	231	38	284	22	202	22	269	38	264	43	290
Mn(mg/g)	0.3	1.2	0.4	1.5	0.5	0.3	1.1	0.6	0.4	0.9	0.6	0.7
Co	41	134	19	51	17	29	14	38	8	25	7	17
Ni	20	218	32	195	3	36	3	43	5	36	7	39
Cu	102	571	155	618	3	30	4	39	4	29	7	35
Zn	17	111	31	123	8	127	5	143	16	142	12	123
Br	3.7	0.7	5.3			0.7	0.3	0.4				0.1
Se	2.8	1.7	4.4	0.7	0.1	0.5	0.1	0.7	0.2	0.1	0.1	0.6
Rb	1	64	1	47	1	44	1	42	1	95	1	116
Sr	0.1	4.9	0.1	4.9	0.4	19.6	0.4	9.0	1.2	15.3	1.0	14.0
Zr	0	210	0	144	2	156	1	157	2	202	2	178
Mo	1.8	12.4	2.0	12.6	0.2	0.7	0.2	1.2	0.4	2.0	0.5	1.4
Ba	33	231	28	291	85	213	170	235	45	443	58	513
La	11.0	30.7	8.7	21.7	0.3	20.1	0.3	16.7	2.2	38.0	1.7	35.2
Ce	10.7	82.2	7.2	61.8	1.1	47.7	0.7	40.5	1.8	83.3	2.3	79.8
Nd	11.0	28.4	9.4	21.6	0.6	25.9	0.5	22.5	3.2	35.1	2.0	32.1
Sm	2.3	4.9	1.7	4.0	0.2	6.2	0.2	5.0	0.7	6.8	0.5	5.9
Pb	2	5	1	4	5	8	2	5	2	8	6	16
Th	3	11	3	11	0	7	0	6	1	16	1	15
U	1030	831	1743	1146	3	3	5	3	1	4	2	4
B	nd	2926	nd	3698	nd	3425	nd	2721	nd	2353	nd	2445
Na	nd	3915	nd	4061	50	4724	52	4915	61	3854	64	4900
Mg(mg/g)	0.3	2.2	0.4	2.9	5.3	22.5	6.5	37.3	4.7	18.4	3.4	13.9
Si(mg/g)	1		1		2		2		3		2	
P	82	431	86	671	69	448	43	672	102	403	193	796
K(mg/g)	0.4	16.6	0.3	13.7	0.3	9.5	0.3	7.6	0.4	21.5	0.4	21.8
Ca	0	194	0	163	40	261	17	481	40	215	25	358
Fe(mg/g)	8.2	78.2	7.9	76.1	5.7	108	5.0	112	10.5	84.1	11.1	86.6
Al(mg/g)	2.4	97.6	2.7	80.8	3.2	85.2	3.3	79.1	4.8	97.8	4.1	96.4
Ti	117	3882	69	3437	17	6521	16	8324	38	5529	53	4287

A5.3 Semiquantitative ICP-MS Data for TAO Extracts and Residuals (μg/g total sample)

Hole	PH55	PH55	PH55	PH55	PH58	PH60	PH60	PH60	PH60	PH60
Depth (m)	14.4	14.4	31.2	31.2	2.2	6.8	6.8	11.5	11.5	20.5
Extract	TAO*	RES**	TAO	RES	TAO	TAO	RES	TAO	RES	TAO
Ge	0.25	0.80	0.99	0.65	0.04	0.09	1.15	0.20		0.09
Y	1.89	39.40	4.01	42.59	0.87	0.90	11.57	1.33	14.12	1.77
Pd	0.02	0.12	0.04	0.28	0.01	0.01		0.02	0.09	0.02
Cd		1.08	0.01	0.35			0.82	0.15	0.82	
Sn		3.38		6.89		0.02	4.12		9.39	0.26
Cs	0.06	0.50	0.26	0.15	0.08	0.11	4.26	0.11	4.48	0.11
Pr	0.39	6.43	0.22	5.36	0.39	0.27	10.50	0.39	9.29	0.29
Gd	0.67	10.82	0.68	10.50	0.33	0.35	7.67	0.45	6.20	0.34
Dy	0.69	13.17	1.06	13.61	0.38	0.40	4.54	0.50	4.68	0.60
Er	0.56	9.54	0.94	9.57	0.19	0.19	2.48	0.27	2.82	0.36
Yb	0.36	9.45	0.96	10.50	0.20	0.15	2.92	0.24	2.78	0.43
Hf		13.02		15.59		0.08	9.60		7.91	0.15
W	2.25	9.07	10.80	18.37	39.73	4.84	8.95	1.47	5.20	2.13
Pt		25618		11136			6135	0	8121	0
Hg	1.34		2.17	1.16	0.81	0.80	0.62	0.67	1.05	0.67
Ga	3.97	15.28	10.40	8.54	0.43	1.14	21.15	1.16	19.12	1.58
As	0.13	1.74	0.42	3.38	0.10	0.07	2.67	0.07	0.93	0.11
Ag		3.00	0.03	0.67	0.00	0.00	0.10	0.00	0.20	0.00
In										
Sb	0.01	0.93	0.02	0.57	0.01	0.03	0.09	0.03	0.24	0.03
Eu	0.12	2.06	0.10	1.89	0.09	0.07	1.39	0.09	1.22	0.06
Tb	0.11	1.95	0.16	2.07	0.06	0.06	0.93	0.09	0.81	0.10
Ho	0.14	3.29	0.30	2.91	0.07	0.07	0.83	0.10	0.90	0.13
Tm	0.05	1.17	0.16	1.43	0.03	0.03	0.39	0.04	0.44	0.06
Lu	0.07	1.41	0.17	1.45	0.02	0.03	0.37	0.04	0.46	0.05
Ta		0.76			0.05	0.01	0.80	0.01	2.82	
Re	0.14	0.68	0.64	2.67	0.08	0.26	0.79	0.09	0.01	0.34
Au		23.45	0.00	30.16	0.03		9.82	0.01	2.77	
Tl	0.11	0.25	0.04	0.13	0.09	0.03	0.97	0.01	0.97	0.04
Bi	0.10	0.48	0.08	1.36	0.07	0.30	0.29	0.20	0.06	0.25

Hole	PH60	PH60	PH60	PH89	PH89	PH89	PH89	PH89	PH90	PH90
Depth (m)	20.5	29.7	29.7	9.8	16.0	16.0	29.7	29.7	11.5	11.5
Extract	RES	TAO	RES	RES	TAO	RES	TAO	RES	TAO	RES
Ge	0.51	0.18	1.06	0.39	0.15	0.15	0.12	1.73	0.13	0.38
Y	22.20	1.41	15.47	10.95	1.02	4.73	0.87	10.20	1.35	10.41
Pd	0.12	0.02			0.01	0.09		0.04	0.03	0.18
Cd	0.16	0.05	1.24	1.00	0.02	0.56	0.01	0.33	0.11	0.50
Sn	3.71	0.03	4.86	5.84		1.16		1.77		2.51
Cs	1.88	0.37	2.24	1.61	0.05	0.35	0.34	2.38	0.03	1.56
Pr	9.40	0.25	11.32	9.78	0.34	1.98	0.11	4.16	0.34	5.86
Gd	7.01	0.35	7.55	6.71	0.39	1.68	0.21	4.03	0.49	4.18
Dy	6.67	0.52	5.54	4.66	0.38	1.43	0.30	3.82	0.49	3.74
Er	4.30	0.28	3.59	1.94	0.23	0.95	0.19	1.89	0.30	2.16
Yb	3.67	0.30	4.36	2.41	0.26	0.86	0.19	2.36	0.20	2.77
Hf	8.53		15.60	7.95		1.85		4.54		5.53
W	6.18	0.61	10.61	3.82	0.57	2.70	0.17	3.68	0.42	3.07
Pt	6217		4890	3594	0	24310		13164		0.53
Hg	0.27	1.11		0.89	0.91	0.54	0.91	0.29	0.40	1.55
Ga	19.91	1.92	31.96	21.72	1.34	5.26	1.38	17.40	1.34	14.25
As	0.48	0.01	1.01	0.92	0.24	0.28	0.03	0.98	0.13	0.25
Ag	0.01			0.35	0.00	0.64		1.56	0.04	0.23
In										
Sb	1.25	0.02	0.38	0.77	0.03	0.21	0.06	0.28	0.01	0.48
Eu	1.59	0.05	1.56	1.40	0.08	0.32	0.04	0.91	0.09	0.81
Tb	1.24	0.08	1.01	0.78	0.06	0.21	0.04	0.47	0.07	0.73
Ho	1.58	0.11	1.21	0.93	0.08	0.37	0.07	0.76	0.10	0.66
Tm	0.63	0.04	0.45	0.33	0.03	0.15	0.03	0.37	0.05	0.36
Lu	0.69	0.04	0.49	0.32	0.04	0.15	0.03	0.32	0.04	0.32
Ta	0.49	0.02	0.70	0.67						
Re	0.69	0.01	0.11	0.29	0.03	0.29		0.46	0.03	0.26
Au	5.73	0.00	1.39	8.81		8.27		11.74		
Tl	0.70	0.10	0.89	0.66	0.01	0.19	0.02	0.45	0.02	0.38
Bi	0.13	0.80	1.00	0.29	0.31	0.13	0.25	0.20	0.32	0.17

Hole	PH90	PH90	PH91	PH91	PH91	PH91	PH93	PH93	PH93	
Depth (m)	16.0	16.0	9.9	9.9	14.4	14.4	9.9	9.9	14.4	
Extract	TAO	RES	TAO	RES	TAO	RES	TAO	RES	RES	
Ge	0.02	0.42	0.22	0.47	0.24	0.28	0.21	0.33	1.17	
Y	0.99	11.65	0.86	6.70	1.99	9.07	3.02	13.97	28.10	
Pd	0.02	0.05	0.02	0.03	0.02		0.02		0.26	
Cd		0.68		0.49			0.20		0.96	
Sn		3.42		2.12		3.21		5.10	4.06	
Cs	0.06	1.68	0.06	0.91	0.11	1.59	0.15	2.01	1.66	
Pr	0.30	7.27	0.27	3.84	0.35	6.03	1.94	10.36	11.02	
Gd	0.38	5.33	0.42	2.50	0.71	4.59	1.46	7.28	10.58	
Dy	0.33	4.47	0.40	2.46	0.74	3.13	1.04	4.78	10.36	
Er	0.24	2.24	0.24	1.37	0.43	2.14	0.59	2.87	7.15	
Yb	0.18	2.83	0.16	1.49	0.44	2.39	0.54	3.16	7.94	
Hf		18.23		19.13		6.38		9.35	12.38	
W	0.20	3.29	0.64	1.92	0.64	3.58	0.67	3.99	0.70	
Pt	1.26						0.18			
Hg	0.53	0.29	0.10	0.64	0.49	10.63				
Ga	0.98	16.97	1.07	5.84	1.89	12.19	1.78	24.99	17.94	
As	0.05	0.47		0.00	0.28	0.21	0.02		0.71	
Ag	0.05	0.45	0.22	0.48		0.26	0.00	0.22	0.31	
In										
Sb	0.00	0.13	0.03	0.07	0.00	0.24	0.01	1.17	0.59	
Eu	0.06	1.01	0.06	0.44	0.14	0.84	0.29	1.31	2.19	
Tb	0.07	0.80	0.04	0.36	0.09	0.60	0.21	1.00	1.67	
Ho	0.08	0.83	0.07	0.49	0.16	0.71	0.21	0.94	2.15	
Tm	0.03	0.41	0.02	0.18	0.08	0.27	0.09	0.55	1.08	
Lu	0.03	0.36	0.02	0.25	0.08	0.38	0.08	0.48	1.25	
Ta		0.31			0.08		0.04	0.12	0.50	
Re	0.07	0.24	0.03	0.14	0.02	0.18	0.03	0.04	0.03	
Au	0.02		0.00			0.12	0.00		0.03	
Tl	0.01	0.43	0.00	0.26	0.01	0.46	0.06	0.95	0.72	
Bi	0.13	0.10	0.05	0.05	4.50	1.35	0.08	0.16	0.60	

Hole	PH94	PH94	PH94	PH94	DDH4	DDH4	DDH4	DDH4	M2	M2
Depth (m)	9.9	9.9	14.4	14.4	11.1	11.1	21.1	21.1	10.00	10.00
Extract	TAO	RES	TAO	RES	TAO	RES	TAO	RES	TAO	RES
Ge	0.14	0.65	0.23		0.08	1.71	0.13	1.03	0.13	0.08
Y	4.62	9.31	0.79	9.36	0.84	46.70	0.86	21.99	4.80	10.71
Pd	0.05	0.04	0.01		0.01	0.48	0.00	0.13		
Cd	0.05	0.51		0.05	0.18	0.98	0.23	1.25	0.36	0.20
Sn		3.35		3.73	0.08	2.94		3.56		4.98
Cs	0.14	0.91	0.08	3.90	0.03	0.41	0.04	0.03	0.19	1.77
Pr	2.38	5.67	0.21	10.92	0.12	8.36	0.19	9.32	3.40	9.37
Gd	2.59	3.18	0.33	5.92	0.21	13.48	0.29	9.95	2.59	5.41
Dy	1.98	3.01	0.33	4.48	0.27	15.81	0.25	6.81	2.22	4.45
Er	1.07	2.10	0.19	2.13	0.21	10.19	0.13	4.64	0.93	3.29
Yb	0.85	2.34	0.20	2.39	0.16	11.68	0.16	5.63	0.91	4.04
Hf		19.60		40.10		13.70		43.06		11.42
W	1.39	2.28	2.63	5.31	2.09	8.64	0.18	8.36	0.10	3.49
Pt						8590		7641		
Hg	0.06	4.59	0.27	2.64	0.74	0.03	1.62		0.07	
Ga	1.71	10.52	1.14	17.59	1.15	17.43	2.82	22.42	0.65	19.55
As	0.52	0.28	0.06	0.11	0.02	2.06	0.02	1.26	0.06	0.26
Ag		0.32	0.00	0.54		0.89		0.57		5.25
In										
Sb	0.13	0.14	0.00	0.06	0.02	0.84	0.01	0.75		0.15
Eu	0.30	0.57	0.10	1.37	0.03	2.46	0.05	1.88	0.38	1.23
Tb	0.45	0.59	0.06	0.84	0.05	2.43	0.05	1.14	0.39	0.76
Ho	0.38	0.68	0.06	0.72	0.07	3.48	0.05	1.58	0.32	0.95
Tm	0.14	0.29	0.03	0.26	0.03	1.70	0.02	0.82	0.11	0.43
Lu	0.10	0.35	0.03	0.43	0.03	1.80	0.02	0.90	0.14	0.49
Ta	0.24	0.17	0.01		0.02	0.86		0.80	0.06	2.44
Re	0.07	0.21	0.38		0.14	1.42	0.02	1.60	0.03	0.01
Au						13.35		3.27		
Tl	0.05	0.22	0.00	0.90	0.04	0.14	0.01	0.09	0.01	0.34
Bi	0.59	0.24	0.20	0.25	0.06	0.90	0.00		0.16	0.77

Hole	M2	M2	M4	M4	M4	M4	M5	M5	M5	M5
Depth (m)	14	14	11	11	15	15	11	11	15	15
Extract	TAO	RES	TAO	RES	TAO	RES	TAO	RES	TAO	RES
Ge		1.08	0.05	1.45	0.05				0.11	
Y	4.86	8.39	1.62	30.85	1.01	23.43	5.13	22.34	3.05	15.67
Pd	0.07		0.03		0.01		0.04		0.04	
Cd	0.38	0.08		3.13	0.10		0.01			
Sn		8.55		2.38		2.49	0.00	3.86		4.38
Cs	0.23	1.19	0.02	1.13	0.01	1.47	0.03	2.09	0.04	2.64
Pr	2.48	7.57	0.19	7.28	0.11	6.61	0.80	11.58	0.59	10.75
Gd	1.89	5.43	0.32	10.87	0.33	7.17	1.57	8.25	0.94	8.27
Dy	1.54	3.46	0.55	12.22	0.36	7.27	1.48	9.51	1.01	6.59
Er	0.74	2.54	0.35	7.80	0.25	6.08	0.83	7.75	0.64	4.59
Yb	0.23	2.68	0.31	8.63	0.17	7.52	0.80	5.81	0.60	4.38
Hf		9.32		9.39		9.25	0.20	5.95		11.28
W	0.21	2.61	1.16	0.64	1.78	0.41	2.98	12.17	3.36	6.06
Pt							0.57	5.67		
Hg	0.16	0.04	0.15		0.06		0.00		0.21	
Ga	0.75	16.80	1.86	17.32	2.54	15.46	1.28	21.38	1.48	22.12
As		0.43	0.01	0.08	0.00	0.20	0.00		0.01	0.33
Ag	0.18	4.87		2.59	6.97		0.05	5.23	0.02	0.33
In						0.56				
Sb	0.01	0.79		0.59		0.24	0.00	0.28	0.01	0.60
Eu	0.51	1.18	0.08	2.60	0.08	1.47	0.27	2.20	0.19	2.00
Tb	0.31	0.64	0.08	1.71	0.06	2.08	0.23	1.49	0.17	0.95
Ho	0.30	0.68	0.13	2.71	0.08	0.96	0.32	1.84	0.21	1.36
Tm	0.15	0.38	0.06	1.25	0.03	1.10	0.11	0.92	0.09	0.73
Lu	0.06	0.37	0.04	1.31	0.03	0.03	0.11	1.03	0.09	0.73
Ta	0.01	2.05		0.49	0.03		0.01	0.10	0.03	1.03
Re	0.05		0.08		0.02		0.17	0.07	0.21	
Au		0.12				0.38	0.02			
Tl	0.04	0.34	0.01	0.34	0.03	0.37	0.02	0.50	0.11	0.89
Bi	0.10	1.31	0.02	0.34	0.03		0.10	0.35	0.10	0.55

* TAO = TAO extract
** RES = TAO residual

APPENDIX 6 URANIUM SERIES DISEQUILIBRIA RESULTS

A6.1 Uranium Series Disequilibria in Accessible (TAO extractable (TAO)) and Inaccessible (TAO residual (RES)) Phases and in Bulk Rock Determined by Alpha Spectrometry

HOLE	DDH52*	DDH52*	DDH52*	DDH52*	DDH52*	DDH52*	DDH52	DDH52*
DEPTH (m)	0-1.1	0-1.1	0-1.1	1.1-2.2	1.9	2.2	2.2	2.2-3.2
TAO [U] (μg/g)***	98 (2)	86 (2)	89 (2)		81 (2)			31
TAO $^{234}U/^{238}U$	0.91 (.01)	0.90 (.01)	0.92 (.01)		0.90 (.01)			0.92
TAO $^{230}Th/^{234}U$	1.87 (.06)	1.70 (.08)	1.61 (.06)		0.99 (.05)			1.11
TAO $^{226}Ra/^{230}Th$								
RES [U] (μg/g)***	**539				**333			**58
RES $^{234}U/^{238}U$	1.44				1.22			1.31
RES $^{230}Th/^{234}U$	1.09				1.51			1.30
RES $^{226}Ra/^{230}Th$								
BULK [U] (μg/g)	637 (12)			383 (12)	414 (9)	66 (2)	36 (1)	89 (2)
BULK $^{234}U/^{238}U$	1.36 (.01)			1.22 (.02)	1.16 (.02)	1.17 (.02)	1.09 (.04)	1.17 (.02)
BULK $^{230}Th/^{234}U$	1.59 (.05)			1.63 (.06)	1.43 (.04)	1.23 (.04)	1.06 (.03)	1.25 (.04)
BULK $^{226}Ra/^{230}Th$	0.68			0.7				0.75

HOLE	DDH52*	DDH52*	DDH52*	DDH52	DDH52	DDH52	DDH52
DEPTH (m)	5.8	6.8	6.9	6.9	7.8	9.7-10.8	9.7-10.8
TAO [U] (μg/g)	6.4 (.2)		16.0 (.3)			86 (2)	87 (2)
TAO $^{234}U/^{238}U$	0.89 (.01)		0.92 (.01)			0.83 (.01)	0.80 (.01)
TAO $^{230}Th/^{234}U$	2.63 (.12)		0.95 (.04)			0.55 (.03)	
TAO $^{226}Ra/^{230}Th$							
RES [U] (μg/g)	**26.6		**152				
RES $^{234}U/^{238}U$	1.20		1.13				
RES $^{230}Th/^{234}U$	1.85		1.47				
RES $^{226}Ra/^{230}Th$							
BULK [U] (μg/g)	33 (1)	965 (20)	168 (4)	173 (4)	88 (2)		
BULK $^{234}U/^{238}U$	1.14 (.02)	1.05 (.02)	1.11 (.01)	1.20 (.02)	1.24 (.01)		
BULK $^{230}Th/^{234}U$	1.97 (.08)	1.12 (.04)	1.46 (.03)	1.33 (.03)	1.29 (.05)		
BULK $^{226}Ra/^{230}Th$	1.21		0.98				

* Nightingale (1988) (USNRC contract, Annual Report 1986-1987)

** Values calculated by difference or summation of other extractions (errors not estimated).

*** Amounts are per gram of whole rock.

Values in parentheses represent uncertainty of 1σ.

HOLE	DDH52*	DDH52*	DDH52*	DDH52	DDH52*	DDH52	DDH52
DEPTH (m)	9.7-10.8	11.9-12.9	14-15.1	17.3	18.3	20	22.3
TAO [U] (μg/g)	90 (2)		1350 (25)		3380 (70)		215 (15)
TAO ^{234}U/^{238}U	0.80 (.01)		0.95 (.01)		0.98 (.01)	0.65 (.01)	0.77 (.01)
TAO ^{230}Th/^{234}U	0.67 (.03)		0.82 (.03)		0.96 (.02)		
TAO ^{226}Ra/^{230}Th							
RES [U] (μg/g)	~302		~620		~720		328 (21)
RES ^{234}U/^{238}U	1.28		1.20		1.0		1.33 (.05)
RES ^{230}Th/^{234}U	1.28		1.22		1.19		
RES ^{226}Ra/^{230}Th							
BULK [U] (μg/g)	392 (8)	692 (16)	1970 (40)	678	4100 (90)	792 (20)	543 (15)
BULK ^{234}U/^{238}U	1.17 (.01)	1.17 (.02)	1.03 (.01)	1.01	0.99 (.01)	1.02 (.02)	1.11 (.02)
BULK ^{230}Th/^{234}U	1.14 (.03)	1.18 (.03)	1.01 (.04)	1.08	1.00 (.02)	0.97 (.02)	1.16 (.02)
BULK ^{226}Ra/^{230}Th	1.01		0.87		0.76		

HOLE	DDH52*	DDH52*	DDH52*	DDH52+	DDH1*	DDH1	DDH1
DEPTH (m)	25	28	29.7	34.5-35.6	2.2	2.2	4.7
TAO [U] (μg/g)	98 (2)	88 (2)		122 (4)			1028
TAO ^{234}U/^{238}U	0.65 (.01)	0.80 (.01)		0.93 (.01)			0.60
TAO ^{230}Th/^{234}U	0.45 (.03)			0.83 (.04)			0.29
TAO ^{226}Ra/^{230}Th							
RES [U] (μg/g)	~121	~231		~91			1277
RES ^{234}U/^{238}U	1.28	1.17		1.10			1.34
RES ^{230}Th/^{234}U	1.18			1.25			1.15
RES ^{226}Ra/^{230}Th							
BULK [U] (μg/g)	219 (5)	319 (6)	133 (3)	213 (3)	641 (12)	835 (11)	2305
BULK ^{234}U/^{238}U	1.00 (.01)	1.07 (.01)	1.00 (.01)	1.00 (.02)	1.12 (.01)	1.18 (.02)	1.01
BULK ^{230}Th/^{234}U	0.99 (.02)	1.00 (.02)		1.03 (.03)	1.17 (.03)	1.09 (.03)	0.92
BULK ^{226}Ra/^{230}Th	0.92			1.12			

HOLE	DDH1	DDH1	DDH1*	DDH1	DDH1*	DDH1*	DDH2*	DDH2*
DEPTH (m)	4.7	9.3	14.4-15.1	19.4-20.5	29.3	34.5-35.6	2.6-3.2	11.9
TAO [U] (µg/g)	~1069			~76130	8.5 (.2)	103 (3)	183 (4)	336 (6)
TAO $^{234}U/^{238}U$	0.61			0.97	0.89 (.02)	1.04 (.01)	0.85 (.01)	0.67 (.01)
TAO $^{230}Th/^{234}U$	0.29			0.87	0.59 (.04)	0.90 (.03)	0.41 (.02)	0.32 (.02)
TAO $^{226}Ra/^{230}Th$								
RES [U] (µg/g)	~1201			~6205	~21.5	~111	~372	~599 (19)
RES $^{234}U/^{238}U$	1.32			1.07	1.07	0.96	1.10	1.17 (.03)
RES $^{230}Th/^{234}U$	1.24			1.70	1.06			1.18 (.04)
RES $^{226}Ra/^{230}Th$								
BULK [U] (µg/g)	2271 (50)	2353 (51)	815 (20)	82300	30 (1)	214 (5)	555 (13)	935 (18)
BULK $^{234}U/^{238}U$	1.00 (.01)	0.95 (.01)	1.03 (.01)	0.99 (.01)	1.02 (.01)	1.00 (.02)	1.02 (.01)	.99 (.01)
BULK $^{230}Th/^{234}U$	1.01 (.02)	0.87 (.02)	1.02 (.02)	1.04 (.03)	0.94 (.04)	1.04 (.04)	0.87 (.02)	0.97 (.02)
BULK $^{226}Ra/^{230}Th$						1.14	1.76	

HOLE	DDH2	DDH2	DDH2*	DDH2	DDH2	DDH3	DDH3*	DDH3
DEPTH (m)	13.2-14.5	15.9-16	17.2-18.5	33-34.3	63.4-64.7	1.2-3.3	5.8-7.0	8.2-9.3
TAO [U] (µg/g)	464 (9)		310 (7)	~17655			120 (3)	
TAO $^{234}U/^{238}U$	0.70 (.01)		0.75 (.01)	1.11			0.70 (.01)	
TAO $^{230}Th/^{234}U$	0.42 (.02)		0.47 (.02)	0.87			0.64 (.03)	
TAO $^{226}Ra/^{230}Th$								
RES [U] (µg/g)	~656		~554	~64845			~316	
RES $^{234}U/^{238}U$	1.21		1.13	0.96			1.06	
RES $^{230}Th/^{234}U$	1.24		1.14	0.97			1.11	
RES $^{226}Ra/^{230}Th$								
BULK [U] (µg/g)	1120 (20)	1070	864 (20)	82500	35700	267 (6)	436 (8)	559 (12)
BULK $^{234}U/^{238}U$	1.00 (.01)	0.89	1.00 (.01)	1.00 (.01)	0.99	0.97 (.01)	0.96 (.01)	1.01 (.01)
BULK $^{230}Th/^{234}U$	1.00 (.02)	0.90	1.04 (.03)	0.99 (.02)	1.00	0.85 (.03)	1.02 (.03)	1.00 (.04)
BULK $^{226}Ra/^{230}Th$	0.91			1.11				

HOLE	DDH3*	DDH3	DDH3	DDH3*	DDH3*	DDH3*	DDH3*
DEPTH (m)	10.5-11.7	10.5-11.7	10.9	14-15.2	14-15.2	14-15.2	16.3-17.5
TAO [U] (μg/g)		~204		456 (8)	426 (9)	441 (9)	288 (5)
TAO $^{234}U/^{238}U$		0.67		0.62 (.01)	0.63 (.01)	0.62 (.01)	0.64 (.01)
TAO $^{230}Th/^{234}U$		0.23		0.45 (.03)	0.40 (.01)	0.39 (.01)	0.35 (.02)
TAO $^{226}Ra/^{230}Th$							
RES [U] (μg/g)		~564		~614		~630	~677
RES $^{234}U/^{238}U$		1.06		1.09		1.08	1.04
RES $^{230}Th/^{234}U$		0.97		1.23		1.07	1.08
RES $^{226}Ra/^{230}Th$							
BULK [U] (μg/g)	769 (25)		820 (12)	1070 (20)			965 (20)
BULK $^{234}U/^{238}U$	0.96 (.02)		0.97(.01)	0.89 (.01)			0.92 (.01)
BULK $^{230}Th/^{234}U$	1.00 (.04)		0.92 (.03)	0.90 (.03)			0.93 (.02)
BULK $^{226}Ra/^{230}Th$			0.99	1.08			

HOLE	DDH3*	DDH3*	DDH3	DDH3	DDH3	DDH3	DDH3
DEPTH (m)	16.3-17.5	16.3-17.5	16.3	22.3-23.3	28-29.3	32.4	32.9
TAO [U] (μg/g)	274 (6)	290 (7)	~275	212 (5)	79 (2)		
TAO $^{234}U/^{238}U$	0.64 (.01)	0.64 (.01)	0.66	0.76 (.01)	0.99 (.01)		
TAO $^{230}Th/^{234}U$	0.32 (.01)		0.27				
TAO $^{226}Ra/^{230}Th$							
RES [U] (μg/g)			~691	~483	~8		
RES $^{234}U/^{238}U$			1.08	1.04	0.97		
RES $^{230}Th/^{234}U$			1.06				
RES $^{226}Ra/^{230}Th$							
BULK [U] (μg/g)				695 (15)	87 (3)	30	9 (.3)
BULK $^{234}U/^{238}U$				0.95 (.01)	0.99 (.02)	1.03 (.01)	1.03 (.02)
BULK $^{230}Th/^{234}U$				0.94 (.04)	1.03 (.05)	0.97 (.03)	
BULK $^{226}Ra/^{230}Th$				1.37		1.55	

HOLE	DDH3	DDH3	DDH4	DDH4	DDH4	DDH4	DDH4
DEPTH (m)	33.4	68.6	3.5-4.7	5.8-7.0	7.7	8.2-9.3	10.5
TAO [U] (μg/g)				163 (4)			71 (8)
TAO $^{234}U/^{238}U$				0.69 (.01)			0.64 (.03)
TAO $^{230}Th/^{234}U$							0.64 (.08)
TAO $^{226}Ra/^{230}Th$							0.41
RES [U] (μg/g)				~283			87 (2)
RES $^{234}U/^{238}U$				1.01			1.01 (.01)
RES $^{230}Th/^{234}U$							2.40 (.16)
RES $^{226}Ra/^{230}Th$							1.04
BULK [U] (μg/g)	11 (.5)	331	15 (.5)	446 (13)	280 (6)	221 (6)	
BULK $^{234}U/^{238}U$	1.07 (.05)	1.00	1.04 (.03)	0.89 (.02)	0.99 (.02)	0.92 (.02)	
BULK $^{230}Th/^{234}U$	0.80 (.03)	1.02	1.32 (.08)	0.88 (.03)	0.85 (.02)	0.92 (.05)	
BULK $^{226}Ra/^{230}Th$				0.86			

HOLE	DDH4	DDH4*	DDH4	DDH4	DDH4*	DDH4	DDH4*
DEPTH (m)	13.3	14-15.2	14	14	18.4	18.7-19.8	21-22.2
TAO [U] (μg/g)		96 (2)	~186	217 (9)			207 (5)
TAO $^{234}U/^{238}U$		0.66 (.01)	0.67	0.69 (.02)			0.64 (.01)
TAO $^{230}Th/^{234}U$			0.29	0.63 (.03)			0.45 (.02)
TAO $^{226}Ra/^{230}Th$				0.20			
RES [U] (μg/g)		~95	~361	372 (17)			~526
RES $^{234}U/^{238}U$		1.16	0.99	0.93 (.03)			0.92
RES $^{230}Th/^{234}U$			1.00	1.23 (.06)			1.00
RES $^{226}Ra/^{230}Th$				0.92			
BULK [U] (μg/g)	88 (3)	191 (4)	536 (12)	~589	3.2 (.1)	536 (13)	733 (17)
BULK $^{234}U/^{238}U$	1.03 (.04)	0.90 (.01)	0.87 (.01)	0.84	0.89 (.02)	0.87 (.01)	0.84 (.01)
BULK $^{230}Th/^{234}U$	1.50 (.04)	0.85 (.05)	0.90 (.02)	1.05		0.90 (.02)	0.88 (.03)
BULK $^{226}Ra/^{230}Th$		1.07		0.79			0.81

HOLE	DDH4*	DDH4*	DDH4	DDH4*	DDH4*	DDH4*	DDH40
DEPTH (m)	21-22.2	21-22.2	23.6	28-29.2	31.8	31.5-32.8	19.5
TAO [U] (μg/g)	199 (4)	206 (5)					
TAO $^{234}U/^{238}U$	0.65 (.01)	0.63 (.01)					
TAO $^{230}Th/^{234}U$							
TAO $^{226}Ra/^{230}Th$							
RES [U] (μg/g)							
RES $^{234}U/^{238}U$							
RES $^{230}Th/^{234}U$							
RES $^{226}Ra/^{230}Th$							
BULK [U] (μg/g)			274 (8)	7.0 (0.2)	2.1 (0.1)	12.4 (0.4)	356
BULK $^{234}U/^{238}U$			0.86 (.03)	1.04 (.01)	1.00 (.02)	0.97 (.01)	1.09
BULK $^{230}Th/^{234}U$			0.82 (.03)			0.95 (.04)	1.03
BULK $^{226}Ra/^{230}Th$							

HOLE	DDH40	DDH54	DDH58	DDH58	DDH58	DDH58	DDH58
DEPTH (m)	25.5	13.5-15	3.03	9.1	18.2	21.2	24.3
TAO [U] (μg/g)		226 (6)		~780	~1927	~358	~259
TAO $^{234}U/^{238}U$		0.73 (.02)		0.67	0.76	0.74	0.78
TAO $^{230}Th/^{234}U$		0.72 (.04)		0.31	0.52	0.40	0.32
TAO $^{226}Ra/^{230}Th$							
RES [U] (μg/g)		~737 (22)		~920	~2693	~732	~467
RES $^{234}U/^{238}U$		1.07 (.02)		1.38	1.23	1.22	1.19
RES $^{230}Th/^{234}U$		1.24 (.07)		1.48	1.39	1.36	1.37
RES $^{226}Ra/^{230}Th$							
BULK [U] (μg/g)	56	963 (22)	234 (6)	1700 (44)	4620(110)	1090 (24)	726 (17)
BULK $^{234}U/^{238}U$	1.01	0.96 (.01)	1.03 (.02)	0.99 (.02)	1.04 (.01)	1.04 (.01)	0.98 (.02)
BULK $^{230}Th/^{234}U$	1.01	1.18 (.03)	0.98 (.03)	1.05 (.04)	1.06 (.03)	1.09 (.03)	1.10 (.03)
BULK $^{226}Ra/^{230}Th$							

HOLE	DDH60	DDH60	DDH60	DDH62	DDH62	DDH85	DDH85	DDH85
DEPTH (m)	3.03	21.2	27.3	9.12	15.2	6.1	9.12	12.2
TAO [U] (μg/g)				¯198	¯3120	¯6.2	¯28	
TAO $^{234}U/^{238}U$				0.76	0.91	0.98	0.79	
TAO $^{230}Th/^{234}U$				0.74	0.80	2.44	0.98	
TAO $^{226}Ra/^{230}Th$								
RES [U] (μg/g)				¯401	¯2812	¯38	¯347	
RES $^{234}U/^{238}U$				1.08	1.07	0.94	1.03	
RES $^{230}Th/^{234}U$				1.22	1.05	2.14	1.19	
RES $^{226}Ra/^{230}Th$								
BULK [U] (μg/g)	87 (2)	150 (3)	4.7 (.02)	605 (14)	5907 (141)	45 (1)	377 (8)	72 (2)
BULK $^{234}U/^{238}U$	0.94 (.02)	0.88 (.01)	1.02 (.04)	0.98 (.01)	0.98 (.01)	0.93 (.01)	1.05 (.01)	0.96 (.02)
BULK $^{230}Th/^{234}U$	0.94 (.06)	0.79 (.03)	1.03 (.06)	1.01 (.02)	0.92 (.05)	2.10 (.06)	1.13 (.02)	0.98 (.04)
BULK $^{226}Ra/^{230}Th$								

HOLE	DDH85	DDH85	DDH85	DDH85	DDH87	PH55	PH55	PH55*
DEPTH (m)	15.2	17.5-18.7	21.2	24.3	24.3	7.6	13.7-15.2	18.3-20
TAO [U] (μg/g)	¯34	110	¯116		¯21		132 (5)	152 (3)
TAO $^{234}U/^{238}U$	0.84	0.77 (.01)	0.80		0.64		0.64 (.03)	0.68 (.01)
TAO $^{230}Th/^{234}U$	0.69		0.40		0.38		0.61 (.05)	
TAO $^{226}Ra/^{230}Th$							2.39	
RES [U] (μg/g)	¯150	¯313	¯325		41 (1)		85 (3)	¯164
RES $^{234}U/^{238}U$	1.06	1.08	1.03		0.95 (.02)		1.24 (.03)	1.08
RES $^{230}Th/^{234}U$	1.21		1.15		1.10 (.08)		1.31 (.07)	
RES $^{226}Ra/^{230}Th$							1.31	
BULK [U] (μg/g)	186 (4)	423 (11)	446 (11)	80 (2)	61 (2)	103 (3)	¯217	316 (7)
BULK $^{234}U/^{238}U$	1.05 (.01)	1.00 (.01)	0.99 (.01)	1.02 (.02)	0.83 (.01)	0.98 (.01)	0.88	0.89 (.01)
BULK $^{230}Th/^{234}U$	1.12 (.02)		1.02 (.02)	0.94 (.05)	0.95 (.02)	0.94 (.02)	1.00	0.83 (.02)
BULK $^{226}Ra/^{230}Th$								0.92

HOLE	PH55	PH56	PH56	PH58	PH58*	PH58	PH58	PH58
DEPTH (m)	18.3	13.5	13.5	1.5	1.5-3	1.5-3	1.5-3	1.5-3
TAO [U] (μg/g)	¯146	¯74	¯68				76 (2)	66
TAO $^{234}U/^{238}U$	0.67	0.75	0.79				0.82 (.02)	0.78
TAO $^{230}Th/^{234}U$	0.33	0.61	0.65				0.42 (.02)	0.42
TAO $^{226}Ra/^{230}Th$							0.08	
RES [U] (μg/g)	¯169	¯262	¯255				71 (5)	
RES $^{234}U/^{238}U$	1.09	1.01	0.99				0.75 (.06)	
RES $^{230}Th/^{234}U$	0.97	1.24	1.30				1.01 (.08)	
RES $^{226}Ra/^{230}Th$							2.50	
BULK [U] (μg/g)		323 (10)		603	235 (5)	623 (9)	¯147	
BULK $^{234}U/^{238}U$		1.00 (.02)			0.96 (.01)	0.97 (.01)	0.78	
BULK $^{230}Th/^{234}U$		1.18 (.03)			0.74 (.03)	0.70 (.02)	0.69	
BULK $^{226}Ra/^{230}Th$				0.96	0.99			

HOLE	PH58*	PH58*	PH60	PH60	PH60	PH60	PH60	PH60
DEPTH (m)	6-7.6	24.4	1.5-3	1.5-3	6.1-7.6	6.1-7.6	10.7-12.2	19.8
TAO [U] (μg/g)		3.5 (.1)	87 (2)		2.2 (.1)	2.5 (.1)	5 (.1)	2.5 (.1)
TAO $^{234}U/^{238}U$		0.80 (.01)	0.82 (.01)		0.84 (.02)	0.86 (.03)	0.87 (.02)	1.02 (.03)
TAO $^{230}Th/^{234}U$		0.73 (.03)	0.32 (.03)		1.25 (.06)		1.21 (.06)	0.88 (.04)
TAO $^{226}Ra/^{230}Th$					0.24		0.11	0.28
RES [U] (μg/g)		¯5.5	¯142			4.0 (.2)	4 (.1)	2.4 (.1)
RES $^{234}U/^{238}U$		1.04	1.02		1.05 (.02)	1.03 (.05)	0.94 (.02)	0.91 (.02)
RES $^{230}Th/^{234}U$		1.15	0.94			1.28 (.06)	1.14 (.06)	1.07 (.07)
RES $^{226}Ra/^{230}Th$						1.15	1.32	1.60
BULK [U] (μg/g)	25 (1)	8.8 (.2)	229 (5)	261 (4)		¯6.5	¯9	¯4.9
BULK $^{234}U/^{238}U$	1.00 (.01)	0.95 (.02)	0.94 (.01)	0.97 (.01)		0.96	0.90	0.97
BULK $^{230}Th/^{234}U$	0.71 (.06)	1.03 (.1)	0.74 (.03)	0.71 (.02)			1.18	0.96
BULK $^{226}Ra/^{230}Th$							0.65	0.88

HOLE	PH60	PH89*	PH89	PH89	PH89	PH89	PH90	PH90
DEPTH (m)	30.5	3-4.6	3-4.6	9.1-10.7	15.2	29	3-4.6	3-4.6
TAO [U] (μg/g)	1 (.05)			2.9 (.1)	11 (.5)	0.9 (.1)		
TAO $^{234}U/^{238}U$	1.21 (.06)			0.88 (.02)	0.92 (.03)	0.67 (.04)		
TAO $^{230}Th/^{234}U$	1.61 (.10)			0.91 (.04)	0.70 (.04)	1.13 (.08)		
TAO $^{226}Ra/^{230}Th$	0.68			0.36		0.24		
RES [U] (μg/g)	5.6 (.2)			6 (.2)	3.6 (.1)	1.1 (.1)		
RES $^{234}U/^{238}U$	0.75 (.03)			0.94 (.02)	1.06 (.04)	1.34 (.07)		
RES $^{230}Th/^{234}U$	0.51 (.03)			1.22 (.13)	1.34 (.07)	1.64 (.13)		
RES $^{226}Ra/^{230}Th$	1.44			1.31		0.97		
BULK [U] (μg/g)	~6.6	225 (4)	263 (5)	~8.9	~14.6	~2.0	51 (1)	63 (2)
BULK $^{234}U/^{238}U$	0.82	0.97 (.01)	0.95 (.02)	0.92	0.95	1.04	1.03 (.01)	0.99 (.02)
BULK $^{230}Th/^{234}U$	0.76	0.69 (.03)	0.69 (.02)	1.12	0.88	1.50	1.11 (.04)	1.08 (.03)
BULK $^{226}Ra/^{230}Th$	1.08	0.92		1.07		0.81	0.87	

HOLE	PH90	PH90	PH91	PH91	PH93	PH93	PH93	PH94
DEPTH (m)	10.7	15.2	9.2	13.7	6.1	9.1	13.7	9.2
TAO [U] (μg/g)	8.6 (.3)	1.3 (.1)	2 (.1)	4.2 (.2)	3.9 (.1)	3.6 (.1)	5.1 (.2)	8.8 (.3)
TAO $^{234}U/^{238}U$	0.93 (.02)	0.87 (.05)	0.95 (.04)	0.84 (.03)	0.81 (.03)	0.80 (.02)	0.76 (.02)	0.86 (.02)
TAO $^{230}Th/^{234}U$	1.40 (.04)	1.71 (.11)	1.01 (.05)	0.94 (.05)	0.65 (.03)	0.93 (.04)	0.98 (.04)	3.04 (.13)
TAO $^{226}Ra/^{230}Th$	1.19	0.77	1.27	0.50	1.30 (.06)	3.65	1.11	0.34
RES [U] (μg/g)	7.7 (.4)	2.5 (.12)	1.3 (.1)	2.4 (.1)	13 (.5)	6.3 (.3)	16 (.4)	3.2 (.1)
RES $^{234}U/^{238}U$	1.18 (.06)	1.84 (.05)	0.97 (.06)	0.96 (.05)	0.95 (.03)	1.00 (.03)	0.82 (.01)	1.05 (.04)
RES $^{230}Th/^{234}U$	1.80 (.11)	1.43 (.12)	1.79 (.10)	1.31 (.07)	0.92 (.04)	1.16 (.07)	1.36 (.06)	1.56 (0.8)
RES $^{226}Ra/^{230}Th$	1.25	1.46	3.05	6.03	1.07 (.07)	0.89	0.90	1.84
BULK [U] (μg/g)	~16.3	~3.8	~3.3	~6.6	~16.9	~9.9	~21.1	~12
BULK $^{234}U/^{238}U$	1.05	0.85	0.96	0.88	0.92	0.93	0.80	0.91
BULK $^{230}Th/^{234}U$	1.61	1.53	1.32	1.08	0.86	1.09	1.27	2.59
BULK $^{226}Ra/^{230}Th$	1.23	1.19	2.23	3.15	1.11	1.63	0.94	0.62

HOLE	PH94	M1	M1	M1	M1 19	M2	M2	M3
DEPTH (m)	13.7	5	13 white	13 red	19	10	14	4
TAO [U] (μg/g)	0.7 (.1)	7.2 (.2)	3.6 (.2)	26 (1)	122 (4)	1423 (88)	1837 (112)	31 (1)
TAO $^{234}U/^{238}U$	0.99 (.12)	0.84 (.04)	0.94 (.05)	0.96 (.04)	0.88 (.04)	0.69 (.01)	0.74 (.01)	0.83 (.03)
TAO $^{230}Th/^{234}U$	3.25 (.44)	1.61 (.09)	1.32 (.07)	1.07 (.06)	0.97 (.05)	0.58 (.04)	0.78 (.05)	0.88 (.04)
TAO $^{226}Ra/^{230}Th$	0.26	1.91 (.10)			1.51 (.07)	1.29	0.67	2.36 (.10)
RES [U] (μg/g)	2.8 (.1)	24 (1)	25 (1)	239 (6)	221 (7)	1012	1574	94 (3)
RES $^{234}U/^{238}U$	0.95 (.04)	1.20 (.05)	0.84 (.02)	1.05 (.04)	1.04 (.04)	1.31	0.99	1.13 (.04)
RES $^{230}Th/^{234}U$	1.26 (.07)	1.41 (.08)	1.49 (.07)	1.09 (.04)	1.14 (.05)	1.19	1.72	1.08 (.05)
RES $^{226}Ra/^{230}Th$	3.74	0.85 (.05)			0.85 (.04)	0.88	0.58	0.76 (.03)
BULK [U] (μg/g)	~3.5	~31.2	~28.6	~265	~343	~2435	~3411	~125
BULK $^{234}U/^{238}U$	0.96	1.12	0.85	1.04	0.98	0.95	0.86	1.05
BULK $^{230}Th/^{234}U$	1.66	1.44	1.47	1.09	1.09	0.93	1.28	1.04
BULK $^{226}Ra/^{230}Th$	2.34	1.06			1.04	0.99	0.61	1.02

HOLE	M3	M3	M3	M3	M4	M4	M5	M5
DEPTH (m)	13 gen.	13 white	13 yellow	20	11	15	5	11
TAO [U] (μg/g)	109 (5)	52 (2)	163 (8)	204 (7)	2 (.1)	5.5 (.2)	19 (1)	0.9 (.04)
TAO $^{234}U/^{238}U$	0.70 (.01)	0.96 (.03)	0.70 (.01)	0.75 (.02)	0.80 (.05)	1.01 (.02)	0.81 (.02)	1.02 (.05)
TAO $^{230}Th/^{234}U$	0.51 (.02)	1.33 (.06)	0.64 (.03)	0.85 (.04)	1.24 (.07)	0.90 (.03)	0.43 (.02)	1.49 (.09)
TAO $^{226}Ra/^{230}Th$				1.07 (.04)	0.89	0.57	1.59 (.06)	0.79
RES [U] (μg/g)	237 (7)	52 (1)	329 (8)	118 (5)	2.3 (.1)	2.9 (.1)	38 (1)	4.3 (.2)
RES $^{234}U/^{238}U$	1.06 (.03)	1.42 (.03)	1.12 (.02)	1.16 (.04)	1.02 (.04)	1.06 (.04)	1.04 (.02)	1.00 (.04)
RES $^{230}Th/^{234}U$	1.13 (.03)	2.94 (.10)	1.39 (.04)	1.26 (.06)	1.37 (.07)	1.34 (.06)	0.94 (.04)	1.31 (.1)
RES $^{226}Ra/^{230}Th$				0.91 (.03)	1.30	1.52	1.02(.02)	0.96
BULK [U] (μg/g)	~346	~104	~492	~322	~4.3	~8.4	~57	~5.2
BULK $^{234}U/^{238}U$	0.95	1.19	0.98	0.90	0.92	1.02	0.96	1.00
BULK $^{230}Th/^{234}U$	0.99	2.29	1.22	1.05	1.32	1.06	0.80	1.34
BULK $^{226}Ra/^{230}Th$					1.15	1.00	1.11	0.92

HOLE	M5	W1	W1	W1	W1	W2	W2	W2
DEPTH (m)	15	3	24	13	13 <10μm	5.2	14 gen	14 yellow
TAO [U] (μg/g)	1.8 (.1)	5.8 (.2)	28 (1)		43 (1)	22 (1)	21 (1)	113 (?)
TAO ^{234}U/^{238}U	0.99 (.03)	0.91 (.03)	0.87 (.02)		0.83 (.03)	0.76 (.04)	0.67 (.02)	0.72 (.02)
TAO ^{230}Th/^{234}U	1.22 (.05)	1.06 (.05)	0.99 (.04)			1.05 (.06)	0.82 (.04)	0.31 (.02)
TAO ^{226}Ra/^{230}Th	0.30					1.32 (.08)		
RES [U] (μg/g)	6.1 (.03)	25 (1)	294 (11)	285 (13)	313 (8.9)	67 (2)	23 (.75)	149 (5)
RES ^{234}U/^{238}U	0.90 (.04)	1.03 (.04)	1.02 (.05)	1.09 (.07)	0.99 (.04)	1.01 (.04)	1.15 (.04)	1.08 (.05)
RES ^{230}Th/^{234}U		1.04 (.05)	0.66 (.03)	0.52 (.03)		1.06 (.04)	0.89 (.04)	1.28 (.07)
RES ^{226}Ra/^{230}Th		1.40 (.06)	1.37 (.03)	1.88 (.09)		0.84 (.03)	1.27 (.04)	
BULK [U] (μg/g)	~7.9	~30.8	~322		~356	~89	~44	~262
BULK ^{234}U/^{238}U	0.92	1.00	1.01		0.97	0.95	0.92	0.92
BULK ^{230}Th/^{234}U		1.04	0.68			1.06	0.87	0.95
BULK ^{226}Ra/^{230}Th						0.94		

HOLE	W2	W2	W4	W4	W4	W5	W7	W7
DEPTH (m)	14 grey	14 <10μm	5	14	24	13	4	13
TAO [U] (μg/g)	32 (2)	225 (8)	520 (12)	239 (10)	4064 (112)	0.30 (.01)	94 (3)	0.9 (.03)
TAO ^{234}U/^{238}U	0.76 (.04)	0.62 (.04)	0.88 (.02)	0.80 (.01)	0.97 (.01)	1.39 (.08)	0.79 (.01)	0.86 (.03)
TAO ^{230}Th/^{234}U	0.31 (.02)		1.03 (.03)	0.83 (.04)	1.08 (.03)	0.84 (.05)	0.89 (.04)	1.53 (.07)
TAO ^{226}Ra/^{230}Th			1.44 (.06)		1.00 (.03)		1.12 (.04)	
RES [U] (μg/g)	28 (1)	201 (4)	300 (11)	115 (12)	158 (6)	3.2 (.1)	214 (5)	6.2 (.2)
RES ^{234}U/^{238}U	1.22 (.05)	1.12 (.05)	1.36 (.04)	1.13 (.17)	1.40 (.06)	0.90 (.04)	1.10 (.01)	0.99 (.04)
RES ^{230}Th/^{234}U	2.02 (.10)		1.25 (.05)	3.77 (.41)	1.46 (.07)	1.14 (.07)	0.72 (.03)	0.73 (.03)
RES ^{226}Ra/^{230}Th			1.18 (.04)	2.28 (.04)	1.73 (.08)		1.88 (.06)	1.45 (.05)
BULK [U] (μg/g)	~60	~426	~820	~354	~4222	~3.5	~304	~7.1
BULK ^{234}U/^{238}U	0.96	0.86	1.06	0.91	0.98	0.94	1.01	0.98
BULK ^{230}Th/^{234}U	1.31		1.13	2.02	1.10	1.10	0.76	0.82
BULK ^{226}Ra/^{230}Th			1.31		1.05		1.67	

A6.2 Radionuclide Concentrations in Rocks Determined by Gamma Spectrometry

Conc (Bq/g)	DDH1 2.2 (m)	DDH1 27.4-29.0 (m)	DDH2 13.7-15.0 (m)	DDH2 38.1-39.6 (m)	DDH3 10.9 (m)	DDH3 13.7-15.0 (m)	DDH3 33.3 (m)	DDH4 7.7 (m)	DDH4 13.3 (m)
^{238}U (^{234}Th)	10.0 (1.3)	881 (1.1)	11.7 (3.6)	1001 (1.1)	10.5 (1.2)	9.6 (3.8)	0.15 (22)	3.70 (2.0)	1.13 (4.6)
^{230}Th	14.7 (6.3)	958 (6.6)	8.41 (26)	985 (7.0)	10.2 (8.3)	ND	ND	2.78 (20)	2.09 (20)
^{226}Ra (^{214}Bi)	ND	815 (1.2)	11.6 (3.8)	1118 (1.1)	10.1 (0.4)	6.9 (5.1)	0.15 (3.0)	1.98 (0.9)	1.03 (1.0)
^{210}Pb	11.2 (1.0)	555 (1.2)	10.5 (2.9)	644 (1.2)	8.54 (1.2)	6.4 (3.9)	0.11 (29)	1.75 (2.9)	0.95 (4.1)
^{235}U	ND	42.6 (13)	0.64 (35)	36.5 (16)	0.58 (1)	ND	ND	0.20 (18)	0.076 (31)
^{231}Pa	0.51 (11)	34.2 (11)	1.01 (20)	31.6 (14)	0.44 (12)	ND	ND	0.18 (18)	0.09 (34)
^{228}Ra (^{228}Ac)	ND	ND	ND	ND	0.045 (44)	ND	0.064 (8.0)	0.040 (28)	0.068 (11)
^{40}K	ND	ND	ND	ND	0.41 (13)	ND	0.56 (3.4)	0.32 (9.7)	0.34 (6.3)
Activity Ratios									
$^{230}Th/^{238}U$	1.47	1.09	0.72	0.98	0.97	---	---	0.75	1.85
$^{226}Ra/^{238}U$	---	0.93	0.99	1.12	0.96	0.72	1.00	0.54	0.91
$^{210}Pb/^{238}U$	1.12	0.63	0.90	0.64	0.81	0.67	0.73	0.47	0.84
$^{231}Pa/^{235}U$	---	0.80	1.58	0.87	0.76	---	---	0.90	1.18

Values in parentheses denote counting error (%).

ND = Not Detected.

Conc (Bq/g)	DDH4 23.6 (m)	DDH30 7.5-9.0 (m)	DDH30 13.5-15.0 (m)	DDH30 22.5-24.0 (m)	DDH52 2.2 (m)	DDH52 6.9 (m)	DDH54 3.0-6.0 (m)	DDH54 13.5-15.0 (m)
^{238}U (^{234}Th)	2.97 (2.3)	6.27 (1.8)	7.40 (2.7)	10.2 (1.8)	0.45 (8.8)	2.09 (3.1)	5.34 (1.7)	9.99 (0.4)
^{230}Th	2.10 (32)	6.02 (7.4)	6.70 (12)	10.0 (3.0)	0.72 (40)	4.16 (12)	4.78 (13)	10.5 (2.2)
^{226}Ra (^{214}Bi)	1.69 (1.0)	5.04 (0.4)	6.65 (0.4)	8.21 (1.1)	ND	2.68 (0.8)	4.02 (0.4)	10.0 (0.2)
^{210}Pb	1.50 (3.2)	4.37 (1.8)	5.60 (2.1)	7.58 (2.9)	0.36 (9.7)	2.23 (2.4)	3.60 (1.9)	12.0 (0.4)
^{235}U	0.13 (25)	ND	0.37 (6.8)	0.60 (19)	ND	0.008 (44)	0.23 (11)	0.54 (3.8)
^{231}Pa	0.13 (23)	ND	ND	0.48 (5.2)	ND	0.11 (27)	ND	1.07 (2.5)
^{228}Ra (^{228}Ac)	0.063 (16)	ND	0.037 (37)	0.061 (9.3)	ND	0.16 (8.0)	0.029 (30)	0.053 (31)
^{40}K	0.36 (8.3)	0.094 (32)	0.67 (6.3)	0.19 (45)	ND	0.35 (10)	0.14 (18)	0.13 (34)
Activity Ratios								
$^{230}Th/^{238}U$	0.71	0.96	0.91	0.98	1.60	1.99	0.90	1.05
$^{226}Ra/^{238}U$	0.57	0.80	0.90	0.80	---	1.28	0.75	1.00
$^{210}Pb/^{238}U$	0.51	0.70	0.76	0.74	0.80	1.07	0.67	1.20
$^{231}Pa/^{235}U$	1.00	---	---	0.80	---	14	---	1.98

Conc (Bq/g)	DDH54 22.5-24.0 (m)	DDH58 9.12 (m)	DDH58 18.2 (m)	DDH58 21.2 (m)	DDH58 24.3 (m)	DDH58 30.3 (m)	DDH60 9.12 (m)	DDH60 18.2 (m)
^{238}U (^{234}Th)	11.1 (0.6)	18.2 (0.8)	48.8 (0.4)	12.6 (0.5)	8.11 (1.0)	2043 (0.4)	6.90 (0.6)	11.5 (0.9)
^{230}Th	11.8 (10)	22.1 (4.4)	54.4 (2.8)	13.3 (3.7)	8.22 (6.9)	3051 (2.4)	7.21 (4.0)	11.2 (6.8)
^{226}Ra (^{214}Bi)	8.58 (8.7)	17.9 (0.6)	38.6 (0.4)	14.6 (0.4)	9.19 (0.6)	3315 (0.2)	5.44 (0.5)	10.3 (0.7)
^{210}Pb	8.12 (0.8)	22.4 (0.7)	45.4 (0.5)	20.4 (0.4)	12.0 (0.8)	1822 (0.5)	6.80 (0.7)	12.5 (1.0)
^{235}U	0.62 (27)	0.78 (11)	2.36 (5.0)	0.58 (6.7)	0.39 (12)	138 (4.6)	0.33 (7.0	0.61 (10)
^{231}Pa	ND	1.79 (6.0)	4.96 (3.0)	1.36 (3.8)	1.02 (5.9)	66.7 (10)	0.83 (3.6)	1.28 (5.5)
^{228}Ra (^{228}Ac)	0.033 (30)	ND	ND	ND	ND	ND	ND	ND
^{40}K	ND	ND	ND	ND	ND	ND	ND	ND
Activity Ratios								
$^{230}Th/^{238}U$	1.06	1.21	1.11	1.06	1.01	1.49	1.04	0.97
$^{226}Ra/^{238}U$	0.77	0.98	0.79	1.16	1.13	1.62	0.79	0.90
$^{210}Pb/^{238}U$	0.73	1.23	0.93	1.62	1.48	0.89	0.99	1.09
$^{231}Pa/^{235}U$	---	2.29	2.10	2.34	2.62	0.48	2.52	2.10

Conc (Bq/g)	DDH60 21.2 (m)	DDH62 9.12 (m)	DDH62 15.2 (m)	DDH62 27.3 (m)	DDH65 7.5- 9.0 (m)	DDH65 13.5- 15.0 (m)	DDH65 22.5- 24.0 (m)	DDH68 7.5- 9.0 (m)
^{238}U (^{234}Th)	1.67 (0.9)	6.65 (0.9)	59.0 (0.5)	44.3 (1.6)	3.77 (1.9)	8.18 (1.2)	56.0 (0.8)	12.0 (2.4)
^{230}Th	1.28 (8.7)	7.36 (5.7)	60.6 (3.2)	44.5 (10)	6.27 (2.0)	9.24 (8.5)	55.5 (4.2)	12.1 (6.7)
^{226}Ra (^{214}Bi)	1.32 (0.8)	5.99 (0.8)	43.2 (0.5)	42.4 (1.8)	5.03 (0.4)	7.72 (0.3)	52.4 (4.2)	10.6 (6.7)
^{210}Pb	1.68 (1.1)	6.82 (0.9)	46.7 (0.6)	39.3 (1.4)	4.36 (1.6)	6.72 (1.4)	47.8 (0.7)	9.59 (0.7)
^{235}U	0.067 (14)	0.33 (11)	2.45 (6.8)	2.35 (1.4)	0.20 (14)	0.47 (14)	3.04 (20)	0.69 (28)
^{231}Pa	0.19 (6.3)	0.38 (6.5)	3.23 (3.6)	2.85 (11)	ND	0.45 (8.1)	2.54 (7.2)	0.60 (8.0)
^{228}Ra (^{228}Ac)	0.058 (16)	ND	ND	ND	0.066 (16)	0.055 (24)	0.14 (25)	0.12
^{40}K	ND	1.64 (9.5)	ND	ND	0.096 (32)	0.62 (6.5)	1.07 (19)	0.30 (14)
Activity Ratios								
$^{230}Th/^{238}U$	0.77	1.11	1.03	1.00	1.66	1.13	0.99	1.01
$^{226}Ra/^{238}U$	0.79	0.90	0.73	0.95	1.33	0.94	0.94	0.88
$^{210}Pb/^{238}U$	1.01	1.03	0.79	0.89	1.16	0.82	0.85	0.80
$^{231}Pa/^{235}U$	2.84	1.15	1.32	1.21	---	0.96	0.84	0.87

Conc (Bq/g)	DDH68 13.5-15.0 (m)	DDH68 22.5-24.0 (m)	DDH85 6.07 (m)	DDH85 9.12 (m)	DDH85 12.1 (m)	DDH85 15.2 (m)	DDH85 18.2 (m)	DDH85 21.2 (m)
^{238}U (^{234}Th)	25.5 (0.2)	10.3 (12)	0.48 (2.5)	4.32 (1.2)	0.75 (1.3)	1.77 (1.2)	4.06 (1.1)	4.98 (1.0)
^{230}Th	25.1 (1.4)	10.4 (16)	0.95 (11)	5.81 (5.7)	0.82 (9.2)	1.97 (7.0)	5.05 (6.8)	4.84 (7.0)
^{226}Ra (^{214}Bi)	21.9 (0.6)	8.85 (0.3)	1.05 (1.2)	4.47 (1.0)	0.81 (0.8)	1.62 (1.0)	4.39 (0.8)	3.57 (1.1)
^{210}Pb	19.5 (1.0)	7.98 (0.5)	0.98 (1.5)	4.91 (1.1)	1.03 (1.1)	1.94 (1.1)	5.53 (1.0)	4.36 (1.1)
^{235}U	1.26 (17)	0.49 (13)	0.018 (30)	0.20 (15)	0.047 (14)	0.071 (19)	0.18 (16)	0.23 (13)
^{231}Pa	ND	ND	0.043 (14)	0.24 (8.7)	0.081 (9.5)	0.11 (7.6)	0.55 (6.3)	0.30 (6.8)
^{228}Ra (^{228}Ac)	ND	0.049 (28)	0.18 (7.5)	0.072 (30)	0.16 (4.8)	0.19 (10)	ND	0.15 (13)
^{40}K	0.17 (50)	0.49 (8.1)	ND	ND	ND	0.77 (7.6)	ND	ND
Activity Ratios								
$^{230}Th/^{238}U$	0.98	1.01	1.98	1.34	1.09	1.11	1.24	0.97
$^{226}Ra/^{238}U$	0.86	0.86	2.19	1.03	1.08	0.92	1.08	0.72
$^{210}Pb/^{238}U$	0.76	0.77	2.04	1.14	1.37	1.10	1.36	0.88
$^{231}Pa/^{235}U$	---	---	2.39	1.20	1.72	1.55	3.06	1.30

Conc (Bq/g)	PH56 6.0-7.5 (m)	PH56 13.5-15.0 (m)	PH56 18.0-19.5 (m)	PH58 1.5-3.0 (m)	PH60 1.5-3.0 (m)	PH73 6.0-7.5 (m)	PH73 13.5-15 (m) <105μm	PH73 13.5-15 (m) 105-250μm
^{238}U (^{234}Th)	4.41 (1.9)	4.36 (1.1)	8.19 (0.6)	7.63 (1.4)	3.46 (2.3)	5.59 (0.3)	2.33 (2.2)	2.16 (2.2)
^{230}Th	4.26 (4.3)	4.39 (3.1)	7.66 (5.0)	5.59 (12)	1.84 (45)	6.23 (5.2)	2.94 (12)	1.87 (17)
^{226}Ra (^{214}Bi)	3.82 (0.4)	3.95 (0.5)	6.55 (0.3)	5.38 (0.5)	ND	5.51 (0.3)	1.88 (2.1)	1.65 (1.0)
^{210}Pb	3.49 (0.6)	3.54 (0.4)	5.21 (1.1)	3.92 (1.8)	2.06 (2.7)	4.71 (1.1)	1.90 (2.1)	1.40 (2.5)
^{235}U	0.24 (10)	0.21 (3.4)	0.34 (22)	0.36 (14)	ND	0.28 (9.8)	0.12 (27)	0.13 (26)
^{231}Pa	ND	ND	0.083 (29)	0.30 (15)	0.17 (20)	ND	ND	ND
^{228}Ra (^{228}Ac)	0.028 (32)	0.032 (33)	0.032 (29)	0.10 (15)	ND	0.025 (40)	0.12 (9.1)	0.13 (9.0)
^{40}K	0.099 (25)	0.30 (11)	0.079 33)	0.29 (16)	ND	0.19 (15)	0.16 (19)	0.16 (19)
Activity Ratios								
$^{230}Th/^{238}U$	0.97	1.01	0.94	0.73	0.53	1.11	1.26	0.87
$^{226}Ra/^{238}U$	0.87	0.91	0.80	0.71	---	0.99	0.81	0.76
$^{210}Pb/^{238}U$	0.79	0.81	0.64	0.51	0.60	0.84	0.82	0.65
$^{231}Pa/^{235}U$	---	---	0.24	0.83	---	---	---	---

Conc (Bq/g)	PH73 13.5-15.0 (m) 250-500μm	PH73 13.5-15.0 (m) 500-1000μm	PH73 13.5-15.0 (m) 1000-2000μm	PH73 18.0-19.5 (m) <105μm	PH73 18.0-19.5 (m) 105-250μm	PH73 18.0-19.5 (m) 250-500 μm	PH73 18.0-19.5 (m) 500-1000μm	PH73 18.0-19.5 (m) 1000-2000μm
^{238}U (^{234}Th)	1.79 (2.9)	1.58 (3.2)	1.11 (1.9)	0.34 (17)	0.21 (11)	0.17 (25)	0.13 (26)	0.12 (32)
^{230}Th	1.34 (27)	1.58 (19)	1.04 (19)	0.43 (38)	ND	ND	ND	ND
^{226}Ra (^{214}Bi)	1.30 (0.8)	1.08 (0.9)	0.88 (1.1)	0.32 (1.7)	0.22 (2.6)	0.18 (2.5)	0.16 (2.7)	0.15 (2.8)
^{210}Pb	1.18 (3.2)	1.08 (3.0)	0.77 (1.7)	0.29 (2.7)	0.19 (9.9)	0.21 (13)	0.12 (17)	0.091 (24)
^{235}U	0.048 (46)	0.076 (27)	0.041 (45)	0.020 (43)	ND	ND	ND	ND
^{231}Pa	ND	ND	0.033 (41)	ND	ND	ND	0.029 (46)	ND
^{228}Ra (^{228}Ac)	0.11 (7.1)	0.095 (9.1)	0.076 (11)	0.080 (6.7)	0.062 (10)	0.080 (9.1)	0.080 (6.3)	0.082 (6.4)
^{40}K	0.079 (25)	0.10 (22)	0.15 (12)	0.15 (12)	0.26 (7.8)	0.28 (7.6)	0.30 (5.8)	0.35 (5.3)
Activity Ratios								
$^{230}Th/^{238}U$	1.79	1.58	1.11	0.34	0.21	0.17	0.13	0.12
$^{226}Ra/^{238}U$	0.75	1.00	0.94	1.26	---	---	---	---
$^{210}Pb/^{238}U$	0.73	0.68	0.79	0.94	1.05	1.06	1.23	1.25
$^{231}Pa/^{235}U$	---	---	0.80	---	---	---	---	---

Conc (Bq/g)	PH89 3.0-4.6 (m)	PH90 3.0-4.6 (m)	KD2 6.0-7.0 (m)	KD2 13.0-14.0 (m)	KD2 19.0-20.0 (m)
^{238}U (^{234}Th)	3.17 (2.4)	0.76 (5.9)	0.48 (4.2)	0.19 (18)	0.21 (18)
^{230}Th	2.30 (24)	0.99 (36)	ND	ND	ND
^{226}Ra (^{214}Bi)	2.12 (0.9)	0.86 (1.0)	0.44 (2.8)	0.17 (2.2)	0.21 (2.3)
^{210}Pb	1.62 (3.2)	0.66 (5.4)	0.43 (6.3)	0.18 (2.2)	0.23 (2.3)
^{235}U	0.18 (20)	ND	0.048 (29)	ND	0.027 (46)
^{231}Pa	0.15 (24)	0.050 (40)	ND	ND	ND
^{228}Ra (^{228}Ac)	0.071 (16)	0.053 (11)	0.045 (13)	0.039 (10)	0.067 (4.4)
^{40}K	0.40 (8.1)	0.35 (5.4)	0.094 (21)	0.16 (8.1)	0.35 (2.2)
Activity Ratios					
$^{230}Th/^{238}U$	0.73	1.30	---	---	---
$^{226}Ra/^{238}U$	0.67	1.13	0.92	0.89	1.00
$^{210}Pb/^{238}U$	0.51	0.87	0.90	0.95	1.10
$^{231}Pa/^{235}U$	0.83	---	---	---	---